EPFL

Thèse n° 8574

Exploring ferroelectricity in HfO2-based thin films by tackling application-relevant challenges

Présentée le 19 février 2021

Faculté des sciences et techniques de l'ingénieur
Laboratoire des dispositifs nanoélectroniques
Programme doctoral en science et génie des matériaux

pour l'obtention du grade de Docteur ès Sciences

par

Matteo CAVALIERI

Acceptée sur proposition du jury

Prof. V. Michaud, présidente du jury
Dr I. Stolichnov, directeur de thèse
Prof. A. Gruverman, rapporteur
Dr C. Lichtensteiger, rapporteuse
Prof. D. Damjanovic, rapporteur

École polytechnique fédérale de Lausanne

2021

To my future self.

Might he be able to look back and
acknowledge his accomplishments

Acknowledgements

Bringing this doctorate home was possibly my toughest personal challenge, which already tells how lucky I am; while this is a very solitary effort on many aspects, it was possible only thanks to the teamwork and support of many people around me. Here is to acknowledge them. I will try to be concise but fear not, what cannot be said here will be said in front of a beer, or whatever drink your diet/religion/beliefs/fads allow.

I would first like to thank the president and members of the jury of my oral exam, who agreed to read my manuscript as their Christmas treat, add their fruitful remarks and then take the time to discuss it with me. Since after more than two hours they were still asking questions, I'm gonna assume that they had a good time there. Thanks to Prof. Véronique Michaud, Prof. Alexei Gruverman, Dr. Céline Lichtensteiger, and Prof. Dragan Damjanovic: having such high-profile researchers in my final exam was an honor other than a pleasure. I also want to reserve a special mention to Dr. Uwe Schroeder who kindly agreed to take part in the oral exam as well but finally could not join due to doctoral school's regulations. This is because a great part of my research was possible thanks to a collaboration with the Namlab group that he manages in Dresden. With this, I then also want to thank all the people there who at different times deposited and characterized materials to send here in EPFL for my experiments. I want to thank finally Prof. Paul Muralt for taking part in my candidacy exam three years ago and for being a plentiful source of tips on PLD processing and anecdotes during these years.

The biggest and warmest thank you however goes to Dr. Igor Stolichnov, my supervisor during these four years. I discovered in you not only a dependable professional and brilliant scientist but also a very kind man, who always sees the person beyond the colleague he is working with. I learned so much from you, and definitely not just about ferroelectrics. It was a pleasure working with you, seeing the shots from your incredible photographic trips all over the world, discussing the best conditions and resorts to go skiing in the weekend (or during the week) and listening to you quoting Lev Tolstoj while we do AFM experiments or telling me amazing anecdotes of all kinds. I don't know what is coming next, but for sure I will miss working with you. Thank you so much for everything and all the best.

Many other people helped me out in the EPFL bubble. As I did a lot of fabrication and experimental work in CMi's cleanroom facility, I had to use countless tools, which have countless ways to break and stop working, normally at 6 PM on Fridays. A very warm thank you goes to the people who advised and assisted me with all the technical issues. This includes especially Rémy Juttin and Patrick Madliger; I hardly saw people as committed and dedicated to their job, yet always with a smile on their faces. Whatever was my problem, it immediately became their problem, and they did all they could

to solve it (CMi, get more of this). Thanks to Solmates and Jeroen van Swigchem in particular for the prompt in-person and remote assistance, long before that became fashion in 2020. However, there is no need for tool failures to be confined to cleanroom. A big thank you goes to Anna Murello, whose invaluable experience helped me more than once sorting out the bizarre behavior of our dear AFM. I want to cite Éamon O'Connor as well, who shared with me many long months of fabrication and characterization of non-working devices, until some eventually did work. What an effort that was! Thank you Éamon!

Other than technical issues, so many practical things of all sorts have to be arranged during a doctorate, and for this I could always rely on Isabelle Buzzi and Karin Jaymes; their work goes under the radar for the most part, but they ensured me a smooth ride in Nanolab during these four years. The same goes for Anne Kolly, Chrystelle Demierre and Sandra Roux from the doctoral school. Your kindness and support was much appreciated all along.

Nanolab was my second home in the last four years, and the place where I first met people when I moved in to Switzerland. Thanks to Prof. Adrian Ionescu for giving me the possibility to be part of this amazing group. Here I found colleagues who turned into friends, and this is not a given. Carlotta, Chiara, Emanuele, Jacopo, Nicolò, you always kept my mood up during this long time; I am extremely grateful for meeting you and I will always value that. All the dinners, nights out, trips, bbqs at the lake, and everything else was simply great with you. Huge thanks also to all my past and present colleagues in Nanolab, from Ali, Maneesha, Francesco and Teodor representing the old guard, to the newer generations with Fatemeh, Andrei, Sadegh, Shokoofeh, Pooya, Felix, Yingfen, Fabio and Ali. In case somebody is wondering, I am the arbitrary threshold for this classification.

Outside of the EPFL bubble, many more people offered me strength, support, fun social moments and much more. A very big thank you to Francesca, you are such a multitasking, smart and generous person. All the time spent together is extremely fun, especially for you when we go skiing. I hope that we will have more of it soon! I then want to thank Mariazel, you are a very inspiring person. I'm so glad that I crossed you in Nanolab for just enough time to start developing this amazing friendship with you, I value it so much. Thank you also to Jana, you are such a funny and strong woman; you exposed me to so many interesting ideas and we had so much good time together, thank you especially for supporting me in the last months during the writing! I also want to thank Alexandre, Cosimo and Rachele (and Victor!), Davide, Georgi, Giulia and Alessandro, James, Ladina, Nadia, Philipp, Sardar, Seb and all the team of Les Cédres, Yassine.

I then want to mention friends who are scattered all over the corners of this too lockdowned planet and often feel very far, yet they always proved to be close to me. I am talking to you Alessia, Ben and Shail! Thank you for the long phone/Skype/Zoom calls at whatever time of the day or night. A great thank you to Santiago as well, who inspired me to pursue a doctorate in the first place, when I was doing my master thesis under his supervision.

Finally, I want to thank all the people from my hometown, those who know me since the longest. My sister Fedi, Franz and Mara, you have been my beacons long before I started all this and you will be it afterwards as well. You don't know how many times

a text message, a short call, a little gift or an ice cream together put everything back in the right perspective and gave me the energy that I needed to keep going. Thank you. Ale, Giova, Ste, Vale, thank you for your support at all times. The time spent together acquired a whole nother value since when we can meet so little. My friendship with you defines for me what being friends means. Long live that! I then want to thank Ale, Benni, Cate, Fede, Hani, Lulo and Ugo. All of you, in a way or another, shaped me into who I am now and supported me through this long effort.

Finally, I want to thank everybody in my family and especially my parents Cinzia and Roberto for their love and continuous messages and phone calls. The big family gatherings that used to be for birthdays or special occasions are now moved to the few days per year that I am available, and I want to thank you for that and for always showing me that I have a place where to seat around the table and have an amazing lunch together.

They say: tell me whom you go with, and I will tell you who you are. All in all, these four years of doctorate are about me as much as they are about you all. Thank you everybody!

Lausanne, 28/01/2021 Matteo Cavalieri

Abstract

Ferroelectric materials offer a broad range of application-relevant properties, including spontaneous polarization switchable by electric field. Archetypical representatives of this class of materials are perovskites, currently used in applications ranging from sensors and actuators to information storage in nonvolatile memories. The latter application poses significant technological challenges because perovskites cannot be easily integrated in CMOS fabrication. The two main issues are a high annealing budget required to obtain functional films and the instability of ferroelectricity at the nanoscale that prevents aggressive scaling.

In this context, the discovery a decade ago of ferroelectricity in hafnia (HfO_2) thin films was groundbreaking: they are readily employed in CMOS processing and were shown to retain their properties down to 5 nm and lower, overcoming the main limitations of perovskites and making them ideal candidates for low-power ferroelectric devices. Research then focused on understanding the physics underlying polarization response of these materials while developing reliable fabrication process for smooth integration in logic and memory devices. This thesis contributes to CMOS-compatible processing of ferroelectric hafnia and addresses intriguing and partly controversial aspects of its switching properties.

The majority of HfO_2 films are grown by Atomic Layer Deposition (ALD), a mature but slow and not so flexible technique. The layers are amorphous and need high thermal budget annealing to become ferroelectric. This work proposes an alternative Pulsed Laser Deposition (PLD) fabrication route for ferroelectric hafnia thin films with conventional TiN electrodes and very low thermal budget, well within the requirements for CMOS compatibility. The superior flexibility of PLD is exploited to obtain already partially crystallized films that only need low thermal budget annealing to become ferroelectric.

Besides the development of a CMOS-compatible fabrication route, detailed investigation of ferroelectricity is performed by off-resonance Piezoresponse Force Microscopy (PFM). Optimization of this technique allowed probing extremely weak response, with vertical resolution below 0.1 pm. This is accomplished without having to rely on resonance amplification, thus avoiding possible related artifacts. The same technique enabled to obtain reliable PFM through a top electrode and dielectric layer.

Ferroelectricity in undoped HfO_2 is explored, giving insight into phase evolution at nanometer scale during the wake-up process. A study on ultrathin HZO demonstrated the potential of such films for future generations of memory devices with mV-range operation. Comparing HZO films of different thickness, an anomalous scaling of coercive field is noted: a new nucleation model is proposed to interpret this, with important

practical implications. Finally, the developed methodology is employed in the analysis of ferroelectric/dielectric bilayers used for Negative Capacitance (NC) applications, offering an alternative look to the debate on intrinsic or nucleation-driven switching.

In this thesis, technological challenges of this new class of ferroelectrics are taken as starting point to propose an alternative fabrication method and explore the physics behind ferroelectricity in thin films. The results reveal the fascinating complexity of hafnia ferroelectrics and the enormous potential that they hold for next-generation applications.

Keywords: ferroelectricity, hafnium oxide, HfO_2, HZO, Gd:HfO_2, off-resonance Piezoresponse Force Microscopy (PFM), Pulsed Laser Deposition (PLD), CMOS compatibility, Nucleation Limited Switching (NLS), Negative Capacitance (NC).

Riassunto

I materiali ferroelettrici possiedono una vasta gamma di proprietà molto utili dal punto di vista tecnologico, tra cui una polarizzazione spontanea che può essere invertita da un campo elettrico. I rappresentanti più tipici di questa famiglia di materiali sono le perovskiti, che hanno trovato numerosi utilizzi da sensori ed attuatori a memorie non volatili. Quest'ultima applicazione presenta sfide tecnologiche significative perchè le perovskiti non sono facilmente integrabili nei processi CMOS. I due problemi pincipali al riguardo sono l'alto bilancio termico necessario per ottenere film funzionali e l'instabilità della ferroelettricità su scala nanometrica.

In questo contesto, la scoperta un decennio fa della ferroelettricità in film sottili di ossido di afnio (HfO_2) ha rappresentato una grande innovazione: questi film sono già regolarmente impiegati in processi CMOS ed hanno dimostrato di mantenere proprietà ferroelettriche fino a spessori di 5 nm e oltre, caratteristiche che li rendono superiori alle perovskiti e candidati ideali per dispositivi a basso voltaggio. La ricerca si è quindi focalizzata da una parte sul comprendere il comportamento della polarizzazione e la fisica sottostante e dall'altra sul trovare processi che permettano di fabbricare ed integrare questi film in memorie ed applicazioni logiche. Questa tesi contribuisce a questo processo di ricerca presentando un metodo di fabbricazione dell'afnio ferroelettrico che è compatibile CMOS, ed esplora gli aspetti affascinanti ed in qualche misura controversi dell'inversione della polarizzazione in questi materiali.

La maggioranza dei film sottili di HfO_2 sono cresciuti tramite deposizione di strati atomici (ALD), una tecnica matura ma lenta e non molto flessibile. I film così ottenuti sono amorfi e necessitano di ricottura ad alte temperature per diventare ferroelettrici. Questo lavoro propone un processo alternativo per la fabbricazione di HfO_2 con elettrodi convenzionali in TiN, basato sulla deposizione a impulsi laser (PLD) e caratterizzato da un bilancio termico molto basso, minore di 450 °C e quindi compatibile con i processi CMOS. Sfruttando la grande flessibilità di questa tecnica è possibile depositare film che sono già parzialmente cristallizzati e che quindi necessitano di un minore bilancio termico durante la ricottura per esibire comportamento ferroelettrico.

In parallelo allo sviluppo di una tecnica di fabbricazione compatibile CMOS, viene effettuata un'analisi dettagliata della ferroelettricità in film sottili tramite microscopia a forza piezoelettrica (PFM) non in risonanza. L'ottimizzazione di questa tecnica permette di rilevare risposte estremamente deboli, con una risoluzione verticale di 0.1 pm. Ciò è ottenuto senza dover ricorrere all'amplificazione ottenuta lavorando in risonanza, e quindi evitandone i possibili artefatti. La stessa tecnica è stata poi usata per dimostrare che è possibile realizzare PFM in alta risoluzione anche attraverso l'elettrodo e uno strato isolante.

L'osservazione di alcuni dettagli nella risposta rilevata tramite PFM non in risonanza ha permesso di confermare la natura genuina della ferroelettricità in questi materiali e di gettare luce sull'evoluzione delle fasi (ferroelettrica e non) su scala nanometrica durante il processo di wake-up. Lo studio di film ultrasottili di HZO ha consentito di esplorare il loro potenziale nell'ottica di una nuova generazione di dispositivi che lavorano a basso voltaggio. Studiando film di spessori diversi dello stesso materiale è stato possibile osservare un andamento anomalo del campo coercitivo, che è spiegato supponendo un nuovo modello di nucleazione che può avere importanti ricadute tecnologiche. Infine, la stessa tecnica è applicata a strutture usate in dispositivi che sfruttano la capacità negativa (NC) e caratterizzate da un doppio strato isolante/ferroelettrico. Questo approccio offre un punto di vista alternativo al dibattito sull'inversione intrinseca o assistita dalla nucleazione di domini.

In questa tesi, le sfide tecnologiche riguardanti questa nuova classe di materiali ferroelettrici sono prese come punto di partenza per proporre un metodo di fabbricazione alternativo ed esplorare la fisica alla base della ferroelettricità nei film sottili. I risultati rivelano l'affascinante complessità dei film di HfO_2 e allo stesso tempo l'enorme potenziale che racchiudono per lo sviluppo di dispositivi di nuova generazione.

Parole chiave: ferroelettricità, ossido di afnio, HfO_2, HZO, Gd:HfO_2, microscopia a forza piezoelettrica (PFM) non in risonanza, deposizione con laser ad impulsi (PLD), compatibilità CMOS, inversione di polarizzazione, inversione limitata dalla nucleazione (NLS), capacità negativa (NC)

Contents

List of Figures

1 | Introduction

The first section of this introductory chapter gives the motivation behind this work on ferroelectric HfO_2-based thin films; the next section introduces electrical and structural arguments for ferroelectricity in crystalline materials and then explains it through a phenomenological theory, introducing relevant quantities that will be used throughout this work. The third section illustrates the status of current research on ferroelectric HfO_2-based thin films, before the last section that gives an outline of this dissertation.

1.1 Motivation

Ferroelectric materials possess a wide spectrum of properties that make them very suitable for many technological applications. Nowadays they are successfully employed in nonvolatile memories (due to their ferroelectric hysteresis), capacitors (for the high permittivity), sensors and actuators (piezoelectric effect), infrared detectors (thanks to the high pyroelectric coefficient) and other applications.

The work presented in this thesis aims to bring a contribution to the understanding of HfO_2-based thin films, a recently discovered class of ferroelectrics with a rather unique set of properties that are anticipated to represent a revolution in the field [1, 2]. In particular, what is considered a game changer is that these films show ferroelectricity for thickness down to very few nanometers. The theoretical study of these materials is primarily concerned with stabilization of ferroelectricity, characterization of polarization reversal mechanism and factors influencing it. The very peculiar conditions associated to the insurgence of ferroelectric behavior in fluorite HfO_2-based thin films at very low thickness bring along a new set of challenges. In particular, some issues that were already known in perovskites, the other important family of ceramic ferroelectrics, such as phase stabilization and accurate interface engineering, are assuming a predominant role here [2].

At the same time, in this new class of ferroelectrics lies the potential for a great step ahead towards overcoming some of the most pressing technological challenges of this time. Namely, the multitude of devices required by latest innovations such as Internet of Things (IoT) or autonomous drive, just to cite some, demand both device scaling and reduction of power consumption. The most promising employment of these newly

discovered materials is surely in the field of nonvolatile ferroelectric memories, but more applications were proposed from supercapacitors to sensors to neuromorphic devices and more [2–4]. With this in mind, the research direction pursued in this work is steered by application-relevant issues. From the industry point of view, several technological requirements have to be met if one wants to commercialize a reliable ferroelectric device, including [2, 5]:

- strong and constant polarization response (i.e. absence of wake-up or fatigue);
- low operation voltage to reduce power consumption;
- good retention for about 10 years;
- polarization switching for 10^{15} cycles with no or minimal degradation;
- CMOS compatibility, meaning low fabrication thermal budget and smooth integration with materials currently used in electronics.

Amorphous thin films of hafnium oxide are routinely employed in electronics as high-κ dielectrics since several years and their integration is therefore mature [6, 7]. However, the annealing step required to crystallize the material and stabilize the correct ferroelectric phase introduces a new fabrication challenge, since temperature in excess of 450-500 °C is necessary to induce ferroelectricity in the vast majority of HfO_2-based thin films [8]. In addition, the presence of an annealing step during fabrication and the extremely small thickness of these layers is causing the interfaces between ferroelectric and electrode materials to play a major role in determining the functional properties of the film and its switching mechanism. Another concern emerging from a number of studies is that the scaling of operation voltage seems to be interrupted for thickness smaller than 10 nm, an issue that can hinder the realization of sub-1 V ferroelectric devices [2, 8].

Overall, the greatest technological advantage of HfO_2-based materials is their retention of ferroelectric properties down to few nm in thickness. The potential for aggressive scaling renovated the interest in ferroelectric memories and opened to other applications in low-power electronics. However, several distinct hurdles in the path of device commercialization were identified; this dissertation is therefore undertaking a complementary approach in tackling the mentioned issues. On one hand by proposing an alternative fabrication path which falls within the requirements of a fully CMOS compatible process and on the other hand by offering in-depth analysis of coercive field scaling and switching mechanisms in films of various thickness and with different interface materials.

1.2 Fundamentals of ferroelectricity

The first time that ferroelectric materials were reported was in 1921, just a century ago: Joseph Valasek noticed a permanent polarization that could be switched in a hysteretic fashion on Rochelle salt [9]. Substantial progress in the field was made starting from 1946, when ferroelectricity was found in $BaTiO_3$ (BTO), an inorganic compound with perovskite structure [10]. Later on, in 1971, also the first ferroelectric polymer,

polyvinylidene fluoride (PVDF), was identified [11]. The last significant discovery in chronological order of a new major class of ferroelectric materials was made public in 2011, just ten years ago, when permanent polarization and hysteretic behavior were detected in silicon doped HfO_2, a ceramic compound with fluorite structure [1].

Several kinds of materials exhibit ferroelectric behavior; among them, ceramics with perovskite structures were the most extensively investigated and as a result BTO and $PbZrO_3$-$PbTiO_3$ (PZT) are currently the most technologically important class of ferroelectric materials. A first phenomenological theory to explain ferroelectricity, which takes into account the crystalline structure of the material, started to be developed by Devonshire already in 1949 taking $BaTiO_3$ as reference model [12].

In this section, ferroelectricity is first introduced from electrical and structural perspectives, that is looking at the displacement of charges in the material and showing the crystal symmetries that allow ceramic compounds to be ferroelectric. Then, the phenomenological theory explaining insurgence of ferroelectricity in crystalline materials will be illustrated; starting from the ideal case described by thermodynamics, the degree of approximation is progressively reduced as domain formation and defects are discussed.

1.2.1 An overview of electrical and structural properties of ferroelectrics

Ferroelectrics constitute a small selected group among all dielectric materials. A common way to explain ferroelectricity is therefore to first define dielectric materials from an electrical point of view and then show, from a crystallographic perspective, what are the requirements that a material must satisfy in order to be ferroelectric [13–15]. When an insulating material is placed into an electric field E_j its positive and negative charges are slightly displaced. In a linear approximation, the material can be considered to polarize following the equation

$$P_i = \chi_{ij} E_j, \tag{1.1}$$

where P_i is the polarization vector and χ_{ij} is the dielectric susceptibility, a symmetrical second-rank tensor. Subscripts in the notation represent orthogonal directions in the three dimensional space. The dielectric displacement D_i caused by the applied field accounts for the contributions of polarization and vacuum charges according to the formula

$$D_i = \epsilon_0 E_i + P_i, \tag{1.2}$$

where the constant ϵ_0 is the dielectric permittivity of vacuum. Combining the previous two equations one can write the displacement field D in the material as a function of

the applied electric field E_j as

$$D_i = \epsilon_0 E_i + \chi_{ij} E_j = \epsilon_0 \delta_{ij} E_j + \chi_{ij} E_j = (\epsilon_0 \delta_{ij} + \chi_{ij}) E_j = \epsilon_{ij} E_j. \tag{1.3}$$

In the above equation, ϵ_{ij} is defined as the dielectric permittivity of the material, also a symmetrical second-rank tensor, and δ_{ij} is Kronecker delta. When dealing with ferroelectrics in the application-relevant plane capacitor configuration, that is with the insulator sandwiched between two conductive electrode plates, a few simplifications can be introduced. First, for ferroelectric materials usually χ_{ij} is much greater than ϵ_0 and therefore $\epsilon_{ij} \approx \chi_{ij}$. This also implies that, in ferroelectrics, polarization is basically the whole contribution to displacement field, or that $D \approx P$. Second, electric field E, polarization P and displacement D are assumed to be all uniformly aligned along the vertical direction; accordingly, $i = j = 3$ and subscripts are usually omitted altogether. In conclusion, Eq. 1.3 can be rewritten for a ferroelectric in plane capacitor structure as

$$D = \frac{q}{A} = \epsilon E = \epsilon_0 \epsilon_r E, \tag{1.4}$$

where q is the charge at capacitor surface and A is the area of electrodes. The term ϵ_r is the relative permittivity or dielectric constant of the material ($\epsilon_r = \epsilon/\epsilon_0$), which is introduced to have a more practical metric to compare dielectrics.

Another important effect that is observed in all dielectric materials is electrostriction, a nonlinear strain caused by the applied field. In ferroelectrics, it is more consistent to formulate the electrostrictive effect as a function of the polarization [13] as

$$x_{ij} = Q_{ijkl} P_k P_l, \tag{1.5}$$

where x_{ij} is a second-rank symmetrical tensor representing the strain of the material and Q_{ijkl} is the fourth-rank tensor of electrostrictive coefficients.

To resume, the above discussion is applicable to all dielectrics with the only caveat that, for ferroelectric materials, the magnitude of P basically represents the total displacement charge D. Now, to really distinguish ferroelectric materials among all dielectrics, it shall be explained what characterizes them from a structural point of view. Crystalline materials are divided in 32 point groups, also called crystal classes, according to their symmetry. Among these, 20 are non-centrosymmetric and therefore become polarized (along one or more polar axes) as a result of an applied mechanical stress. This effect, called piezoelectricity, is owed to the fact that, when strained, the displacement of atoms is such that the unit cell becomes polar. This behavior is used for example in piezoelectric sensors. The opposite holds true as well, meaning that an externally applied electric field generates a deformation in the material. This is called converse piezoelectric effect and is at the basis of the working principle of piezoelectric actuators.

The direct piezoelectric effect can be written as

$$D_i = d_{ijk} X_{jk}, \tag{1.6}$$

where X_{ij} is the second-rank symmetrical stress tensor and d_{ijk} is the direct piezoelectric coefficient, a third-rank tensor. The converse piezoelectric effect instead describes the strain that is caused when an electric field is applied as follows:

$$x_{ij} = d_{kij} E_k. \tag{1.7}$$

From thermodynamic arguments it can be demonstrated that direct and converse piezoelectric coefficients are the same, that is to say

$$d_{ijk}^{direct} = (d_{ijk}^{converse})^T, \tag{1.8}$$

where T indicates the transposed matrix. Once again the notation can be simplified: it was mentioned that strain and stress tensors, x_{ij} and X_{ij} respectively, are symmetrical. This allows to introduce the Voigt notation by which subscripts ij and kl can be substituted by a single subscript m or n [13]. In literature and practical applications the piezoelectric and electrostrictive coefficients are then usually reported as:

$$\begin{aligned} d_{ijk} &\rightarrow d_{mk} \\ Q_{ijkl} &\rightarrow Q_{mn}, \end{aligned} \tag{1.9}$$

Once the main properties of piezoelectrics have been highlighted, a further step can be made in the subdivision of crystalline materials: amid the 20 non-centrosymmetric classes, there is a subset of 10 crystals which present a spontaneous polarization P_s even when no external electric field is applied; in addition, its magnitude is a function of temperature. These materials are therefore called pyroelectrics. Ferroelectrics are in turn a subset of pyroelectrics, in which the direction of stable spontaneous polarization can be reversed. Notice that from the crystallographic point of view there is no difference between pyroelectric and ferroelectric materials: the only way to distinguish them is by trying to switch the polarization direction. If it can be reversed, the material is ferroelectric. Fig. 1.1 shows this classification from dielectrics to ferroelectrics using Venn diagrams, which is a useful way to understand how each ferroelectric has to be both pyroelectric and piezoelectric while the opposite is not true.

In summary, what makes ferroelectric materials different from other dielectrics is that, even in absence of an external electric field E, they possess a spontaneous polarization P_s. Even more interesting from a technological point of view is the fact that the direction of spontaneous polarization can be switched if a field stronger than the coercive field E_c is applied in the opposite direction. This behavior implies the insurgence of hysteresis in

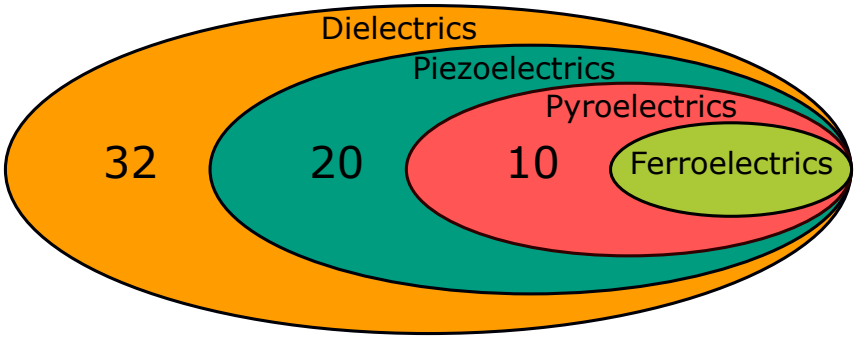

Figure 1.1: Venn diagram showing the crystallographic classification of dielectric materials. For each set, the number of point groups belonging to it is indicated.

the polarization response when sweeping the electric field, as can be seen in Fig. 1.2b. There, the intercepts on the y-axis are called positive and negative remanent polarization P_r: this slightly differs from P_s in the practical case in which multiple ferroelectric domains are formed within the material, as it will be explained in more detail later, but this difference can be ignored for now. Such P-E curve can be actually obtained as time integration of the transient current I that is measured across the capacitor stack when applying an electric field (with amplitude higher than E_c). An example of I-E plot obtained from this measurement is given in Fig. 1.2a.

The intuition of Devonshire was that the root cause of hysteresis has to be searched into the crystal structure of the material. A ferroelectric that presents two values of P_r as in Fig. 1.2b must also possess two distinct stable configurations at the atomic level, which correspond to energetic minima. This is depicted in Fig. 1.2c, which represents the Gibbs energy landscape of a ferroelectric.

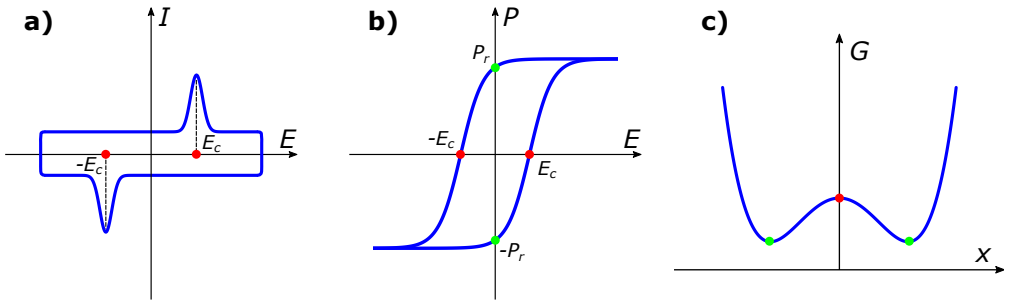

Figure 1.2: a) Displacement current versus field (I-E) plot of a ferroelectric material and b) typical hysteresis loop (P-E) that is derived from it; c) double well potential of the Gibbs energy G as a function of position x. Red dots indicate the coercive field and the potential energy to overcome in order to switch from one stable state to the other, whereas green dots show the two stable polarization states when no field is applied.

1.2.2 Phenomenological theory of ferroelectricity

After the discovery of ferroelectricity in $BaTiO_3$ the research intensified and a phenomenological thermodynamic theory was developed to explain the observed results. The theory describes formation of two energetic minima as result of a phase transition from a parent non-polar (paraelectric) to a polar (ferroelectric) phase with decreasing temperature (Landau-Ginzburg-Devonshire or LGD theory) [16–18]. The phase transition in ferroelectric materials is best described when expressing the Gibbs energy in the elastic form, because it shows the direct dependence of G on displacement field D. This is convenient because D is related via Eq. 1.2 to the polarization P, that is the order parameter analyzed during the phase transition. A simplified derivation of the double-well potential of Fig. 1.2c and of other relevant coefficients is offered below. For a more detailed derivation starting from constitutive equations and in the most general case of tridimensional space the reader is referred to [13, 18]. Here, for the sake of simplicity, only the simpler case of one spatial dimension is considered where polarization and field are applied along the same direction.

The Gibbs energy G is related to the elastic Gibbs energy G_1 by the relation

$$G = G_1 - ED, \tag{1.10}$$

where it can be seen that, for $E = 0$, the two are equal. The contribution of an externally applied field is contained in the term -ED: it is worth considering here how a reduction of the Gibbs energy can be obtained only when E and D (in a ferroelectric: P) have the same sign, which means they are parallel. If they were antiparallel, they would result instead in an increase of Gibbs energy that will eventually lead to polarization switching in the same direction of the field (or to breakdown).

After appropriate manipulation, a small variation of the elastic Gibbs energy G_1 can be written as [13]

$$\mathrm{d}G_1 = -S\mathrm{d}T - x\mathrm{d}X + E\mathrm{d}D, \tag{1.11}$$

where S and T are two scalar quantities defining entropy and temperature, respectively; x and X are instead the tensors mentioned earlier and representing strain and stress. When the latter is kept constant, G_1 can be expanded in a Taylor series around the state of equilibrium G_{10} as

$$G_1 = G_{10} + \frac{\alpha}{2}D^2 + \frac{\beta}{4}D^4 + \frac{\xi}{6}D^6, \tag{1.12}$$

where β and ξ are regarded as temperature-independent coefficients. It can be shown that β can be positive or negative and that will give a second or first order phase

transition, respectively. In addition, ξ must always be positive. Both these higher order coefficients are correction factors and therefore get smaller in magnitude as the order increases. Finally, assuming that the parent non-polar phase is centrosymmetric (which is the case for most ferroelectric taken into consideration), the coefficients of the odd powers have to be zero due to symmetry reasons [13].

The coefficient α deserves further explanation, since it includes the temperature dependence of the Gibbs energy. This has to be in a form that satisfies the requirements of minimization of G for both the parent paraelectric phase and the ferroelectric one. In addition, G has to be continuous at the phase transition, which occurs at what is called the Curie temperature T_c. Remembering that in a ferroelectric D can be substituted by P, the requirements for α will be:

$$\alpha(T) \mid \begin{cases} \text{for} \quad T > T_c: & G_1 = G_{10} \quad \text{and} \quad P = 0 \\ \text{for} \quad T = T_c: & G_{1paraelectric} = G_{1ferroelectric} \\ \text{for} \quad T < T_c: & G_1 < G_{10} \quad \text{and} \quad P \neq 0. \end{cases}$$

The solution is a simple linear dependence of α with temperature,

$$\alpha = \frac{(T - T_0)}{C}, \tag{1.13}$$

where C is the Curie constant and T_0 is the Curie-Weiss temperature. In a first-order phase transition $T_0 < T_c$, whereas in a second-order phase transition the two coincide. Eq. 1.13 is called the Curie-Weiss law and the coefficient α is actually the reciprocal of the electric susceptibility χ seen in Eq. 1.1. Since we are looking for a minimum of Gibbs energy we need to derive and equal to zero Eq. 1.12 in conditions of fixed temperature and electric field. Assuming stress equal to zero, this yields

$$E = \frac{\partial G_1}{\partial D} = \alpha D + \beta D^3 + \xi D^5. \tag{1.14}$$

To make sure this is a minimum we need to impose the second derivative greater than zero, which gives

$$\frac{\partial E}{\partial D} = \frac{\partial^2 G_1}{\partial D^2} = \alpha + 3\beta D^2 + 5\xi D^4 > 0. \tag{1.15}$$

As stated before, in a ferroelectric material with no electric field applied ($E = 0$), D can be substituted by P_s and therefore Eq. 1.14 becomes

$$P_s(\alpha + \beta P_s^2 + \xi P_s^4) = 0. \tag{1.16}$$

As shown below, this equation presents the two possible solutions

$$0 = \begin{cases} P_s & \rightarrow \quad \text{paraelectric phase,} \\ \alpha + \beta P_s^2 + \xi P_s^4 & \rightarrow \quad \text{ferroelectric phase,} \end{cases} \tag{1.17}$$

that can be applied to the two different phases involved in the transition. The trivial solution, $P_s = 0$, corresponds to the paraelectric phase. In the ferroelectric phase on the contrary $P_s \neq 0$, and the solution is:

$$P_s^2 = \frac{-\beta + \sqrt{\beta^2 - 4\alpha\xi}}{2\xi}. \tag{1.18}$$

It can be shown that for $\xi \approx 0$, $\beta > 0$ and $T < T_0 = T_c$, the spontaneous polarization takes the simple form

$$P_s^2 = -\frac{\alpha}{\beta} \tag{1.19}$$

and presents indeed two possible values, $+P_s$ and $-P_s$, that correspond to the two polarization states of a ferroelectric material. The polarization changes in a continuous way during the phase transition, which is hence said of second order. The susceptibility χ undergoes a discontinuity and tends to infinity at Curie temperature as it can be understood by looking at Eq. 1.13.

The opposite case, where P_s shows a discontinuity at the phase change, is instead a first-order phase transition, and occurs when $\xi > 0$ and $\beta < 0$. Here ξ cannot be neglected and therefore this yields a more complex equation of P_s; more information on that can be found in [18, 19]. Fig. 1.3 summarizes the behavior of P_s and χ (or, equivalently, ϵ_r) for both the first- and second-order phase transition of a paraelectric into ferroelectric material.

In a similar way to what was done to extract polarization, by manipulating and deriving Eq. 1.11 with the appropriate boundary conditions it is possible to obtain other coefficients which have important physical meaning [13]. For example, remembering the electrostrictive effect described in Eq. 1.5, it is expected that ferroelectrics possess a spontaneous strain x_s caused by P_s when both $X = 0$ and $E = 0$:

$$x_s = \frac{\partial G_1}{\partial X} = Q P_s^2. \tag{1.20}$$

Another important quantity that was mentioned earlier and that will be extensively discussed throughout this work is the piezoelectric coefficient *d*. With appropriate bound-

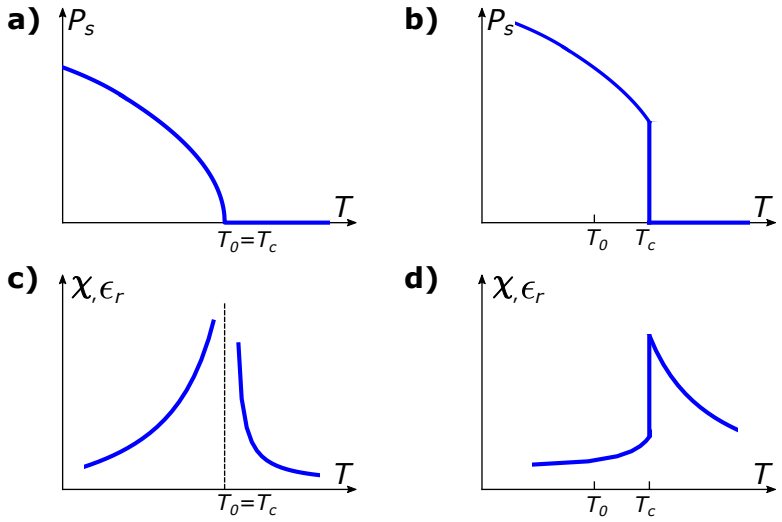

Figure 1.3: Temperature behaviour of spontaneous polarization P_s and electric susceptibility χ (or equivalently relative permittivity ϵ_r) for second-order, a) and c), and first-order, b) and d), phase transition.

ary conditions this can be derived from Eq. 1.11 as

$$d = \frac{\partial^2 G_1}{\partial X \partial D} = 2\epsilon_0 \epsilon_r Q P_s. \tag{1.21}$$

The thermodynamic theory outlined here, that shows how the spontaneous polarization is allowed by looking at the energy landscape of a ferroelectric, adds to the crystallographic considerations presented previously. While it provides a very useful tool in approaching the study of ferroelectric materials, it remains an idealization of the complex reality of phase transition. This is not to say it has to be disregarded, however the first hypothesis of energy landscape described as a symmetrical polynomial can be easily violated in a real ferroelectric. The next step will be therefore to see how polarization develops in a material, looking at what happens at the atomic scale and how that reflects at the macroscale.

1.2.3 Ferroelectric domains and polarization switching

Polarization was so far regarded as a macroscopic effect that can be recognized by the presence of surface charges on a material. When looking at the *P-E* hysteresis loop of Fig. 1.2b the two stable polarization states can be observed. However, it can be seen that the switching from one polarization state to the other is not abrupt and punctual (that is, occurring at one precise value of the field). The positive and negative coercive fields are conventionally defined as the points where the loop intercepts the x-axis, but polarization reversal is a continuous process that starts before and continues after that value of the

field. This behavior can be understood using the Preisach model for hysteretic systems, which describes macroscopic hysteresis as the integral of many microscopic bistable units [20].

As discussed earlier, when a crystalline material cools down the phase transition, spontaneous polarization appears along the crystal axes that allow it, which can be one or more according to the material. However, due to different electrical and mechanical local boundary conditions, these crystal axes (and hence polarization) can be oriented differently throughout the material. In ferroelectrics, small continuous regions of the crystal that share the same orientation of the spontaneous polarization are called domains. Each domain possesses its own hysteretic behavior with different $\pm E_c$ and bias field E_{bias}, which shifts the switching along field axis. This splitting of the material into domains is therefore responsible for the spread of polarization switching with respect to applied field.

An exemplary P-E hysteresis loop is shown in more detail in Fig. 1.4: when a positive electric field E is first applied to the material, some domains start to switch until the coercive field is reached, at which point most of the ferroelectric response is already measured (from A to C). Polarization is saturating at this point because less and less domains are left to switch, and there is an approximate linear relationship between P and E (from C to D). If the field applied to the ferroelectric starts to decrease, the polarization reduces because some domains backswitch very early on. Still, polarization becomes zero only at the negative coercive field -E_c, and in fact crosses the point of zero field with a positive residual value P_r, that is the remanent polarization discussed earlier (from D to F). The field becomes more negative and P completely reverses (from F to G). Upon increase of the field, polarization reduces until eventually it switches at the positive E_c (from G to D). The hexagons in Fig. 1.4 sketch the domain configurations at all the critical points of the loop, that is when $E = 0$, for $P = 0$, and at saturation. A monodomain configuration is reached for high E while a mixed state is observed at the coercive fields. Notice the difference between the remanent and the saturation polarization, P_r and P_s, respectively: the latter is the projection on y axis of the linear dependence observed for high fields, when polarization saturates. However, when the field is lowered, some domains already start to switch back and thus $P_r < P_s$. For the monodomain case in a single crystal, the two would coincide. Notice that, ideally, this loop is symmetrical with respect to both x and y axes but there can be many reasons for that not to be the case, as will be discussed in the next section.

The reason for domains formation to occur is the minimization of Gibbs energy: if the polarization were to be uniformly aligned everywhere in the material, there would be two oppositely charged surfaces. The consequence of that is the insurgence of a depolarization field E_d inside the material, in the direction opposite to the polarization and proportional to it, which has a high energy cost. This effect is indeed reduced by creating ferroelectric domains, as shown in Fig. 1.5. Adjacent domains are separated by a very fine region (1-10 nm) called ferroelectric domain wall, where the direction of polarization changes from that of a domain to that of the next one. Two neighboring domains can be oppositely aligned, and in that case there is a 180 ° domain wall between them, as in Fig. 1.5. However, also 90 ° domain walls (or with different angles according

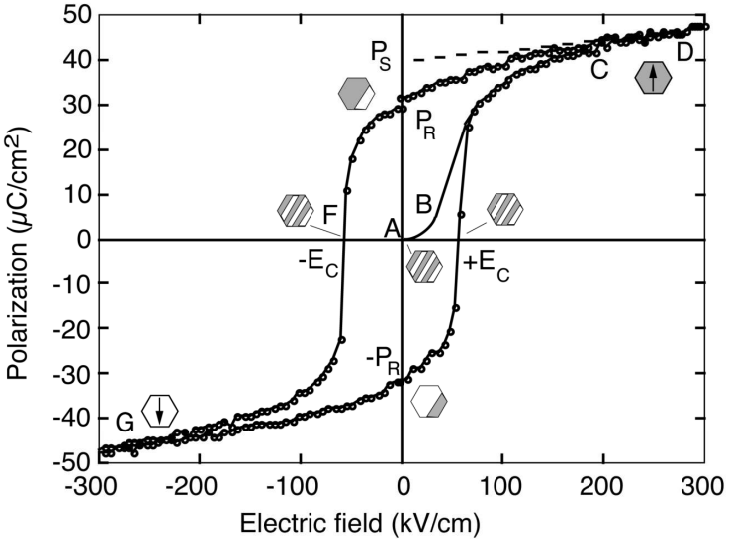

Figure 1.4: Ferroelectric hysteresis loop (P-E) measured on a PZT sample, where the exagons sketch domain configuration of the material at different points of the loop. Reproduced and adapted from [14].

to the crystalline structure of the material) exist if the domains are aligned differently. In this case there is also strain associated to them, which are then ferroelastic domain walls.

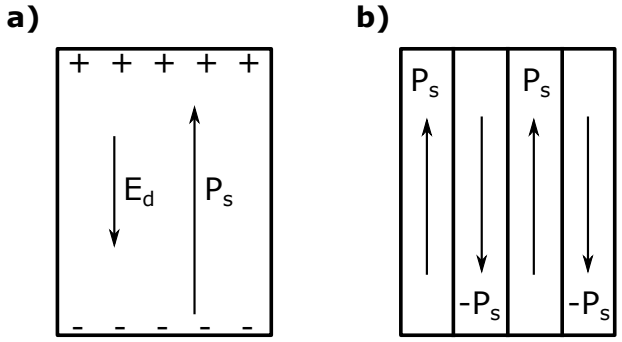

Figure 1.5: a) A ferroelectric material with uniformly aligned polarization P_s presents surface charge, which gives rise to a depolarization field E_d; b) a more favourable, lower energy configuration with ferroelectric domains of opposite P_s, which ideally enables the cancellation of E_d.

It should be noted here that insurgence of depolarization field is an unavoidable consequence of polarization if there is insufficient screening and charges are not compensated: inside the material, displaced charges always create a field opposite to the polarization direction, and this leads to an increase of the Gibbs energy. The sources of such compensation can be external or internal: at the outer surface, compensation charges can be electrons coming from a conductive electrode or ionic species from air (external),

whereas at domain walls as well as at the outer surface, charged species can come from within the material (internal) [21].

However, given that domain walls are interfaces and appear as defects of the crystal structure, it follows that also splitting into domains has an energy cost. Domains formation upon phase transition is then the result of a complex energy minimization process which takes into account the surface energy, that of domain walls, and that associated to electric and elastic fields [2, 14, 19]. Ideally, the fully poled state of a ferroelectric corresponds to all domains in the material aligned with the polarization direction. In a single crystal such monodomain configuration can occur, whereas in polycrystalline materials many domains can still be observed, oriented along the polarization direction or as close as possible to it. In addition, some domains can exist which are still aligned in the opposite direction (their local E_c or E_{bias} are such that they have not switched yet). The real picture thus often includes the presence of multiple domains with different alignment even in a poled state.

Now that the concept of ferroelectric domains has been introduced, what is left to discuss is what happens to them during polarization reversal. In the ideal case, according to the phenomenological theory presented earlier, the applied field increases to a point where it causes an instability in the crystal, which suddenly switches to the opposite stable state: this is defined as intrinsic or thermodynamic switching. In reality, the polarization reversal is gradual and domains of opposite direction start to form at the interfaces already at lower fields; this switching is called extrinsic. The mechanism involves two parts: domain nucleation and growth. However, it was very soon found by Landauer that nucleation of new domains from a perfect interface require still prohibitively high E_c, whereas polarization switching was experimentally measured at lower fields: this contradiction is therefore usually termed Landauer paradox [22, 23]. A solution is found by considering the presence of defects which locally stabilize domain nuclei, that do not have to be newly created at every switching event but now only need to grow.

The most widely accepted description of polarization switching in bulk, single crystal materials is the Kolmogorov-Avrami-Ishibashi (KAI) model [24–26], which describes the switching kinetics in terms of volume fraction change. According to the KAI model, nuclei of opposite polarization initially germinate, but at high surface energy cost; if the nuclei can reach a certain critical size, their growth becomes favorable and newly formed domains keep increasing in size. This germination happens simultaneously in multiple random places in the material and therefore at a given moment the growing domains will start to touch one another and their growth rate will slow down again. Assuming the nucleation of opposite phase domains to be uniformly diffused in the material, this model suggests that the limiting factor for polarization switching is the growth rate that is determined by domain walls motion. The plot of fraction of switched polarization $\Delta P(t)/2P_s$ versus time t will therefore be a sigmoid, with a steep slope at the center (high switching rate) and a smaller slope at the beginning and at the end of the process (low switching rate). This behavior is analytically described by Eq. 1.22, where τ is a decreasing function of E which includes the velocity of domain walls motion and the number of nuclei per volume, whereas m is a purely geometrical constant that depends

on the shape of growing domains (being higher for higher dimensionality):

$$\frac{\Delta P(t)}{2P_s} = 1 - e^{-(t/\tau)^m}. \tag{1.22}$$

This model works well in a continuous crystal in which domain walls can move with very little energy, and randomly nucleated domains just grow until they touch one another [27]. On the other hand, it fails to describe the switching behavior of polycrystalline thin films: here, polarization reversal is no more a widespread phenomenon that involves the whole crystal homogeneously, but rather a region-by-region process. The domain nucleation rate within such independent regions becomes the limiting factor of switching, that is to say that the domain wall motion takes a negligible time compared to that required for a nucleation event. Therefore, polarization switching in polycrystalline thin films can be better described by a nucleation limited switching (NLS) model [27] via the formula

$$\frac{\Delta P(t)}{2P_s} = \int_{-\infty}^{\ln t} g(z)dz, \tag{1.23}$$

where *g(z)* is the statistical distribution of nucleation times, that is a logarithmic function with exponentially wide range. The nature of these regions is such that each of them can switch independently and they do not influence one another. If a region is large enough to contain a high number of nucleation sites (a single crystal being the limiting case), it can in principle switch following the KAI model. For smaller regions, however, the statistical distribution of nucleation rates gives a more appropriate description of polarization reversal. One way to experimentally discriminate between the two mechanisms is to apply increasingly higher field and see the changes in switched polarization versus time. In KAI model, higher field leaves the shape of switching curve unaltered but shifts it to shorter times. On the contrary, in NLS scenario higher field increases the slope of switching curve [28]. More discussion on switching scenarios will be done in this work when results are presented, since this is a current research topic in ferroelectric HfO_2 and many factors are found to play a role in it, such as interfaces and thickness of the film.

In this section the main domain formation mechanism was described and it was introduced how different polarization switching processes take place when the material is in the bulk state or a polycrystalline thin film. This was the first time that a deviation from the ideal case was introduced, but real materials always differ from a perfect crystal to some extent. In many cases materials are even engineered to differ from a perfect crystal in order to enhance ferroelectric properties. Hence, an explanation of ferroelectricity would be incomplete without a look at the role of inclusions, charged species, interfaces and all other kinds of defects that are normally found in a material. The next subsection will therefore present the impact of defects on ferroelectric properties of materials.

1.2.4 Structural defects and their impact on ferroelectric properties

This subsection goes further away from the ideal case and shows that defects are always found in ferroelectric materials and have a decisive role in defining their properties. The phenomenological theory presented before explains the double-well potential of Fig. 1.2c in qualitative terms but without giving any insight into the energies involved in the process. The contradiction of an observed coercive field that is considerably lower than theoretical expectations was discussed earlier and termed Landauer paradox; alternative mechanisms to explain the nucleation and growth of domains were proposed, namely KAI and NLS. Despite their differences, they both rely on the assumption that nucleation of opposite polarization domains is initiated in some preferential locations in the material. This is due to the presence of structural defects, alterations of the crystalline lattice which act as preferential nucleation centers by locally lowering the energy barrier for switching.

Defects can be of multiple kinds. Impurities like atoms of foreign elements are an example of point defects: they can be charged or neutral with respect to the element that they substitute in the crystal lattice, and that will have an impact on the material when exposed to electric field. They also are larger or smaller in diameter, and this will locally influence the strain of crystal lattice. As mentioned previously, this phenomenon is greatly used as a way to engineer ferroelectric materials and is called doping. Another example of point defect, among the most studied in ferroelectric oxides, are oxygen vacancies: they are mainly formed in the material fabrication process in order to compensate dopant charge but can change their amount and distribution for instance by phase transition and electrical cycling [29].

Increasing the dimensionality, dislocations represent a line defect: they occur when there is an error in the stacking of atoms in the lattice and cause a sudden modification from one atomic layer to the next. The local stress is increased and the ability of the material to deform is higher in correspondence of a dislocation. Grain boundaries are instead an example of surface defects: all crystalline materials that are not single crystals present grain boundaries. Their amount intuitively depends on the grain size (smaller grains give more grain boundaries and vice versa) that is in turn related to the film thickness, which then becomes an important parameter to control in order to modify ferroelectric properties [30–32]. Interfaces with other materials, normally top and bottom electrodes, are another example of critical surface defect, one that is receiving a lot of attention by researchers due to its impact on both stress and electric fields inside the ferroelectric [2, 33].

Finally, a volume defect that is found especially in HfO_2-based thin films is the presence of second-phase regions that did not stabilize in the desired ferroelectric phase [2]. As expected, given how many types of defects always coexist in a material, their influence is paramount when one aims to enhance ferroelectric properties. However, defects are also related to detrimental phenomena, and these will now be discussed.

A problem that hinders the technological development of ferroelectric devices is imprint, that is the shift of coercive voltages to higher or lower values. When looking at

P-E plots of imprinted ferroelectrics, a shift of the loop in horizontal direction is observed as depicted in Fig. 1.6b. This indicates that one of the two polarization directions is harder to switch (higher field is required): as a result, the material will preferably polarize in the other direction [2, 34]. This is a typically unwanted phenomenon in memory applications because it means that more voltage has to be applied overall in order to have a functional device. Another consequence of imprint that hampers device functionality is that the material might switch back to its preferential polarization direction even when no voltage is applied. On the other hand, imprint can be exploited in Negative Capacitance (NC) devices as will be explained later [35]. Imprint is mostly originated by interface defects and trapped charges that pin domains in their current state. When a field of opposite direction is applied, these domains cannot freely switch but instead require more activation energy. A way to see that in terms of energy potential is to imagine that one of the two wells sits at a lower value and thus its potential barrier is larger, as depicted in Fig. 1.6a. Imprint might occur upon phase transition from the parent non-polar phase if certain constraints are present (such as particular stress and electric field conditions) [29]. Another possible mechanism that originates imprint is the incomplete screening of charges at one of the two interfaces, which induces a built-in field inside the material: this is particularly evident when the two electrode materials are different. However, it is often possible to greatly reduce imprint in ferroelectric capacitors by electrical cycling: the continuous alternation of positive and negative fields has the outcome to redistribute defects more homogeneously within the material [29, 36].

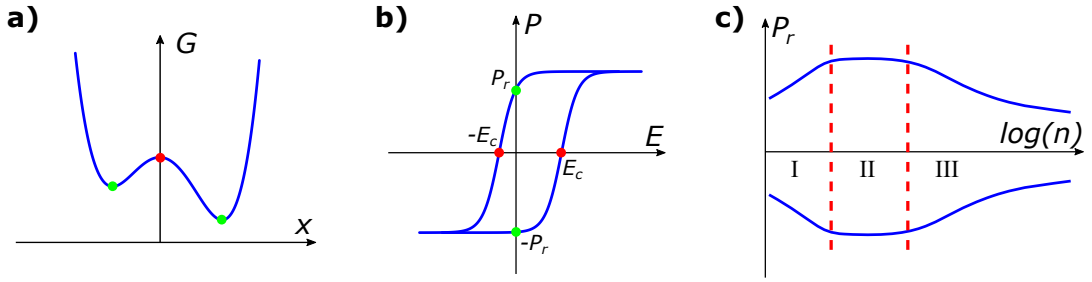

Figure 1.6: a) Asymmetric double-well potential resulting in imprint; b) a *P-E* loop of an imprinted ferroelectric: notice the difference between positive and negative E_c; c) a typical endurance diagram plotting P_r versus number of electric cycles n. During cycling, three regions can be distinguished: wake-up (I), stable state (II) and fatigue (III).

The role of cycling is not limited to removing imprint: even in materials that do not show any initial bias field, cycling can play a vital role in enhancing the ferroelectric properties at first (wake-up) and in degrading them afterwards (fatigue). A typical plot that is often shown in literature is the endurance plot, which shows the remanent polarization in both directions (or the sum of their absolute values, $2P_r$) as a function of number of cycles, the latter normally plotted in logarithmic scale. Understandably, this is critical for most applications where switching reliability has to be guaranteed over long time. A sketch of such plot is given in Fig. 1.6c, where the regions of wake-up (I) and fatigue (III) are highlighted. Notice that, despite very commonly observed, a material does not necessarily have to show both (or any) of these features: from a

technological perspective that would actually be the ideal case. Wake-up can occur if the formation of ferroelectric phase did not lead to a uniform distribution of defects, which might be preferentially located at the interfacial regions. Upon cycling, much like it was explained before for imprint, the most mobile defects are displaced from interfaces to bulk and distribute more evenly inside the material. This allows a homogeneous field distribution across the ferroelectric and enables the switching of a higher portion of material: as a result, net increase of P_r is observed [2, 4, 29].

Further cycling, though, implies repeated domain reversal and continuous migration of charged defects: this means a lot of domain walls movement through a crystal structure that is becoming denser of high-energy regions. With a high concentration of defects in the material, domain walls might not have enough energy to move and thus remain pinned. In addition, defects at the interfaces can inhibit domain nucleation and growth, further reducing the switching area of the material and decreasing the measured P_r. These two phenomena are at the basis of fatigue in ferroelectric materials [2, 4, 37].

Now that the basics of ferroelectricity have been presented, it is time to look more in detail to the class of ferroelectric materials that will be the subject of this work: HfO_2-based thin films. The next section will show the state of the art in the research field. Despite the novelty, with first paper appearing in 2011, much progress has been done already; parallels will be naturally drawn to PZT and other perovskites since they are the closest ferroelectrics and are extremely well characterized since longer time.

1.3 State of the art of HfO_2-based ferroelectrics

HfO_2 is a ceramic oxide with $\approx$ 5.5 eV bandgap and fluorite crystal structure, where the Hf^{4+} cations are located at the corners and faces of a parallelepiped whereas the O^{2-} anions occupy the tetrahedral interstitial sites. At room temperature the crystal structure of bulk material is monoclinic, while a temperature increase induces a phase transformation first into tetragonal (>1700 °C) and then into cubic phase (>2600 °C) [38]. If high enough pressure is applied, there can be the development of an orthorhombic (o-) phase between monoclinic (m-) and tetragonal (t-). Furthermore, it was shown that doping can lead to stabilization of cubic and tetragonal phases to lower temperatures [2].

Since neither of these phases is noncentrosymmetric, ferroelectricity was not immediately discovered despite HfO_2 was already commonly used as high-κ dielectric layer in electronics [6, 7]. In the first report of ferroelectric Si:HfO_2 thin film the authors claimed stabilization of a previously unnoticed noncentrosymmetric $Pbc2_1$ orthorhombic phase, developed in place of (or rather together with) the well-known and usually reported tetragonal and monoclinic phases [1, 39]. In their investigation, they ascribed this fact to capping of Si:HfO_2 with a TiN top electrode before the annealing step, that is when the material is still amorphous. Annealing only after top electrode deposition and Si doping were suggested to build an in-plane strain in the thin film that stabilizes the otherwise unstable orthorhombic phase, see Fig. 1.7 [1].

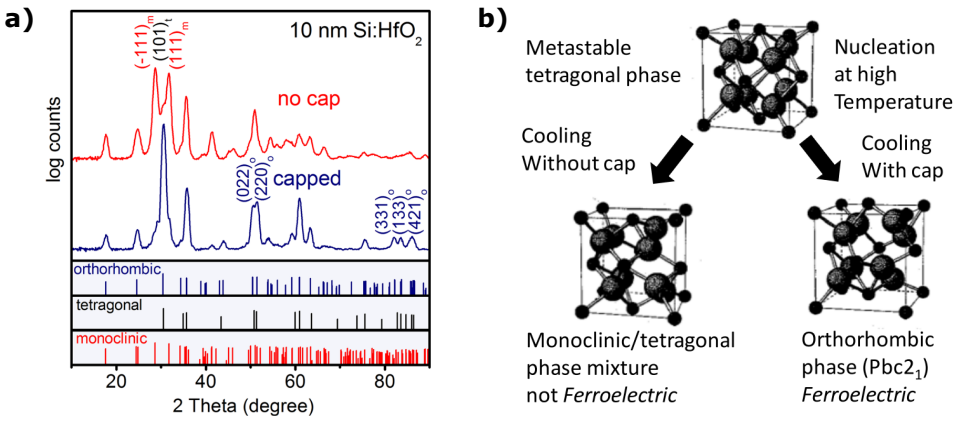

Figure 1.7: a) An XRD micrograph showing two thin Si:HfO_2 films annealed with and without top electrode (reproduced from [1]); b) the proposed phase transition that leads to o-phase formation (reproduced from [39]).

This was a rather unexpected finding since ferroelectric ceramics such as PZT or BTO usually have perovskite structure, where the polarity is determined by displacement of the central Zr^{4+} or Ti^{4+} cation in the octahedral interstitial site of the unit cell. HfO_2-based materials are the first example of fluorite structure ceramics showing ferroelectricity: the mechanism involves a movement of O^{2-} anions inside the tetrahedral interstitial sites of the orthorhombic unit cell. Both fluorite HfO_2 and perovskite PZT unit cells are depicted in Fig. 1.8, where the polarization direction can be understood looking at the position of O^{2-} and Zr/Ti^{4+}, respectively.

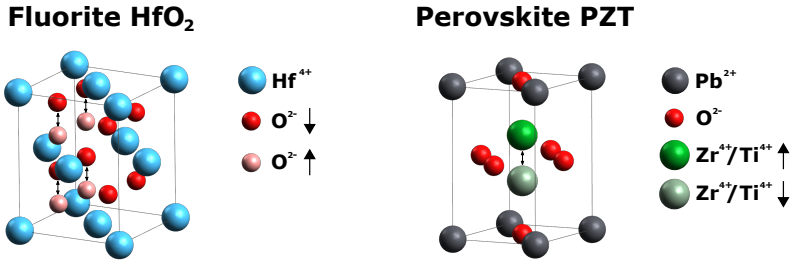

Figure 1.8: Simplified sketch of fluorite HfO_2 and perovskite PZT unit cells showing the elements position and corresponding polarization direction. The structures were created with Avogadro v1.2.0 [40].

The discovery reignited interest in ceramic ferroelectrics for nonvolatile memory and FeFET applications: technologies based on PZT scaled down to 130 nm node already in 2007 but could not go any further due to instability of the material at smaller thickness [4, 41, 42]. On the contrary, first report of ferroelectricity in Si:HfO_2 was for a film thickness of 10 nm only. As many researchers started to investigate this material, it was soon discovered that chemical composition and top electrode capping are far from being the only factors impacting the microstructural properties (and thus the ferroelectric response) of HfO_2-based thin films: influences of film thickness, oxygen vacancies,

annealing conditions and top electrode material have been observed and investigated.

After Si, the effect of different dopants such as Al [43], Gd [44], La [45], Sr [46] and Y [47] was among the first topics to be investigated. The reason is that dopants distort the lattice structure of the material and this, if appropriately engineered, could lead to the stabilization of the orthorhombic phase observed in Si:HfO_2, thus enabling ferroelectricity. Such lattice distortion is mainly caused by the larger or smaller atomic radius and valence of the doping element, but no univocal trend was found and the precise mechanism is not completely understood yet [2, 48, 49].

In addition, for each dopant there seems to be an optimal concentration window that stabilizes o-phase: while this is relatively wide for La, it is usually quite small for other elements as it can be seen in Fig. 1.9, where polarization response is plotted for many dopant concentrations of different elements [2]. One HfO_2-based chemical compound that is intensely studied and deserves a special mention is $Hf_xZr_{1-x}O_2$, normally referred as HZO when x=0.5. The peculiarities of this material, with respect to slightly doped HfO_2-based thin films, are its higher tolerance to concentration variations, high P_r and endurance, and low thermal budget required for fabrication. All these properties are very promising for applications and make it probably the most studied among all the HfO_2-based ferroelectrics [2, 50–53].

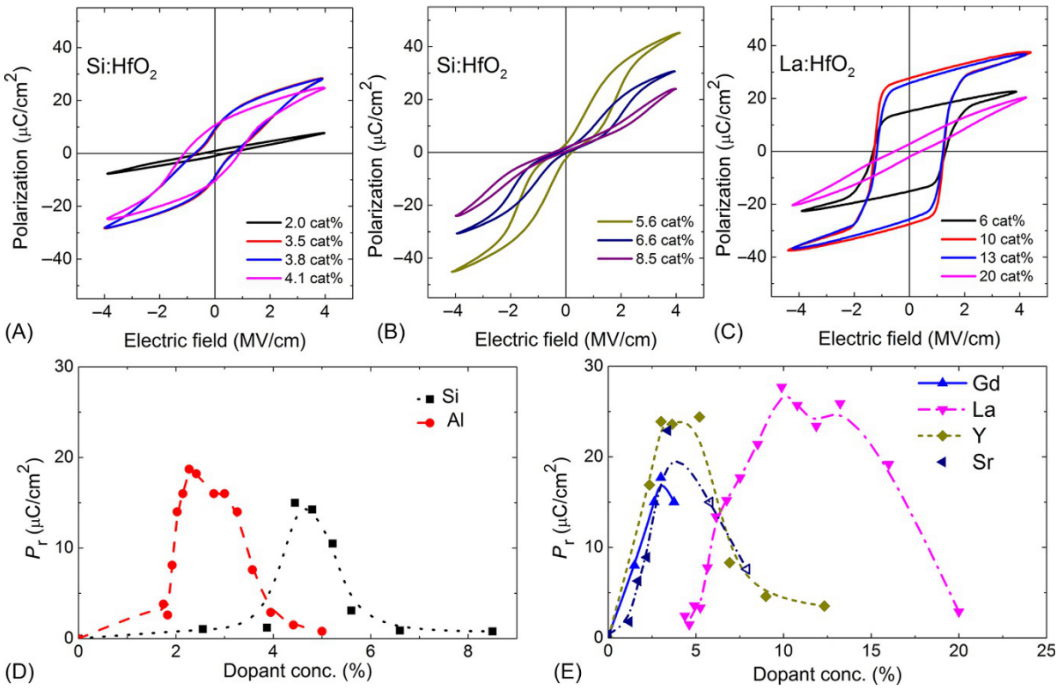

Figure 1.9: Polarization loops of HfO_2 thin films with different doping concentrations of Si (A,B) and La (C). Remanent polarization versus doping concentration for elements smaller (D) and larger (E) than Hf (reproduced from [2]).

Another important feature experimentally observed in HfO_2-based thin films is a trend showing lower amount of o-phase (and thus P_r) with increasing film thickness [2, 54–56].

This was later investigated also theoretically, and it was found that in order to determine the most favorable phase in a thin film, many parameters have to be taken into account, including notably the grain free energy [51, 57]. This is given by an interplay of bulk and interface energies that depend on the grain size, in turn limited by the film thickness. Since the interface energy of the o-phase is lower than that of m-phase, the former is more favorable when the grains are small, as it is the case for thinner films, as shown in Fig. 1.10a and b [51, 56]. Here, the authors reported that the incorporation of an Al_2O_3 1 nm layer in the middle of an HZO film further stabilizes the o-phase by effectively creating two films with half thickness each (and therefore smaller grain size) [56]. It is worth mentioning that there are notable and not yet understood exceptions to this trend, namely Gd- and La-doped films [31, 58, 59].

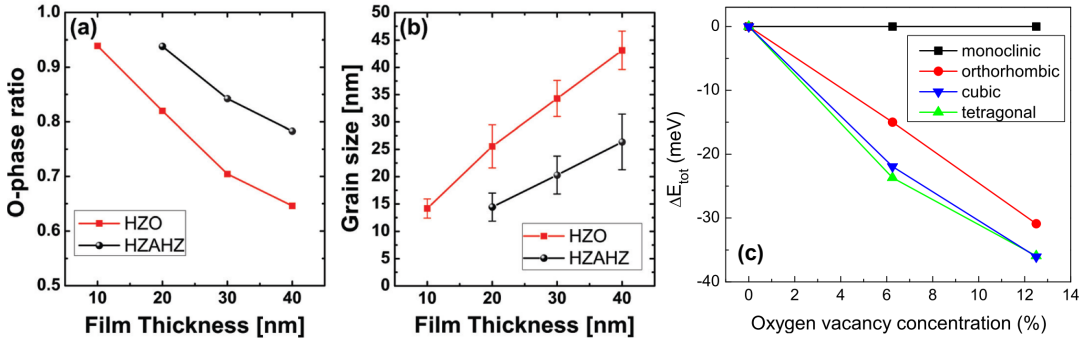

Figure 1.10: (a) Ratio of o-phase/(o-phase + m-phase) versus film thickness dependency for HZO and HZAHZ (identical structure but with Al_2O_3 1 nm layer deposited at exactly half thickness of the HZO film); (b) grain size versus film thickness dependency for the same two structures (both reproduced and adapted from [56]); (c) formation energy of crystalline phases of Gd:HfO_2 with respect to O vacancy concentration (reproduced from [31]).

Similarly to what was done in PZT, which is very often taken as a model to benchmark and define research directions in HfO_2-based ferroelectrics, the effect of O vacancies is investigated and reported to play a major role. A large amount introduces a lattice distortion that makes the m-phase less prone to crystallize, but too many O vacancies ultimately favor the development of t-phase, as shown in Fig. 1.10c [31]. It is evident that only a delicate equilibrium of many factors can correctly stabilize the ferroelectric phase. Oxygen vacancies have been studied in perovskite ferroelectrics already and are known to form preferentially at the electrode interfaces and migrate to grain and domain boundaries, causing degradation of ferroelectric properties [32, 60–62].

The amount and distribution of oxygen vacancies in HfO_2-based thin films are especially dependent on the electrodes due to the critical annealing step that is required to obtain ferroelectricity. The most widely reported electrode in literature is TiN, which is considered very suitable to CMOS processing due to its chemical and thermal stability and good electrical and mechanical properties [7]. The main drawback of TiN however is that it easily binds with O to form TiO_xN_y or rutile TiO_2 [63]. Since the TiN is in direct contact with the HfO_2, it can efficiently scavenge O from it during the annealing process,

effectively creating an interfacial dead layer which will be rich in oxygen vacancies and thus predominantly in the t-phase [2, 29, 64, 65]. Clearly all these effect are enhanced with a reduced film thickness, when the size of dead layer becomes comparable with that of the film. Negative effects caused by this dead layer include higher coercive voltage, presence of depolarization field, lower polarization and reduced endurance.

Given the importance of interfacial layers between ferroelectric and electrodes, it follows that also annealing conditions (thermal budget and atmosphere) greatly affect the ferroelectric response of thin films [66–69]. In particular, it was found that annealing in inert atmosphere (N_2) and at temperatures ranging between 450 and 800 °C gives the best results for most ALD HfO_2 films [69]. A summary of the complex phase formation trends with thermal budget during annealing, dopant content and film thickness is given in Fig. 1.11.

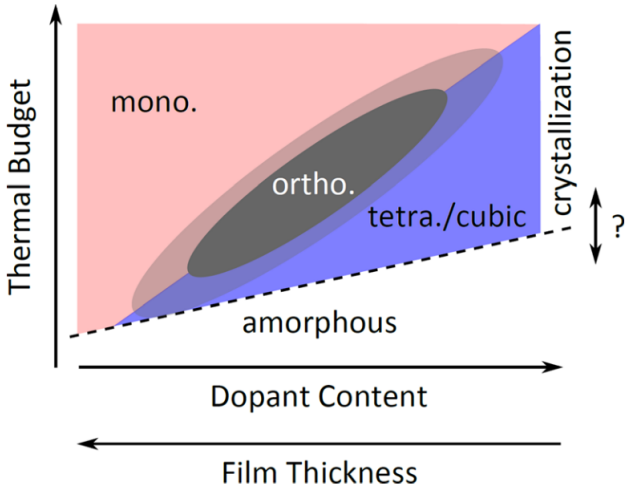

Figure 1.11: Qualitative summary of the phase formation trends of HfO_2-based thin films according to thermal budget, dopant content and film thickness (reproduced from [31]).

From what has been discussed so far it emerges that the importance of top electrode is twofold: on the one hand it contributes to the properties of interfacial layer and can act as a tool to control the amount of oxygen vacancies; on the other hand, it imposes the mechanical constraint that induces stress in the thin film during annealing. Similarly to PZT, it was shown that an oxide electrode such as RuO_2 reduces the scavenging of O at the interface with the ferroelectric and prevents the formation of an oxygen vacancy-rich dead layer in HZO [70]. Clearly top electrode materials also differ in their thermal expansion coefficients and thus can induce more or less stress in the thin film upon annealing. It is not surprising therefore that many materials were investigated such as TaN, Pt, Pd, Au, TiN, W, Al and Ta: the reported trend is that lowering the thermal expansion coefficient of the electrode increases tensile stress and P_r of the ferroelectric films [31, 71]. Even for the same electrode material a higher thickness can increase the stress and consequently the o-phase formation in the film [72]. The great importance of stress imposed by annealing after top electrode deposition can be better understood

considering that even undoped HfO_2 was shown to be ferroelectric, implying that this can be an intrinsic effect, not dependent on doping [73].

With such great importance relying on imposing the appropriate strain level to the film, it is not unexpected to think that also a rational choice of the bottom electrode on which the film will be deposited, which takes into account the lattice mismatch between the two materials, can be critical. This is especially true if epitaxial layers are to be obtained: several groups reported indeed the fabrication of ferroelectric thin films deposited by PLD at high temperature (usually > 700 °C) on appropriately engineered substrates that favour o-phase formation such as yttria-stabilized zirconia (YSZ) or $La_{0.67}Sr_{0.33}MnO_3$ (LSMO), [74–78]. It is interesting to remark that such films do not require neither top electrode deposition nor annealing to show ferroelectric behavior. Notably, high temperature PLD fabrication of epitaxial thin films also allowed to propose the existence of a ferroelectric rhombohedral phase in HZO for the first time [75].

As illustrated so far, the magnitude of P_r depends on the amount of o-phase in the film; in the previous section it was mentioned that this can transform with electrical cycling and thus P_r can change with the creation and distribution of defects in the film. It is extensively reported that ALD HfO_2-based ferroelectric thin films first present a wake-up phase before showing a stable P_r and then undergoing fatigue [29, 31, 34, 36, 79–82]. In contrast to that, epitaxial ferroelectric films deposited by PLD at high temperature and already in the ferroelectric phase do not need such wake-up procedure [74, 75, 78].

The *P-E* loop of a ferroelectric HfO_2-based thin film in the pristine state often shows a pinched hysteresis, with a double peak in the *I-E* characteristic. This is mainly due to the accumulation of charged defects, mostly O vacancies, at the interfaces between ferroelectric and electrodes, with the top electrode being the most critical one [2]. The O vacancies-rich interfaces are an unavoidable byproduct of the fabrication process, with ALD process temperature occurring in the range 250-300 °C and annealing reaching in some cases even 1000 °C. Due to the fabrication route of the capacitor stack, the oxidation of bottom and top electrode is also asymmetrical, leading to different defect concentrations in the material [2]. Interfaces with electrodes become responsible of local bias field in one direction and therefore enable parallel aligned domains to switch at lower field (whereas antiparallel ones switch at higher field), giving the peculiar shape of *I-E* and *P-E* plots observed for pristine samples. Both initial imprint in pristine films and t-phase relaxation into o-phase upon cycling are related to the initial charge accumulation at the iterface [29, 83]. The possibility to reduce imprint by having a higher thermal budget during the fabrication process was reported, but the downside is a higher leakage current and an earlier breakdown [55]. Electrical cycling, however, can reduce imprint and this is thanks to a redistribution of defects across the film, preferentially in higher energy regions such as grain boundaries [29]. It was shown that the size of interface dead layer is reduced during cycling, with t-phase transforming in o-phase, due to the migration of O vacancies away from it [29, 84]. The macroscopic effect that is observed is an increase in P_r and a merging of the two peaks in the *I-E* plot, as shown in Fig. 1.12a and b, respectively.

While electrical cycling and defect redistribution is at first beneficial, giving a re-

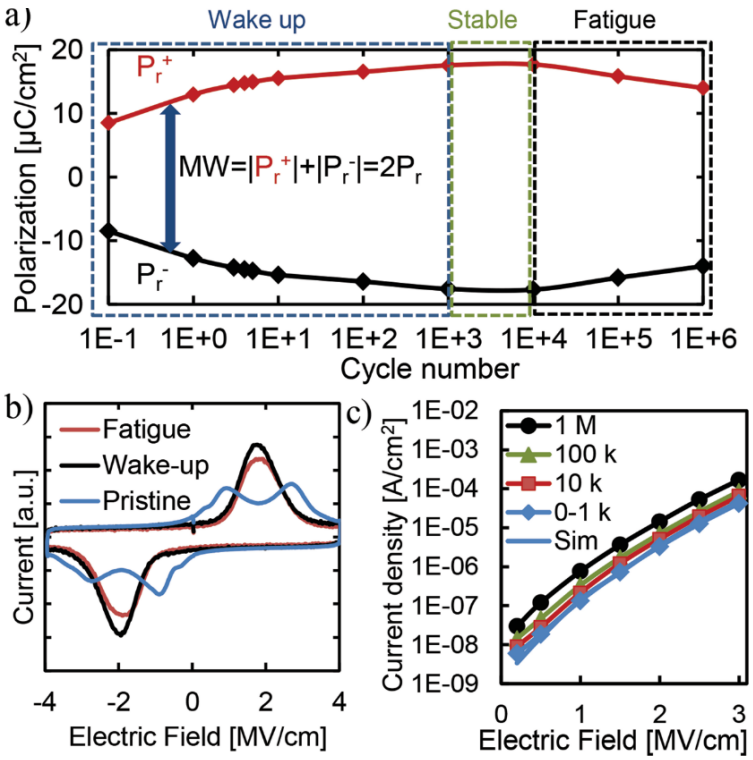

Figure 1.12: Electrical cycling behavior of a Sr:HfO_2 ferroelectric. Wake-up, stable and fatigue regions can be identified by the value of P_r versus the number of cycles in a) and by I-E plots in b); c) leakage current measurements with increasing field at different cycles (reproduced from [29]).

duction of imprint and an increase of P_r, it becomes detrimental when the continuous polarization switching starts to induce the generation of too many defects in the crystal structure. P_r decreases, leakage current increases, and the material eventually shows hard breakdown, see Fig. 1.12. The fatigue process leads to a permanent degradation of the film that can only be partially recovered by exposing the film to high temperature [85]. Leakage current measurements allowed to infer that, oppositely to what happens in the wake-up process where defects are mainly redistributed across the material, in the fatigue process there is also a creation of new defects [29]. The high amount of O vacancies and other charged defects created during cycling preferentially accumulates along domain and grain boundaries, requiring a higher energy cost for domain walls to move [29, 37]. This also suggest that control of domain size can influence leakage in thin films [4]. When an increasing portion of the material does not switch due to domain pinning the P_r will reduce, as it is observed in fatigue. At the same time, the accumulation of defects along domain and grain boundaries creates preferential conduction paths which are responsible for the film breakdown [29, 37]. A further challenge in HfO_2 ferroelectrics is that sudden breakdown is particularly difficult to avoid, because the ratio between coercive field E_c and breakdown field E_{bd} is relatively high, around one order of magnitude higher than the one of perovskite ferroelectrics [2, 52].

One of the unclear aspects of ferroelectricity in HfO_2-based thin films is the polarization reversal mechanism. Among the many techniques that were employed to unveil the switching dynamics, a very powerful one is Piezoresponse Force Microscopy (PFM), which enables to detect the local electrochemical response of the ferroelectric thin film. Here, with a dc + ac voltage applied to the probing tip in contact with the film, it is possible to image the domain structure and measure the switching of a very localized region under the tip, typically in the order of few tens of nm. More details on this will be offered in chapter 2 as this characterization technique constitutes a large part of this work. An example of the application of PFM to the understanding of switching properties of HfO_2-based ferroelectrics is the analysis of films in the pristine state and then after wake-up [86]. PFM has been particularly useful to correlate the incomplete domain switching in pristine films with their low P_r and pinched polarization loop detected by microscopic P-E measurements. When those films were trained and showed a higher P_r, also the PFM images showed a more complete polarization across the film, as seen in Fig. 1.13 [2].

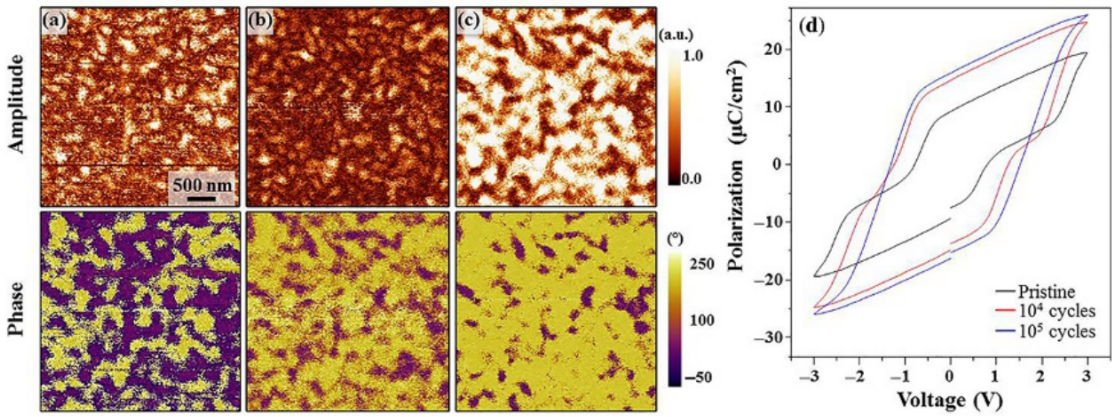

Figure 1.13: (a-c) Amplitude and phase PFM images of a La:HfO_2 capacitor positively poled at 4 V in (a) pristine state, (b) after 10^4 and (c) 10^5 electrical cycles; (d) the macroscopic P-V loops measured at the corresponding training conditions (reproduced and adapted from [2]).

The polarization switching mechanism in HfO_2-based thin films is not yet univocally determined, even though more and more studies are indicating a NLS scenario greatly affected by interface effects [2, 86–88]. This finding is in agreement with the expected behavior of polycrystalline thin films as explained in the previous section. However, late results coming from the investigation of Negative Capacitance (NC) heterostructures are casting doubts concerning the switching mechanism and suggesting that in particular conditions a different scenario can be at play [35, 89].

The concept of negative capacitance was first theorized by Landauer already in 1976 by looking at the shape of the double-well potential, where a region of negative curvature can be seen between the two stable polarization states [90]. This region of the curve is however unstable and therefore very elusive, and corresponds to a polarization switching that follows the S-shaped profile depicted in Fig. 1.14. This is however not accessible

in classic experiments where the electric field E is imposed to the structure in order to measure the polarization P. What is commonly observed instead is the switching from one polarization state to the other that was widely described so far.

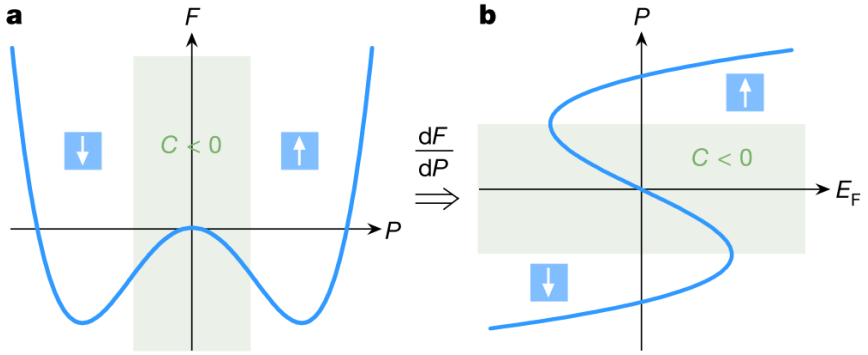

Figure 1.14: a) The free energy (F) double-well landscape of a ferroelectric material; b) the S-shaped profile of polarization P versus field E_F is obtained by deriving the energy. Green shaded regions are where the capacitance is negative (reproduced and adapted from [35]).

The conceptualization of a working NC device came from Salahuddin in 2008, where it was suggested that a way to obtain the desired effect was to place a dielectric and a ferroelectric in series inside a capacitor [91]. The direct observation of the S-shaped curve was achieved only very recently by sandwiching ferroelectric HZO and dielectric Ta_2O_5 between two TiN electrodes: the experimental technique consisted in applying nanosecond pulses which did not allow for charge compensation and domain stabilization at the ferroelectric/dielectric interface [35]. More details on this can be found in chapter 6 where NC and related switching mechanisms are discussed.

What is important to remark however is that the whole theory behind NC is grounded on a fundamental hypothesis, namely the intrinsic switching of the ferroelectric, which excludes the possibility of domain formation. As explained so far, this is in open disagreement with extrinsic switching of ferroelectric thin films theorized by NLS scenario. These conflicting results are opening questions on whether intrinsic switching can occur in HfO_2-based thin films or rather NC can be achieved even with domain formation as proposed by some authors [92, 93].

The recent demonstration of NC devices using HZO thin films embodies the fact that HfO_2-based materials are at the forefront of ferroelectric technology. These materials already enabled to reach impressive results in a relatively short amount of time, though it is clear that more fundamental research is necessary in order to clarify the deepest aspects of ferroelectric nature in these films. This thesis aims to expand the understanding of switching behavior in HfO_2-based ferroelectrics by evaluating the impact of thickness in thin to ultrathin films and the role of interfaces in NC heterostructures.

1.4 Thesis outline

Chapter 2 presents the fabrication and characterization techniques employed in this work. The first section explains how thin films were deposited and capacitor structures were created for functional characterization. The appendix provides more detailed information regarding this section, detailing the samples that were received after the deposition and annealing steps from the ones that were entirely fabricated as part of this work. The second section shows the characterization methods that were used in analyzing the samples with a detailed explanation of the off-resonance PFM technique, which constitutes the most consistent part of this work.

Chapter 3 discusses the development of a CMOS-compatible fabrication route which enables to deposit ferroelectric Gd:HfO_2 by PLD. The first section details the influence of different parameters in the fabrication process, while the following two sections present the results of microstructural and functional characterizations, effectively proving the ferroelectric nature of the deposited film.

Chapter 4 showcases the effectiveness of off-resonance PFM in assessing genuine ferroelectricity in thin films with low piezoresponse. Detection of subtle features in amplitude and phase loops is brought as proof of the true nature of ferroelectricity and demonstrates the capabilities of this technique, that is extensively used throughout this work to investigate HfO_2-based ferroelectrics. The second section presents PFM results on the cycling behavior of undoped HfO_2, with quantitative estimation of tiny variations in effective d_{33} caused by voltage cycling.

Chapter 5 analyzes in details the effects of scaling on the switching behavior of thin to ultrathin HZO films. Remarkably, the observation of millivolt-range complete polarization switching in 7 nm films is considered a promising achievement for the realization of low-power ferroelectric devices. This result is reported together with an unexpected coercive field trend observed for film thickness lower than 10 nm, which leads to the proposition of a different switching mechanism for ultrathin films.

Chapter 6 presents the analysis of NC heterostructures where ferroelectric layer is in contact with a dielectric. The impact of interfaces is discussed and PFM findings are related to previous literature work on same NC structures by other techniques. The last section is taking these results as starting point to discuss the different polarization switching mechanisms encountered in ferroelectric HfO_2-based thin films.

Chapter 7 summarizes the contributions of this dissertation to the field and discusses the research paths that are left open by this work and in the wider context of HfO_2-based ferroelectric thin films.

2 | Methods: fabrication and characterization techniques

This chapter is divided in two sections: the first one will describe the fabrication route used to create the devices that are investigated in this work. In particular, it will introduce the main thin film deposition techniques and highlight the differences between them. After that, the conventional photolithography and etching steps to obtain capacitor structures are explained. The second section of the chapter will describe the microstructural, electrical and electromechanical characterization techniques that were used to analyze the ferroelectric properties of HfO_2-based thin films, with a special focus on Piezoresponse Force Microscopy (PFM).

2.1 Fabrication techniques

The analysis of ferroelectric HfO_2-based thin films requires the fabrication of micrometer-size devices that are suitable for structural and functional characterization. The structure that is used throughout this work to investigate ferroelectricity is the application-relevant capacitor structure, consisting in sandwiching the ferroelectric layer between two electrodes made of conducting materials. Other heterostructures including an insulating layer are also employed in order to examine Negative Capacitance (NC) in HZO and Si:HfO_2. The fabrication of capacitors and other heterostructures takes place in cleanroom environment, and the process starts from a Si wafer on top of which the appropriate material layers are deposited. Then the patterning of such materials stack is executed by means of photolithography and etching, and the desired structure is created. In addition, for the particular kind of ferroelectrics studied in this work, an optimized annealing step is required after the fabrication of the stack and before the patterning. Here the process flow will be qualitatively presented, paying special attention to the deposition techniques which play a major role in obtaining the correct ferroelectric properties. For all the quantitative information regarding deposition, annealing, photolithography and etching recipes, the reader is referred to the appendix.

2.1.1 Deposition of ferroelectric thin films and annealing

The deposition of HfO_2-based ferroelectric thin films is currently achieved by three main techniques:

- Chemical Vapor Deposition (CVD), normally Atomic Layer Deposition (ALD);
- Physical Vapor Deposition (PVD), usually sputtering or Pulsed Laser Deposition (PLD);
- Chemical Solution Deposition (CSD).

This work made use of thin films fabricated exclusively through the first two techniques, therefore CSD will not be presented here (further information on that is available in literature [2]). The first reports about ferroelectricity in Si:HfO_2 employed ALD as deposition method [1, 39]; this fact should not surprise since ALD is a mature technique which was already routinely used to deposit HfO_2 in the microelectronics industry. This is due to advantages such as the great control over thickness and properties of the deposited film, relatively low process temperature compared to other CVD techniques, high conformality and strong chemical selectivity, together with the possibility to be scaled industrially [94, 95]. ALD consists in growing thin films by means of controlled chemical reactions on the substrate. This is achieved thanks to the use of reactants, also called precursors, that are injected into the chamber and chemically react with the substrate. The two precursors are never injected simultaneously inside the chamber, and a purging step takes place between the two to ensure that they are never in contact. This effectively creates a self-limiting mechanism in which every cycle of reactant can only grow a limited amount of film (a few Å normally) and prepares the surface of the substrate to react with the other precursor. An ALD process thus typically requires a certain number of reactive and purging cycles in which the film is deposited layer by layer until the desired thickness is reached and the process is stopped. The control of dopant concentration in ALD is obtained by selecting the appropriate ratio of dopant/Hf precursor cycles, which could introduce concentration gradients and potentially pose a limit to fabrication of ultrathin films with very small dopant concentration.

The main drawbacks of ALD are the low growth rate of about 0.1 nm/cycle, the formation of potentially toxic byproducts (especially if Cl-based precursors are used) and the film contamination (mainly by C, but also Cl if present in the reactant) [2, 96]. In addition, since the growth mechanism is governed by chemical reactions of precursors with substrate, the chamber temperature has a strong impact on the deposition, usually narrowing the available range for HfO_2 based materials to the 200-300 °C window [2]. In general, there is no univocal temperature dependence of crystalline phase formation in ALD films, which strictly depends on the material [97]. As a result, HfO_2 based ALD films are usually amorphous after deposition and need a subsequent annealing step to crystallize the ferroelectric phase.

The ALD thin films used in this work, neither of them fabricated as part of this work, are $Hf_{0.5}Zr_{0.5}O_2$ (HZO) and Si:HfO_2: the former was fabricated in Namlab, whereas the

latter in the CMi cleanroom facility in EPFL. More information on the ALD deposition procedure can be found in [35, 89, 98], while the detailed process flows and recipes are reported in appendix.

Soon after ferroelectricity was discovered in many HfO_2 systems deposited by ALD, it was reported also on a sputtered Y:HfO_2 [47]: this proved that ferroelectricity is not strictly related to process parameters specific to ALD, and opened to the possibility of using PVD fabrication routes too, such as indeed sputtering and, later, PLD. PVD techniques are different to ALD mainly in that film growth is not led by a chemical reaction occurring on the surface of the sample but rather by the kinetic energy of atomic species when they hit the surface. Here, the substrate and a target made of the desired material are placed facing one another into a chamber where high vacuum is created: the target is then bombarded with highly energetic particles that possess sufficient kinetic energy to eject atomic species from the target into a plasma plume, which will deposit on the substrate and grow the film. The irradiating particles are usually an ionized inert gas (Ar^+, Kr^+) in sputtering and coherent photons, that is a laser, in PLD. The advantages of PVD techniques are mainly given by the great control over processing parameters such as chamber pressure, temperature and atmosphere, kinetic energy of the incoming particles, and possibility to deposit virtually every element or inorganic compound, without having to rely on chemical reactions. Different materials can also be deposited in sequence without breaking the vacuum just by implementing a carousel system for carrying multiple targets. The deposition rates, in the order of 10 nm/min, are also way higher than in ALD and can be adjusted (and further increased). Finally, the contamination given by precursors in ALD (normally C) is absent here, and the only contaminants can come from dirt inside the chamber or the target, which has then to be of high quality and carefully controlled. A typical drawback of PVD techniques is the poor conformality of deposited thin films, meaning that features which are out of the line of sight of the target are not deposited. In addition, in order to ensure a long enough mean free path to the ablated particles, high vacuum is often required. Finally, targets are usually quite small and very wide areas cannot be deposited, especially with a good thickness control. However, industrially scalable tools are being developed that are able to overcome these issues.

The electrode films used in this work, made of TiN, and the contact materials such as Pt and W, as well as the dielectric Ta_2O_5 and the undoped HfO_2 analyzed in chapter 4, are all deposited by sputtering, either internally in CMi or at Namlab [35, 99]. Detailed process flows and recipes are provided in appendix.

Looking at PLD more in detail, since the Gd:HfO_2 samples discussed in the next chapter were fabricated as relevant part of this work, a few more things can be added. Most importantly, in PLD the target stoichiometry is normally well maintained in the sample because the laser is applied in pulses and ablates the material, bringing it locally to such high temperature that the different elements composing it reach their vapor point regardless of their nature. In general, this very strong and localized heating of the target enables the whole process to take place at overall lower temperature, eventually even at room T [100]. Another important aspect is that a generous O_2 flow has to be normally provided in PLD because the plasma plume and the eventual contaminants in

the chamber are usually creating a reduced atmosphere [101]. A problem often found in PLD is that chunks of ablated material are ejected from the target and deposit on the substrate and contaminate it, unless some mechanisms such as a droplet trap are put in place.

The PLD setup used in this work is a custom version of SP800 by Solmates. This system uses a KrF laser (λ = 248 nm) which, through a series of mirrors and lenses, is focused on the circular target surface with an incident section of 2x2 mm^2. The converging lens is mounted on a motorized stage which allows to swipe the incident point of the laser along the radius of the target surface, which is rotating in the meantime. This configuration enables the material deposition on a larger substrate surface while guaranteeing a uniform wear of the target at the same time. A rotating droplet trap, whose speed is synchronized with the laser pulses, is placed between the target and the substrate (100 mm wafer) and allows only the generated plasma plume to hit the substrate, preventing the incorporation of inclusions in it. A set of Hg lamps heat up the wafer from the back side and a pyrometer installed inside the heating chamber is touching the back of the wafer holder and ensures a live temperature reading during deposition.

Figure 2.1: PLD setup used in this work. The laser module (A), deposition chamber (B) and pyrometer (C) can be seen from this angle.

In all fabrication procedures mentioned before, either depositing the films by ALD or by sputtering/PLD, an annealing step is necessary in order to crystallize the material in orthorhombic phase and induce ferroelectricity. Since this is a crucial step, different optimal conditions exist for every material analyzed in this work (HZO, Si:HfO_2, Gd:HfO_2 and undoped HfO_2). In the case of externally produced HZO and undoped HfO_2 the films were received already annealed and more information can be found in [99, 102]. However, and for the sake of clarity, all annealing details are explained in the process flows shown in appendix and will be reminded in the main text when results on those

films will be presented.

The last step before patterning the desired structures is to deposit another layer of a more conducting element, which facilitates the subsequent electrical and electromechanical analysis; in this work, a thin layer of Pt or W is sputtered, and this is always performed in CMi. The resulting materials stack that will be patterned into capacitors is, from bottom to top, Si/TiN/FE/TiN/Pt (or Si/TiN/FE/TiN/W), where FE stands for the ferroelectric material.

2.1.2 Fabrication of capacitor structures

As mentioned in the introduction of this chapter, the last part of the device fabrication route after film deposition and annealing is the patterning of capacitors and other structures: this involves multiple cleanroom steps that can be overall classified as photolithography and etching. Contrary to the film deposition steps, the preparation of the structures was always part of this work and performed internally in CMi.

The typical photolithography process requires the spin coating of a photoresist, that is a polymer sensible to UV light, on top of the deposited thin films. A subsequent hardbake is performed on a hotplate in order to prepare the resist for the exposure step. A photolithography mask is prepared and fed to a laser writer, which exposes the selected regions of the chip. In order to realize the pattern, the chip is dipped in a solvent that dissolves the exposed photoresist.

Now the pattern is on the top polymer layer but not yet on the material stack. The pattern transfer is accomplished through physical etching, which is stopped upon reaching the ferroelectric film: the desired structures are now obtained. Finally, the chip has to be cleaned in order to remove the residual photoresist and be ready for analysis.

The main steps involved in the fabrication of ferroelectric capacitors, namely thin films deposition, annealing, top contact deposition, photolithography and etching are illustrated in Fig. 2.2. More details about the steps and quantitative explanations for each process flow used in this work are provided in appendix.

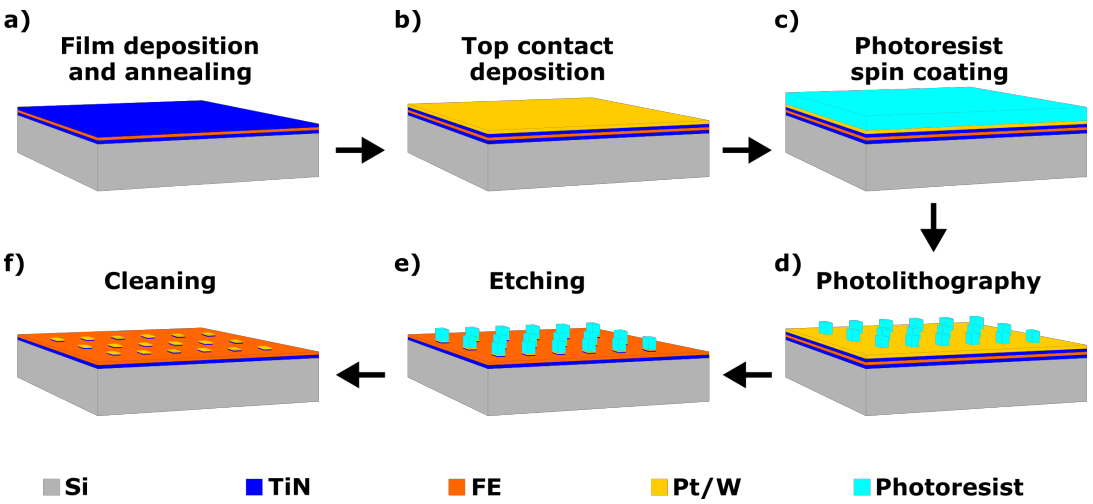

Figure 2.2: Process flow for the fabrication of devices presented in this work. a) Deposition of TiN/FE/TiN on Si wafer and annealing; b) deposition of top contact, either Pt or W; c) spin coating of the photoresist; d) creation of the pattern by photolithography; e) etching to transfer the pattern from the photoresist to the substrate; f) devices are ready to analyze after cleaning the photoresist away.

2.2 Characterization techniques

Once the device fabrication was discussed, the characterization techniques will be presented, together with the setups used in this work. HfO_2-based materials are known to be ferroelectric thanks to the stabilization at room temperature of a non-centrosymmetric orthorhombic phase. Hence, the microstructural characterization already offers an important piece of information about ferroelectricity, and will be examined in the first subsection. Structural information on the samples fabricated in this work was primarily obtained through Grazing Incidence X-Ray Diffraction (GIXRD); Transmission Electron Microscopy (TEM) was also employed to clearly determine the thickness of the films and their composition. Finally, X-Ray Photoelectron Spectroscopy (XPS) was used in order to determine the effect of the annealing ambient on the diffusion of chemical species. However, the most important features of ferroelectric materials are related to their electrical properties, which present a hysteretic behavior; the second subsection will then explain the principles of Polarization-Voltage (P-V), Capacitance-Voltage (C-V) and leakage measurements. The last subsection will finally give a rather detailed description of the working principle of Atomic Force Microscopy (AFM) and its variation Piezoresponse Force Microscopy (PFM), an extremely powerful technique that enables to measure electromechanical properties of ferroelectric materials.

2.2.1 Microstructural characterization

The importance of the newly discovered orthorhombic phase was understood since the first paper reporting ferroelectricity in Si:HfO_2 [1, 39]. Accordingly, one of the most commonly used techniques for microstructural investigation of ferroelectric HfO_2 thin films is GIXRD. The principle of XRD measurements is that a beam of X-rays is directed against the material surface where it hits atoms that scatter it: the wavelength of the incoming X-rays is comparable to the atomic distances and therefore the strong interaction causes the formation of a diffraction pattern according to the Bragg's law. This is collected by a movable detector and plotted as a function of the diffracted angle 2θ, that is the angle formed between the incident beam and the diffracted beam. In GIXRD, in order to ensure that the diffraction pattern is generated only by the topmost layers of the material, a very low angle ω is chosen for the incoming beam, usually below 2 °, which reduces the penetration of X-rays inside the material to a few nm only. All the XRD data reported in this work have been taken in EPFL with this GIXRD configuration, called ω-2θ scan, with an Empyrean diffractometer by Panalytical, equipped with a PIXcel-1D detector and using a Cu (λ = 1.54 Å) X-ray beam. The beam was generated with a voltage of 45 kV and a current of 40 mA. The incident angle ω was always fixed at 1 ° whereas the 2θ angle was scanned either for a few degrees around 30 °, close to the relevant peaks of o-, t- and m-phase in HfO_2, or from 20 to 70 ° for wider scans.

Fig. 2.3 shows a picture of the setup and the incident and diffracted beam accessories that were used for analyzing the samples. The incident X-ray beam comes out of the tube (A) and passes through a 1/32 ° divergence slit (F) before entering the parallel beam mirror (B): these two devices ensure that only a very thin and not diverging beam hits the sample, which is very important especially when the incident angle is as low as it is in GIXRD. A 10 mm mask (H) is placed to limit the width of the incident beam and make sure that none of it goes out of the sample surface. The X-ray beam hits the sample that is sitting on an xyz movable stage (C) and gets diffracted and collected by the movable detector (E) after passing through a parallel plate collimator (D), a 0.04 rad soler slit (I) and a Ni filter (J). The devices on the diffracted path enable to maximize the signal to noise ratio of the diffracted rays by filtering out noise and non-perfectly aligned X-rays. Finally, before any measurement, a proper alignment must be reached, in this case using an HZO reference sample kindly provided by Dr. Éamon O'Connor. During this procedure, a slightly different configuration is used and a manual beam attenuator (G) is also included in the incoming beam. The alignment is found and a measurement is performed on the reference sample before placing the chips under investigation, ensuring reproducibility between different measurement sessions.

The plot resulting from a GIXRD analysis contains the number of counts versus the 2θ angle, and once acquired and fitted with LIPRAS [103] it is compared to reference patterns found in databases for phase identification. In particular, the XRD patterns used in this work are PDF 04-005-5597 (o-HfO_2), 04-034-0104 (m-HfO_2), 04-011-8820 (t-HfO_2) and 00-038-1420 (c-TiN) retrieved from the ICDD database [104] and mp-390 and mp-2657 (t-TiO_2) retrieved from The Materials Project [105]. It should be noted here that samples characterized by GIXRD only consist of the annealed Si/TiN/FE/TiN

stack since other materials such as Pt or W are not relevant to the analysis. In addition, it shall be specified that there is no interest or benefit in having patterned structures on the sample, simply because the area analyzed by GIXRD is way larger (10 mm^2 approximately) than the features themselves (2500 μm^2 for the largest), so they could not be distinguished anyway.

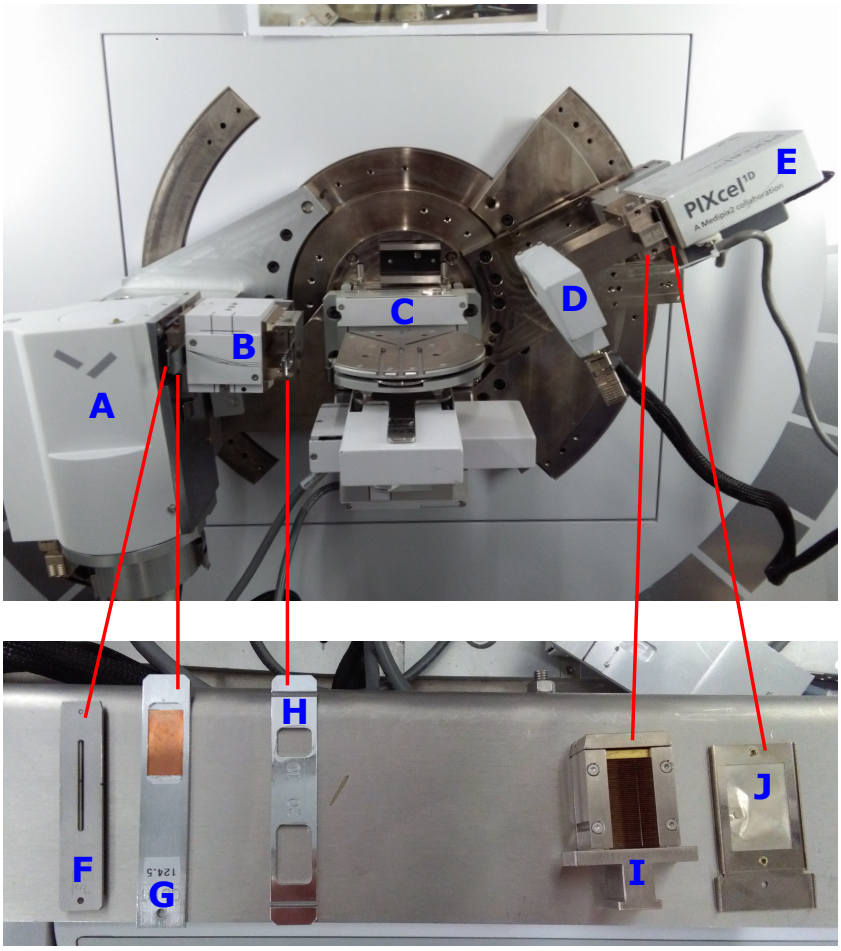

Figure 2.3: GIXRD setup used in this work to characterize ferroelectric thin films. At the left of the xyz movable stage (C), the incident beam path includes X-ray tube (A), parallel beam mirror (B), divergence slit (F), beam attenuator (G) and mask (H). On the right, the diffracted path includes a parallel plate collimator (D), a soler slit (I), a Ni filter (J) and the detector (E).

The other microstructural characterization technique that was used in this work is TEM. This allows to observe materials and their structure at the finest possible resolution and was thus used both to assess the film thickness and to see the amorphous and crystallized regions in Gd:HfO_2. During a TEM experiment the sample, which is thinned down to a few tens of nm of thickness, is placed in Ultra High Vacuum (UHV) and bombarded with a converged beam of highly energetic electrons: by collecting the ones

which are scattered a dark field image is obtained. Another powerful application of TEM is the possibility to implement Energy Dispersive X-Ray Spectroscopy (EDX): here, the incoming electron beam is used to hit and eject electrons from their valence shell. An electron belonging to an outer shell transitions to the free inner position and in doing so releases an X-ray. The energy of the emitted X-ray is related to the transition energy, which is different, and thus provides a univocal footprint, for every element. By recording this signal it is therefore possible to obtain qualitative and quantitative information on the elements present in the sample (with the lighter elements usually more difficult to detect). A FEI Tecnai Osiris in the Interdisciplinary Center for Electron Microscopy (CIME) in EPFL was used for the TEM analysis in this work, with an acceleration voltage of 200 kV and a current of 1 nA. This, in combination with EDX analysis, allowed to measure the thickness of Gd:HfO_2 thin films deposited by PLD and to assess the Gd concentration in the film.

The last microstructural characterization technique described in this work is XPS, which makes use of the photoelectric effect: here the sample is also placed in a UHV chamber and irradiated by soft X-rays (penetration depth $\approx$ 1-10 µm), which cause it to emit electrons whose kinetic energy is recorded. This makes possible to calculate the electron binding energy, which gives information about the species and atomic bonds in the material. A PHI VersaProbe II scanning XPS microprobe by Physical Instruments with an Al Kα X-ray source was used in this work to detect the diffusion of species and oxidation of TiN electrodes during annealing in different environments. The tool is also equipped with an ion gun which allows to bombard the sample, eject material from it and then take measurements at different depths, thus enabling to obtain a composition profile along the thickness.

2.2.2 Electrical characterization

In view of potential applications, among the most interesting functional properties of ferroelectric materials are remanent polarization P_r, coercive voltage V_c, relative dielectric constant ϵ_r, endurance and leakage current. All these quantities can be easily measured through the planar capacitor structure that was described in the first section of this chapter: the main tool used in this work for extracting macroscopic ferroelectric properties of HfO_2-based thin films is a TF 2000 analyzer with FE module by AixACCT. In this measurement, two conductive probes are in contact with bottom and top electrodes of the capacitor, and are connected by triaxial cables to the FE module which is in turn connected to the computer. A magnifying lens is used to facilitate the operation of the micromanipulators to which the conductive probes are attached. Once a good connection is established, a typical measurement performed on ferroelectrics is the Dynamic Hysteresis Measurement (DHM): the voltage is swept through the capacitor keeping one of the two electrodes virtually grounded and the current passing through it is detected. The resulting current versus voltage (I-V) plot ideally shows a flat value of current with two peaks in correspondence of coercive voltages, that is when the polarization switches direction. The current is then integrated in order to compute the charge, and the polarization versus voltage (P-V) or field (P-E) is plotted. This measurement is widely

reported in literature as it allows to easily quantify significant properties such as P_r and V_c; from the P-V loop it is also possible to determine whether the material displays a full polarization response or on the contrary the loop is pinched or degrading [2, 29, 31, 66, 73, 83, 84, 106]. The voltage in DHM is applied in a triangular wave, with the user being able to define maximum amplitude and frequency of the measurement. The frequencies used in this work range from 100 Hz to 2 kHz, whereas the amplitude depends on the film thickness. For the optimization of the resulting curve, an appropriate current range has to be defined, and that normally lies around 1-100 µA. As good practice, the first measurement is taken on a reference capacitor in order to make sure that the right capacitance is detected and the system is working correctly.

This ferroelectric tester also enables to electrically cycle capacitors and test the endurance of the material. The excitation voltage in this experiment is applied by a square wave, whose amplitude and frequency can be set by the user and varied according to the thickness of tested samples. After cycling, a DHM can be taken to see if there was any change in the polarization properties of the material, which could indicate wake-up or fatigue. It is possible to define how many cycles the sample has to undergo and how many DHMs are to be performed for every cycle decade, so that the evolution of the polarization response can be closely followed. The typical plot in this case shows the values of P_r versus the number of cycles, with the latter in logarithmic scale [2, 29, 31, 73, 79, 81, 84, 85].

Another relevant quantity that is usually reported in HfO_2-based ferroelectrics is the relative dielectric constant ϵ_r, which can be used to infer the present phases in the material since each of them possesses a different value [2, 66, 107, 108]. In addition, the ϵ_r-V plot of a ferroelectric should have a peculiar butterfly shape, with peaks in correspondence of the polarization switching, a feature that further confirms ferroelectricity. The relative dielectric constant of a material can be easily calculated once the capacitance is known: the capacitor structure offers the perfect conditions for performing such analysis. In fact, the same tool used for DHM also allows to perform Capacitance Measurements (CM) which give a C-V plot that can be converted into a ϵ_r-V plot by knowing the thickness t of the material and the area A of the capacitor, as shown in Eqn. 2.1 below, where ϵ_0 is the vacuum permittivity:

$$C = \epsilon_r \epsilon_0 \frac{A}{t}. \tag{2.1}$$

A CM consists in the application of a triangular voltage wave similarly to what is done in DHM; in addition, a small ac signal is superimposed in order to generate an ac current, integrate it and measure the capacitance. In this work ac amplitude of 200 mV and frequencies in the range 1-5 kHz were used.

A very useful feature of the AixACCT ferroelectric tester is the patented dynamic leakage current compensation mechanism, which facilitates measurements and enables to obtain clean polarization and capacitance loops by removing the effect of leakage current. This implies that another instrument is required if one wants to measure leakage. In

this work a Keithley 4200A parameter analyzer was employed for this purpose. The setup is similar to the previous one, but this time the two probes contacting the device are connected by triaxial cables to Source Measurement Units (SMUs) which are in turn connected to the computer. After an open and short circuit calibration, the measurement simply consists in applying the usual triangular voltage wave and detecting the current that is passing through the capacitor, which will increase with higher applied voltage. The leakage current is usually plotted in literature as the logarithm of the current versus applied voltage [2, 29, 85, 109].

2.2.3 Electromechanical characterization

The electromechanical characterization of HfO_2 by PFM makes the most consequential part of this work, therefore the technique will also be explained in more detail. Atomic force microscopy, and especially PFM, is an ideal investigation method in that it allows integrating and strengthening structural and electrical characterization results by locally probing the material and measure its electromechanical response. In addition, some unique opportunities are given by this technique which are precluded to other investigation methods, such as the visualization and manipulation of ferroelectric domains. In this subsection, the working principle of contact and non-contact AFM will be reviewed before presenting the PFM technique. In particular, the distinction between resonance and non-resonance PFM will be explained and it will be shown why the latter was chosen in this work.

Contact and non-contact AFM

Atomic force microscopy is a very powerful and non-destructive technique for local analysis of materials: in its simplest form, a very small probe is scanned on top of the sample surface and relevant information such as the topography can be obtained. According to the kind of interaction between probe and sample, the contact or non-contact mode is obtained. A list of the main components that constitute an AFM and an explanation of its working principle is given here and shown in Fig. 2.4:

- a scanning probe, made of cantilever and tip;
- an XY scanner to move the sample;
- a Z piezo actuator;
- a laser and a photodetector;
- a feedback loop.

The probe is defined by two main parts: one is the cantilever, that is a beam having one end clamped to its holder and the other end loose and free to oscillate. The other part is a pyramidal-shaped tip, located on the bottom side of the cantilever at its loose end. A typical tip is several µm high and with an end radius that can be as little as a few

nm. On the top side of the cantilever, in correspondence of the tip location, is shined a laser that is reflected against a photodetector. As a result, the deflection of the cantilever corresponds to a position of the laser spot on the photodetector, which is divided into four quadrants to separate vertical and horizontal components. The laser position becomes an input of the feedback loop which has the task to ensure that cantilever deflection (contact mode) or oscillation (non-contact mode) remain constant and equal to the value set by the user. This is accomplished by Z piezo actuators, vertical stacks of piezoelectrics connected to the sample holder that can modify its vertical position according to the output of the feedback loop. A surface scan is acquired by moving the sample on the horizontal plane thanks to an XY scanner while the probe always remains fixed in its position. This is usually achieved by placing the sample with carbon tape on a disc which is then magnetically connected to the scanning stage and actuators.

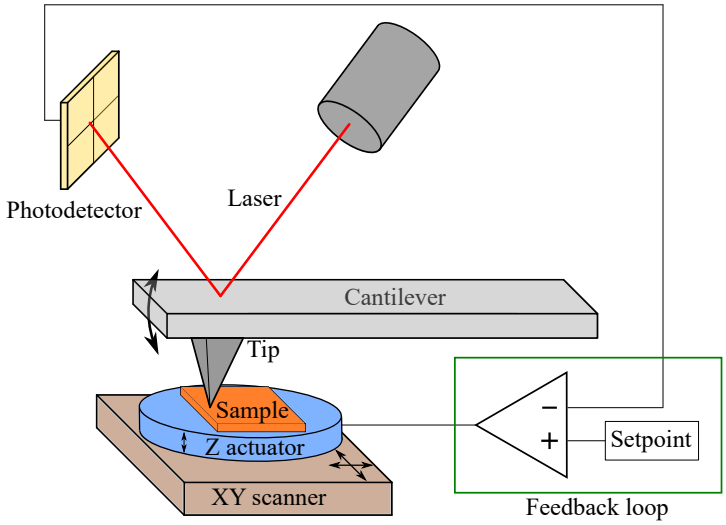

Figure 2.4: Schematics representing (out of scale) the main components of an atomic force microscope: cantilever and tip (forming the probe), a laser that is reflected on the cantilever and hits a photodetector, and a feedback loop that processes this input to maintain the probe in right position by driving piezoelectric Z actuators. An XY scanner allows for surface scan on samples (the probe does not move in the XY plane during scanning).

While the contact mode is the most intuitive technique, with the tip simply dragged on the sample surface, its most evident drawback is that the tip is in constant contact with the sample, leading to a faster wear and possibly damaging the sample too, especially if soft. A worn tip clearly has lower lateral resolution (because the tip radius increases) and, in case a conductive coating is present, this can quickly wear out too [110]. The non-contact or tapping mode addresses these issues by reducing the contact time between tip and sample surface and especially by avoiding the drag. Here the cantilever oscillates and the tip just taps the sample surface, with a force proportional to the amplitude of oscillation and set by the user. The main advantage of this second mode is that the tip is not constantly dragged on the surface and therefore wears less than in contact mode.

Typical in-plane resolution that can be achieved by AFM is in the order of few tens of nm whereas in the z-axis, that is the vertical displacement of the tip, it can reach even fractions of nm. This superior precision makes it an ideal tool to investigate properties of piezoelectrics and ferroelectrics at the nanoscale: their electromechanical behavior indeed induces a very small displacement when they are subjected to an electric field, which can be detected by the AFM tip. The next subsection shows more in detail how this is achieved in practice.

Resonance and off-resonance PFM

PFM is a form of scanning probe microscopy which stems from contact mode AFM: here, the conductive probing tip is used to simultaneously apply an electric field and detect the induced electromechanical response of the material. This technique is especially powerful in analyzing piezoelectric and ferroelectric materials, where a strong electromechanical coupling is observed due to the converse piezoelectric effect. Since its invention in mid-90s, numerous methods were developed to characterize polarization reversal in ferroelectrics, including imaging of nanoscale size domains and acquisition of piezoelectric loops which locally induce domain switching thanks to a voltage sweep [111]. This technique was therefore also applied to ferroelectric HfO_2-based thin films to obtain information with respect to domain pinning and growth, presence of nonferroelectric phases, polarization switching mechanisms and other features that no other method can unveil with this resolution [2, 86, 112–116].

In a typical PFM experiment the investigated material is deposited on a bottom electrode and the conductive AFM tip acts as the top electrode to which the voltage V_{tip} is applied in the form

$$V_{tip} = V_{dc} + V_{ac}cos(\omega t). \tag{2.2}$$

The applied voltage is the summation of a switching bias V_{dc} and a probing ac bias V_{ac} with frequency ω. The applied voltage V_{tip} causes a field E inside the film region below the tip; as a consequence of that, a polarization state is induced in the material along the field vertical orientation. This, thanks to the converse piezoelectric effect, produces a static displacement and a vibration of the sample, related to the dc and ac component of the field. However, the collected signal represented by the vertical tip displacement can include other contributions of physical and electromechanical nature [117]. In particular, a relevant effect on the measurement is played by electrostatic interactions caused by the applied voltage [117–120]. The total response amplitude in the vertical direction Δz, normally in the sub-nm range, can therefore be expressed as

$$\Delta z = \Delta z_{piezo} + \Delta z_{es}, \tag{2.3}$$

where only Δz_{piezo} is the piezoelectric response of the material. The term Δz_{es} repre-

sents contributions of electrostatic forces acting on tip and cantilever body, related to free moving or injected charges on the sample surface [111, 121]. Clearly, the reliability of PFM measurements depends on being able to maximize piezoelectric response while minimizing electrostatic contributions. The latter are caused by capacitive forces F_{es} which can be written as

$$F_{\text{es}} = \frac{1}{2} V_{tip}^2 \frac{dC}{dz}, \tag{2.4}$$

where dC/dz is the derivative along the vertical direction z of the capacitance C of the sample-cantilever system which includes local and nonlocal interactions [111]. It shall be remembered here that V_{tip} is constituted of dc and ac contributions, and therefore the electrostatic force will also have ac and dc components. In view of this consideration, dc-on and dc-off loops were always compared in this work as this is a way to quantify the electrostatic interaction and confirm the genuine ferroelectricity of the material, as explained in more detail in chapter 4. The displacement caused by the electrostatic force is then given by

$$\Delta z_{es} = \frac{F_{es}}{k^*}, \tag{2.5}$$

where k* is the contact stiffness. The geometry and mechanical properties of the cantilever influence both F_{es} and k*, thus having a strong impact on the electrostatic contribution. It follows that a good practice in order to minimize Δz_{es} is the use of adequate contact force and stiff cantilever, that is with spring constant as high as 40 N/m [28, 111, 121, 122].

Another precaution is to use a top electrode instead of applying the voltage through the tip directly on the bare surface of the dielectric. In fact, measuring through a top conductive layer which acts as top electrode is greatly reducing the electrostatic artifacts in the measurements, which can induce ferroelectric-like behavior from materials which are known not to be ferroelectric [117–121]. While this is not so dramatic when analyzing materials with strong piezoresponse, it becomes critical for thin films analyzed in this work. This brings another benefit to the measurement: while the response is still probed locally under the tip, the applied electric field becomes uniformly distributed across the whole capacitor and well aligned in the vertical direction, producing a homogeneous rather than local domain switching [28]. The drawback of having a layer between the film under measurement and the PFM probe is clearly a reduction in resolution and the potential contribution of such layer to the measurement [28, 111, 123, 124]. For this reason the top electrode has to be as thin as possible and was always kept below 40 nm (TiN + Pt) in this work.

The main sources of electrostatic interactions which prevent a correct piezoresponse quantification have been highlighted; in summary, the two most important actions to reduce such contributions are identified as using a stiff cantilever and measuring through

a top electrode. The first section of chapter 4 will present results which show how reliable PFM data was obtained in this work following these criteria.

Once the electrostatic contribution has been eliminated, the piezoresponse term Δz_{piezo} in Eqn. 2.3 is left to characterize. In all dielectrics it exists a nonlinear coupling between elastic strain x and polarization P, called electrostriction, which can be expressed as

$$x = QP^2, \tag{2.6}$$

where Q is the electrostrictive coefficient. As explained before, x and Q are, respectively, a second and fourth rank tensor, and the indices are here omitted for simplicity. In ferroelectrics the material presents polarization, and hence strain, even when no field is applied. In the case of PFM analysis the polarization from an external field with dc and ac components is added to that and therefore the resulting strain can be written as

$$x = Q(P + \delta P)^2 = QP^2 + 2QP\delta P + Q(\delta P)^2, \tag{2.7}$$

where P is the polarization of the material and δP is the small polarization change due to the applied ac bias. The term QP^2 is a static surface displacement induced by the polarization state of the material which is not detected by the lock-in, which is acquiring the tip oscillation signal corresponding to the applied ac bias. This is included in δP in the above equation: in practice, $Q(\delta P)^2$ is very small and can be neglected. The second term of Eqn. 2.7 is then the one of interest; when the probing ac electric field is weak, as it is the case in PFM experiments, the polarization response depends linearly on it and can be written as

$$\delta P = \epsilon_r \epsilon_0 E_{ac} = \epsilon_r \epsilon_0 \frac{V_{ac}}{h} cos(\omega t + \phi), \tag{2.8}$$

where ϵ_r and ϵ_0 are second rank tensors representing the relative dielectric permittivity of the material and of that of vacuum, respectively, and h is the film thickness (assuming the field uniformly aligned in the vertical direction) [13]. The phase shift ϕ indicates the delay of polarization response with respect to applied voltage. The strain component related to the small ac driving voltage, x_{ac}, is then

$$x_{ac} = 2QP\epsilon_r \epsilon_0 \frac{V_{ac}}{h} cos(\omega t + \phi), \tag{2.9}$$

Finally, if the above equation is multiplied by the film thickness h, the vertical displacement Δz_{piezo} caused by the probing ac voltage is found:

$$\Delta z_{piezo} = 2QP\epsilon_r \epsilon_0 V_{ac} cos(\omega t + \phi). \tag{2.10}$$

The multiplication factor that relates the vertical tip displacement to the applied tip bias is the converse piezoelectric coefficient d_{33} and thus equation 2.10 can be written as

$$\Delta z_{piezo} = d_{33} V_{ac} cos(\omega t + \phi). \tag{2.11}$$

Later in this subsection the calibration procedure that enables to obtain Δz in pm will be explained, since the acquired signal is actually in V.

It shall be noticed here that the d_{33} coefficient in the above equation has to be regarded as a measured effective d_{33} and in general differs from the true d_{33} of the material. This draws from the considerations that thin films are usually polycrystalline, with randomly oriented domains, and their mechanical displacement is strongly influenced by the clamping effects given by the encapsulation between top electrode and surface [2, 28, 71]. Due to these caveats, the effective d_{33} measured by PFM can be considered as a lower limit of the material's true d_{33}.

A substantial challenge with the HfO_2-based ferroelectric materials analyzed throughout this work is that their d_{33} is very small, in the order of few pm/V [125, 126]. This implies that, even applying tens of V, only a few tens of pm displacement is expected by the material. Such low response can very well be close to the noise floor of the instrument and besides that it can be totally covered by minimal electrostatic interactions or surface roughness [110, 121]. In reality it is not even possible to apply such high voltages, because a breakdown of the thin film would occur.

It follows that some form of response amplification is necessary in PFM. The most common way to achieve this is to apply a small ac voltage to the tip with a frequency that corresponds to the resonance frequency f_r of the sample-tip system. The naturally occurring amplification happening at this precise frequency makes the signal stronger and easier to be detected by the lock-in. This technique has allowed for great improvement of PFM analysis, enabling to detect d_{33} of very few pm/V. However, this approach relies on being able to track and maintain same quality of resonance frequency of the tip-sample system during the scan, something that is not always so straightforward: in fact, f_r changes with the tip-sample mechanical interaction, which can be affected by surface topography features, presence of electrostatic charge, tip wear, surface contamination and so on.

The classic method to track the f_r of the tip-sample system is Phase Locked Loop (PLL). PLL-based method works by calculating the phase lag between the excitation and response signal defined in Eqn. 2.8: if that can be efficiently monitored, the frequency of excitation signal can be modified in order to closely follow f_r. However, ferroelectric materials present the obvious problem that they possess two stable phase states and can even switch during measurement if the applied ac voltage is too high, so resonance tracking by PLL cannot work for these materials [127]. Two more sophisticated techniques were developed to circumvent this problem: Dual-Frequency Resonance Tracking (DFRT or DART) and Band Excitation (BE) [127, 128].

DART method makes use of two lock-ins to send two reference excitation signals with separate frequencies very close to the f_r of the system, one immediately before and one right after the resonance peak. By detecting the amplitude response at these two reference frequencies and by imposing them a constant amplitude, it is possible to track and follow the resonance shift [127]. In BE an excitation signal (with complex, non-sinusoidal waveform) is applied to the tip not at a single frequency but simultaneously in a range of frequencies enclosing f_r. The detected response of the cantilever is Fourier transformed and allows to obtain the resonance frequency and phase of the response [128]. Ultimately, both these techniques allow to work in resonance and have a higher signal to noise ratio, producing appreciable results in short acquisition times. These techniques enable to obtain PFM images in reasonably short times and collect large arrays of loops in Switching Spectroscopy PFM (SSPFM) [129].

Yet the response quantification remains uncertain due to the unknown quality and shape of the resonance, which is dependent on many factors as stated before; even just a variation in the laser spot position on the cantilever can contribute to make the data more ambiguous and their interpretation more challenging [2, 111, 130]. These aspects can play a minor role when the ferroelectric response is strong such as in PZT, but they become more relevant when the expected d_{33} is as small as in HfO_2-based ferroelectrics, where it can be in the order of 1-10 pm/V [125, 126].

With the aim to reduce as much as possible the sources of artifacts and simplify the data interpretation, this work makes use exclusively of off-resonance PFM. All the measurements presented in this work were performed on a Asylum Research Cypher AFM, using an external HF2LI lock-in amplifier by Zurich Instruments commanded by a LabView script in order to have full control on the measurement parameters; this custom setup is shown in Fig. 2.6. With this setup the tip is driven by an ac signal whose frequency can be arbitrarily chosen, as long as it is kept far from the f_r of the system. In addition, in order to prevent frequency limitations imposed by RC of the system, very small capacitors of 5x5 μm^2 were always used. Since resonance amplification does not come into play, quantification of the response after proper calibration is more straightforward, since there is no unknown modification of the response by the quality factor of resonance peak. Ultimately this ensures that response signal is frequency independent, a feature which adds strength to the measurement.

It is clear that one main disadvantage comes along with the decision of working off-resonance: the lower response of the material (1 to 2 orders of magnitude lower than in resonance) requires a much higher integration time in order to have a good signal to noise ratio. For loops presented in this work the time constant ranges from $\approx$ 70 to 600 ms, whereas for images it is about 45 ms. This implies a longer time to take loops ($>$ 5 min per loop) and scans ($>$ 4 hours for a 1x1 μm^2 scan).

A potential issue related to this is the thermal drift, which can cause the sample to move and make the comparison of images taken at different times more difficult. With the purpose to have a stable temperature during multiple scans and prevent this problem, the experiments were always conducted at least one day after the samples were inserted into the AFM chamber. Fig. 2.5 below shows two topography images (acquired at the

same time of PFM scans) taken with a delay greater than 14 hours between each other; from the surface features it can be recognized that the thermal drift was minimal.

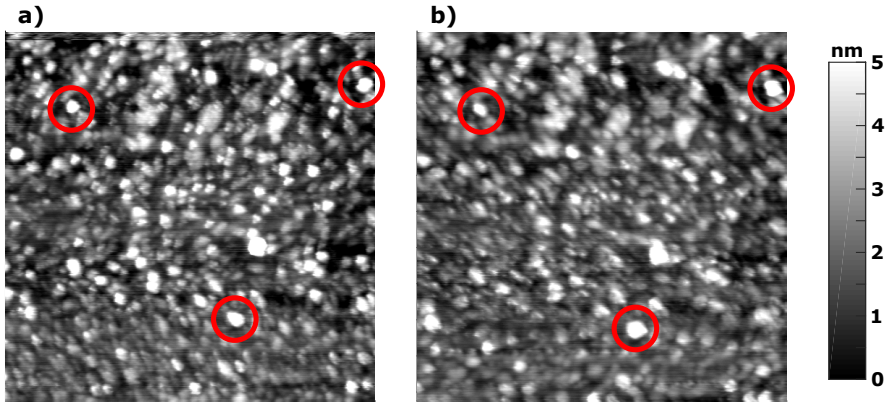

Figure 2.5: Topography data acquired during PFM scan: both images are 1x1 μm^2. The scan on the right (b) was performed over 14 hours after the scan on the left (a). The very small movement of the highlighted features attests to a minimal thermal drift.

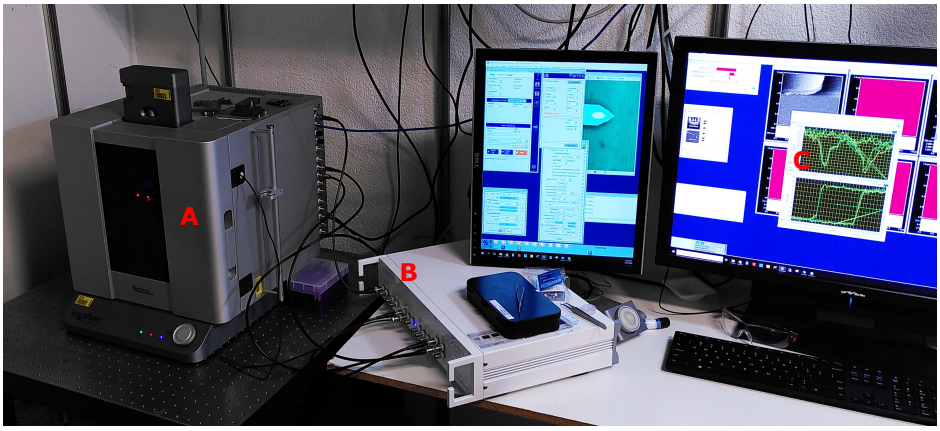

Figure 2.6: PFM setup used in this work. The Asylum Research Cypher (A) is connected to an external HF2LI Zurich Instruments lock-in amplifier (B) which in turn is commanded by a LabView script (C).

From what was said before it follows that, in order to fully exploit the advantages of off-resonance PFM and obtain a reliable quantitative assessment of the ferroelectric response, the choice and calibration of the cantilever is fundamental. Here, MikroMasch HQ:DPER-XSC11 Pt-coated conductive tips with a nominal spring constant of 42 N/m were used. To the extent of preserving the integrity of the thin conductive coating layer of the tip, the sample was always approached in tapping mode with a force that was just enough to ensure the image acquisition. This allows to locate the small 5x5 μm^2

capacitor and position the tip for subsequent PFM analysis limiting as much as possible wear of the coating layer.

The cantilever calibration was performed with a reference Sc:AlN piezoelectric kindly provided by the group of Prof. Paul Muralt, which was first characterized by double-beam laser interferometer and a d_{33} of 6-6.5 pm/V was found. Then, by performing PFM analysis on the same sample and on 5x5 µm^2 Pt electrodes, a calibration factor C was found which enabled to relate the vertical displacement in pm with the measured response in µV. By taking Eqn. 2.11 and rearranging it to highlight the calibration factor C and the detected response amplitude A in V, one obtains:

$$d_{33} = \frac{\Delta z}{V_{ac}} = \frac{C \cdot A}{V_{ac}}. \tag{2.12}$$

The calibration factor is then computed as

$$C = \frac{d_{33eff} \cdot V_{ac}}{A} = 0.07 \left[\frac{pm}{\mu V}\right] \tag{2.13}$$

During a measurement, since the applied ac is known and set by the user, it is now possible to use Eqn. 2.12 and calculate the effective d_{33} of the material.

All the precautions taken during the off-resonance PFM experiments performed in this work and ad hoc calibration of the tip response have been explained here. The first section of chapter 4 will show how all this is reflected in PFM loops features which attest to the genuine ferroelectricity of investigated materials.

2.3 Summary

This methodology chapter presented the fabrication and characterization techniques that were used throughout this work. In the first section, difference between ALD and PLD fabrication techniques was highlighted: while the samples analyzed in chapter 4, 5 and 6 were received already deposited by ALD, with the exception of undoped HfO_2 which was sputtered, the Gd:HfO_2 thin films analyzed in chapter 3 were grown by PLD as relevant part of this work. The device fabrication was always performed as part of this work and is also explained in the first section. Techniques employed in this work for analysis of ferroelectric thin films are presented in the second section, with a particular focus on the electromechanical characterization by off-resonance PFM, which constitutes the most relevant part of this work.

3 | CMOS-compatible PLD deposition of ferroelectric Gd:HfO_2

This chapter reports the findings on ferroelectric Gd:HfO_2 thin films fabricated by PLD in a CMOS BEOL compatible process. After an introduction to explain the interest in PLD method and the state of the art, the work is presented. The development of a process which meets the constraint of CMOS compatibility is discussed first and then, once the deposition and annealing parameters have been fixed, the microstructural analysis and electrical characterization of the ferroelectric film are shown.

Ferroelectric HfO_2-based thin films have been extensively studied in recent years, and are of particular interest for both non-volatile memory applications and steep-slope devices such as negative capacitance field effect transistors. As already explained in the introduction, they offer several advantages over more traditional ferroelectrics such as perovskites, demonstrating improved scaling potential and offering superior integration capability with Complementary Metal-Oxide-Semiconductor (CMOS) processes [2, 49, 131]. Ferroelectric behavior associated to the polar orthorhombic phase has been demonstrated by numerous groups for HZO, a compound where Hf and Zr are present in equal amounts [2, 96, 131–133]. Ferroelectricity has also been observed by incorporating small concentrations of a number of different dopant atoms in HfO_2, among them Si [1, 39, 54, 55, 134], Y [47, 74, 85, 135, 136], Gd [31, 44, 106, 108, 137], Sr [29, 34, 46, 83, 106], and La [46, 58, 59, 68, 138]. Of particular relevance to the work presented in this study, the ferroelectricity of Gd:HfO_2 thin films has been reported to be tolerant to a wide thickness, doping and annealing range [2, 31, 106, 137].

For hafnia-based ferroelectrics, the vast majority of literature reports are for ALD-grown thin films, a process that is well established and enables full compatibility with CMOS Front-End-Of-Line (FEOL). Some studies also report sputtering and Pulsed Laser Deposition (PLD), techniques which offer great flexibility thanks to the possibility to tune a variety of parameters during the process, which in turn affect the properties of the deposited film. These include the laser power and repetition rate, the pressure and composition of the gas(es) in the PLD chamber, and the deposition temperature. With regard to formation of ferroelectric hafnia thin films, the development of a PLD pro-

cess to form the necessary orthorhombic phase is not trivial given the interdependence of a number of these parameters and the matrix is further complicated by subsequent annealing steps.

One of the great advantages in having the possibility to tune many deposition parameters independently is that a process can be engineered to obtain epitaxial growth. With this purpose, a number of previous studies have employed PLD to deposit hafnia-based epitaxial thin films showing promising ferroelectric properties [75–77, 136, 139, 140]. Deposition temperatures in the case of the aforementioned works were always in the range from 550 to 825 °C and made use of carefully engineered substrates such as epitaxial Yttria Stabilized Zirconia (YSZ), $La_{0.67}Sr_{0.33}MnO_3$ (LSMO) on $LaAlO_3$ (LAO) or $SrTiO_3$ (STO). Given the delicate selection of substrates and deposition conditions, a subsequent annealing step is normally not necessary in order to observe ferroelectricity.

However, when epitaxial films were not sought, other PLD studies reported lower temperatures for depositing polycrystalline thin films. Amorphous Y:HfO_2 was deposited at 200 °C but required a subsequent annealing step at 600 °C for 60 seconds to crystallize in the ferroelectric phase [85]. HZO was deposited at the slightly higher temperature of 250 °C; in this case, a lower annealing temperature of 530 °C for 60 s was necessary to see ferroelectric behavior [141]. It is therefore possible to envisage an appropriate choice of deposition and annealing conditions which can maintain the temperature lower than 450 °C throughout the whole process, thus enabling a CMOS-compatible PLD fabrication route. Indeed, when considering the future incorporation of ferroelectric hafnia-based films in applications, this is still one of the open challenges.

Here, a low thermal budget PLD fabrication route for ferroelectric gadolinium doped hafnia thin films is demonstrated. The films were deposited on a conventional TiN/Si substrate, with a PLD deposition temperature of 330 °C and subsequent anneal at maximum 450 °C, therefore within the confines required for CMOS Back-End-Of-Line (BEOL) compatibility. The use of Gd doping might help achieving this result since the appearance of ferroelectricity for relatively low annealing temperature in ALD Gd:HfO_2 films was previously demonstrated [69, 106]. In addition, since PLD films usually report a higher concentration of O vacancies and Gd is a trivalent dopant, thus further contributing to O vacancies creation, the annealing was explored not only in the standard N_2 atmosphere but also in O_2.

The fabrication of the material stack used in this work is explained in detail in appendix. After the annealing step, 30 nm of W were deposited in order to have a good contact for electrical characterization, which was performed on squared capacitor structures of 50x50 μm^2.

3.1 Development of the fabrication process

The investigation of the optimal fabrication route, that is finding the right deposition and annealing conditions, was performed bearing in mind one main constraint: the

maximum temperature of the process should never exceed 450 °C in order to ensure CMOS BEOL compatibility. It is also relevant to be able to deposit the film on TiN bottom electrode, widely reported as the best material for HfO_2-based ferroelectrics due to its superior mechanical and electrical properties coupled with its strong thermal and chemical stability [7]. It will be shown how this requires a delicate balance between the thermal budget seen by the sample during the deposition and the annealing. Tab. 3.1 summarizes the six parameters that were taken into account for the process development procedure, together with their range of variation: temperature, pressure and gas flow inside the chamber during film deposition, presence of top electrode capping during annealing, and annealing atmosphere and thermal budget.

Process parameter	**Value range**
Deposition temperature	220 - 420 °C
Deposition pressure	0.05 - 0.2 mbar
O_2 flow	0 - 50 sccm
Top electrode capping	Yes - No
Annealing temperature	$<$ 450 °C
Annealing atmosphere	N_2 - O_2

Table 3.1: Parameters and respective ranges for the process development.

The choice for the characterization technique at this early stage of the study fell on GIXRD, given the high output of samples: this technique is relatively quick and does not require the whole photolithography steps that are very time consuming, while at the same time offers already a first indication of the goodness of the film. For instance, it is already possible to detect the amorphous or crystalline nature of the film, and the presence of m-phase with respect to o- and t-phases. To this extent, annealed $Si/SiO_2/TiN/Gd:HfO_2/TiN$ structures (without top contact layer and patterning) were tested by GIXRD in the 2θ range from 27 to 33 °, that is where the main m-, t- and o-phase peaks are located. After the fabrication conditions such as temperature and pressure were found, capacitors structures were patterned and the polarization response of the samples was analyzed by means of P-V measurements in order to fine tune other parameters such as the O_2 flow during deposition.

The deposition temperature was the first parameter to be analyzed: it can be clearly seen from Fig. 3.1a how a partial crystallization already occurs during the film deposition, that is without top electrode encapsulation and annealing. The crystallization becomes stronger with increasing process temperature from 220 to 420 °C. The only observed peak is at $2\theta \approx 30.2$ ° which, while not being enough to univocally discriminate between t- and o-phases, already allows to exclude major presence of m-phase, whose peaks lie at $2\theta \approx 28.3$ and 31.7 °. The observed temperature trend is expected and, while the deposition conditions and the temperature range explored in this study are not directly comparable, this is in agreement with what is reported in literature for

epitaxial depositions of HfO_2-based materials by PLD. Several studies show that for high deposition temperature the material is already crystalline and ferroelectric without subsequent annealing [75, 77, 136, 140].

This result highlights the different nature of PLD with respect to ALD technique, where deposition only takes place in the 200 - 300 °C temperature range and gives mainly amorphous films which require further annealing. The film growth dynamics in PLD is regulated by the kinetic energy that atoms possess when they hit the substrate, which in principle can be defined just by the laser energy and repetition rate. The higher the energy of the ejected atoms, the longer they can migrate on the substrate and rearrange themselves in a densely packed and more stable configuration, as opposed to forming an amorphous layer for lower energy. In this context, deposition temperature contributes to the increase of kinetic energy and allows for a higher mobility and close-range ordering of the deposited atoms [142, 143].

In Fig. 3.1b the film deposited at 420 °C, which showed the strongest crystallinity when as-deposited (see Fig. 3.1a), is compared to a film deposited at 330 °C and subsequently annealed at 400 °C for 40 s in N_2 after top TiN electrode encapsulation. The annealed film shows a much stronger peak, meaning a more complete crystallization of the film. In addition, a peak shift of approximately 0.2 ° to the right can be observed, suggesting a higher stress in the film as expected from the annealing under top electrode [2, 33, 66]. To further confirm that a ferroelectric response is not achieved on the as-deposited samples despite the observed peak, capacitor structures were fabricated and tested on this film. The typical behavior of a dielectric with no hysteretic response was obtained, a result clearly suggesting that only a partial crystallization can be achieved by PLD deposition and the annealing step after top electrode encapsulation is necessary to further transform the remaining amorphous phase.

However, samples deposited at 220 °C and which showed no crystallization remained amorphous even after annealing at 400 or 450 °C. Crucially, this suggests that PLD technique can be exploited in order to lower the required annealing temperature to complete the phase formation if a partial crystallization can already be achieved during deposition.

A critical parameter in PLD deposition is the chamber pressure. The GIXRD signatures of films deposited at 330 °C with different pressures and all annealed at 400 °C for 40 s in N_2 are presented in Fig. 3.2, showing how narrow the optimal window is. Increasing the chamber pressure from 0.05 to 0.2 mbar produces three films dramatically different, from one displaying an important monoclinic peak to one that does not crystallize even after annealing.

Due to the nature of this technique, as it was the case for deposition temperature, the effect of oxygen pressure is also described in terms of the kinetic energy that ejected target atoms possess when they hit the substrate. A higher pressure causes a larger scattering of atoms in their path from the target; as a consequence, when they reach the substrate they possess less kinetic energy to diffuse around and achieve a denser packing, leaving an amorphous film [142–145]. It can be speculated that the same argument could

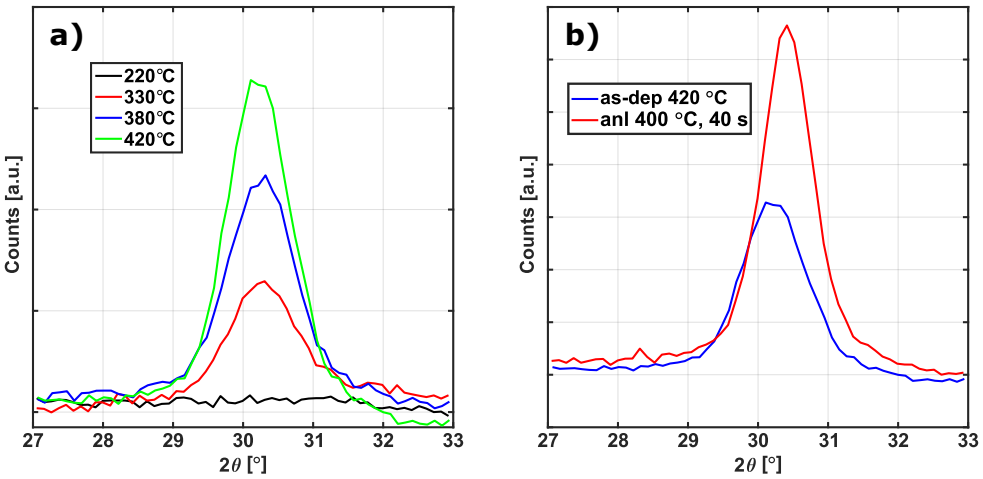

Figure 3.1: a) GIXRD analysis on as-deposited samples showing the impact of deposition temperatures; b) GIXRD comparison of samples in as-deposited state and annealed after top electrode encapsulation. In all cases, the main t- or o-phase peak is observed at $2\theta \approx 30.4$ ° and there is no sign of m-phase, whose peaks should appear at 28.3 and 31.7 °.

explain the formation of monoclinic phase for the lowest pressure: here atoms hit the substrate with high kinetic energy which allows them to relocate on the film and cluster in the most favorable crystalline configuration, which for this class of ferroelectrics is indeed the non-ferroelectric m-phase.

The last deposition parameter that was investigated is O_2 flow during deposition. Fig. 3.3a shows the result of GIXRD on three films deposited with increasing O_2 flow and subsequently annealed. Notice that 20 sccm of N_2 flow were used to reach and maintain the chamber pressure when zero O_2 flow was tested. No major differences were found except a considerable peak shift to the left of ≈ 0.3 ° for the sample deposited with no O_2. No other peaks are reported in close vicinity of the o-111 or t-101 peak; therefore, it is assumed that it is the same peak but shifted. This can indicate a lower in-plane tensile stress, which can also imply crystallization of a different phase. These samples were also analyzed electrically, and the results are shown in Fig. 3.3b. All films show hysteresis but the one deposited with no O_2 flow has a clear dielectric behavior, whereas the other two films present ferroelectricity. It is clear from the horizontal shift that the highest O_2 flow during deposition is strongly oxidizing the bottom electrode and degrading the switching characteristic. Regarding the film deposited with lack of O_2, a possible explanation is that the film crystallizes in tetragonal phase, which is not ferroelectric and also shows a peak in correspondence of the orthorhombic phase as discussed earlier. The peak shift to the left could be due to a lower in-plane tensile stress of the tetragonal phase [2, 33, 66].

In conclusion, the optimal fabrication conditions for PLD deposition of ferroelectric Gd:HfO_2 thin film were found to be a temperature of 330 °C with a chamber pressure of 0.1 mbar and an O_2 flow of 20 sccm. This enables to obtain ferroelectric behavior with a subsequent annealing already at 400 °C, as will be shown in the next section.

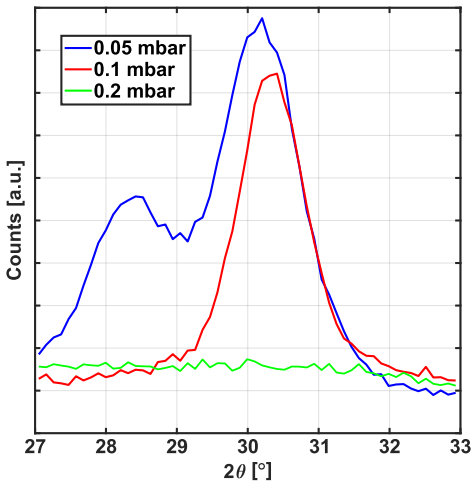

Figure 3.2: d) GIXRD analysis showing the influence of deposition pressure on crystalline phase formation in Gd:HfO_2. The diffraction peak at 28.6 ° for a chamber pressure of 0.05 mbar is given by the monoclinic phase.

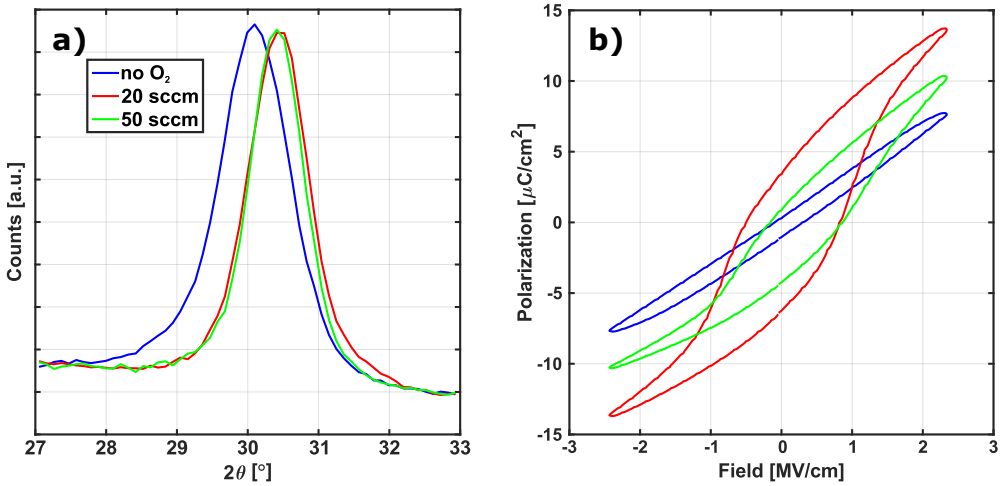

Figure 3.3: Influence of O_2 flow in a) crystalline phase formation and b) polarization response of thin Gd:HfO_2 thin films.

3.2 Microstructural analysis: hints of ferroelectric phase

Once the development of a recipe for deposition of Gd:HfO_2 has been illustrated, a more detailed characterization of the thin film is presented here. A TEM micrograph of the W/TiN/Gd:HfO_2/TiN/Si structure is shown in Fig. 3.4a for a sample that was annealed at 450 °C for 80 s in N_2. The thickness of all layers of interest can be measured: bottom and top TiN layers are $\approx$ 25 nm, while the top W is $\approx$ 35 nm thick. Finally, the Gd:HfO_2 layer is $\approx$ 21 nm thick and shows good uniformity. However, it can be observed that ferroelectric interfaces are not extremely sharp and extend for a few nm: interface quality can be optimized in PLD by carefully controlling temperature, O_2 flow and pressure in the chamber during deposition, but this was not an objective of the work at this stage.

The EDX elemental profiles in Fig. 3.4b, taken across the red area highlighted in Fig. 3.4a, show some interdiffusion of species; most notably, oxygen migration towards the electrode layers is observed due to the known scavenging effect of TiN, as it will be discussed later. A good stoichiometric ratio is detected for the Gd:HfO_2 film (the counts of Gd have been multiplied by a factor 10 for better comparison with other elements). The detected amount of Gd in the HfO_2 film is 3.0 %, which is very close to the ceramic target stoichiometry of 3.5 % and acceptable given the resolution of the analysis. The HRTEM image in Fig. 3.4c further confirms that the annealing at 450 °C was sufficient to bring the thin films to a crystallized state, in contrast to what is observed on the as-deposited sample in Fig. 3.4d, which consists of a mostly amorphous film with some locally crystallized regions. It is in principle possible to distinguish between t- and o-phase with this technique but the measurements required to accurately detect O ions position in the unit cell are beyond the scope of this work.

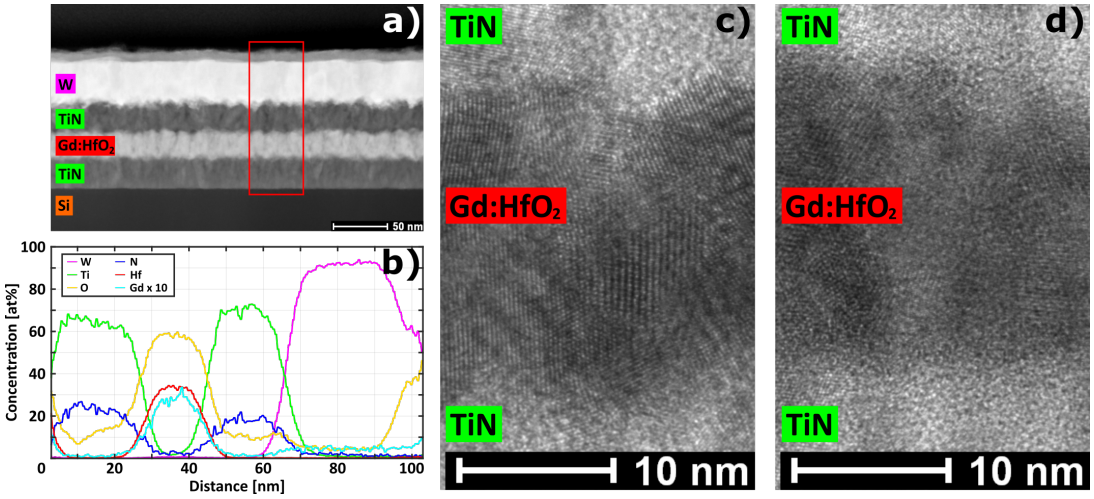

Figure 3.4: a) TEM image of annealed sample where the W/TiN/Gd:HfO_2/TiN/Si capacitor structure can be seen; b) EDX along the red box indicated in a), where Gd signal is amplified by a factor 10 for better visualization; c) HRTEM detail in which a stronger crystallization of the N_2 annealed film can be seen with respect to the d) as-deposited sample.

GIXRD results are exhibited in Fig. 3.5. It is common to plot XRD results in the 2θ region from 27 to 33 °, where the characteristic peak for the ferroelectric orthorhombic phase is observed at ≈ 30.4 °. In Fig. 3.5a and b it is clear that a peak at 30.4 ° is detected for all annealing conditions starting from 400 °C. This provides evidence for the presence of ferroelectric orthorhombic phase in these Gd:HfO_2 PLD films, although it is noted that XRD is limited in this respect because it is difficult to separate the contributions of ferroelectric orthorhombic phase and non-ferroelectric tetragonal phase [146]. This scan range also enables detection of the presence of non-ferroelectric monoclinic phase, characterized by diffraction peaks appearing at ≈ 28.3 and 31.6 °; no such peaks were observed though, suggesting a mostly m-phase free film. The XRD plots unequivocally show how crystallinity is significantly enhanced by an annealing of just 40 s at 400 °C as inferred by the much higher magnitude of the XRD peak for this condition with compared to as-deposited. A further increase of the annealing thermal budget, up to 450 °C and for a longer annealing time, does not result in a remarkable change of the XRD peak at 30.4 °. Fig. 3.5a and b also show that the quality of the main diffraction peak at 30.4 ° does not seem to depend on the annealing ambient, with both O_2 and N_2 giving nearly identical diffraction profiles. This is in agreement with other previous reports which explored different annealing atmospheres on HZO [147, 148].

However, the wider scan range for the two samples annealed at 450 °C for 80 s shown in Fig. 3.5c, which includes other secondary HfO_2 and TiN peaks, highlights a few differences between the two films. First, the O_2 annealed sample presents a very small peak at ≈ 25.2 ° which could possibly be associated to the (011) orientation of the m-phase: the N_2 annealed sample does not show it and instead displays a stronger reflection at ≈ 35.4 °, in correspondence of the o-002/t-110 peak. This might indicate that the

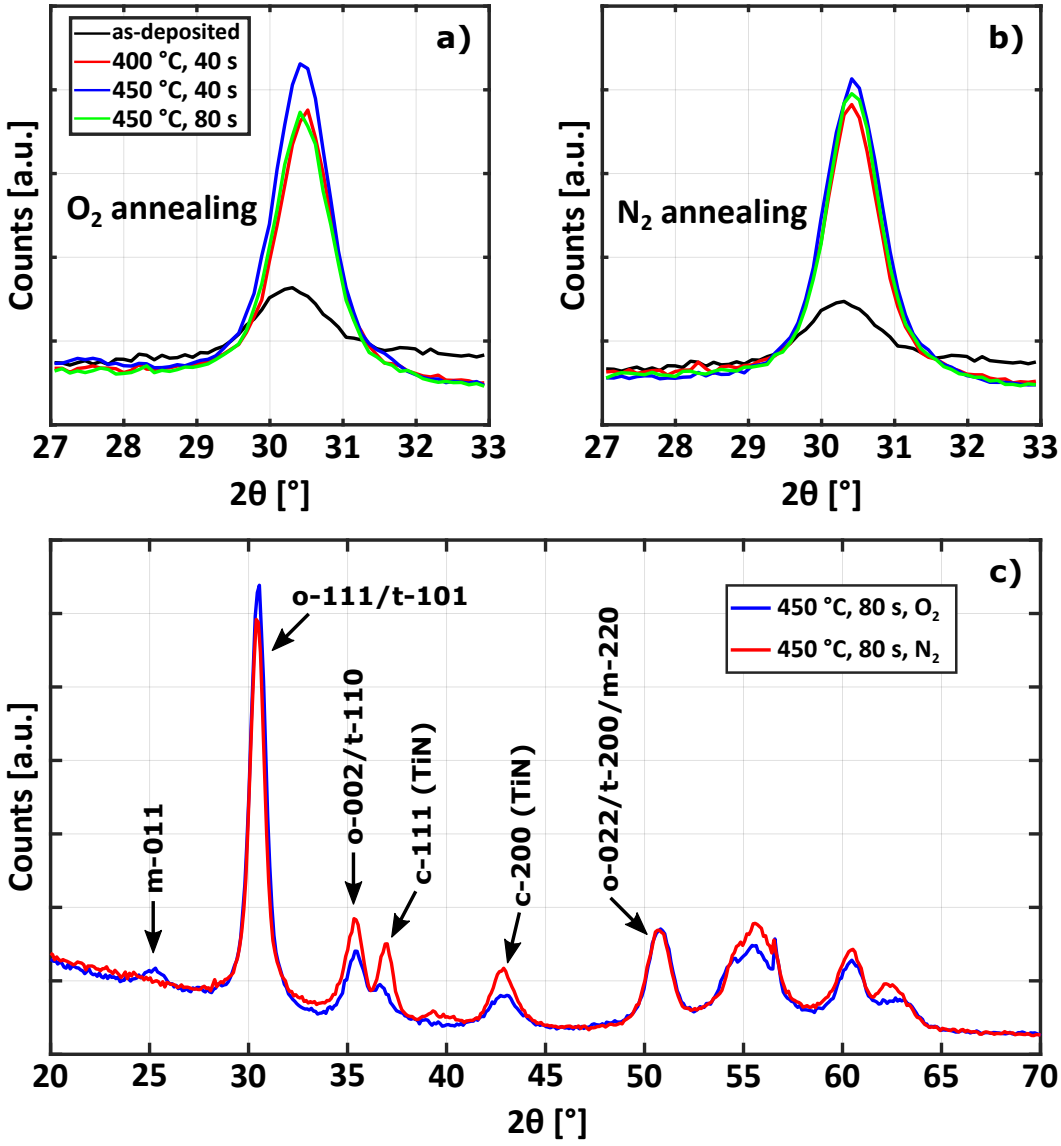

Figure 3.5: GIXRD characterization of Si/TiN/Gd:HfO_2/TiN stack in the 27-33 ° 2θ region for samples annealed a) in O_2 and b) in N_2; c) a wider scan taken on the two samples with highest annealing budget and showing other secondary HfO_2 and TiN peaks.

annealing in N_2 is more efficient in preventing m-phase formation, even though both samples seem to be almost entirely free from it. The second feature that can be noticed in the wider scan is a weaker signal of the c-TiN peaks at $\approx$ 36.8 and 42.9 ° for the O_2 annealed film. This might indicate an expected stronger TiN oxidation into TiO_xN_y or rutile TiO_2 for the O_2 sample, for which however no matching peaks were found. As for the peaks detected for $2\theta > 50$ °, they could not be clearly attributed because many phases present higher order diffraction peaks at very close angles.

The oxidation state of the TiN electrodes is investigated by means of XPS by comparing as-deposited, N_2 annealed and O_2 annealed (450 °C, 80 s) samples. The results are shown in Fig. 3.6, where the element concentrations are superimposed for the three cases: here, the as-deposited sample can be considered as reference in order to see the effect of annealing. Looking at the O counts, it is possible to see how indeed there is higher diffusion in both electrodes for the O_2 annealed sample; the effect is particularly evident in the top electrode, meaning that the formation of TiO_xN_y or TiO_2 is likely. Other features that can be noticed in the same sample are a slightly higher migration of Ti in the ferroelectric layer and of Hf in the bottom electrode. The XPS analysis illustrated in Fig. 3.6 does not allow having such high resolution as EDX results reported in Fig. 3.4b, however the concentration profiles in the N_2 annealed and as-deposited films look overall very similar, having sharper interfaces and a lower intermixing of species compared to the sample annealed in O_2. It is therefore arguable that the two films might also have a different electrical behavior.

From microstructural characterization it emerges that the quality of electrodes and ferroelectric/electrode interfaces is an aspect where there is certainly room for improvement and optimization. One example is the in-situ deposition of TiN by PLD, which would ensure that full capacitor stack is obtained without breaking vacuum. Exploiting the great flexibility of PLD, an appropriate control of O_2 and N_2 flows during deposition of each different layer can be achieved and higher quality interfaces could be obtained.

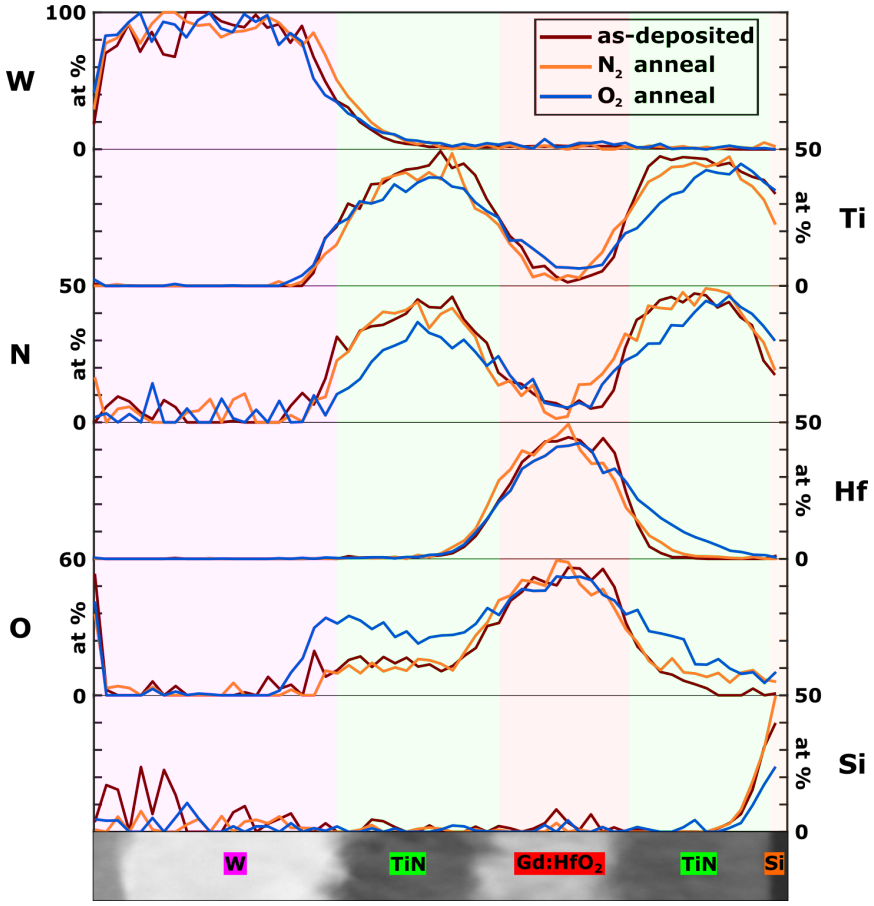

Figure 3.6: XPS analysis revealing the atomic concentration on Si/TiN/Gd:HfO_2/TiN/W structures for as-deposited, N_2 and O_2 annealed samples (450 °C, 80 s).

3.3 Ferroelectricity in low thermal budget Gd:HfO_2 films confirmed

Further to the structural signatures of ferroelectric orthorhombic phase, electrical characterization has been used to confirm whether Gd:HfO_2 PLD films are truly ferroelectric. Polarization versus electric field (P-E) measurements were performed on the capacitor structures with a triangular signal having an amplitude of 5 V (2.4 MV/cm) and a frequency of 1 kHz. All devices in this study required a wake-up procedure in order to reach the optimal hysteretic polarization reversal, which in the present case consisted of 1000 cycles at 2.6 MV/cm at 1 kHz. This wake-up effect has been observed previously for various Hf-based ferroelectric films [2, 31, 47, 48, 77, 83, 99, 106, 137, 139, 149]. Fig. 3.7a and b show P-E characteristics for the as-deposited and annealed (in O_2 and N_2 respectively) devices. The as-deposited sample displays nearly non-hysteretic response even after a wake-up procedure. For all the N_2 and O_2 annealing conditions the P-E plots show a pronounced hysteretic behavior, and this is further illustrated by the typi-

cal butterfly loop described by the relative dielectric constant ϵ_r in Fig. 3.7c and d, for annealing in O_2 and N_2 respectively.

C-E curves were measured independently on the same setup used for P-E, and the relative permittivity ϵ_r was calculated from those. This clear ferroelectric behavior indicates that the diffraction peak previously observed in the XRD is attributable mainly to the ferroelectric orthorhombic phase of Gd:HfO_2. The ϵ_r-E curves of Fig. 3.7c and d show a higher relative dielectric constant, and a greater variation, for the O_2 samples. It is known that o-phase of HfO_2 has a lower value of permittivity than t-phase, therefore a higher presence of o-phase in the N_2 samples could be speculated [2, 66, 107, 108]. The stronger polarization response detected in the P-E loops might support this claim. A competing scenario is to consider the TiN electrode layers as partially oxidized into TiO_2 and thus having a higher dielectric constant, as suggested in a previous study [108].

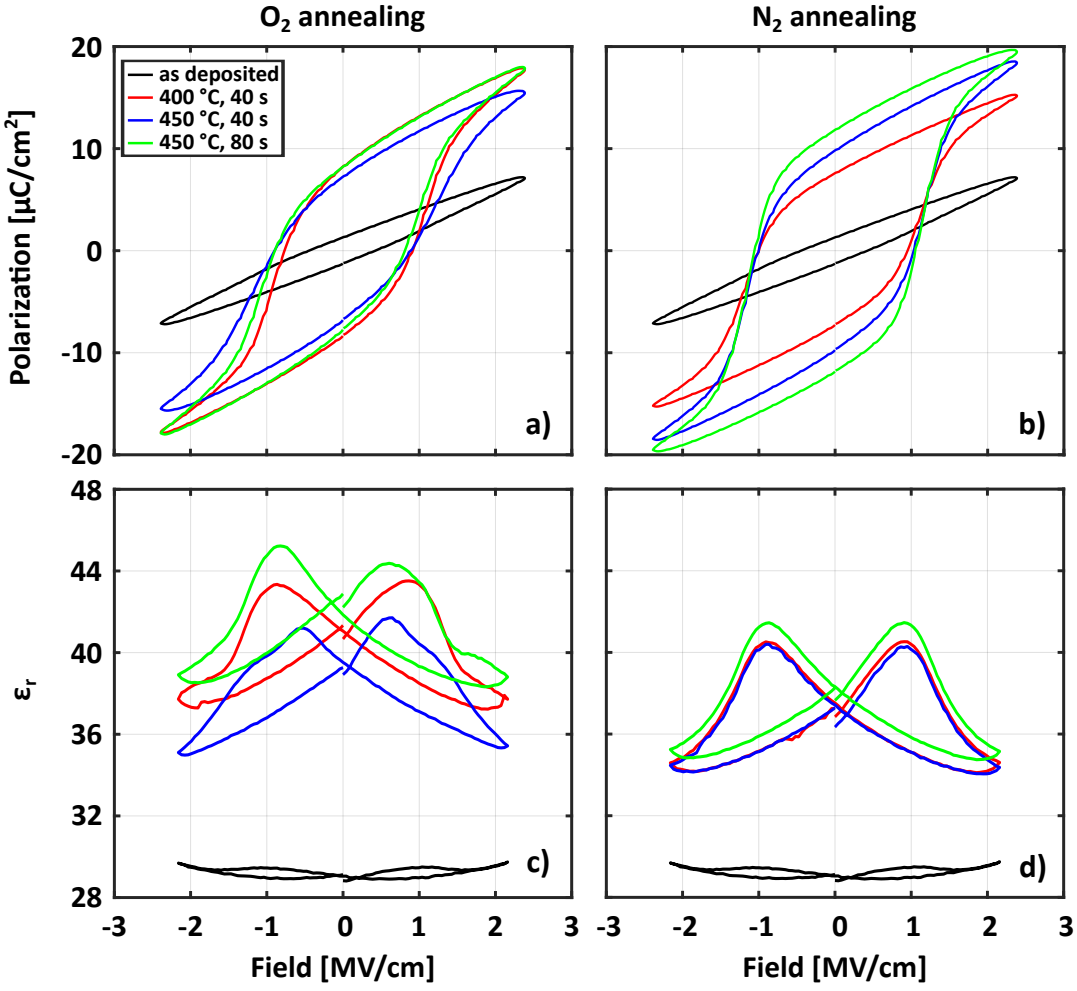

Figure 3.7: Effect of different annealing conditions on ferroelectric properties of Gd:HfO_2 thin films: a) P-E and c) ϵ_r-E curves for samples annealed in O_2; b) P-E and d) ϵ_r-E curves for samples annealed in N_2.

It was alluded to earlier that partial crystallization of the PLD film occurs during the

330 °C deposition itself. The P-E characteristics in Fig. 3.7 confirm however that the combined thermal budget of the PLD deposition (330 °C) plus annealing (400-450 °C) is necessary in order to observe ferroelectric P-E loops. As mentioned before, PLD growths were also performed at 220 °C but no crystallization was observed in the XRD and a higher thermal budget exceeding CMOS compatibility was necessary in the subsequent annealing in order to induce crystallization. Films deposited at higher temperature (380 °C and above) instead resulted in greater crystallization but these samples did not exhibit ferroelectric P-E loops as-deposited, and subsequent annealing rendered polarization characteristics which were dominated by leakage. This aspect of the work demonstrates one advantage of the PLD process where the deposition temperature can be tuned to minimize the annealing thermal budget.

Further analysis of the data in Fig. 3.7a and b shows that both the thermal budget and the annealing environment make a noticeable difference with respect to the ferroelectric behavior of the device, something that was not so clearly appreciable in the XRD diffraction pattern. The sample annealed in N_2 at 450 °C for 80 s shows a remanent polarization $P_r = 12$ µC/cm^2. The thermal budget plays a significant role in N_2 annealing for the samples investigated here, with a P_r increase of 60 % on increasing the anneal temperature and time from 400 °C to 450 °C and 40 s to 80 s respectively. The samples annealed in O_2 ambient exhibit lower polarization, with a maximum measured P_r of 8 µC/cm^2, and there seems to be a reduced influence of annealing thermal budget. In order to see whether the trend of ferroelectric response increasing with higher thermal budget continues further, annealing at 500 and 550 °C was performed. This though leads to a loop degradation regardless of the annealing ambient at 500 °C, or just leakage at 550 °C, to the extent that samples could not be measured at all.

The fact that it was possible to electrically measure the ferroelectric response of the O_2 annealed HfO_2 films attests to the fact that the oxidation of the top electrode speculated after the XPS analysis (see Fig. 3.6) is not so dramatic. At the same time, it should be noted that the P-E loops shape is clearly different when comparing the N_2 and O_2 annealing: all N_2 annealed samples show a sharper and symmetrical switching at $E_c = \pm 1$ MV/cm, compared to the less saturated loops for O_2 annealed samples, where E_c changes according to the thermal budget. A small horizontal shift of ≈ 0.1 MV/cm towards the right is noticeable for the samples annealed in O_2, suggesting a small asymmetry of the interfaces and more uneven defect distribution in those sample. However, the measurements of Fig. 3.7 were collected after a wake-up procedure of 1000 cycles, when defects such as O vacancies might have mostly redistributed and reduced this effect. A similar behavior for N_2 and O_2 annealed samples was observed before [147].

Another difference in the P-E curves between the samples annealed in different conditions is the overall lower polarization measured for the samples annealed in O_2. This can be linked to the partial oxidation of the top electrode suggested by the XPS results of Fig. 3.6: it is indeed possible that the voltage actually applied to the ferroelectric during the measurement is reduced from the nominal value and thus the ferroelectric response is smaller. Pristine capacitors were also measured in order to investigate the initial imprint, but they show just a slightly leaky dielectric behavior. By taking consecutive measurements (up to 15-20) the leakage progressively reduces but the loop does

not open up yet. The training procedure described before for the wake-up (1000 cycles) is necessary to obtain any ferroelectric response: as a consequence, the initially pinched loops that are sometimes reported in literature could not be observed here.

Leakage tests were performed on these devices after the same training procedure of the measurements shown in Fig. 3.7: current densities in the order of 10^{-6}-10^{-3} A/cm^2 were measured on the devices at a field of 2 MV/cm, within the range of values commonly reported in literature for hafnia-based ferroelectrics [77, 99, 133, 140, 149, 150]. It is noted however that a higher leakage is consistently measured for O_2 annealed samples. It is possible to think that the partial oxidation of the electrodes and larger interdiffusion of species observed in Fig. 3.6 introduced more defects close to the ferroelectric/electrode interface, which is also more energetic. The increased number of defects and their high mobility can explain the larger leakage current density observed for the O_2 annealed samples with respect to N_2 annealed ones.

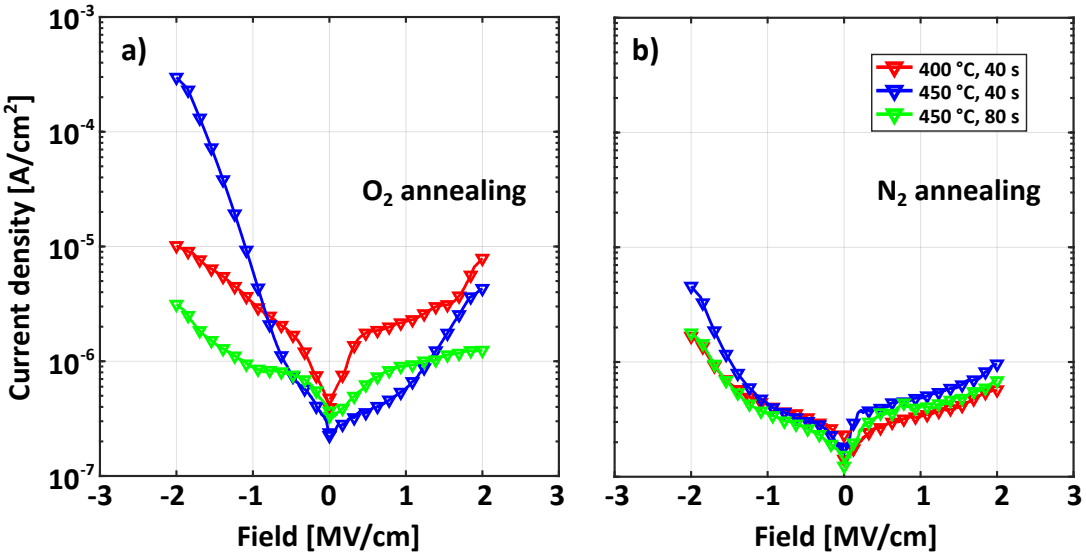

Figure 3.8: Leakage current density versus electric field for a) O_2 and b) N_2 annealed samples.

An application-relevant property of ferroelectrics is their endurance, that is their resistance to voltage cycling, hence this is now evaluated: fatigue tests were conducted using a rectangular wave with amplitude 2.6 MV/cm and frequency 1 kHz. Endurance plots for the two samples whose annealing thermal budget gave the best polarization response, that is 450 °C for 80 s, are shown in Fig. 3.9a. Both samples undergo a similar wake-up phase in the first 10^3 cycles but then exhibit markedly different behavior. Fig. 3.9b compares the P-E loops measured at 10^3 cycles (wake-up) and the last loops acquired before breakdown for both samples. It can be seen that in the case of the N_2 sample the E_c remains constant and the P_r increases from 10 to 12 µC/cm^2 (20 % improvement), until sudden breakdown (BD) occurs after 10^6 cycles. Hoffmann et al [31] similarly observed breakdown after 10^6 cycles for 10 nm Gd:HfO_2 films deposited by ALD where a 10 minute 450 °C annealing in N_2 was employed. In examining the O_2 sample, Fig. 3.9a

shows that the fatigue process occurs instead gradually, with a progressive reduction of the P_r from 8.8 to 5.7 µC/cm^2 (35 % loss). Despite this degradation, the O_2 annealed film was able to sustain more than 10^7 cycles. For the film annealed in O_2, Fig. 3.9b gives an even clearer picture of the gradual degradation of the film: the loop becomes more rounded, an increase of E_c and decrease of P_r are registered. Looking at Fig. 3.9a it can also be noticed that the onset of fatigue comes slightly before 10^4 cycles for the O_2 sample, indicating that the recovery process occurring during wake-up is not yet fully accomplished for this sample.

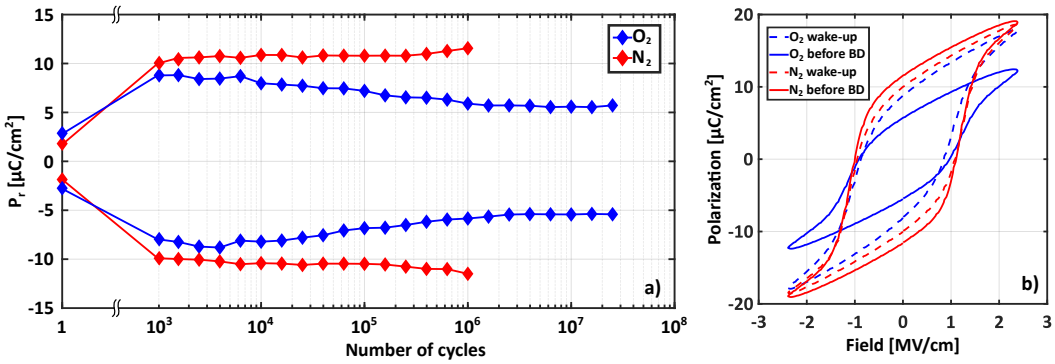

Figure 3.9: Fatigue behavior comparison between N_2 and O_2 annealed samples (450 °C, 80 s); after an initial wake-up procedure of 10^3 cycles, the evolution of P_r vs number of cycles is plotted in a); the comparison of loop degradation at 10^3 cycles and before breakdown (BD) for both annealing conditions is shown in b).

An improvement of fatigue endurance associated with higher leakage conduction has been observed in earlier studies of perovskite ferroelectric capacitors [37], however a similar model of fatigue has not been established yet for HfO_2-based ferroelectrics. Assuming that fatigue is due to the inhibition of nuclei of opposite polarization domains caused by trapped charge, it can be speculated that oxygen annealing alters the structure and energy of defects and reduces the nuclei blockage. The N_2 annealed film on the contrary undergoes a small change in the P-E loop profile during the test, up to 10^6 cycles where sudden breakdown occurs. It is expected that sharper hysteresis loop and high spontaneous polarization result in a relatively early breakdown after voltage cycling. One explanation for this phenomenon is that during polarization reversal the interface-adjacent layer of the ferroelectric is always exposed to a very high transient electric field, with consequent charge transport and defects formation in the near-by-interface region of the film [151]. In view of the previous discussion, it is also possible that a field lower than nominal was applied to the O_2 annealed sample, and this might also cause the higher endurance observed for that film. Overall, the difference in endurance behavior according to annealing environment suggests that the composition of annealing atmosphere could be viewed as a parameter to tune in order to find the best trade-off between switching polarization and endurance, but further work is necessary to clarify this effect.

To summarize, the best P_r value achieved in this work was 12 µC/cm^2 for the sample

annealed in N_2 at 450 °C for 80 s. In comparing this with relevant studies in the literature it is noted that Sharma et al. [139] reported a P_r of 12 µC/cm^2 for Gd:HfO_2 deposited using PLD at 650 °C. Remanent polarization values > 30 µC/cm^2 and comparable to the state of the art for hafnia films have been demonstrated in previous PLD reports on HZO [75, 76, 150], although the thermal budget requirements in those cases was much higher with PLD growth temperatures ranging from 700 °C to 800 °C. For previous studies employing the ALD technique to grow Gd:HfO_2 it is noted that Mueller et al [44] and Park et al [137] reported P_r of 12 µC/cm^2 and 10 µC/cm^2 with annealing temperatures of 1000 °C to 800 °C respectively, while Hoffmann et al [106] reported $P_r \approx$ 15 to 18 µC/cm^2 with annealing in the range 450 °C to 800 °C.

Therefore, while it is clear that the P_r for the films in this work is lower than state of the art values obtained for ferroelectric hafnia, it is comparable to that reported in other studies using Gd:HfO_2 material grown with either PLD or ALD, and is achieved using a competitive thermal budget. The doping level of Gd in the hafnia films in this study is 3.0 %, and it is possible that a slightly different doping level may be required in order to optimize P_r. This is however beyond the scope of this study as for the PLD technique this requires obtaining a new target material, and is not simply a matter of changing the cycle ratio as would be the case for ALD process.

3.4 Summary

A low temperature process for the fabrication of ferroelectric Gd:HfO_2 on TiN layer by PLD was demonstrated. The maximum thermal budget never exceeds 450 °C and ferroelectric behavior is reported already after a 400 °C annealing, which renders this method compatible with CMOS BEOL processing.

A remanent polarization of 12 µC/cm^2 and a coercive field of 1 MV/cm were obtained, comparable to previous reports on ALD films. The annealing in O_2 was investigated besides the most common N_2 environment. This most notably led to an increased endurance of the film under electrical cycling, which came along with a significant degradation of polarization response. Such behavior is strikingly different from that of films annealed in N_2 with equivalent thermal budget, which show no degradation and incurred a sudden breakdown after shorter number of cycles. This suggests that annealing atmosphere can be tuned in order to achieve a better trade-off between fatigue behavior and switching characteristics. In addition, the O_2 annealing enhances the compatibility with functional oxides which do not tolerate well N_2 environments.

While this work only represents a starting point and further optimization of the process is still necessary, it reveals how to exploit the advantages of PLD technique with respect to more commonly used ALD, namely the kinetically as opposed to chemically driven deposition mechanism, which gives a greater flexibility in the choice of process parameters. In particular, it was illustrated how the appropriate balance between thermal budget during deposition and annealing is a crucial requirement in order to meet the constraints of CMOS compatibility. Specifically, an increase in deposition temperature

is essential in order to achieve some initial crystallization, which is completed after the annealing under top electrode encapsulation. On the contrary, in order to crystallize samples annealed at lower temperature, a higher thermal budget was necessary, that is not suitable with CMOS BEOL processing.

4 | Robust PFM technique to analyze ferroelectricity in HfO_2

This chapter demonstrates the strength of off-resonance PFM analysis by showing how it can not only corroborate results coming from other characterization techniques but also integrate them by accessing properties otherwise undetectable: examples are domains behavior or subtle features in piezoelectric coefficient d_{33}, which can be related to presence and stability of different phases. The chapter comprises two sections: in the first one, the aspects that ensure a reliable off-resonance PFM investigation are discussed, showing how this techniques makes it possible to obtain both excellent qualitative and quantitative results, even for thin ferroelectrics with very small electromechanical response. The second section reports a study on the endurance behavior of undoped HfO_2, where electrical P-V results are taken as a starting point for in-depth PFM analysis of phase evolution in the material.

Ferroelectric materials are characterized by their electromechanical coupling: as piezoelectrics, they can change in size if exposed to an electric field and vice versa generate a field when mechanically strained. In addition, they possess two or even more equilibrium states, with presence of spontaneous polarization pointing in different directions when no field is applied. The characterization of electromechanical properties of ferroelectric devices is therefore very important both for applications and to understand the nature of polarization switching. In fact, since its invention in the mid-90s, PFM has been used to investigate ferroelectrics and reach deeper insights into the mechanisms governing the electromechanical response of materials [117].

The working principle of AFM and PFM were introduced in chapter 2. Specifically, it was stressed that a few key aspects are of paramount importance in order to obtain a genuine quantification of ferroelectric response in very thin films with low piezoresponse, namely:

- measuring off-resonance, that is far from f_r of the tip + sample system;
- detecting the response through a top electrode;
- using a hard cantilever.

The first point ensures that a quantification is possible, the last two that electrostatic

interaction is absent from the collected response. Here, a more in-depth account of the subtle details noticeable in ferroelectric loops acquired by off-resonance PFM is given in the first section, showing what the criteria to recognize a true ferroelectric response are and how to quantify it. Two elements are highlighted in this section: the shape of on-field loop and the comparison with relative off-field measurement, and the analysis at different frequencies. The accuracy and reliability of off-resonance PFM measurements is a preeminent aspect for the quantification of true ferroelectric response of thin films with such low d_{33} as the ones analyzed in this work.

The second section presents a study on undoped HfO_2, where the endurance behavior of the material is explored by analyzing both collections of local loops and surface scans taken by off-resonance PFM at different stages of voltage cycling. In this work, some features observed in the electrical characterization are taken as starting points to dig deeper into the evolution of switching behavior at the domain level. A qualitative and quantitative account on the effect of electrical cycling is achieved inspecting the changes in electromechanical response by measuring the effective d_{33}. Overall, the presented results not only confirm findings from electrical measurements but also enrich them offering an alternative look into the transformations taking place at different stages of cycling with nanoscale resolution.

4.1 Quantifying genuine ferroelectricity in thin films with low piezoresponse

The class of HfO_2-based ferroelectrics is intensely investigated since its discovery due to the peculiar property of retaining ferroelectricity at very low thickness. While this is of interest scientifically and technologically, the electromechanical characterization of such materials is more challenging than for example PZT, due to their lower response. In this context, it is not easy to quantify such response even with high-resolution techniques such as PFM. A number of publications report PFM measurements on HfO_2-based ferroelectrics where polarization response is normally plotted either in V or in arbitrary units, effectively limiting the analysis to a qualitative description [86, 113, 114, 117, 118]. This is due to the acquisition method that always relies on working close to the resonance frequency of the tip-sample system and makes quantification very challenging. Here, a method to obtain good qualitative results and at the same time quantify them is employed: the key aspect of this approach is to work off-resonance. This makes the technique slower but surely more straightforward since no processing of the measured response has to be performed: as a consequence of that, the interpretation of results also becomes more unequivocal.

In order to make sure that the off-resonance measured piezoresponse can be correctly quantified, a few experimental conditions have to be satisfied as reminded before. These reflect in some distinct features in the collected loops which will be highlighted in this section: the shape of the loops and comparison between on- and off-field, and the frequency independence of the collected signal in a range of frequencies that is clear of

resonance.

Planar capacitors were realized for this analysis as explained in appendix: HZO is sandwiched between two TiN electrodes and a top layer of Pt is deposited for electrical contact; the measurement is performed through the top electrode which is ≈ 30 nm thick in total (TiN + Pt). HZO was chosen among the many HfO_2-based ferroelectrics because it is one of the most studied and well characterized due to its excellent properties. In particular, a film of 10 nm is used because it is usually reported as an optimal thickness for this material [2, 51, 98]. What just said makes the 10 nm thick HZO film analyzed in this work an ideal candidate to explore the subtleties of electromechanical response in PFM characterization. Results on a 30 nm thick film are also reported: this thickness is considered to be close to the point where ferroelectricity in HfO_2-based thin films becomes unstable. It will be shown how PFM analysis can be used to investigate also this aspect of ferroelectrics.

4.1.1 On-field loop shape and comparison with off-field

The main reason behind measuring on- and off-field loops is to check that the detected signal is actually coming from the electromechanical response of the material and no other interactions such as electrostatic forces are present. This analysis also shows whether the film retains its polarized state. The sample is probed by an ac signal superimposed to a step-like dc voltage function: the resulting waveform employed for the measurement is illustrated in Fig. 4.1a. The on-field loop is acquired when the bias is applied; when it is removed, the small ac bias is used to acquire the off-field.

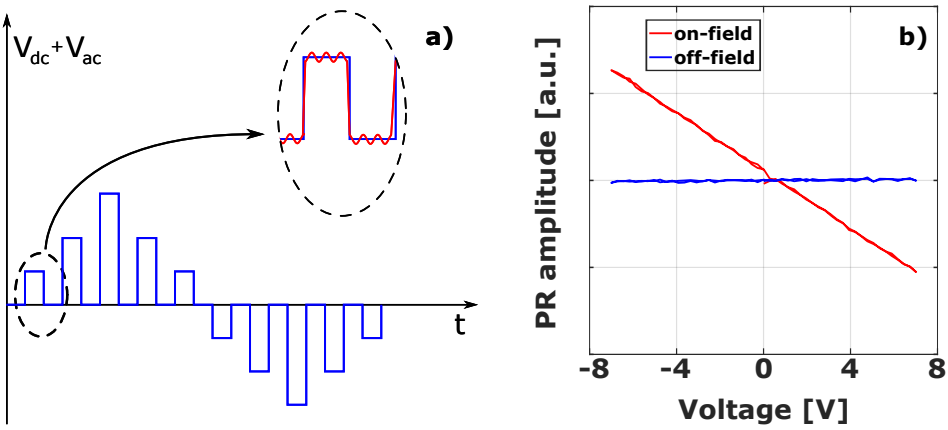

Figure 4.1: a) The complex voltage waveform used to acquire on-field and off-field loops in PFM, consisting in a superposition of dc and ac voltage; b) expected effect of electrostatic interaction when a strong ac signal of 1.5 V is applied (on-field) with respect to the case when ac bias is not present (off-field).

It is important to remind here that the collected signal is proportional to the applied ac voltage V_{ac} as illustrated in Eqn. 2.11 in chapter 2: as a consequence, higher V_{ac} is

preferable in that it gives a stronger signal to noise ratio. However, an upper limitation to V_{ac} comes from the nature of ferroelectric materials: it is indeed crucial to maintain probing voltage lower than V_c, otherwise the film is switched during the measurement itself. In this work, the probing ac voltage was maximum half the coercive voltage for every measured sample, and in most cases even smaller.

The first step in order to distinguish between ferroelectric and electrostatic contribution is to appreciate that the latter is expected to have linear dependence on the voltage applied to the tip, a very different behavior than ferroelectric response [117]. A clear indicator of electrostatic contribution is, in the on-field case, the superposition of a constant slope to the ferroelectric loop that makes it look as if it was partially rotated clockwise. A qualitative visualization of how a pure electrostatic response looks like can be obtained by performing a dc voltage sweep while keeping the tip detached from the sample but in close proximity to it, as illustrated in Fig. 4.1b. This measurement is carried out with a very high ac voltage of 1.5 V (which was never used in practice for any measurement in this work) and shows the expected slope for the on-field case and an almost completely flat response for the off-field loop. As discussed previously, this follows from the two precautions that were adopted in order to eliminate the electrostatic contribution: measuring through a conductive top electrode and using a cantilever with high spring constant, since the electrostatic interaction is inversely proportional to the cantilever stiffness. These two actions can greatly reduce or even eliminate the problem [117, 121].

An example of on-field and off-field amplitude loops comparison is given in Fig. 4.2a for 10 nm thick HZO. The measurement was taken with a frequency of 92 kHz and probing ac voltage of 0.5 V, lower than the measured coercive voltage of ≈ 1 V. The two loops are very similar, which is another important indicator of the absence of electrostatic contributions and genuine ferroelectric nature of the measured response. The corresponding phase plot in Fig. 4.2c shows a perfect 180 ° phase jump, as expected from a good PFM measurement.

However, even with a very hard cantilever as the one employed in this work which possesses a nominal spring constant of 42 N/m, a little negative slope of the saturated signal, i.e. tips pointing down, can be observed in the on-field loop. This feature has a different nature and should not be confused with an electrostatic effect: it is actually a fingerprint of true ferroelectric behavior. The small decrease of the response signal for higher voltage is due to a delicate interplay of competing phenomena. In fact, d_{33} depends linearly on the polarization P but also on the relative permittivity of the material ϵ_r, via the equation

$$d_{33} = 2\epsilon_r \epsilon_0 Q P, \tag{4.1}$$

where Q is the electrostriction coefficient of the material. Considering only the region of the loop in which the applied voltage and the polarization are parallel, that is for example in the first quadrant after the positive coercive voltage in an increasing voltage sweep, ϵ_r and P have completely different behaviors. The relation of polarization with

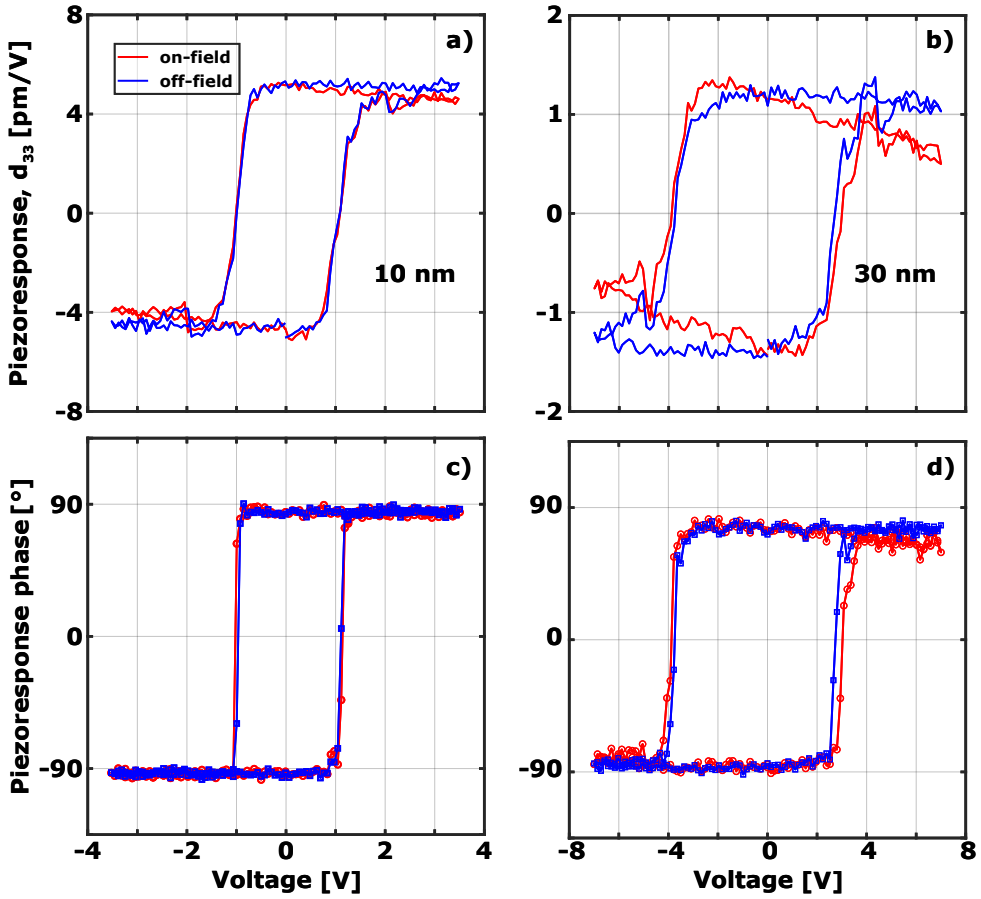

Figure 4.2: Off-resonance PFM amplitude loops on a) 10 nm and b) 30 nm HZO showing distinctive features of ferroelectric behavior; the loops were taken at 92 kHz with an ac voltage of 0.5 and 1.1 V, respectively; their corresponding phase plots are in c) and d).

voltage is quite straightforward, since it consists in a strong surge right after switching and then a slight linear increase with the voltage when saturation is reached. The relative permittivity on the other hand shows an opposite trend, starting from a peak value at V_c and decreasing nonlinearly when voltage increases [28, 102]. According to the balance between the two, the value of d_{33} at saturation can display a small reduction for increasing voltage, which is precisely what happens in Fig. 4.2a.

The PFM loop shown in Fig. 4.2b and d is acquired on 30 nm thick HZO with an ac voltage of 1.1 V and frequency of 92 kHz. Another distinctive characteristic of genuine ferroelectric response is the hump which can be seen in the fourth quadrant of the on-field loop: with increasing voltage amplitude in the direction antiparallel to the polarization state, the material response still increases right before it reduces to zero at V_c, where the polarization state switches. This apparently contradicting behavior is actually expected for this material and explained by the same d_{33} dependence discussed above. The 30 nm thickness is considered close to the ferroelectric-paraelectric transition for HZO: from other ferroelectrics such as PZT it is known that a phase transition is where the relative

permittivity ϵ_r presents the highest nonlinearity [28, 102, 152]. In the case of 30 nm sample the spike in ϵ_r is stronger than the decrease in P and therefore the behavior of Fig. 4.2b is observed. It is worth noting that measured d_{33} for 30 nm HZO is only ≈ 1 pm/V, attesting to the very high resolution achieved by off-resonance PFM technique.

4.1.2 Comparison of loops at different frequencies

Working away from resonance is done with the purpose to avoid an unknown or difficult to quantify signal amplification: this implies that ferroelectric responses acquired at different frequencies should all reasonably look alike and with very similar amplitude. This further adds credibility to off-resonance PFM technique and related quantitative results [102, 117]. A demonstration is given by taking consecutive ferroelectric loops on the same spot at different frequencies: here, 12, 92 and 230 kHz are chosen because the noise of the system is small and guarantees the best visualization and comparison of fine details, but other frequencies are possible too. The resonance frequency in air of the stiff cantilever is in the range 350-400 kHz and, once in contact, this value is usually multiplied by a factor 3-5. It follows that the three chosen frequencies are very far below the first f_r of the system. The results of this analysis are demonstrated on a 10 nm thick HZO film in Fig. 4.3, using a probing ac voltage of 0.5 V.

Looking at one frequency at a time, the quality of the measurement is testified once again by comparing on- and off-field and by seeing the peculiar behavior of tips pointing down for higher voltages. Looking at the phase plots, the clear polarization switch can be observed and the coercive field can be easily extracted. The 12 kHz frequency produces a slightly noisier signal but, when the three frequencies are compared, it can be seen that even the smallest kinks and other features are closely reproduced as expected. A remarkably small d_{33} of 5-5.5 pm/V is measured on this spot at all three frequencies, demonstrating the potential and reliability of off-resonance PFM.

To summarize, the presented results showed that peculiar elements such as tips pointing down in the on-field loop, the comparison between on- and off-field and an invariant response over a wide frequency range, are the key factors which prove that off-resonance PFM can reliably measure the genuine ferroelectric response of thin films with d_{33} as small as 1 pm/V. In conclusion, it shall be reminded that three things make this measurement method trustworthy, namely: using a stiff cantilever, performing the measurement through a thin conductive top electrode (TiN + Pt), and working off-resonance. As long as these requirements are satisfied during the analysis, it is expected that quantification is reliable on other ferroelectric thin films as well, as it will be shown later.

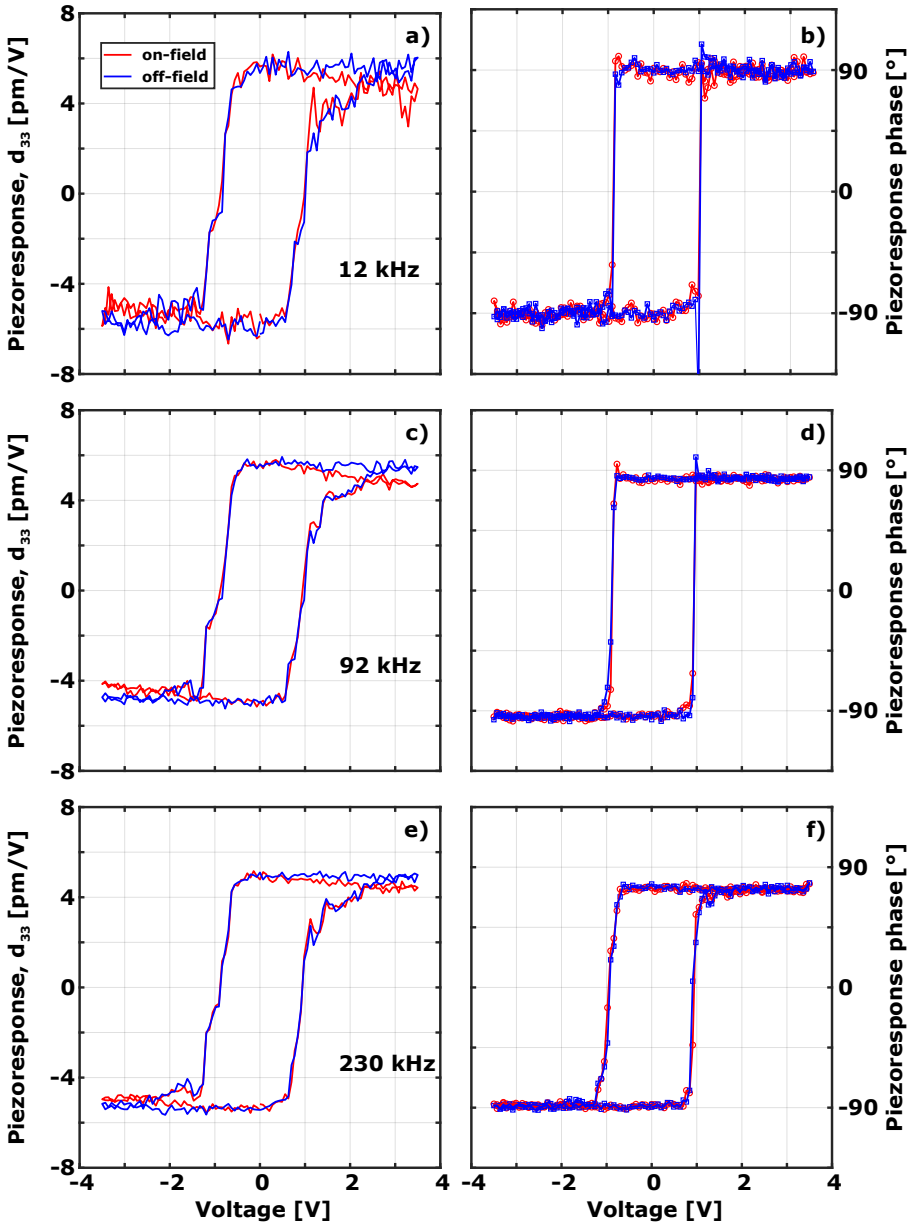

Figure 4.3: Off-resonance PFM amplitude (a,c,e) and phase (b,d,f) response on 10 nm HZO measured at 12 , 92 and 230 kHz respectively with ac voltage of 0.5 V.

4.2 Off-resonance PFM to unveil cycling behavior of undoped HfO_2

After ferroelectricity was demonstrated for HfO_2-based thin films doped with a great number of species, it was eventually reported also in pure, undoped HfO_2 [73]. At first the stability of orthorhombic phase seemed restricted to films thinner than 10 nm, quickly degrading for larger thickness as is common for the majority of HfO_2-based ferroelectrics [2]. It was later proved that depositing undoped HfO_2 by sputtering can extend the stability of orthorhombic phase up to 30 nm, and this was related to the different film growth dynamics with respect to ALD. A higher annealing thermal budget was reported in order to induce ferroelectricity, which was correlated to the room temperature sputtering deposition [99].

In particular, the authors noted a strong ferroelectric response already in the pristine state for films annealed at 1000 °C, and this has been attributed to the more homogeneous distribution of defects and ferroelectric domains in the film which is enabled by the high thermal budget [99]. However, a wake-up is still necessary in order to completely unlock the polarization of the material. This is related by several studies on HZO and other HfO_2-based ferroelectrics to the transformation of residual nonpolar m- or t-phase into ferroelectric o-phase [29, 108, 112, 115]. Here it is shown that PFM is a powerful technique to investigate the changes induced by electrical cycling in a thin film, observing the behavior of ferroelectric domains at the nanoscale and acquiring local d_{33} loops. The sample analyzed in this study is 10 nm undoped HfO_2 annealed at 1000 °C for 1 s; this sample was provided by Namlab group and further details about the fabrication process can be found in appendix. All PFM characterization is performed on 5x5 μm^2 capacitors, whereas the size for electrical characterization is 50x50 μm^2. For the sake of clarity, it shall be specified now that the bottom electrode is always grounded and the voltage is dynamically applied to the top electrode directly by the tip.

The analysis of pristine film reveals an internal bias field which causes an incomplete poling in the negative direction [99]. Fig. 4.4a-c show PFM amplitude, phase and topography obtained on 1x1 μm^2 scan for the pristine sample poled at -3 V for 1 s, also reported in [99]. The images were acquired with an ac voltage of 0.5 V, well lower than V_c, and frequency of 92 kHz. The amplitude plot shows some active regions (lighter) surrounded by areas with lower response (darker); very interesting is also the phase scan, which again testifies the incomplete switching of the material, with some regions positively poled even after the negative poling. The switching in positive direction is instead complete, as it can be seen in [99]. The topography plot is shown to prove that no crosstalk is interfering with the PFM acquisition. The PFM loops of Fig. 4.4d and e are also acquired with a frequency of 92 kHz and ac voltage of 0.5 V after negative prepoling and confirm the strong bias seen in the scan. Analyzing the amplitude plot, it can be noticed how the signal starts from a low value, indicating low retention: accordingly, the phase signal is noisier in the negative state than it is in the positive state. This shows that the sample tries to backswitch to its preferred orientation, that is with polarization pointing down. Another feature observed in PFM amplitude plot is that polarization

response of the material is stronger in the positive than in the negative direction, a detail which suggests the superposition of a ferroelectric response with another contribution, as will be explained later.

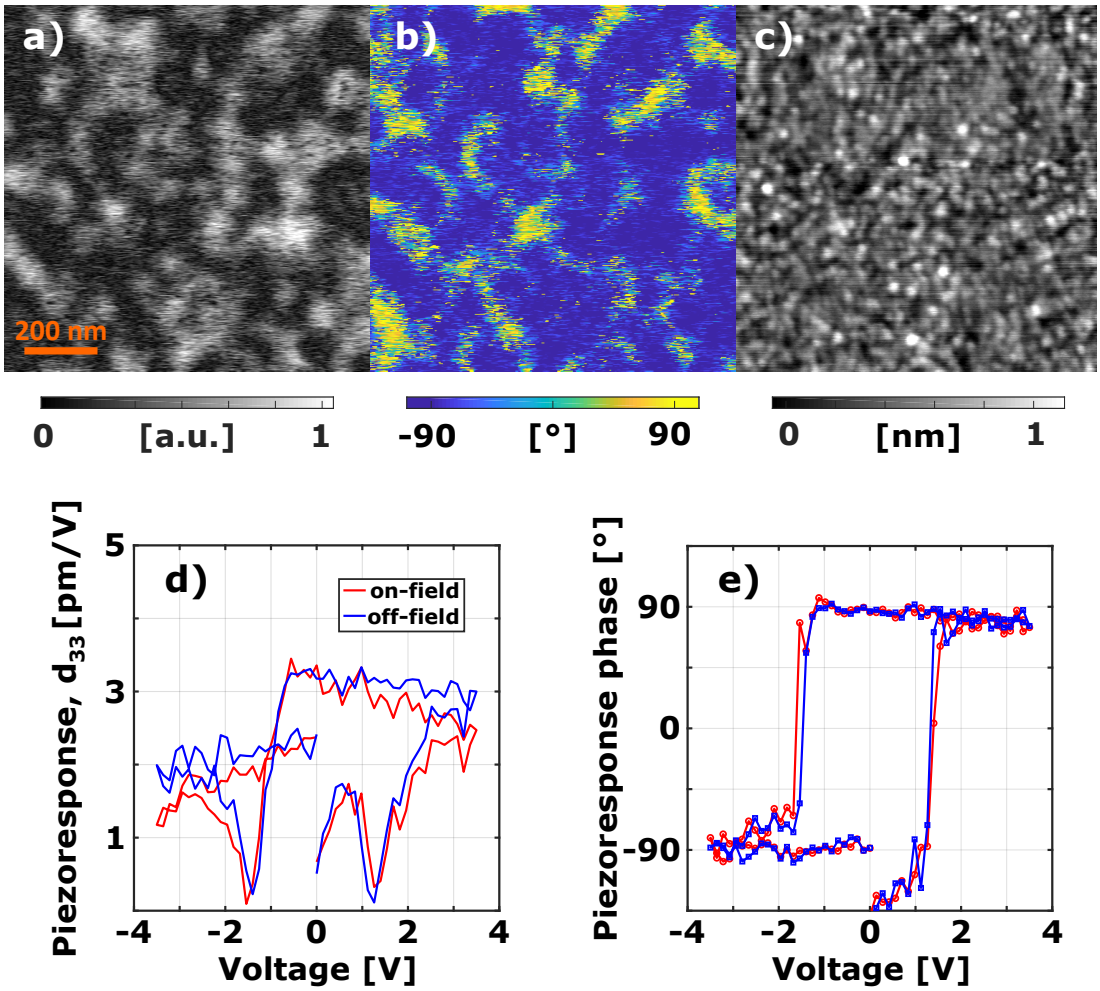

Figure 4.4: a-c) PFM scans showing piezoresponse amplitude, phase and topography signal, respectively, on pristine sample poled at -3 V. The scanned area is 1x1 μm^2; d) PFM amplitude and e) phase measured after negative prepoling also confirming the lack of retention in the negative state.

These results effectively indicate that imprint is present in the pristine material right after annealing: electrical cycling can be used to remove it and increase the polarization response of the material, as shown in [99]. In order to see the evolution of P_r and imprint in this film, an endurance test was performed; a square wave with frequency of 1 kHz and amplitude of 3 V (3 MV/cm) was employed for cycling the material, whereas measurements were taken at the same amplitude but with frequency of 2 kHz. Fig. 4.5 shows the resulting endurance plot, where an increase of P_r was indeed observed. A wake-up is achieved at 10^3 cycles, after which the polarization stays constant until sudden

breakdown at 10^6 cycles, in agreement to what was reported in [99]. The polarization increase is only around 20 % from ≈ 9 to 11 µC/cm^2: as discussed earlier, this is owed to the fact that the material already shows relatively high P_r in the pristine state.

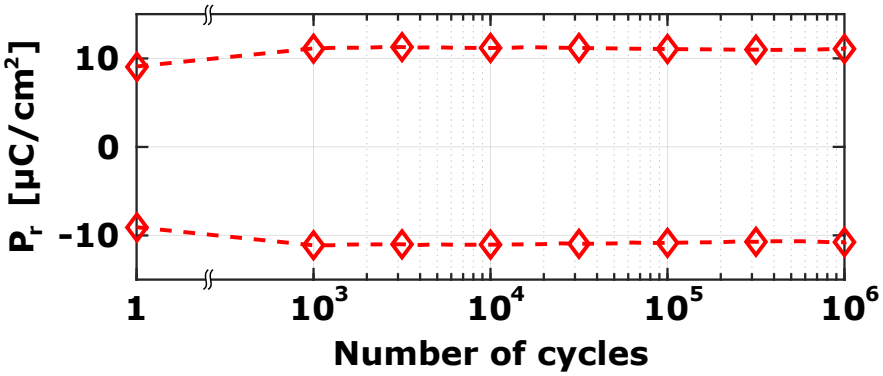

Figure 4.5: Endurance test of 10 nm thick undoped HfO_2. The training voltage is a square wave with amplitude of 3 V and frequency of 1 kHz.

The increase in polarization underlines a change in the material response to electric field; PFM analysis of films at different cycling states can shed light on this matter, given the ability to resolve the local domain switching. To this extent, PFM scans were taken at three relevant points highlighted by the fatigue plot. Pristine state is analyzed first; the sample is then tested at 10^3 cycles when wake-up seems to be fully achieved. Finally, one last analysis is performed before breakdown at 10^6 cycles. A LabView script uses the built-in signal generator of the Zurich Instruments lock-in amplifier described in chapter 2 to bias the tip and cycle the small capacitor. Same settings of the endurance test are used, namely a square wave with an amplitude of 3 V and frequency of 1 kHz.

The results are presented in Fig. 4.6. For each cycling state (pristine, 10^3 and 10^6 cycles) both PFM amplitude and phase images are shown. Scans were acquired at the negatively poled state, -3.5 V, then at 1.7 V where the positive switching initially occurs in the pristine material, and finally in the positively poled state at 3.5 V. The poling was achieved by applying a pulse of 1 s at the desired voltage. Each scan covers an area of 1x0.5 µm^2 and was taken with an ac voltage of 0.5 V and frequency of 92 kHz. The first thing that can be noticed by comparing pristine with trained film is that a more complete switching is achieved after training, and this can be seen by the phase plots. The entire analyzed regions switches to a homogenous phase both for -3.5 and 3.5 V. This was not the case for pristine material.

Looking at the respective amplitude plots, it can be seen that trained material displays an overall larger area with strong response, which appears brighter in the scan, especially in the negatively poled state. This observation indicates that a broader region of the sample became active and started to switch after electrical cycling, a fact that agrees with the picture of a field-induced transformation of residual t-phase in o-phase. The lower amplitude obtained for all cases in the middle column, which is around the coercive voltage, is an expected result: the polarization value is at its minimum, domains of two opposite orientations exist, and the positively poled ones are still very small and

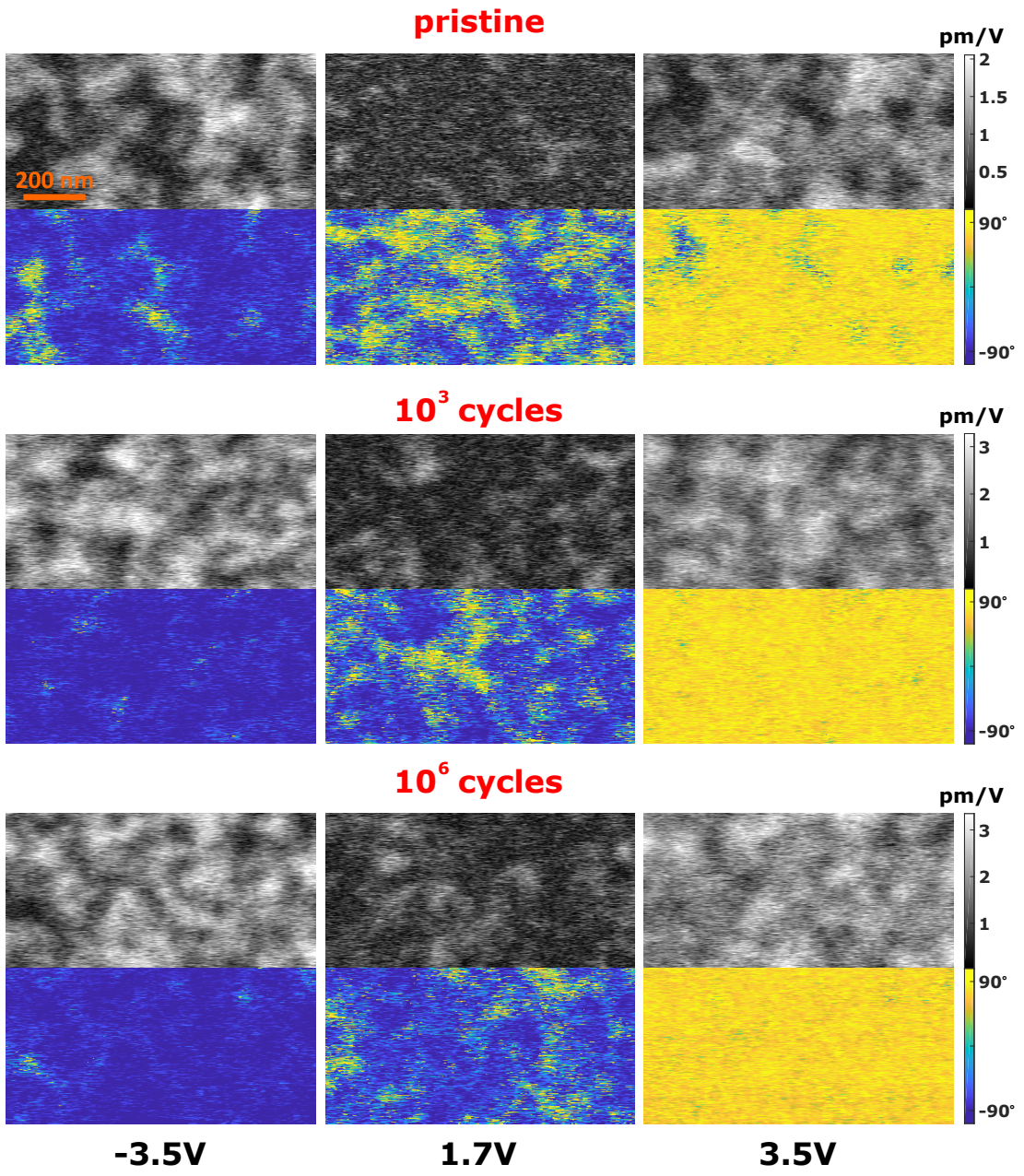

Figure 4.6: PFM amplitude (grayscale) and phase (color) acquired on undoped HfO_2 in pristine, 10^3 and 10^6 cycling state. Three poling conditions are analyzed: from left to right column the poling is -3.5, 1.7 and 3.5 V. The scan size is 1x0.5 µm^2. The intensity scale is the same for both trained conditions and is reduced only in pristine measurement in order to make features more visible.

growing. It is however possible to correlate the phase and amplitude scans at 1.7 V and see individual switching regions. The smallest identifiable domains are around 50 nm wide. It is expected that smaller features can be resolved through the top electrode, but here the very weak d_{33} of the material is probably the main obstacle to the detection.

Paying attention to the scale bars of amplitude plots, which express the effective d_{33} in pm/V, it can be noticed that a higher response is measured on average for the trained film, irrespectively of the number of cycles, in agreement with the endurance plot shown in Fig. 4.5. This response is still exceedingly low, at about 3 pm/V for the strongest spots, which corresponds to a maximum detected displacement of barely 1.5 pm.

When the poled states on the trained sample are analyzed, a full polarization can be inferred from the phase response while the amplitude still reveals brighter and darker regions. The continuum of values detected in the amplitude plot can be ascribed to a misalignment of the polarization orientation with respect to the vertical, out-of-plane direction. This response pattern however can also be associated to the presence of non-ferroelectric phase in the film; while a small amount cannot be excluded, it shall be said that the film was characterized and showed mostly presence of o-phase [99].

A more detailed quantification of the changes induced by electrical cycling was carried out by acquiring series of loops in the scanned region after each cycling condition. Arrays of 5x10 loops were collected and a wealth of results could be obtained from them, such as the distributions of coercive fields and average d_{33}. An ac voltage of 0.5 V and frequency of 92 kHz was used to measure the ferroelectric response. Results are presented in Fig. 4.7.

	V_c^+ [V]	V_c^- [V]	V_{bias} [V]	d_{33} [pm/V]	Δd_{33} [pm/V]
Pristine	1.29 ± 0.59	-2.08 ± 0.48	0.40	1.71 ± 0.39	0.62
10^3 cycles	1.67 ± 0.17	-1.68 ± 0.20	0.01	1.95 ± 0.22	0.11
10^6 cycles	1.69 ± 0.21	-1.71 ± 0.21	0.01	1.93 ± 0.23	0.01

Table 4.1: Quantitative results showing for each cycling condition the positive and negative coercive voltages, V_c^+ and V_c^- and the calculated internal bias V_{bias}; the average d_{33} and the difference between positive and negative response Δd_{33} is also reported.

A comprehensive summary of the quantitative findings is offered in Tab. 4.1. For each loop of the array, positive (V_c^+) and negative (V_c^-) coercive voltages are calculated. The average of the two is computed, changed of sign, and reported as V_{bias}. The d_{33} is also calculated for each loop in the following manner: a polynomial of first order is fitted to the saturation response for both the positive and negative sides of the loop. The intersections of resulting lines at zero voltage is taken as d_{33}. The Δd_{33} represents the difference between positive and negative measurements. To better visualize these quantities, an example showing how the data were calculated is given in Fig. 4.8a for a loop on the pristine sample, where a significant Δd_{33} can be observed. The average and error values reported in the table are calculated by fitting a Gaussian to all the loops collected in each single array.

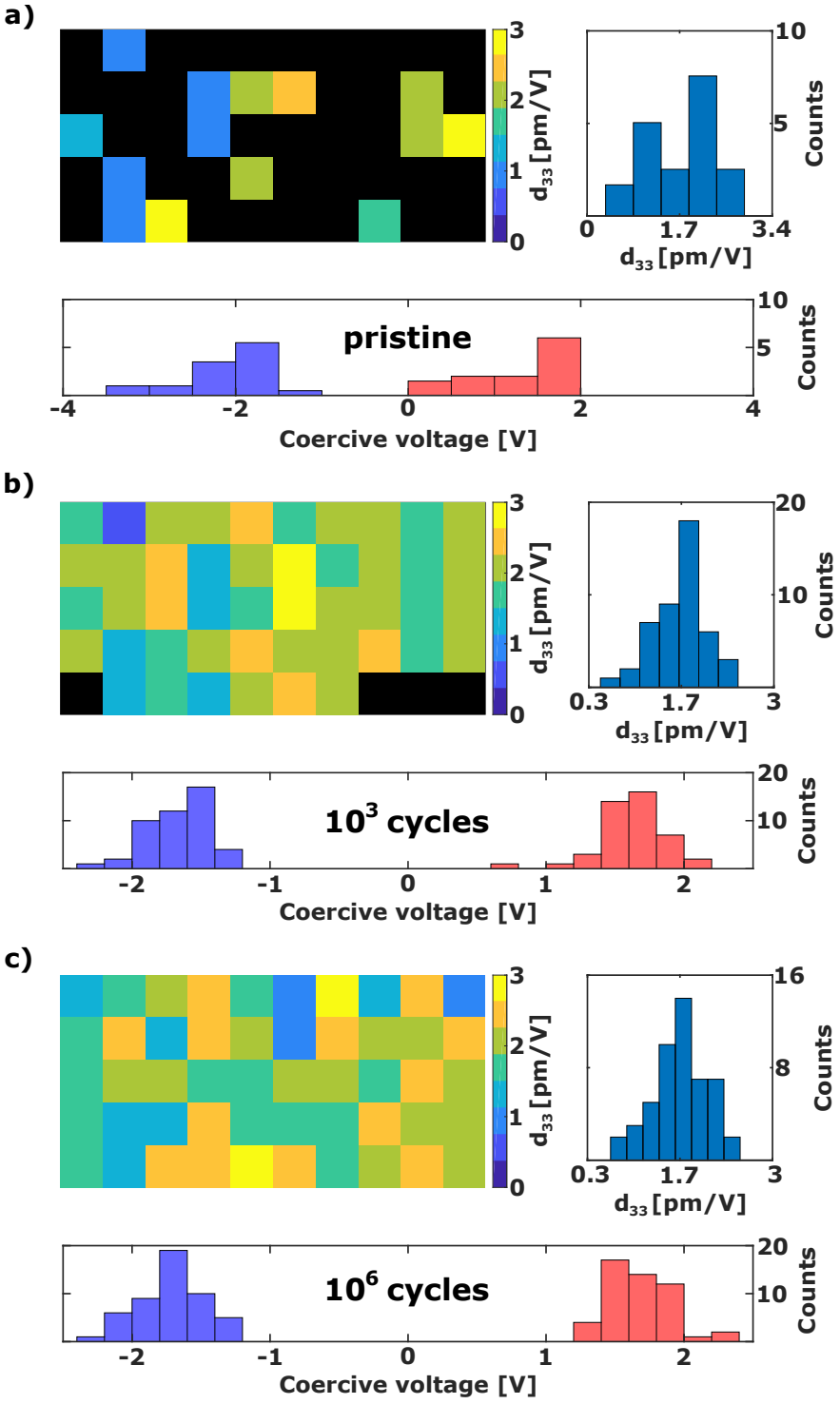

Figure 4.7: Map and distributions of average d_{33} together with positive and negative coercive voltages calculated on 10 nm thick undoped HfO_2 at three different cycling stages: a) pristine, b) after 10 10^3 and c) after 10^6 cycles.

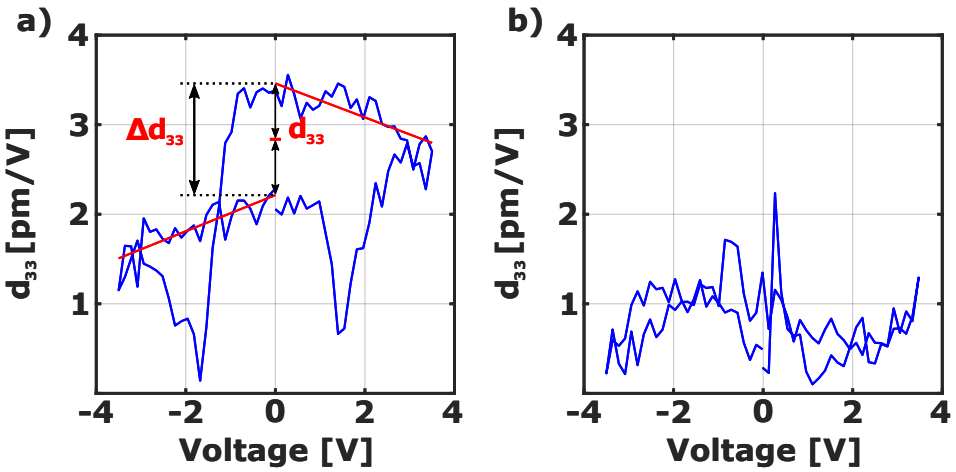

Figure 4.8: a) Procedure adopted to extract d_{33} and Δd_{33} from a PFM loop; b) Example of a measurement that could not be analyzed.

The first clear result is that for the cycled cases almost the totality of measurements could be used for the analysis, whereas in the pristine sample most spots were not showing ferroelectric response, as the one in Fig. 4.8b. Such measurements were probably taken on the non-active region of the material and were therefore discarded. Only about a quarter of the pristine area was useful for analysis, and this explains the greater error reported for the pristine sample in Tab. 4.1. This fact agrees with the findings of Fig. 4.6 where a lower response and less active regions could be identified in the pristine sample.

Looking at the numbers in Tab. 4.1, the effect of cycling is evident. An initial bias of 0.4 V is found, which entirely disappears already at 10^3 cycles. This wake-up phenomenon is commonly reported in HfO_2-based thin films and based on the defect redistribution taking place with electrical cycling [29]. Upon training, average d_{33} increases of about 12 % but the most remarkable result concerns the asymmetry in the response amplitude, which is quantified as Δd_{33}. In the pristine sample, an overall stronger response is found for the positive direction; in contrast, the difference between the two polarization orientations is greatly reduced at 10^3 cycles and practically brought to zero after 10^6 cycles.

A suggested explanation for this behavior is the superposition to ferroelectric response of a piezoelectric signal which vanishes with cycling. A piezoelectric does not switch polarization state and its d_{33} response is a linear signal which adds to the response of the ferroelectric and shifts it in the vertical axis. As a consequence, the amplitude of the response is decreased in one direction and increased in the other, as the loop in Fig. 4.8a shows. Other than o-phase, which is also ferroelectric, there are no other known piezoelectric phases in HfO_2-based ferroelectrics but as discussed earlier it is established that residual m- or t-phase is present in the material and transforms in ferroelectric o-phase upon cycling. It is known that o-phase is normally not stable in bulk or thin HfO_2 films but can be induced in the latter by peculiar stress conditions obtained with

mechanical confinement between electrodes and subsequent annealing [2]. In particular, a favorable stress condition can transform the very close tetragonal structure into orthorhombic. Accordingly, it is possible to conceive a distorted tetragonal phase which is not yet ferroelectric but polar, and hence piezoelectric. The precise quantification of d_{33} response achieved by off-resonance PFM enables to detect the aforementioned contribution, which is present in pristine state and disappears with cycling when the distorted t-phase transforms in o-phase.

While many insights could come on the wake-up behavior of this material, the endurance test presented in Fig. 4.5 and the corresponding PFM analysis were aimed to also investigate fatigue in undoped HfO_2. This stage is normally correlated to a progressive degradation of the polarization response. Decrease of P_r and inhibition of switching within some regions of the material are expected for a sample which undergoes fatigue [29]. In this case no fatigue-related phenomena could be noticed either in P-V or PFM analysis since breakdown occurred suddenly and at 10^6 cycles.

However, further insights into the switching dynamics of the thin film can be obtained by observing the domain evolution with different applied bias close to the V_c, which after wake-up is $\approx$ 1.7 V as seen in Tab. 4.1. Scans at three increasing bias voltages were therefore collected after 1000 cycles of training: the material was first poled negatively at -3.5 V and then gradually poled in the positive direction at 1.5, 1.7 and 1.9 V before obtaining the fully poled state at 3.5 V. The results of such analysis at the three intermediate states are presented in Fig. 4.9a-c (the two fully poled states can be found in Fig. 4.6). As discussed before, since the film is close to the coercive voltage, the collected response is expected to be very weak. Therefore, the amplitude range was adapted for each scan in order to highlight the weak response; a qualitative rather than quantitative analysis is proposed here, so the scans are plotted in arbitrary units. The simultaneously acquired topography scan is shown in Fig. 4.9d, showing a good surface with RMS $<$ 1 nm and excluding crosstalk between PFM and topography features.

Observing the phase plots of Fig. 4.9 it is possible to notice the existence of neighboring independently switched regions. Two main conclusions can be drawn from this: first, looking at the size of uniformly poled regions (some larger than 100 nm) and comparing it to the average grain size for this film of $\approx$ 25 nm [99], it can be inferred that grain boundaries do not provide a barrier to domain growth. In other words, an independently switching region can span across multiple grains. The second and more interesting aspect regards the presence of adjacent regions of oppositely oriented polarization. This is highlighted in the amplitude scan in Fig. 4.9c: the regions enclosed by yellow and blue lines each show a relatively strong response but are in an opposite polarization state. This characteristic behavior of independently switching regions is in agreement with NLS theory, which seems to offer the most appropriate frame for describing switching dynamics of thin films and was reported in other studies on HfO_2-based ferroelectrics [28, 86–88].

In summary, this work investigated the evolution of switching behavior of 10 nm thick undoped HfO_2 by off-resonance PFM. By achieving a lateral resolution in the range of tens of nanometers, domains evolution with electrical cycling is highlighted. In partic-

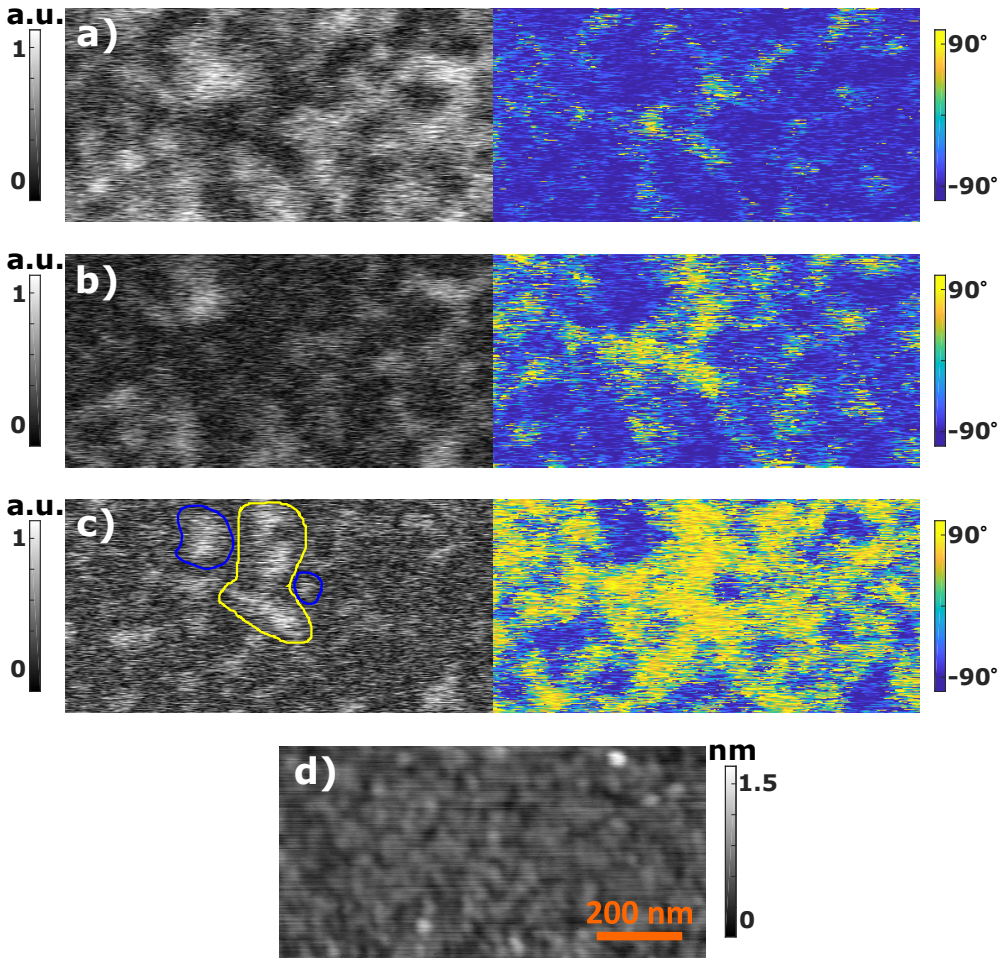

Figure 4.9: 1x0.5 µm^2 PFM amplitude and phase scans on undoped HfO_2 after wake-up. The domain configuration is shown at a) 1.5, b) 1.7 and c) 1.9 V; the blue and yellow regions marked in the amplitude plot in c) denote the existence of adjacent oppositely poled regions in the film; d) the simultaneously acquired topography showing RMS $<$ 1 nm.

ular, the activation of previously non-switching regions is ascertained and correlated to the wake-up process. The effect of pulses at increasing voltage bias was investigated in the film after wake-up: the domain growth behavior showing isolated independently switching regions is collocated in the frame of NLS theory for ferroelectric thin films.

At the same time, the collection of off-resonance PFM loops at different cycling stages enabled to quantify the response intensity and its evolution during wake-up and further cycling, drawing a parallel to what could be observed by electrical measurements. Acquiring arrays of loops, a statistics of relevant properties such as V_c, V_{bias} and d_{33} was obtained for each cycling stage. In particular, the average d_{33} of 10 nm undoped HfO_2 is showing the remarkably low value of $\approx$ 2 pm/V.

In addition, the electromechanical characterization allowed to access a richer set of information like the subtle difference in d_{33} between the two polarization states of a domain. Notably, the analysis of such fine features enabled to detect a piezoelectric contribution which vanishes with electrical cycling. In the context of a field-induced phase transition suggested by previous authors, this response was ascribed to a distorted tetragonal phase transforming into ferroelectric o-phase. Off-resonance PFM is then offering a unique way to characterize the electromechanical contribution of such unwanted phase on the ferroelectric properties of the material.

4.3 Summary

In the first part of this chapter a qualitative and quantitative analysis of off-resonance PFM loops was shown with the purpose to highlight the traits of a genuine and robust ferroelectric response of the material. Specifically, the impact of measuring through top electrode and with a stiff cantilever was demonstrated, resulting in the absence of electrostatic interactions from the collected signal. Moreover, the analysis of response at different frequencies far below the resonance frequency f_r of the system was conducted, showing that the amplitude and fine features of acquired loops are maintained. These two important results allow one to consider the collected signal as the true piezoresponse of the ferroelectric thin film, which can then be quantified.

Following from this meaningful realization, the analysis of cycling behavior in undoped HfO_2 was presented. By collecting series of surface scans and arrays of loops, it was possible to characterize the ferroelectric response of the material and detect the initial presence of a piezoelectric response superimposed to the expected ferroelectric behavior. Thanks to the perks of off-resonance PFM, this could be quantified and associated to the contribution of other polar phases which transformed into ferroelectric o-phase with cycling. This phenomenon is described in literature as responsible of the wake-up commonly observed in HfO_2-based ferroelectrics and its contribution could be visualized here in great resolution.

5 | Quest for millivolt-range ferroelectric devices: a PFM analysis

This chapter presents the findings of off-resonance PFM investigation of HZO thin films of thickness 5, 7, 10 and 30 nm. The first section discusses the measurement of complete, saturated switching in the sub-1 V bias range for the 7 nm film, a relevant result with implications for low-power electronics. This is accompanied by an unexpected thickness trend of coercive field, which shows a reduction with decreasing thickness. This leads to the proposition of an alternative domain nucleation scenario that could be applicable to ultrathin ferroelectrics. The second section introduces qualitative preliminary results on 5 nm which seem to indicate a continuation of the observed trend in ultrathin films.

The discovery of ferroelectricity in HfO_2-based thin films [1] offered new appealing possibilities for device applications: this material was already used as CMOS-compatible high-κ dielectric so its integration in the fabrication process is already well understood. In particular, among all doped HfO_2 ferroelectrics, $Hf_xZr_{1-x}O_2$ (HZO) is one of the most studied because it stands out as the one with lowest required annealing thermal budget, as low as 400 °C [2].

Many studies have found a robust and stable polarization for HZO thin films, and 10 nm is often regarded as optimal thickness [51, 52, 66, 98]. The retention of ferroelectricity in such thin films is of great interest from the application point of view: indeed, one can think of reducing the operation voltage of devices such as nonvolatile memories since that ideally scales with thickness. CMOS compatibility and scalability are the most important practical differences between this class of ferroelectrics and conventional PZT in view of application, and represent a clear advantage for HfO_2-based ferroelectrics.

From the application point of view, coercive voltage of ferroelectrics is an important figure of merit: the lower it is, the less voltage is required to switch between the two polarization orientations, which represent the two logical states. The typical coercive field reported for HZO is approximately 1 MV/cm, which is about an order of magnitude higher than PZT [8]. Despite such high value, this implies that films thinner than 10 nm should anyway be able to show coercive voltages in the sub-1 V range. It seems, however, that such trend is not followed for extremely thin films, which do not possess a

coercive voltage lower than 1 V in practice: a 5.5 nm HZO film was reported to have V_c < 1 V but its macroscopic switching polarization was degraded with respect to thicker samples [80]. Another report of extremely thin HZO calculated a V_c = 0.8 V on a 2.5 nm thick film (E_c > 3 MV/cm), when in practice the applied voltage across the stack required to measure it by PFM was as high as 2 V [68].

Inspecting the ferroelectric behavior of ultrathin films requires visualization of extremely small phenomena related to domain switching mechanisms. In order to clarify the transformations induced by the polarization reversal at the domain level, it is necessary to have a nanometer size resolution and visualize the local electromechanical response of the material. PFM analysis emerges as an appropriate tool for this task. Indeed, domain switching dynamics of HZO thin films has been subject to PFM investigation already: this is not only serving the practical purpose of obtaining devices working in the sub-1 V range, but it sparks a theoretical interest too. The findings however did not include an in-depth analysis of PFM loops, which can be a useful tool to quantify the ferroelectric response of a material [113, 115, 116]. This can be due to the fact that very small d_{33} in the order of only 1-10 pm/V is reported for HfO_2-based ferroelectrics, which makes the quantification very challenging [125, 126].

To shed light on this matter, an off-resonance PFM investigation of thin HZO films on capacitor structures is reported here: in particular, this work will present results on films with thickness ranging from 5 to 30 nm. The structures used in this work are, from bottom to top, Si/TiN/HZO/TiN/Pt, and only differ in the thickness of the ferroelectric layer. The PFM is acquired through the top electrode which has a combined thickness (TiN + Pt) of ≈ 35 nm. Further details about the fabrication can be found in appendix. The first section will present a complete characterization of the films in the 7-30 nm thickness range, whereas the second section presents some preliminary data on 5 nm HZO and discusses how they relate with the previous findings.

5.1 Ferroelectricity in thin to ultrathin HZO films

Ferroelectricity in thin films of 7, 10 and 30 nm is first assessed by electrical measurement. Fig. 5.1 shows *P-E* loops acquired after wake-up on 50x50 µm^2 capacitors at a frequency of 100 Hz for all three samples. Clear hysteretic behavior is appreciable in all cases, with similar P_r of 18 and 20 µC/cm^2 for the 7 and 10 nm thick HZO, respectively. The 10 nm film displays the best response of the three films, with highest P_r and sharpest switching characteristic, confirming that this thickness is optimal for HZO. The 30 nm sample on the other hand shows a markedly weaker response, with a P_r of 7 µC/cm^2: this might be explained by the fact that this thickness is closer to the limit of stability of o-phase in this material [52, 66].

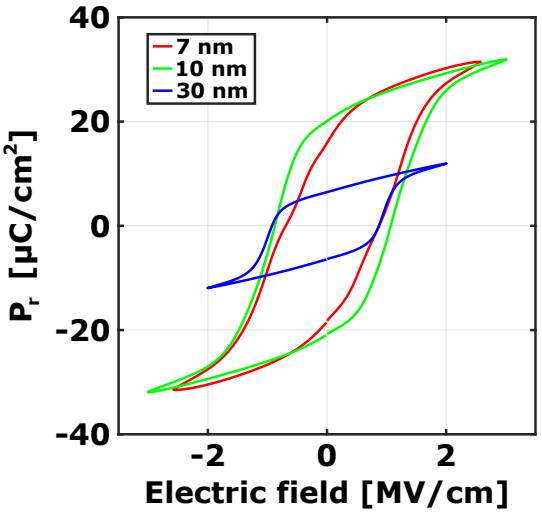

Figure 5.1: P-E loops showing the ferroelectric behavior of HZO films of 7, 10 and 30 nm thickness.

5.1.1 Enabling millivolt-range switching in HZO ultrathin films

Once the ferroelectric behavior is determined in all samples, a detailed off-resonance PFM analysis is conducted. Fig. 5.2 shows piezoresponse loops obtained on 5x5 μm^2 capacitors for the three films after a training procedure of 10^4 cycles at 1 kHz, where the amplitude of the signal was adjusted according to the thickness in order to be ≥ 2 MV/cm. The loops are acquired at a frequency of 92 kHz and with ac voltage of 0.3, 0.5 and 1.1 V for 7, 10 and 30 nm respectively. The probing ac voltage was carefully maintained below half of V_c for each film and close to $V_c/2$ only for the thinnest film in order to get enough signal. Measurement at 12 and 230 kHz were also performed as explained in chapter 4, which proved the frequency independence of on- and off-field loops within this range, far from the resonance frequency of the system. This allows confidently regarding the detected amplitude as the true response of the material. Hence, the displacement was calculated by converting the detected voltage signal after the calibration procedure explained in chapter 2 and the resulting data are plotted showing d_{33} in pm/V. The similarity of on- and off-field loops further attests to the genuine ferroelectricity of the films.

In agreement to the P-E characterization reported in Fig. 5.1, the 10 nm sample shows the strongest response also in PFM measurements, with a d_{33} of ≈ 5.5 pm/V. The 30 nm sample confirms the lower polarization strength observed by P-E analysis, with $d_{33} < 1.5$ pm/V. Further examining the quantitative data emerging from the PFM investigation, one remarkable result has to be mentioned: the noise floor detected for the 7 nm thick HZO film is ≈ 0.2 pm/V as it can be seen in Fig. 5.2a. This loop was acquired with an ac voltage of 0.3 V; as a result, the noise floor is lower than 0.1 pm, which testifies the sensitivity of the measurements performed in this work.

As discussed in chapter 4, the saturation of d_{33} for off-field loops and their similarity to the respective on-field loops certify the genuine ferroelectric response of these thin films. This element adds to characteristic features such as tips pointing down for high voltages in the on-field loops and the hump that is visible for the 30 nm film. Both have been discussed in chapter 4 and are correlated to the dependence of d_{33} on ϵ_r (see Eqn. 4.1), which displays a nonlinear response with field.

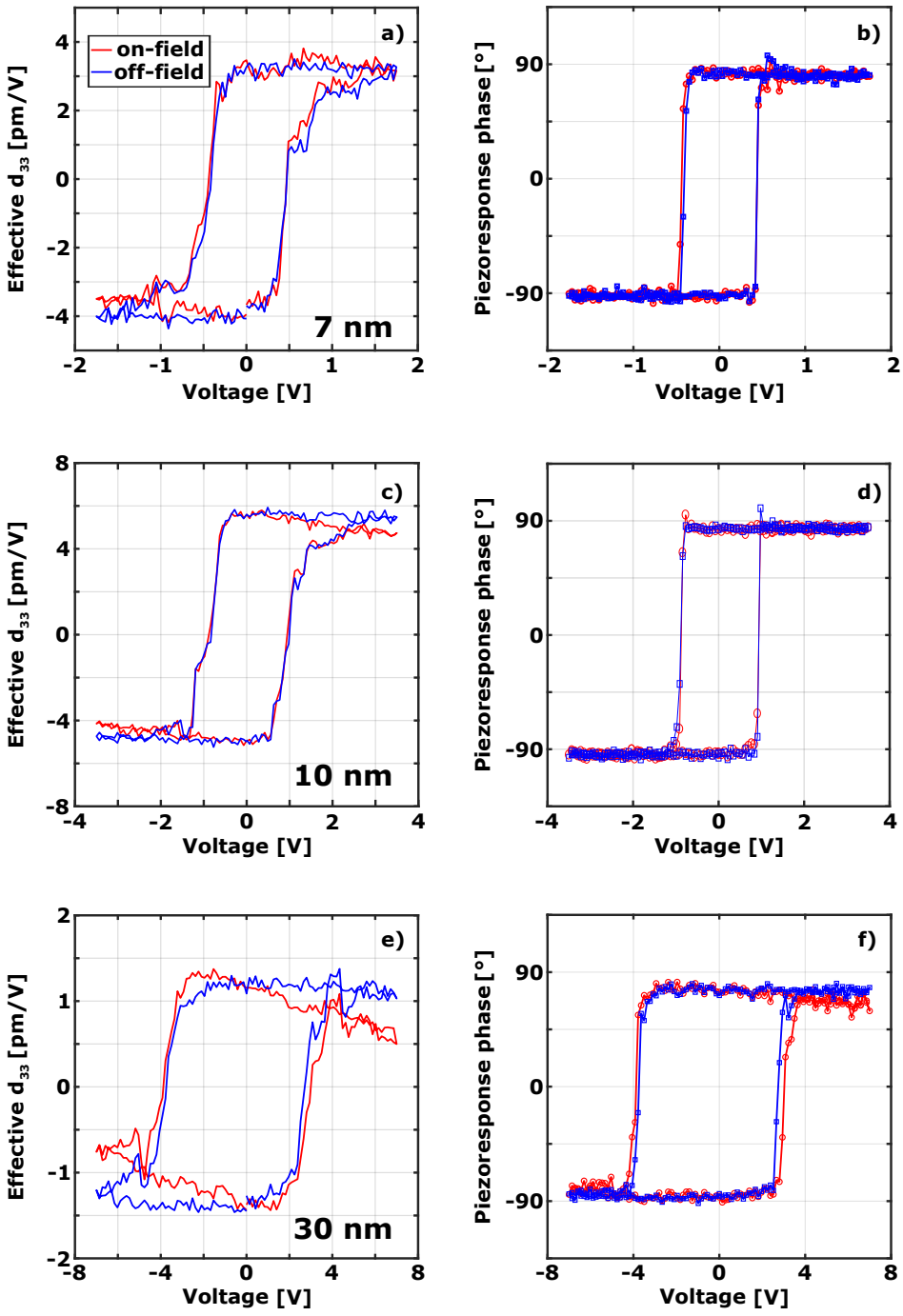

Figure 5.2: Piezoresponse amplitude and phase for a,b) 7, c,d) 10 and e,f) 30 nm thick HZO. Loops were acquired through top electrode with a probing voltage signal of amplitude 0.3, 0.5 and 1.1 V, respectively, and a frequency of 92 kHz.

Looking at the 7 nm film it is possible to observe a sharp switching for fields lower

than 1 V, and saturation is well reached for the maximum bias field of 1.8 V, see Fig. 5.2a. This suggests the possibility to obtain a saturated loop with dc bias sweep lower than 1 V: this is reported in Fig. 5.3, where the loop is also acquired with ac voltage of 0.3 V and frequency of 92 kHz. A clear phase switch is observed with a V_c of $\approx$ 400 mV. This result indicates a robust polarization reversal for the ultrathin 7 nm HZO film and opens to the possibility of millivolt-range operation voltage in low-power electronics.

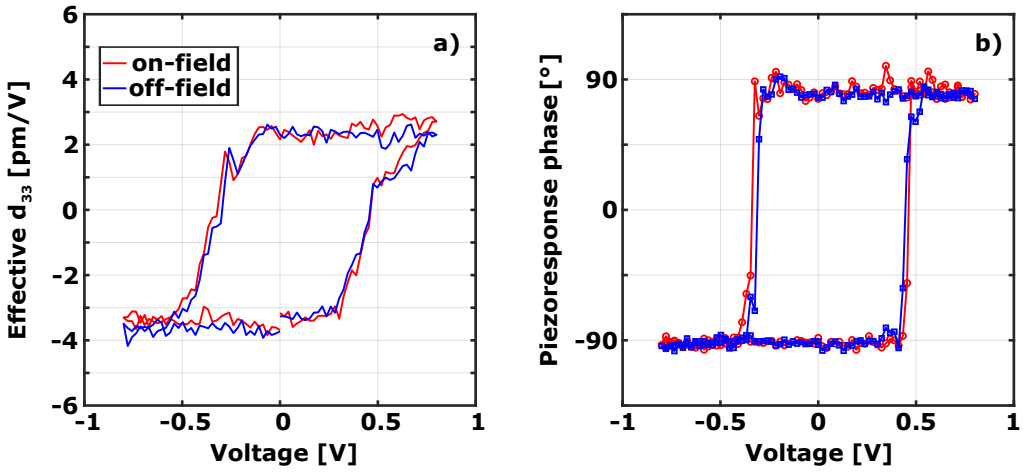

Figure 5.3: Piezoresponse a) amplitude and b) phase measured with a maximum dc bias of 800 mV on a 7 nm thick HZO film.

5.1.2 Unexpected thickness dependence of coercive field in HZO thin films

Following the analysis of the switching characteristic in single locations, PFM scans were also acquired for the three capacitors. In order to visualize the domains evolution, scans at consecutive voltage steps were collected after the same poling procedure reported for PFM loops. Fig. 5.4 shows the results for 10 nm thick HZO. The film was poled by pulses of 1 s at -3 V (negative state), then 1.3, 1.7, and finally 3 V (positive state). The poling is applied by grounding bottom electrode and varying the voltage at top electrode. The image is acquired with a probing ac voltage of 0.5 V and frequency of 92 kHz. The corresponding topography with rms $<$ 1 nm did not interfere with the PFM acquisition.

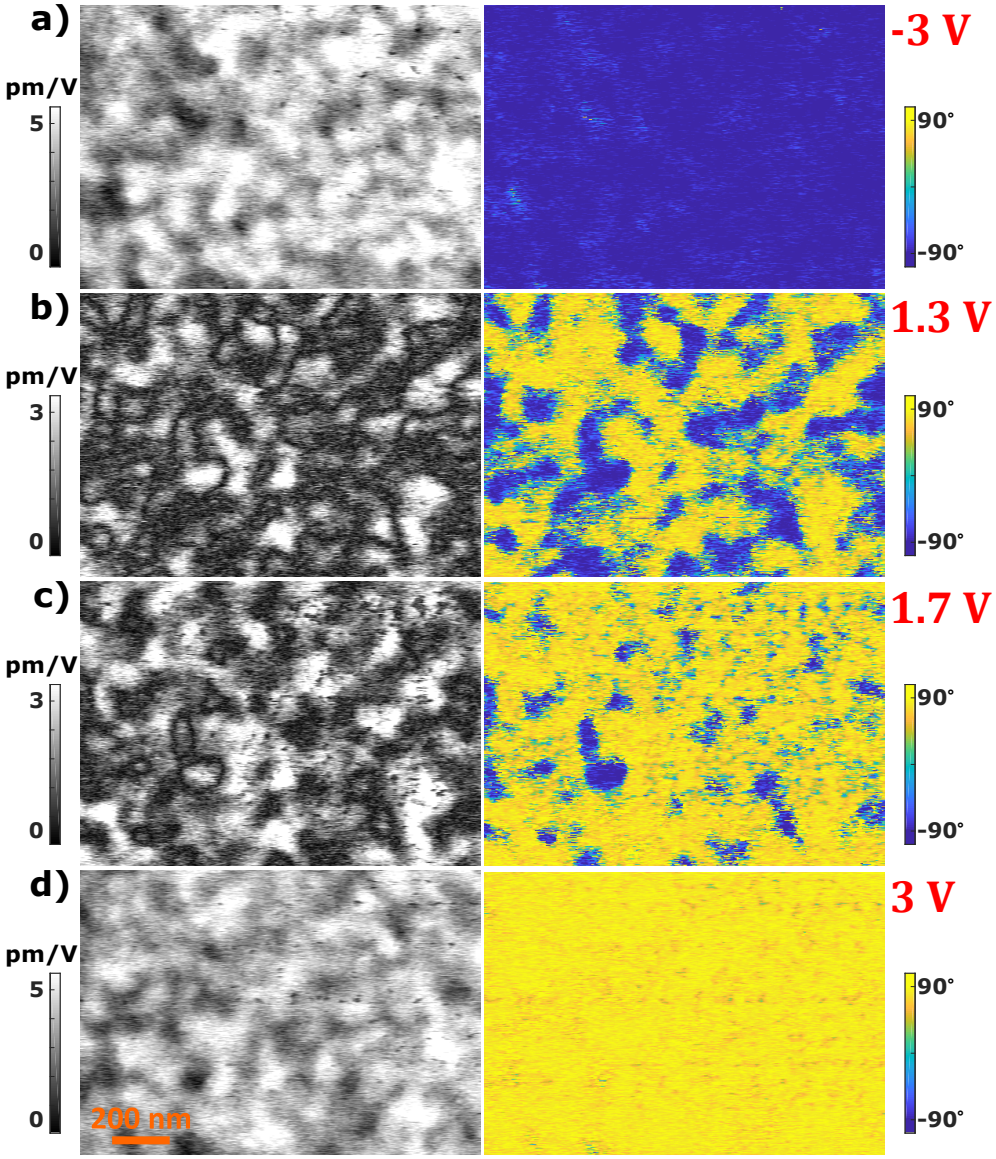

Figure 5.4: 1.4x1 μm^2 scans showing PFM amplitude and phase on 10 nm HZO; after poling at a) -3 V, the sample is progressively poled at b) 1.3 V, c) 1.7 V, and finally at d) 3 V. The probing signal has ac voltage of 0.5 V and frequency of 92 kHz.

The first observation is that a complete switching can be achieved for the two opposite polarization states, as it can be inferred by the phase plots in Fig. 5.4a and d. The corresponding amplitude response on the other hand does not render a completely uniform response but rather a distribution of d_{33} values that can be due to both the misalignment of the polarization axis with respect to the vertical direction and the presence of secondary non-ferroelectric phases. This is common in thin HfO_2 ferroelectrics due to the complex energy interactions that can stabilize m-, t- or o-phase [2, 98]. More interestingly, the two scans at intermediate voltages close to V_c show a very complex

domain pattern. The smallest features that can be resolved are in the order of 30 nm but overall larger regions showing homogeneous switching can be identified, up to $\approx$ 200 nm; for a comparison, grain size in this film is expected to be $<$ 10 nm [98]. This dense arrangement of independently switched regions supports a switching dynamics which follows the NLS theory, analogously to what was reported for the undoped HfO_2 film of the same thickness in the previous chapter.

A similar experiment was conducted on 7 nm HZO, and results are shown in Fig. 5.5. Here the fully poled negative state is achieved at -1.8 V, then the sample is progressively reversed and scans are taken at 0.7, 0.9 and 1.8 V, in the opposite polarization state; higher voltage could not be tested due to high leakage or even failure of the device. While the scans show a similar pattern to the 10 nm film for the steps close to V_c, an important difference comes in the fully poled state, which cannot be reached in neither of the two polarization directions. The phase plots in Fig. 5.5a and d reveal oppositely poled regions even for the largest bias magnitudes, which can be explained by a local injection and trapping of charges in the film or by presence of non-switching domains. Observing Fig. 5.5b, that is the intermediate state poled at 0.7 V, it can be seen that a portion of the film switched already, in agreement to the findings of Fig. 5.2a. The smallest area that switches at such low voltage is in the order of about 100 nm: it is then possible to envision devices entirely located on a single switching region, which would reverse their polarization state in the millivolt range. It is clear however that a better film quality has to be achieved first, where a homogeneous switching such as the one observed for state of the art 10 nm film can be reached.

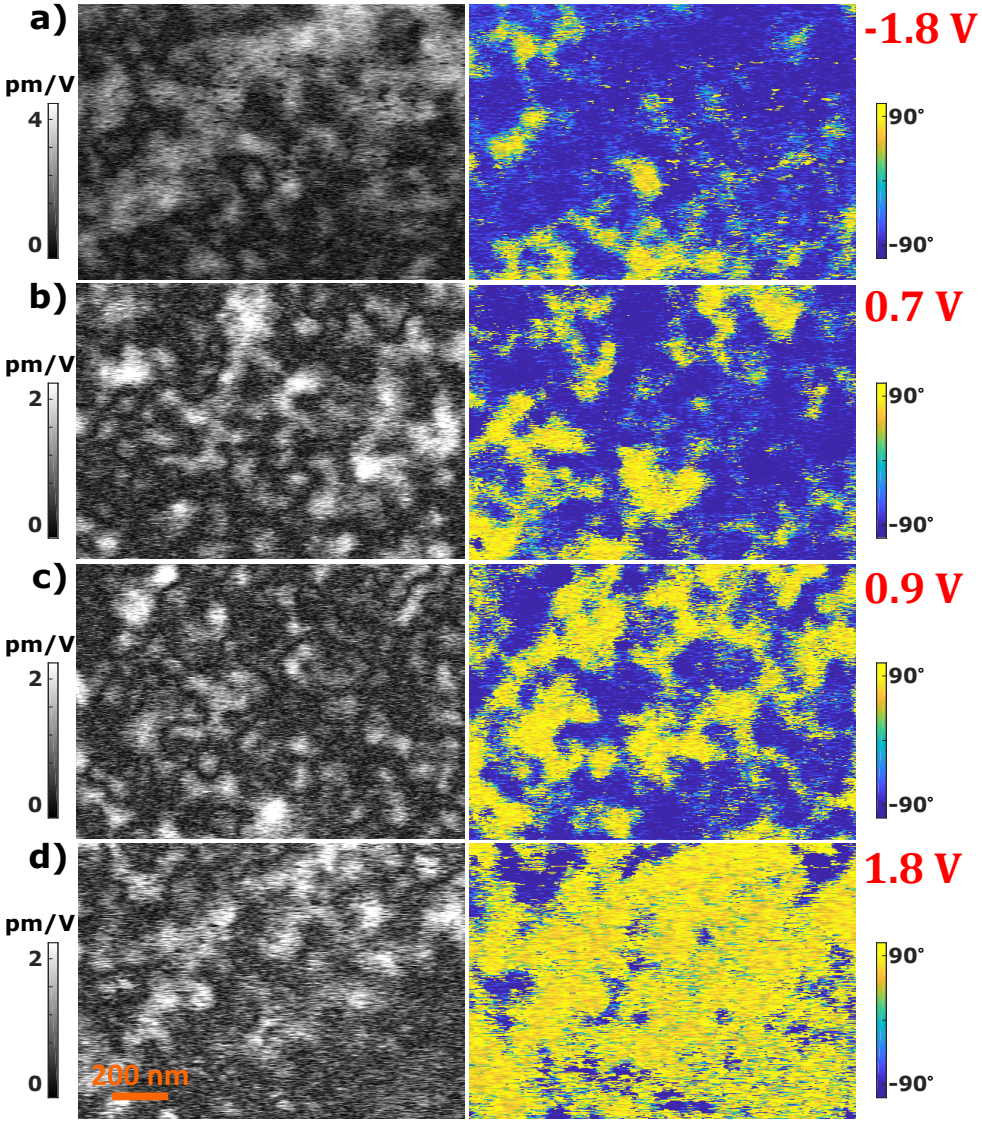

Figure 5.5: 1.4x1 µm^2 scans showing PFM amplitude and phase on 7 nm HZO; after poling at a) -1.8 V, the sample is progressively poled at b) 0.7 V, c) 0.9 V, and finally at d) 1.8 V. The probing signal has ac voltage of 0.3 V and frequency of 92 kHz.

The polarization switching on 30 nm thick sample is showing essentially analogous features to the 10 nm film. Fig. 5.6 shows a scan acquired at 2.5 V poled state, that is close to the positive V_c, after the sample was prepoled negatively. The response is overall lower as expected and discussed earlier, and this makes details less sharp in the amplitude and phase plots. The simultaneously acquired surface height profile is also shown, which enables to exclude a crosstalk between topographic features and PFM response.

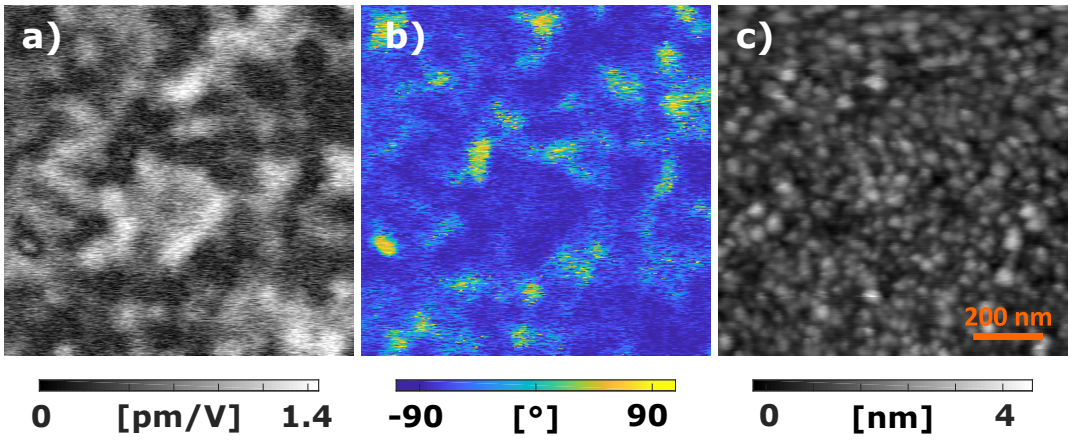

Figure 5.6: 1x1 µm^2 scan showing PFM a) amplitude and b) phase on 30 nm HZO close to the positive V_c at 2.5 V; the probing signal has ac voltage of 1.1 V and frequency of 92 kHz. The c) height profile map is shown to exclude the presence of topographic crosstalk.

To the extent of having a statistical representation of switching data, arrays of 10x10 loops were collected on the three samples on a 1x1 µm^2 area with same settings as measurements in Fig. 5.2. Fig. 5.7a shows the V_c maps for positive and negative V_c of 7 nm thick HZO, where it can be confirmed that the totality of collected loops switches at a field < 1 V. The black spots represent locations where measurements could not be obtained or interpreted, and as such were discarded from the dataset ($\approx$ 85 % of all collected loops were analyzed). The histogram in Fig. 5.7a shows a wide distribution of positive and negative V_c, which is in line with the results obtained by the PFM scan in Fig. 5.5 where a fully poled state could not be reached and some regions showed strong bias.

Analogous maps were obtained for d_{33} and are plotted in Fig. 5.7b for the three samples. The scale is kept the same in order to offer a better comparison of the films: the 10 nm thickness confirms to be in the optimal range for the stabilization of o-phase in HZO, showing the strongest response. The thicker 30 nm film shows the lowest d_{33} amplitude, which is expected since the presence of secondary m-phase is usually higher in thicker HfO_2 ferroelectric films, effectively diluting the o-phase and causing an overall lower response [31, 51]. In addition, this thickness also presents $\approx$ 15 % of non-switching points, which may be related to regions where monoclinic phase stabilized already.

The analysis of the switching data is presented in Tab. 5.1, where the average V_c, E_c and d_{33} are listed for each film thickness. When for each sample V_c is divided by the film thickness to obtain E_c, an unexpected trend is found, shown in Fig. 5.8. By comparing the coercive fields calculated for 30 and 10 nm thick samples one can notice that they are almost identical and equal to 1.22 MV/cm. As reminded previously when discussing the loop shape of Fig. 5.2e, literature reports indicate that 30 nm thick film is closer to transitioning to a non-ferroelectric phase. Then, according to the thermodynamic

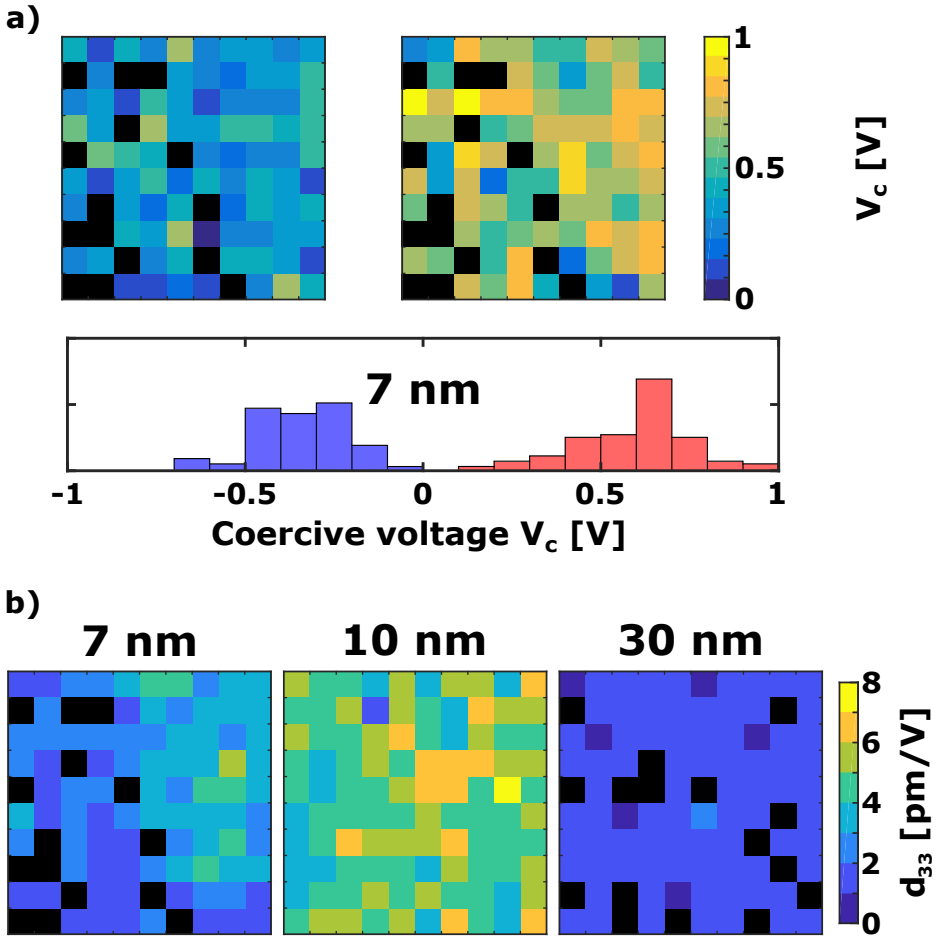

Figure 5.7: a) 1x1 µm^2 maps and distribution of negative and positive coercive voltages V_c for 7 nm thick HZO; b) analogous d_{33} maps for 7, 10 and 30 nm thick HZO, plotted using the same scale for comparison. The black spots represent discarded points.

LGD theory, this sample is also expected to show a lower E_c. In other words, the lattice is "softer" and easier to polarize. Such thickness trend is not encountered in the present study, which suggests that the origin of switching has to be found elsewhere. This is not unexpected, taking into account also the switching dynamics observed in Fig. 5.4: considering the polarization reversal as a phenomenon promoted by the nucleation of opposite polarization domains, a different behavior can be envisaged. This agrees with literature reports stating that intrinsic thermodynamic switching is not correctly depicting the polarization reversal of thin films, which are better described by NLS theory [28, 86–88].

However, the most striking aspect of the behavior observed in Fig. 5.8 is the unexpected reduction of coercive field at the lowest thickness of 7 nm, where the calculated value is 0.68 MV/cm, that is almost two times lower than for thicker films. The coercive field is correlated to the thickness d of the ferroelectric film by the empirical equation E_c

	V_c [V]	E_c [MV/cm]	d_{33} [pm/V]
7 nm	0.48 ± 0.09	0.68 ± 0.13	2.68 ± 0.94
10 nm	1.22 ± 0.09	1.22 ± 0.09	4.88 ± 0.99
30 nm	3.66 ± 0.27	1.22 ± 0.09	1.34 ± 0.26

Table 5.1: Quantitative results showing the average coercive voltage V_c, coercive field E_c and d_{33} for each HZO film thickness.

$\propto d^{-2/3}$, known as Janovec-Kay-Dunn law [102]. This behavior comes from the assumption that critical size for nucleating domains is decreasing with increasing field. However, this equation fails to account for interface effects that become predominant when the thickness of ferroelectric film is comparable to that of the interface, which is precisely the case for very thin films. The depolarizing field associated to an incomplete charge compensation at the electrode interfaces is often suggested as the reason why lower coercive fields can actually be observed for very thin films [153, 154]. This interpretation was adopted in a study on ultrathin HZO films where reduction of E_c was observed for thickness of 5.5 nm [80]. However, according to this model, since a decrease of the maximum field effectively applied to the ferroelectric is brought as a cause for the E_c reduction, a consequent degradation of the polarization is also expected.

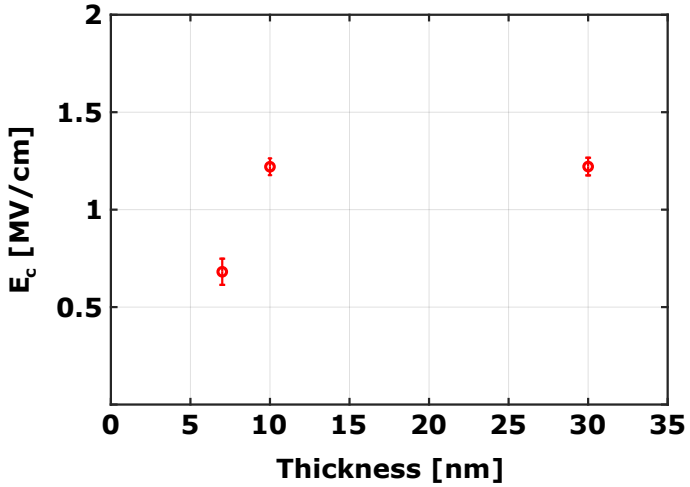

Figure 5.8: Coercive field trend with thickness for thin HZO films.

Remarkably this was not observed in the present work. Fig. 5.9a shows two ferroelectric loops acquired on the 7 nm thick film in identical conditions. The only difference is in the dc bias sweep, which in one case reaches 0.8 V (E = 1.1 MV/cm) and in the other case 1.8 V (E = 2.6 MV/cm). According to the model explained above a significant degradation should be expected in the d_{33} response for the loop taken at lower maximum bias, since d_{33} depends on the polarization which is expected to reduce when the applied field is lower. Most importantly, a different E_c is expected. On the contrary,

the piezoresponse loops of Fig. 5.9a show that saturated d_{33} response is reached even for the lowest field case and the switching occurs at the same coercive voltage for both loops. This fact suggests that the effect of depolarizing field is not playing the main role in the switching dynamics of this film and a different phenomenon has to be accounted for.

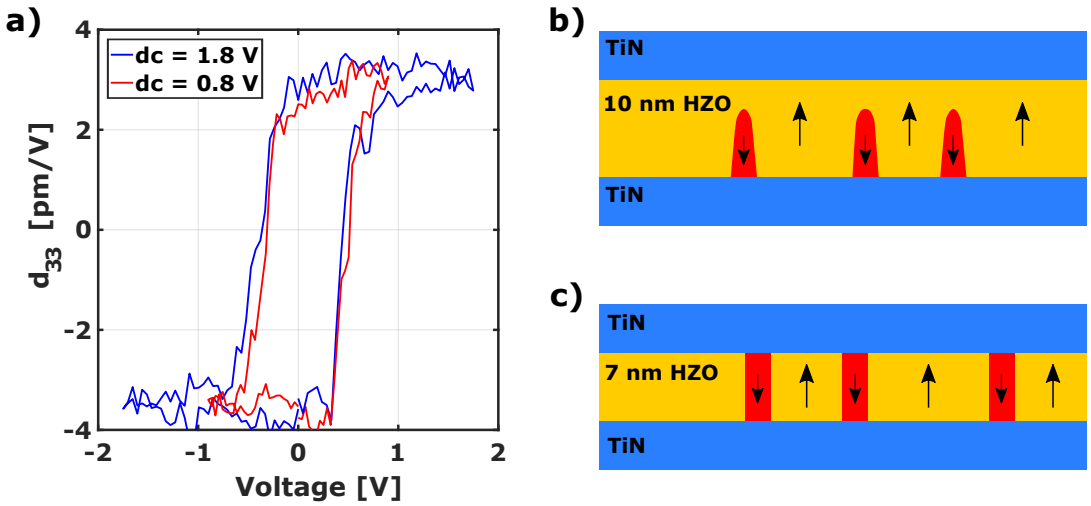

Figure 5.9: a) Comparison of d_{33} loops acquired with different dc voltage amplitude on 7 nm thick HZO film; b) standard nucleation mechanism applied to 10 nm thick films and c) different scenario applicable to thinner 7 nm HZO films.

In order to clarify the switching mechanism, a different nucleation model can be conceived, one that draws from NLS kinetics as this is considered to best describe ferroelectric thin films. In NLS scenario, the energy of a domain contains several contributions: bulk and surface energy, presence of interfaces, defects and electric fields. Domain growth is usually regarded as two-step mechanism: a fast development of the nucleus along polarization direction first allows the domain to reach through the opposite electrode and then a lateral expansion follows. The activation energy is higher for the first part of the process, when growth is parallel to the surrounding polarization and against it, and lower for the second part, because lateral growth is perpendicular to it [155, 156].

Germinating nuclei are usually described as prolate semispheroids of radius r and height l originating at the ferroelectric/electrode interface. Their energy U is defined by the complex balance of a function which includes several parameters [23, 155, 156]:

$$U = -ar^2 l + brl + c\frac{r^4}{l} - dr^2, \tag{5.1}$$

with

$$a = \frac{4\pi P_s E}{3}, \quad b = \frac{\pi^2 \sigma_w}{2}, \quad c = \frac{4\pi P_s^2}{3\epsilon_0 \epsilon_a}\left[ln\left(\frac{2l}{r}\sqrt{\frac{\epsilon_a}{\epsilon_c}}\right) - 1\right], \quad d = \pi\gamma. \tag{5.2}$$

In Eqn. 5.2 the term a represents the "bulk" energy of the domain: the negative sign is because polarization P_s inside the domain is pointing in the same direction as the electric field E and therefore reduces the total energy U. Nucleation of a region with different properties than the surrounding environment always has an energy cost too. The interface between two regions in this case is the domain wall, which is accounted for in the term b, where σ_{w} is the domain wall energy density. The third term in the equation above includes the depolarization energy that is given by the divergence of polarization that exists at the domain wall; ϵ_{a} and ϵ_{c} are the ϵ_{r} components perpendicular and parallel to the polarization, respectively. Both b and c are positive terms, adding to the energy of nucleating domain and competing against the energy gain expressed by factor a. These three terms were originally formulated by Landauer in his first treatment of the subject while term d was introduced later to account for the ferroelectric/electrode interface energy density γ, which is linearly proportional to the polarization and accordingly changes sign with it [23, 155, 156].

A nucleation event successfully takes place when a domain overcomes the nucleation energy barrier, a condition which corresponds to a critical nucleus size. This model is therefore considered not to be dependent on film thickness as long as the critical dimension of the nucleus is lower than that. Fig. 5.9b depicts nuclei of opposite polarization (in red) as they are usually conceived in NLS model, for a 10 nm thick film. Fig. 5.9c instead illustrates a sketch of the nuclei configuration proposed following a different scenario, whose main assumption is a cylindrical shape of the domains, elongated in the direction of film thickness [102]. Here, the critical domain size required for nucleation is equal to or larger than the film thickness for the case of 7 nm HZO film. This implies that domain nuclei for this thickness span across the whole film, from one electrode interface to the other. When this is the case, the required energy for domain growth only corresponds to the wall motion perpendicular to the applied field, as there is no more need to overcome the depolarizing field. Looking at equation 5.1, all terms are expected to be slightly different with a cylindrical shape, but the third one (including parameter c related to divergence of polarization at domain walls) would be greatly reduced, ideally cancelled in case of perfect 180 ° domain walls. This phenomenon is causing the observed reduction in $\mathrm{E_c}$. In addition, such nuclei extending through film thickness can be stabilized by charged defects at the interface and become nonvolatile, a feature that agrees with the observation of Fig. 5.5 [102].

It is possible to picture this switching scenario for thicker films as well. However, the different energy contributions do not make the proposed cylindrical shape the most favorable one for larger nuclei. The nucleation of films in the range of 10-30 nm is therefore following a classic mechanism, where coercive field is independent of thickness; on the other hand, thinner 7 nm films present cylindrical nuclei which enable switching

at lower E_c [102]. The data presented so far cannot be considered conclusive and require a theoretical validation of the nucleation model. In addition, from the experimental point of view, it is interesting to systematically analyze films with thickness smaller than 7 nm in order to see whether the model holds, as thinner films are expected to have a similar behavior. Such investigation however is anticipated to be challenging due to the presence of higher leakage in ultrathin films and because the detection of very small V_c requires very small probing voltages and therefore long integration times.

5.1.3 5 nm: approaching the ultimate limit of stable ferroelectric switching?

The nature of the switching scenario proposed to explain the E_c reduction in 7 nm HZO films is implying the possibility that thinner films would also present such low coercive field. In order to investigate this and find a further confirmation, a 5 nm HZO film is analyzed. As anticipated before, the acquisition of PFM data demonstrated to be very challenging. A complete set of data as for thicker films, comprising a set of scans and high number of loops, could not be obtained. Therefore, the data presented in this section is regarded as preliminary observations.

The 5 nm HZO film is first cycled similarly to what was done for the previous samples, namely by 10^4 cycles with a square waveform with amplitude of 1 V (2 MV/cm) and frequency of 1 kHz. In view of a possibly very low V_c, the probing ac bias is set to 0.2 V only. Even increasing the acquisition time, with a time constant of 1 s, this provides a very noisy signal in the 12-230 kHz frequency range employed for previous analyses, which renders uncertain results. However, by increasing the ac bias frequency to 460 kHz, still comfortably far from f_r of the system, a better signal to noise ratio is obtained. Since the detection at different frequencies could not be achieved, the quantification is not possible and the amplitude is reported in arbitrary units.

Fig. 5.10a and b show amplitude and phase of a PFM loop acquired on the 5 nm HZO film. The data is still noisy but the presence of two stable and saturated regions can be identified for the two polarization states, achieved using a maximum dc bias of 0.4 V only. Inspecting the phase loop, it can be seen that in positive direction the off-field switching occurs at a voltage ≈ 0.1 V higher than the on-field case. Given the quasistatic nature of the measurement, this could indicate a low retention of the polarization state, which was noticed as well in other loops acquired on this film and is further complicating the analysis. However, overall $V_c < 250$ mV is observed for the switching in both positive and negative direction. For a 5 nm thick film, this value corresponds to a remarkably low value of $E_c < 0.5$ MV/cm. This result is suggesting that the trend observed in Fig. 5.8 could continue to smaller thickness, supporting the nucleation mechanism proposed earlier.

The quasistatic measurements attempted with the previous settings induced leakage and charging of the film, hence it was not possible to collect more conclusive information. Thus, another approach was attempted, in order to reduce the acquisition time needed to collect loops and obtain a higher signal to noise ratio. In another set of measurements,

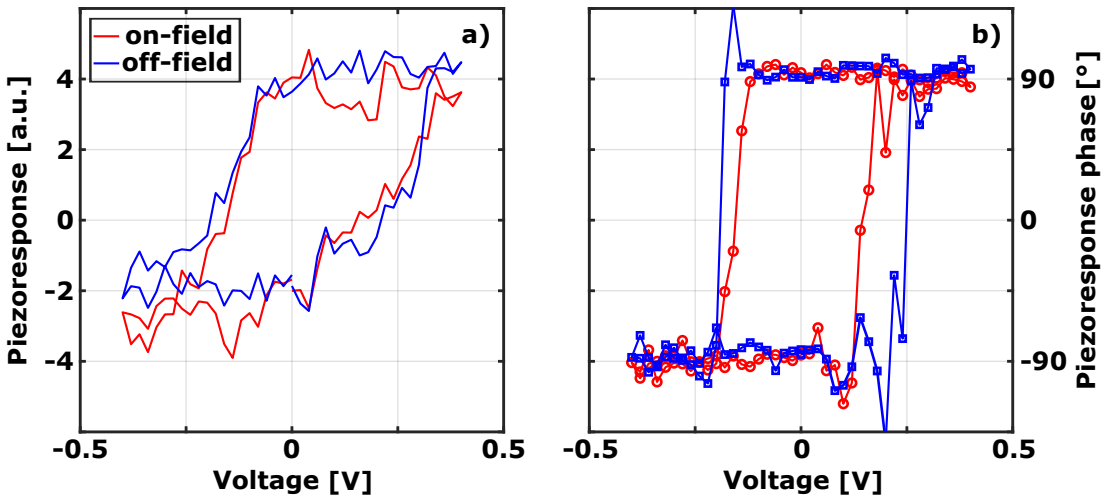

Figure 5.10: Off-resonance PFM preliminary analysis on 5 nm HZO. a) Amplitude and b) phase loops taken on a single spot at a frequency of 460 kHz and probing ac voltage of 0.2 V.

a pristine sample was analyzed in order to prevent leakage induced by cycling. Also, the ac bias frequency was brought closer to f_r of the system, while the ac was left at 0.2 V. The f_r was detected at 1.3 MHz: the results reported in Fig. 5.11 are acquired at a bias frequency of 1.2 MHz, that is still lower than f_r but close enough to be on the peak shoulder and benefit from resonance amplification. Fig. 5.11a and b represent a PFM loop acquired on 5 nm HZO film whereas Fig. 5.11c-e are PFM amplitude, phase and topography scans, respectively, at the poling bias of -0.2 V.

As expected, signal to noise ratio of the PFM loops collected close to f_r is greatly improved. A clear phase switching is detected, with no shift between on- and off-field. A complete saturation can be observed in both polarization states, together with an anomalous bump for the on-field loop in the saturated region, which was detected in other loops too. This feature was not observed before and at present its origin is not clear. An internal bias of ≈ 0.12 V in the positive direction is forcing the maximum dc voltage of the measurement to a higher value. Nonetheless, the saturated loop is collected within a 0.8 V dc bias and an average V_c of 0.37 V is detected, corresponding to E_c of 0.74 MV/cm. This value is slightly higher than what was measured at lower frequencies and comparable to E_c reported for 7 nm film in Tab. 5.1. This result can be explained by the fact that E_c decreases for a longer pulse length in a NLS scenario [87]. Once again, only very few loops could be obtained in this analysis before insurgence of leakage.

The PFM scans in Fig. 5.11c-e, taken after poling at 0.8 V and then at -0.2 V for 1 s, show the presence of two regions, similarly to what was observed in the off-resonance measurements but with much sharper features. Other images were collected at different poling states but there were not significant changes in the amplitude and phase image, then degradation of the film caused by leakage occurred. It is noted that,

since the measurement was performed close to f_r without any resonance tracking system, some crosstalk is present with the topography which does not make this image fully trustworthy.

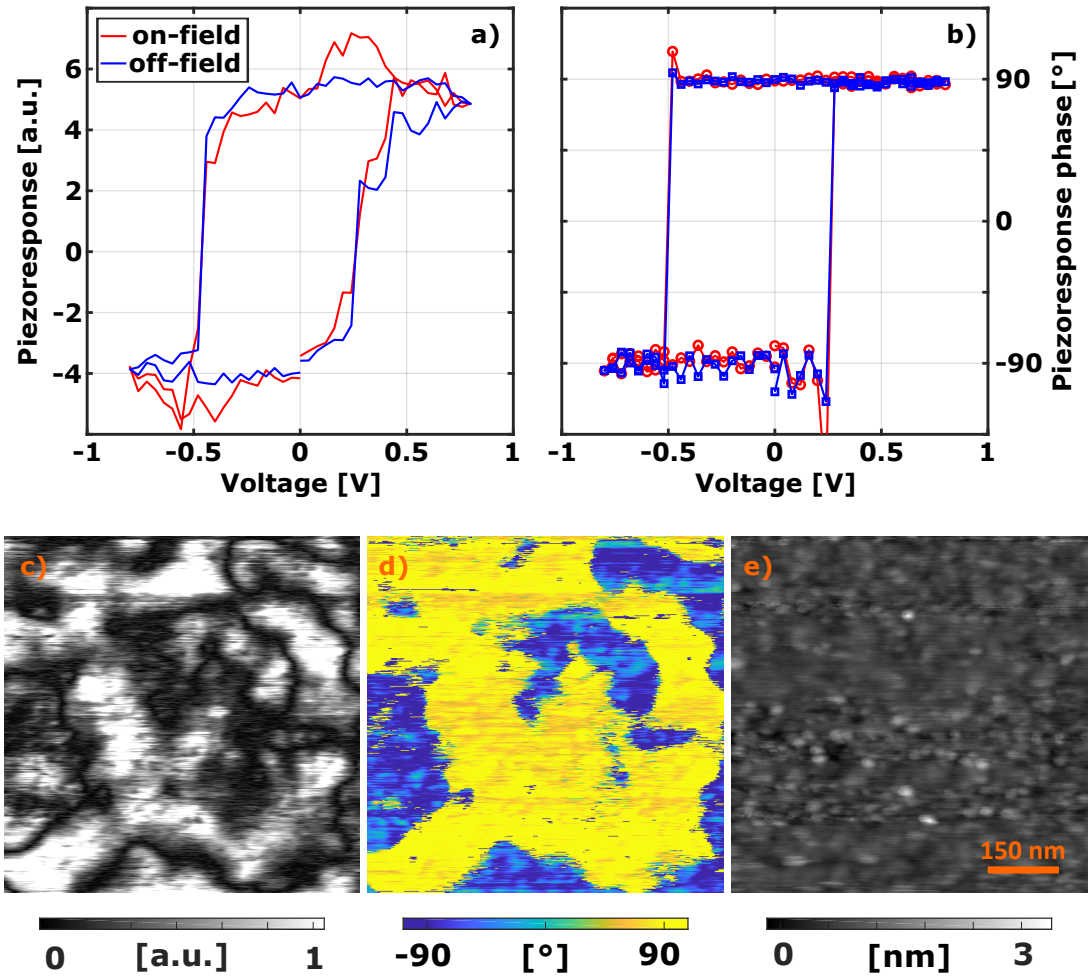

Figure 5.11: Resonance PFM preliminary analysis on 5 nm HZO. a) Amplitude and b) phase loops taken on a single spot and c) amplitude, d) phase and e) topography scans taken on a 0.75x0.75 μm^2 area after -0.2 V poling. All measurements were taken with a probing ac voltage of 0.2 V and frequency of 1.2 MHz, smaller but close to f_r of the system.

However, the presence of imprint and permanently poled regions was noticed also in off-resonance measurements on 7 nm film of Fig. 5.5, where no crosstalk was present. These results seem to support the view of a more difficult switching for thinner films at the global scale, with major presence of strongly pinned areas. At the same time, in the regions where switching is possible, the extreme reduction of film thickness and the scenario of nuclei of cylindrical shape which extend through the entire film could explain

why they possess such low coercive field.

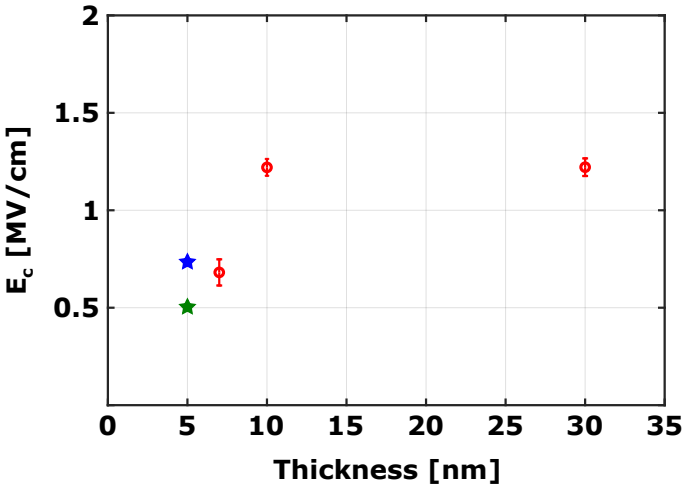

Figure 5.12: Proposed coercive field extrapolation for 5 nm HZO films based on preliminary data collected off-resonance (green star) and close to resonance (blue star).

In conclusion, measurements on 5 nm HZO were attempted but proved to be very challenging due to the combination of leakage of the film and quasistatic nature of off-resonance PFM technique. The analysis could be partially improved by measuring close to f_r, but without implementing any resonance tracking system the results cannot be conclusive. The very limited set of collected data however includes a few PFM loops which consistently switch at voltages lower than 0.5 V ($E_c \approx 0.5$ MV/cm). For the sake of comparison, the two values of coercive field extracted in this preliminary analysis with the two different approaches are plotted against thickness in Fig. 5.12. This suggests the possibility to achieve stable sub-1 V operation voltage on ultrathin HZO films (< 10 nm), possibly leading to further E_c reduction if high quality thin films of even smaller thickness can be produced.

5.2 Summary

This chapter presented a set of off-resonance PFM data including the qualitative and quantitative characterization of HZO thin films of 30, 10 and 7 nm. Very precise measurements allowed the quantification of d_{33} in these films, demonstrating a vertical resolution < 0.1 pm with the lowest bias applied to the 7 nm films. Their switching behavior was analyzed, showing a high presence of nonswitching regions in the thinner 7 nm film. The most remarkable findings however concern the unexpected thickness dependence of coercive field that was found in this work. The same value of E_c is observed for 10 and 30 nm samples, implying that the effect of thickness plays a marginal role in HZO thin films. Unexpectedly, E_c decreases almost by half when the thickness is further reduced to 7 nm. This implies that entire saturated loops could be obtained in the sub-1 V region, with switching occurring near 500 mV.

This result is explained in the frame of a nucleation scenario which introduces a different shape of the domain nuclei, which are suggested to pass through the entire film thickness. In order to test the proposed nucleation mechanism, the analysis of even thinner films is attempted, in the logic that such model should be applicable to them as well. Some initial results on 5 nm thick HZO are presented in the second section: the analysis proved to be extremely challenging due to the very low signal of such thin films which required longer integration time and introduced significant leakage. A few PFM loops possessing very low coercive field could be obtained nonetheless, but the presented data can only be the groundwork for a more thorough investigation of ultrathin films, possibly even thinner than 5 nm. It is clear that very high quality films need to be prepared for that, and the measurement technique has to be pushed at its very limit since extremely small voltage of 0.1-0.2 V are necessary to detect millivolt range PFM loops. The challenge is hard, but the implications for low-power electronic devices are equally strong.

6 | Switching in ferroelectric/dielectric bilayers: competing scenarios in HfO_2-based thin films

This chapter turns to the investigation of heterostructures where a dielectric layer is placed in contact with the ferroelectric. This configuration is of great interest in that it allows accessing Negative Capacitance (NC) regime in the ferroelectric material. Results of off-resonance PFM investigation on MFIS and MFIM structures, on which NC was previously demonstrated, are presented in the first two sections. The third section discusses the open questions issued from the findings on different switching mechanisms observed in HfO_2-based ferroelectric thin films in this chapter and throughout this work.

The capacitor structures analyzed so far always dealt with ferroelectric-metal (F/M) interfaces. The role of defects at such locations is considered paramount in influencing the switching behavior of ferroelectric HfO_2-based thin films, as they can interfere with domain nucleation and growth. Interface charge injection and trapping are also associated to wake-up, fatigue and bias fields [29]. HfO_2-based thin films are generally polycrystalline in nature unless deposition of epitaxial layers on special substrates is pursued, which introduces another source of defects in the film and at the interfaces in the form of grain boundaries [2]. All the interface-related phenomena are amplified in thin films because, despite interfacial layers being really thin (estimated around 0.8 and 1.5 nm for HZO and Gd:HfO_2, respectively [29, 65]), their thickness ratio with respect to the film is higher than in bulk ferroelectrics, even comparable for ultrathin films.

For these reasons, the conventional Kolmogorov-Avrami-Ishibashi (KAI) theory that is used for describing domain nucleation and growth mechanism in bulk ferroelectrics fails to explain the switching behavior of thin films; it was shown that such mechanism is instead best described by Nucleation Limited Switching (NLS) [27]. The salient difference between the two approaches is that KAI theory explains switching as the practically simultaneous nucleation of domains in the crystal which then coalesce, pointing at domain wall movement inside the crystal as the switching liming factor; on the other hand, NLS theory considers the switching as locally confined to multiple small regions of the

material, where it happens independently from other regions. Here, the limiting factor becomes the domain nucleation time within each region. Since interfaces are defect-rich regions, they act as preferential nucleation sites for domains in polycrystalline thin films, a fact that explains the better fit of NLS with respect to KAI in explaining domain nucleation dynamics.

In this chapter the investigation focuses on structures where the ferroelectric layer is in contact with an electrode on one side and an insulator on the other side. Metal-Ferroelectric-Insulator-Semiconductor (MFIS) and Metal-Ferroelectric-Insulator-Metal (MFIM) structures are of high technological interest in devices aiming to stabilize and exploit a reversible Negative Capacitance (NC) regime to reduce operation voltage and power loss [91, 157]. A crucial requirement of low-power consumption negative capacitance FET (NCFET) is that polarization reversal needs to be avoided and the device should show no hysteresis. The basic assumption underlying most works on NC devices is then intrinsic polarization switching of the ferroelectric [35, 157, 158], even though theoretical studies suggesting NC on polydomain ferroelectrics exist too [92, 93].

However, as discussed in the introduction, this clashes with the commonly accepted explanation of domain nucleation and growth in HZO and other HfO_2-based thin films, which is happening at fields lower than thermodynamic E_c and implies hysteretic behavior as discussed before. The polarization reversal is usually examined in terms of NLS or KAI scenarios [86, 87]: intrinsic switching is simply disregarded as it is considered impossible to reach without first activating another extrinsic mechanism at lower voltage. It follows that understanding the switching dynamics in heterostructures used for NC devices is of theoretical interest other than of primary importance for reliable applications.

Given the critical role that interfaces play in ferroelectric thin films, a heterostructure where the ferroelectric is in contact with a dielectric instead of a metal could potentially show different switching mechanisms. In particular, a ferroelectric-insulator (F/I) interface is expected to behave very differently than a F/M one. When a ferroelectric thin film is polarized, there is a net charge at its two opposite surfaces; in the capacitor configuration, the top and bottom metal electrodes readily compensate it. When the stack includes a dielectric, the charge compensation is hindered by the insulator at the F/I interface.

The slow charge compensation finds a particular interest in the quest for NC devices, due to the possibility to access the NC state in the ferroelectric which is enabled by the adjacent dielectric layer [35]. Experimental findings showed that, by application of extremely short voltage pulses in the direction opposite to the stable polarization, it is possible to follow the usually inaccessible S-shaped curve in the P-E plot, as expected by Landau theory [35, 89].

This chapter presents a PFM investigation carried out in order to elucidate the nature of switching mechanisms in MFIS and MFIM heterostructures where NC was already successfully demonstrated. It is important to notice that off-resonance PFM investigation situates at the opposite time scale with respect to the extremely fast analysis that

is usually employed to observe NC effect. The switching pulses applied during PFM measurements are in the order of seconds, whereas pulses used to observe NC are in the order of hundreds of nanoseconds. Therefore, switching is achieved during this analysis whereas it is avoided in the nanosecond pulse experiments. It will be discussed how the results obtained by these two very different approaches can be compared and allow to speculate about the switching scenario in such heterostructure configurations.

The first section of this chapter will present results on a Si/SiO_2/Si:HfO_2/TiN/Pt (MFIS) stack, depicted in Fig. 6.1a. Here the dielectric layer is a thin SiO_2 layer thermally grown on Si; the ferroelectric Si:HfO_2 is then deposited on top of it [89]. The detailed fabrication process can be found in appendix. This is a very application relevant heterostructure, since it constitutes the gate stack of a FET. However, a very strong imprint is found for this structure, which prevented a full analysis of the switching behavior; the reasons and a way to overcome this problem will be discussed. The second section will instead investigate a Si/TiN/HZO/Ta_2O_5/TiN/Pt heterostructure where the dielectric layer is deposited on top of the ferroelectric, depicted in Fig. 6.1b. The results obtained by quasistatic off-resonance PFM analysis are found to be in good agreement with the nanosecond-range pulse measurements previously performed on the same structure [35]. The implications of this finding will be discussed in the third section, where an overview of the different and sometimes conflicting switching kinetics reported for HfO_2-based thin films is presented.

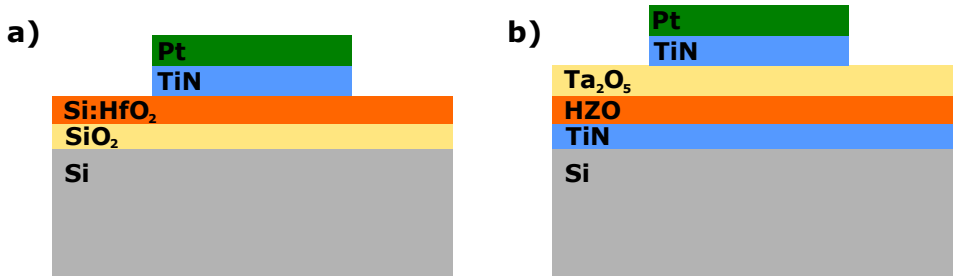

Figure 6.1: Negative capacitance a) MFIS and b) MFIM heterostructures analyzed in this work; the orange and yellow layers are the ferroelectric and dielectric, respectively.

6.1 Off-resonance PFM in NC gate structure: challenges and limitations

The MFIS heterostructure investigated here is very relevant for applications as it constitutes the gate stack of a NCFET. The layers, from bottom to top, are Si/SiO_2/FE/TiN/Pt, where FE is the ferroelectric Si:HfO_2 layer (Fig. 6.1a). The structure was first analyzed by GIXRD and only a low amount of monoclinic phase (< 5 %) was detected, meaning that the Si:HfO_2 film mainly crystallized in the orthorhombic or tetragonal phase, as can be seen in Fig. 6.2 [89].

The electrical analysis of the device revealed positive and negative V_c of 5.5 and -7.5

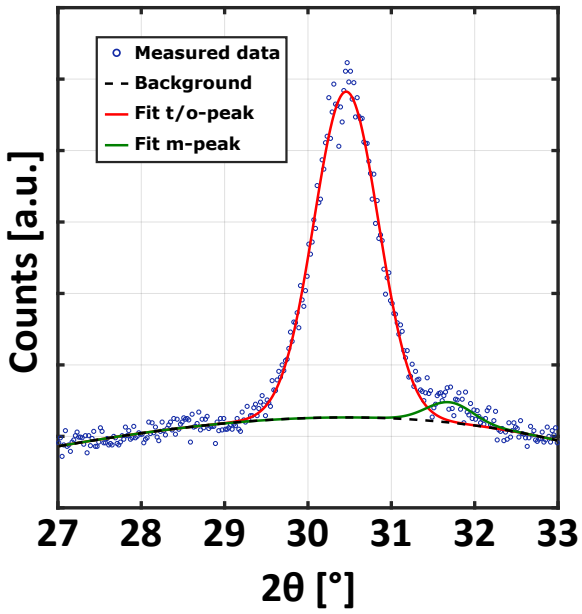

Figure 6.2: GIXRD characterization of Si:HfO_2 showing a good crystallization in t/o-phase with very little (< 5 %) amount of m-phase.

V, respectively, indicating a positive imprint of 1 V across the whole stack [89]. It was observed that, before application of external voltage, the stable state of polarization is the one pointing towards the dielectric SiO_2 layer. Consequently, the NC effect could be detected by applying negative pulses to the top electrode while keeping bottom Si layer at constant bias. Since the pulses are very short (500 ns), the charges cannot be compensated at the F/I interface and the polarization state cannot stabilize, meaning that as soon as the voltage is removed the sample switches back to the stable state, with polarization pointing down.

Such strong bias was observed in off-resonance PFM analysis as well. Fig. 6.3 shows piezoresponse loops collected on the structure with ac signal of 1.3 V and frequency of 92 kHz. The applied dc field reached 8.5 V, close to the maximum allowed by the setup, for which ac + dc cannot exceed 10 V. This was necessary in order to switch the sample in negative direction. Despite the longer pulse times applied in off-resonance PFM, the retention problem was evident when the sample was poled in negative state. The loop is acquired with a voltage sweep starting in negative direction: looking at piezoresponse amplitude loops, the on- and off-field signals are in good agreement until the material switches in the negative state, then the off-field loop displays a constantly lower response amplitude than on-field. This suggests that the film cannot retain the negative polarization state even after second-long pulses. When applied negative bias is reduced in magnitude, even the on-field loop response is decreasing, meaning that it is not sufficient to overcome the bias in the film and fully switch it in the negative state. As a result, from about -1 V onwards, the on- and off-field coincide again, and with a very low response. This extremely low amplitude is also causing the phase signal to become very noisy, as observed in Fig. 6.3b. Then, once polarization switches to the preferential

direction (positive bias, polarization vector pointing down), both amplitude and phase are again showing a strong signal. A further aspect complicating the PFM analysis is leakage, which is evident in Fig. 6.3a by the response at high fields: it is not flat and saturated but some clockwise loops can be observed, indicating charge injection.

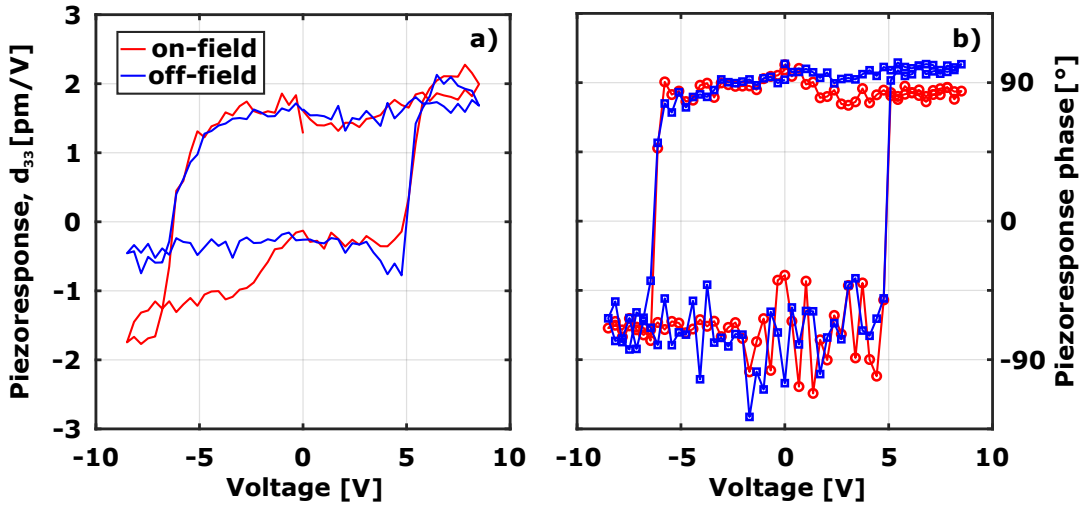

Figure 6.3: a) Amplitude and b) phase off-resonance PFM loops acquired with probing ac voltage of 1.3 V and frequency of 92 kHz on MFIS heterostructure showing a very poor retention of the negative polarization state in the ferroelectric.

When films present strong built-in bias, collecting scans showing the two polarization orientations could be very challenging due to the extremely high acquisition time required by off-resonance PFM. Fig. 6.4a-c show 1x1 μm^2 scans of the sample positively poled at 5.5 V (a), then close to the negative V_c at -6.5 V (b) and finally negatively poled at -9.5 V (c). As expected, the sample could be uniformly poled in positive direction as it can be understood by checking the phase scan in Fig. 6.4a; looking at the amplitude scan a pattern of more or less strong areas can be visualized, but this never exceeds the very low value of 2 pm/V, similarly to what was observed in piezoresponse loops. However, it is not possible to analyze their evolution because the amplitude at negative V_c and negatively poled state are too low. This is coming along with a noisy phase response, which is especially evident in Fig. 6.4c when the sample was poled at -9.5 V. The scan acquired at -6.5 V displays some different regions indicating that possibly a partial switching was achieved. The related amplitude scan shows some features vaguely corresponding to the pattern observed in the phase scan, but the extremely low response is making an interpretation very difficult.

Looking at the negatively poled state, the impact of built-in field is evident: the image is acquired scanning from top to bottom, and a phase gradient can be noticed in that direction. This indicates that during the acquisition time (> 4 hours) the polarization is slowly switching back to its preferred state. Since the poling procedure employed a 1 s pulse at -9.5 V, which surely introduced some leakage and charged defects at both ferroelectric interfaces, it is expected that a charge redistribution is taking place at such long timescale.

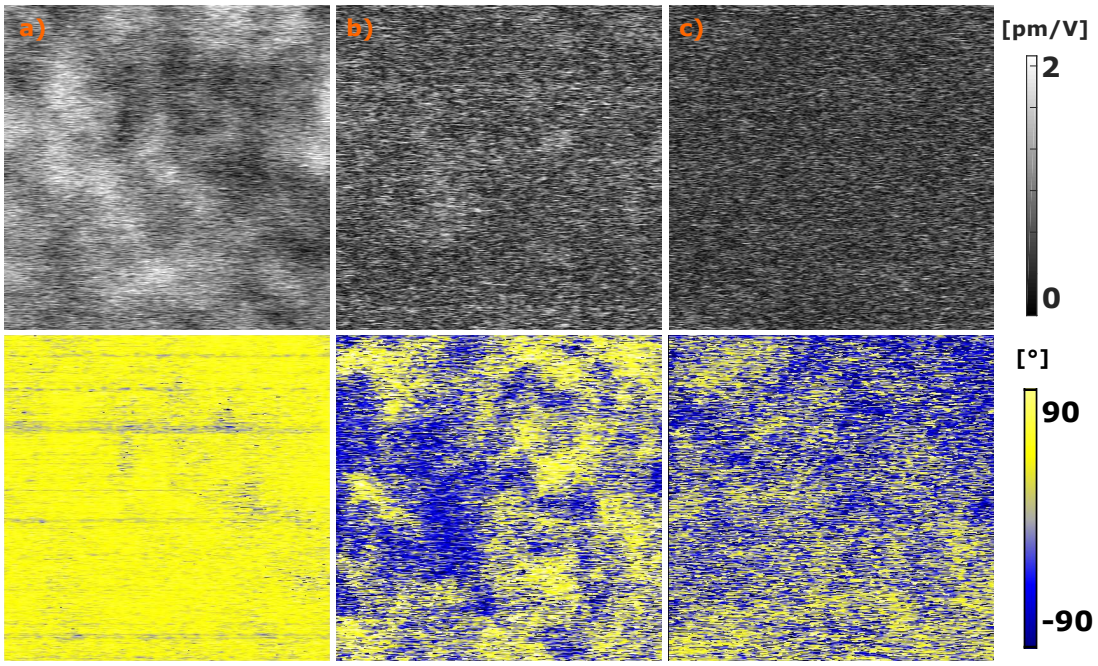

Figure 6.4: Amplitude and phase PFM scans acquired on MFIS heterostructure with ac bias of 1.3 V and frequency of 92 kHz. The stack was first poled at a) 5.5 V, then reversed to b) -6.5 V and finally to c) -9.5 V, and shows a low retention in the negatively poled state.

To summarize, the dramatic effect of built-in field in stabilizing one polarization state was observed by PFM, a result that is in agreement with reported I-V curves and pulse measurements used to investigate NC in this structure [89]. However, a clear analysis of polarization reversal mechanism could not be performed on this structure due to the internal bias which prevented from stabilizing one of the two polarization states. This can be ascribed to the p-doped Si which has a higher work function than TiN, and creates an asymmetry in the structure, even though more in-depth analysis is necessary on this regard [89]. Overall, the proposed MFIS structure, while being very relevant for applications requiring a NCFET, might not be ideal for investigating the ferroelectric/dielectric interface.

This consideration however suggests that fabricating a more symmetrical structure, where both top and bottom electrodes are of the same material, can be a way to overcome this issue. Substituting Si with TiN allows obtaining a more idealized structure where the effect of dielectric-ferroelectric interface can be better isolated and is not masked by a strong voltage drop across the whole stack.

6.2 MFIM as ad hoc heterostructure for investigating intrinsic switching in ferroelectrics

The Si/TiN/HZO/Ta_2O_5/TiN/Pt structure shown in Fig. 6.1b is analyzed in this work. The previously reported GIXRD characterization of the ferroelectric film showed predominance of t-/o-phase and only very little amount of m-phase, as is often reported for thin HZO layers, and indeed good ferroelectric behavior was reported on this film [35].

On this structure, PFM experiments are carried out as usual by respecting all criteria detailed in chapter 2, namely measuring with stiff cantilever, through a top electrode, and off-resonance. Reliable PFM loops and scans could therefore be obtained which enabled to quantify the very small d_{33} of the material. However, a major difference with respect to previous measurements reported in this work is the presence of a Ta_2O_5 dielectric layer between ferroelectric and electrode, with a thickness slightly larger than the ferroelectric itself. This means that the detection is occurring through a > 40 nm thick stack. This layer is further clamping the ferroelectric film and possibly affecting the response, and this adds to the slow charge compensation at the F/I interface that was discussed earlier; overall, it is not trivial to anticipate what the contribution of a thick dielectric layer will look like in PFM measurements.

Fig. 6.5 shows a loop acquired with probing ac bias of 1 V and frequency of 92 kHz. It can be seen that on- and off-field loops are very similar, attesting to the genuine ferroelectric origin of the response signal; in addition, they present an unusual shape with increasing amplitude in the positive voltage and lower response for negative bias. This anomalous behavior was not observed before in other capacitor samples so it is attributed to the presence of a thick dielectric layer. The effect of leakage is also observed, by looking at the high voltage response, in form of regions with clockwise rotation of the amplitude signal: the onset of leakage appears earlier for negative applied bias, in agreement with observation of an easier breakdown for negative poling [35].

Interestingly, a qualitative difference is noted when comparing the loop of Fig. 6.5 with the ones obtained on the MFIS structure investigated in the previous section, see Fig. 6.3: no remarkable intrinsic bias is observed across the capacitor, suggesting that a considerable part of the strong asymmetry observed in the MFIS structure studied earlier can indeed be related to the different electrode materials. Only a few measurements could be obtained before capacitors breakdown, therefore a statistical study of the switching properties could not be presented. However, averaging 5 loops, positive and negative $V_c \approx 2.7 \pm 0.2$ V and -2.5 $\pm$ 0.2 V were obtained. At V_c, since the ferroelectric has approximately zero polarization, a voltage divider equation to find the voltage of the ferroelectric V_F as a function of the applied voltage to the stack V, can be written as

$$V_F = V\left(1 + \frac{d_D \epsilon_F}{d_F \epsilon_D}\right)^{-1}. \tag{6.1}$$

In the previous equation, d and ϵ are thickness and relative dielectric constant, whereas

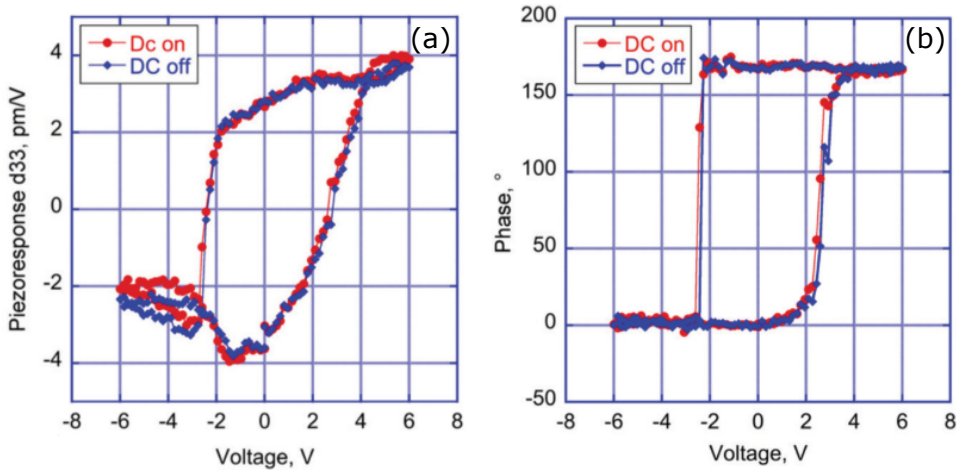

Figure 6.5: a) Amplitude and b) phase off-resonance PFM loops acquired with probing ac voltage of 1 V and frequency of 92 kHz through dielectric layer and top electrode on MFIM heterostructure (reproduced and adapted from [159])

subscripts F and D refer to ferroelectric and dielectric layer. Values for this structure are d_F = 11.6 nm, d_D = 13.5 nm, ϵ_F = 42 and ϵ_D = 23.5 [35]. This corresponds to a true V_c for the ferroelectric layer of 0.84 V, equal to a coercive field of 0.72 MV/cm, which agrees very well with the value of 0.7 MV/cm extracted from the S-shaped curve analysis [35, 159]. Notably, this implies that results obtained by PFM are consistent with intrinsic polarization switching scenario.

A way to investigate the switching model by PFM is to collect surface scans at different polarization states. Fig. 6.6a-c show sequential PFM amplitude and phase maps acquired on a 1.5x1.5 μm^2 area: the results are on a sample first poled for 1 s at -6 V, then at 6 V, and then again at -6 V, respectively [159]. The amplitude images enable to spot very fine details of single switching regions down to $\approx$ 30 nm; the phase scans show instead that for both polarization orientations the sample does not reach the fully poled state. Looking more carefully at Fig. 6.6a and c, it is remarkable to observe features in negatively poled state that are maintaining almost identical shape after being first poled in the positive direction and then back again. Red circles in Fig. 6.6a and c highlight two of these regions but many more can be observed. This result is unexpected, since the usual picture predicts domains that nucleate and grow with applied field at every switching event. What these findings suggest is rather the presence of local nanometer-size ferroelectric regions that switch independently of one another.

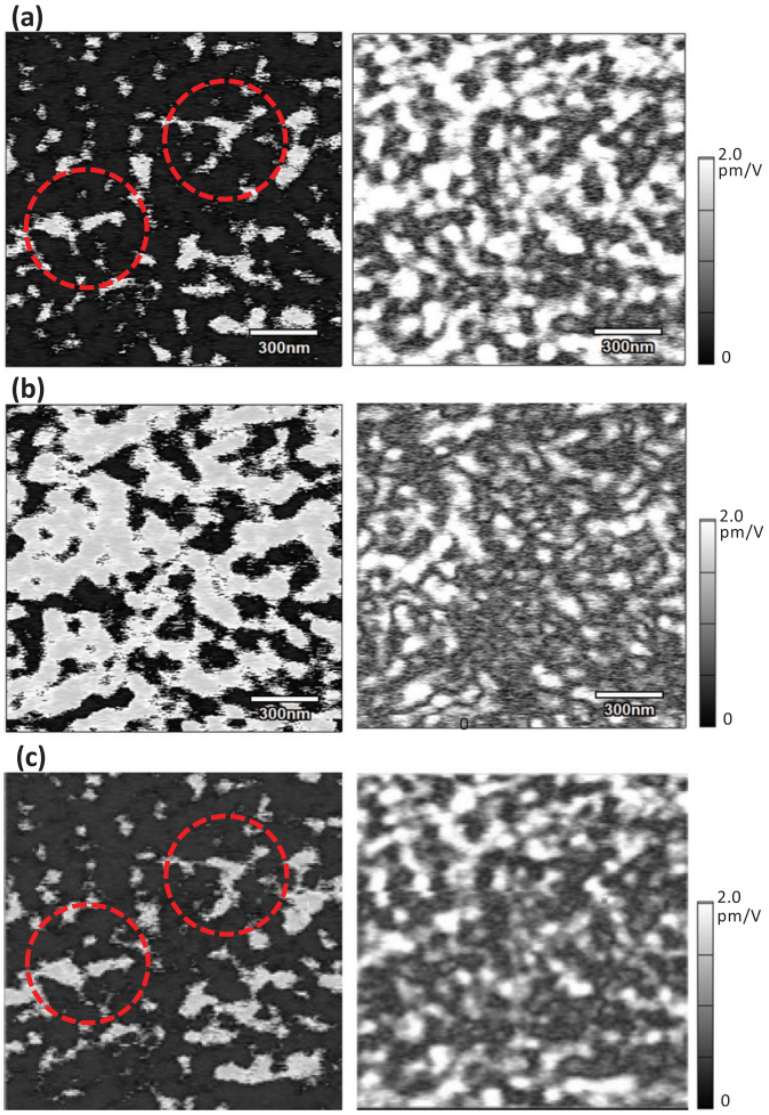

Figure 6.6: 1.5x1.5 µm^2 off-resonance PFM scans acquired with ac probing voltage of 1 V and frequency of 92 kHz showing the sequential poling at a) -6 V, then b) 6 V, and then again c) -6 V (reproduced from [159])

When analyzing the switching mechanism of this stack, it is important to consider the possible impact of trapped charges at the F/I interface [151]. It was shown on this structure that the total field applied to the dielectric is very high and ultimately is the factor causing breakdown [35]. It is then reasonable to think that, with increasing applied field during a switching cycle, leakage occurs and charges get injected and trapped at the F/I interface. If this is the case, subsequent switching to the opposite polarization state will occur at higher coercive field due to the trapped charges acting against the applied field [151]. This effect is expected to be dependent on the maximum applied voltage, as this will cause more charge injection at the interface. This explanation could

justify a detected higher E_c in this structure when analyzed by PFM, which applies very long pulses and can induce more injected and trapped charges. In this context, a switching following NLS model is still possible and higher values of E_c will be detected, comparable to the one related to intrinsic switching by fast pulse measurements.

This hypothesis can be tested experimentally by acquiring PFM loops on the same spot at increasing maximum dc bias. The effect of trapped charges should be visible as an increase of the coercive field with increasing maximum dc bias if the previously explained mechanism applies. Fig. 6.7a-f present such series of loops, with maximum dc bias ranging from 5 to 7.5 V. As it can be seen in Fig. 6.7g however, no such dependence is observed, with V_c being independent on maximum applied bias until 6.5 V, when a weak increase is noticed only for the switching in negative direction. The coercive field seems not to be affected by charges trapped at the interface, therefore the value obtained by PFM loops (see Fig. 6.5) can be regarded as intrinsic.

The remarkably close coercive field values obtained by two very different techniques such as ultra-fast pulses and off-resonance PFM suggest that intrinsic switching is taking place in this heterostructure, as opposed to different values predicted by NLS scenario. PFM scans display a region-by-region switching which is usually invoked in thin films when describing NLS model [86]. In principle this does not contradict the possibility of intrinsic switching; however, the two look very similar because in both cases the switching occurs independently in nanometer-size regions. A crucial difference reported here is the fact that such individual regions have well defined boundaries which do not change shape even after consecutive repoling in different directions. The presence of secondary phase or localized charged defects could explain such behavior. This renders a scenario depicting growing domains less applicable to these regions, which instead have to be treated as independently switching islands within the material. In addition, the weak dependence of V_c on the maximum applied voltage is showing that trapped charges at the interface are not playing a major role in the switching, which is on the contrary expected if polarization reversal is governed by NLS scenario.

In this work, slow PFM measurements were used to analyze the case in which both polarization states are reached and maintained, in opposition to the ultra-fast experiments already conducted on this structure which relied on the slow charge compensation at the F/I interface to avoid stabilization of opposite polarization state [35]. This study can therefore investigate the switching behavior and bring forward indications that switching in this MFIM heterostructure is intrinsic. This has relevant consequences also for memory applications which do not need NC, as intrinsic switching is faster and less temperature dependent than NLS; it also relies less on the interface properties which prove to be so critical in thin films. From this work emerges also the need to obtain a higher uniformity of the deposited film: achieving a lower defect concentration and avoiding presence of non-ferroelectric phases are both expected to improve the switching properties.

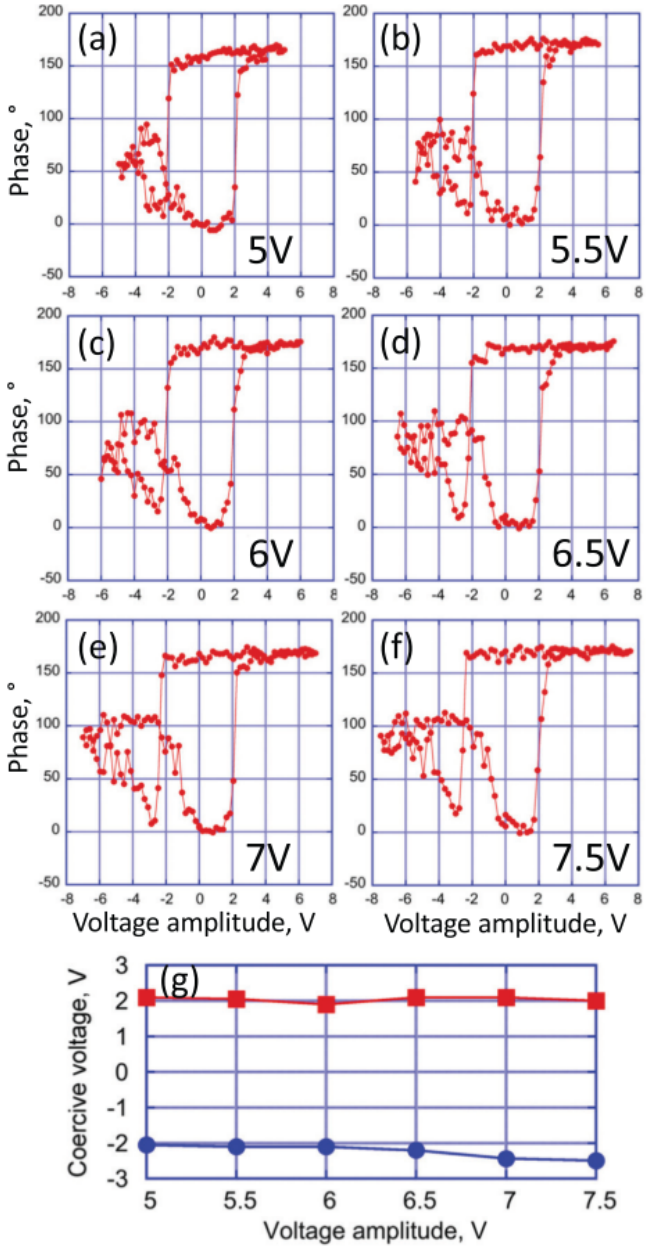

Figure 6.7: V_c dependence on maximum applied voltage. a-f) Loops acquired with increasing voltage from 5 to 7.5 V; g) extracted V_c for each maximum applied voltage (reproduced from [159]).

6.3 Interface modulated switching scenarios in HfO_2-based thin films

Huge progress has been made in understanding ferroelectricity in HfO_2-based thin films since their discovery; major features differentiate them from perovskites, the other extensively studied class of ceramic ferroelectrics. Notably, it was found that the scaling behavior of ferroelectric properties is nearly opposite between these two materials. Perovskites are reported to have a lower limit to retention of stable ferroelectricity, given by the insurgence of a strong depolarizing field for thickness smaller than few tens of nm [131]; on the contrary, HfO_2-based materials rather show an upper limit approaching the few tens of nm, caused by the stabilization of non-ferroelectric phases in the film, and are reported to be ferroelectric down to less than 2 nm [2, 160].

The extremely small thickness that can be achieved in these films is causing ferroelectric interfaces to play a major role in the switching behavior of the material. More specifically, it is often reported that nucleation of opposite polarization domains is an interface-mediated phenomenon. PFM is a very powerful tool for investigating domain dynamics in ferroelectric materials, because it allows tracking polarization switching with nanometer size resolution. Throughout this work off-resonance PFM was used to investigate HfO_2 and HZO in conventional capacitor structures and Si:HfO_2 and HZO in ferroelectric/dielectric heterostructures. The emerging picture is far from univocal.

The analysis of capacitor structures in chapters 4 and 5 corroborated the widely accepted interpretation of polarization switching described by NLS model. In the case of undoped HfO_2 it was shown that electrical cycling initially improves the switching properties of the film. A greater area of the film is observed to switch in trained device than in pristine one, a fact that is usually associated to defects redistribution, mainly O vacancies, from interface to bulk, which allows domain depinning. Concurrently to this phenomenon, as tetragonal phase is most stable when there is high concentration of O vacancies, a relaxation of distorted t-phase into ferroelectric o-phase is usually noted at the interfaces [29]. The results presented in chapter 4 on undoped HfO_2 agree with this picture. In particular it was suggested that t-phase could be polar, and hence detected as a piezoelectric contribution to PFM signal, due to the distortion induced by the high interfacial stress.

Within the NLS scenario, interface stress and defects are closely related to polarization reversal as well. The nucleation of domains with opposite orientation is given by a complex energy balance, which is locally altered by the interface topology. Critically, pinning sites for domains can come from structural defects such as grain boundaries or just different local strain between ferroelectric and electrode materials. This adds to charged defects which can inject from electrodes and become bound. Such irregularity of topography and charged defects concentration at the interfaces is responsible for the preferential switching of some regions over others, and this is causing the typical distribution of switching times described by NLS. This effect was noted in HZO capacitors analyzed in chapter 5 but, as the thickness was decreased to 7 nm, an unexpected behavior was revealed: the film could no more be fully polarized and the polarization reversal

occurred at much lower field, almost half than what was found for 10 nm films.

The origin of this anomalous behavior is proposed to be a nucleation mechanism which still follows NLS model but requires a different shape of domain nuclei, which are proposed to be cylindrical and crossing the whole film. According to this model, the very small thickness of the film is comparable to that of stable nuclei of opposite polarization: consequently, once nucleated, they do not have to grow against the depolarizing field but are only expanding sideways, demanding less energy. This scenario is therefore strongly dependent on the film thickness (it becomes less favorable for thicker films) and interface properties. Indeed, in some areas of extremely thin films where favorable conditions develop, nuclei can stabilize and through-domains become permanent: this can happen for instance due to insurgence of local, nanometer-size charged regions on one F/M interface, which can occur both in the deposition process and during electrical cycling.

Other than the discussed interfacial defects and stress distribution which influence the energy of domain nucleation and growth, the nature of interface is crucial in defining the switching mechanism of ferroelectric films. The typical picture of domain nucleation and growth for oppositely applied field is achieved thanks to the prompt availability of charges at the F/M interfaces with conductive electrodes, which stabilize newly formed domains. If one of the two sides of the ferroelectric is placed in contact with a dielectric, as in the NC structures examined in previous sections, an asymmetry is introduced and this is no longer the case. Charge compensation is very slow at the F/I interface with a dielectric material, and this is found to affect the nature of polarization switching. In these structures, starting from the polarization orientation that is pointing towards dielectric layer, it is possible to access NC by applying voltage pulses in the opposite direction.

Results on the MFIM structure shown before allude to an altogether different mechanism of polarization reversal. Here, the E_c detected by PFM is very close to the one calculated by the fast pulse analysis conducted on the same structure to observe NC effect. Remarkably, the coercive field is also not showing major variations when the maximum voltage applied to the stack is increased up to 50 %. In addition, isolated nanometer-size switching regions are observed which are confined by sharp boundaries that do not change even after poling in opposite direction and repoling back the film. These findings do not agree with NLS model and therefore support the claim that switching in the film is intrinsic, which is the core hypothesis of NC detection. The picture is however complicated by the fact that independent isolated regions observed by PFM surface scans look similar to the features expected in NLS scenario with very slow domain walls.

It is worth mentioning that calculated intrinsic E_c is found to be ≈ 0.7 MV/cm in the MFIM heterostructure, whereas usually reported values for extrinsic switching in HfO_2-based thin films are around 1 MV/cm in capacitors. This is at odds with the fact that extrinsic switching scenarios are introduced precisely to explain the observation of polarization reversal at fields lower than intrinsic E_c. This result then highlights the major detrimental role played by thin interfacial layers that are formed between

ferroelectric and electrodes in the usual capacitor configuration.

The unforeseen findings on the coercive field of HfO_2-based thin films presented throughout this work were correlated to variations in thickness of ferroelectric layer and different materials at the interfaces. Accordingly, contrasting scenarios were proposed in this dissertation to explain polarization reversal. The confusion is generated by the inherent difficulty of studying extremely thin films, where bulk properties of materials are less relevant and become mostly dominated by external energy contributions related to complex stress and electric fields. Examples are surface energy of different phases, roughness and charge distribution at the interface, electrode material, injection and trapping of charges, stress induced by the annealing under top electrode, and so on. To add further ambiguity to the interpretation, these are often concomitant and difficult to isolate experimentally. Despite the apparent mayhem, this chapter shows that comparing results of conceptually different techniques such as fast pulses and off-resonance PFM offers a way to analyze the problem from different angles and gain insights into the complex switching behavior of ferroelectric thin films.

6.4 Summary

This chapter presented off-resonance PFM results on switching behavior of heterostructures where a dielectric layer is placed in contact with the ferroelectric. The MFIS and MFIM stacks analyzed in the first two sections are usually adopted in the investigation of negative capacitance. The proposed inspection method, laying in the timescale at opposite end with respect to fast pulse analysis commonly used, enables to study the case in which the ferroelectric switches to the opposite polarization state, a phenomenon that is avoided in NC experiments.

The MFIS heterostructure is showing a strong internal bias that prevented from stabilizing one of the two polarization states, therefore PFM analysis was somewhat limited on this sample. On the other hand, the PFM study of individual loops and surface scans on MFIM structure is revealing an unconventional switching behavior, that is framed in the context of intrinsic switching, as proposed for the explanation of NC effect previously detected in the same sample.

The polarization reversal caused by intrinsic switching in MFIM structure occurs at very low field, and this is in contrast with commonly published results on similar films which report extrinsic switching (by NLS) at higher field. The third section resumes the findings of this thesis regarding polarization switching mechanisms, and addresses the contradicting pictures showing the key role that film thickness and interfaces play in HfO_2-based ferroelectrics.

7 | Conclusion

This dissertation explored the ferroelectric behavior of HfO_2-based thin films taking as starting point some of the current technological challenges. From the fabrication point of view the thermal budget required during the annealing process still represents a hurdle, since it does not meet CMOS compatibility requirements for most dopants. In the perspective of possible applications, another main issue is the characterization of switching properties of thin and ultrathin films. In particular, the polarization reversal mechanism is influenced by many parameters and it is difficult to analyze films below 10 nm thickness, which are considered crucial in reducing operating voltage in applications. Finally, NC heterostructures including HfO_2-based thin films were recently demonstrated which rely on thermodynamic switching of the ferroelectric layer, which though was never confirmed before and contradicts the expected nucleation-limited switching scenario.

This work took then a dual approach. On the one hand it demonstrated a fully CMOS-compatible production path for Gd:HfO_2: this required the development of a recipe in which the influence of several process parameters on material properties was assessed. On the other hand, well-established ferroelectric materials deposited by ALD or sputtering were investigated by off-resonance PFM to clarify the switching behavior. The main findings and perspectives for future work are summarized below.

Demonstration of fully CMOS-compatible PLD fabrication process for Gd:HfO_2

It was demonstrated that Pulsed Laser Deposition (PLD) can be exploited in order to meet CMOS BEOL fabrication requirements for production of Gd:HfO_2 ferroelectric thin films with conventional TiN electrodes. The recipe development highlighted the need of a delicate balance between thermal budget during fabrication and annealing. By increasing the temperature during deposition, it was possible to reduce it in the annealing step, eventually obtaining ferroelectricity already for a maximum process temperature of 400 °C, with best behavior for 450 °C annealing. This result is suggested to stem from the high flexibility of PLD with respect to ALD, where chemical reactions between precursors are constraining the choice of fabrication conditions.

This work is however only a first step and it would be interesting to see if similar findings can be replicated with other dopants than Gd, making PLD a competitive fabrication method for CMOS-compatible hafnia ferroelectrics. In addition, fine optimization

of process parameters such as deposition pressure and oxygen flow is still needed in order to improve interface quality, which has a decisive impact on ferroelectric properties. In this regard, a promising path to follow is the in-situ fabrication of the whole capacitor structure, that is with top and bottom electrodes deposited by PLD without breaking the vacuum.

Optimization of off-resonance PFM for the analysis of ultrathin films with extremely weak piezoresponse

The arduous challenge of detecting and quantifying very weak ferroelectric response in hafnia thin films, which is orders of magnitude smaller than in PZT, is undertaken by optimizing off-resonance PFM. This technique was pushed to a new limit and allowed to obtain reproducible and artifact-free measurements of genuine ferroelectric features with vertical displacement lower than 0.1 pm in 7 nm films. The presence of secondary phases or the vicinity of a phase transition could be indirectly observed thanks to the quantification of ferroelectric response. With the same technique, high-resolution PFM analysis could also be accomplished on ferroelectric gate structures, where the detection of extremely low piezoresponse was obtained through a dielectric layer of thickness comparable to that of the ferroelectric.

These findings show that off-resonance PFM can be considered as the ultimate technique to investigate ferroelectric properties of thin films at the nanoscale. Among the strength of this method there is the possibility to characterize hafnia thin films directly in their application-relevant configuration, from capacitors to gate structures; in addition, thanks to the quantitative results, it is possible to envision a more complete comparison of ferroelectric response between different thickness and materials.

Analysis of evolution of ferroelectric response with cycling in undoped HfO_2

Off-resonance PFM extensive analysis of undoped HfO_2 allowed to examine and quantify in great detail the evolution of ferroelectric response with cycling. In comparison to pristine film, the amount of switchable area increases and imprint decreases when the material is electrically cycled. In particular, the quantified asymmetry of d_{33} between positive and negative polarization direction detected by off-resonance PFM on pristine sample is associated to the presence of tetragonal phase at the interface. This was already observed by other techniques but here its contribution to the ferroelectric response is directly assessed assuming that high local strain can render the unit cell polar and therefore piezoelectric.

The investigation of cycling behavior in undoped HfO_2 was interrupted by an early breakdown at 10^6 cycles, before any appreciable sign of fatigue could be detected. Given the potential of off-resonance PFM technique in quantitative determination of ferroelectric properties, it would be interesting to perform this study on a material with greater endurance to see what can be revealed about fatigue mechanisms.

Formulation of a nucleation mechanism to explain E_c reduction in ultrathin HZO films

Ferroelectric properties of 30, 10 and 7 nm thick HZO films were investigated by off-resonance PFM. Arrays of many piezoresponse loops and scans of polarization response at different poling states enabled for in-depth evaluation of thickness effect on ferroelectric properties. In particular, an unexpected decrease of E_c for thickness lower than 10 nm was unveiled.

This behavior was rationalized in the context of a switching scenario that proposes a different shape of nucleating domains, which becomes more favorable for extremely thin films. The proposed cylindrical domain nuclei go through the whole film and therefore only need little energy for side growth. The analysis of 5 nm thick HZO film was attempted in order to substantiate this hypothesis but it proved to be very hard to obtain a reliable set of data. Some preliminary results however seem to indicate that E_c is very low also in this film. A corroboration of the proposed alternative nucleation scenario clearly requires more evidence on 5 nm and possibly even on thinner films, as well as the development of a theoretical model.

Investigation of polarization switching in NC heterostructures

Negative capacitance heterostructures including a ferroelectric/dielectric bilayer were studied by off-resonance PFM in the context of examining the role of interfaces in switching behavior of ferroelectric HfO_2-based thin films. In particular, on a MFIM structure with HZO/Ta_2O_5 bilayer it was possible to obtain remarkably good PFM through the dielectric and top electrode stack and measure a coercive field corresponding to the value calculated on the same structure during NC analysis by fast pulses. The fact that two such different investigation techniques, operating at opposite time scales, give the same result supports the claim of thermodynamic switching required to observe negative capacitance. However, the calculated E_c value in this heterostructure is lower than what is commonly reported for extrinsic switching of HZO films, a discrepancy that implies a very important role of interface-adjacent layers in TiN/HZO/TiN ferroelectric capacitors.

In outlook, HfO_2-based ferroelectrics show a strong promise for further reduction of operation voltage for true mV-range applications. Ferroelectric layers of thickness < 2 nm have been already reported and this analysis suggests that there is no fundamental bar for the coercive voltage to scale down accordingly. It is believed that the techniques and approaches addressed in this work will contribute to the exploration of these fascinating systems in view of achieving new generation of low-power ferroelectric devices.

A | Appendix: Detailed process flows for samples fabrication

The samples analyzed in this work consist of five different structures:

- HZO capacitors;
- undoped HfO_2 capacitors;
- Gd:HfO_2 capacitors, whose film deposition was also part of this work;
- Si:HfO_2 Metal-Ferroelectric-Insulator-Semiconductor (MFIS) heterostructures;
- HZO Metal-Ferroelectric-Insulator-Metal (MFIM) heterostructures;

As mentioned in chapter 2, top contact deposition and device patterning was always performed in EPFL. The description of the process flows is therefore organized as follows: the first section refers to the deposition and annealing of the different material stacks with appropriate references when they were not part of this work. The second section will present the process flow, identical for all samples, that was used for creating the devices.

A.1 Thin films deposition and annealing

HZO capacitors

The bottom and top TiN electrodes were fabricated by reactive sputtering in N_2 ambient starting from Ti targets. The HZO films were instead grown by ALD at 260 °C using TEMA-Hf and TEMA-Zr as metal organic precursors, employing water as oxygen source. The chamber was purged by Ar, which was also the precursors carrier gas. The sample structure was annealed at 600 °C in N_2 for 20 s. The final stack, from bottom to top, is Si/TiN/HZO/TiN, see Fig. A.1a. The fabrication and annealing of this stack was not part of this work, and further details can be found in [98, 102].

Undoped HfO_2 capacitors

The bottom and top electrodes were sputtered starting from a Ti target in N_2 atmo-

sphere in order to obtain TiN, whereas the undoped 10 nm thick HfO_2 was sputtered in Ar ambient. The annealing of the material stack was performed at 1000 °C in N_2 for 1 s. The final stack, from bottom to top, is Si/TiN/HfO_2/TiN, see Fig. A.1b. The fabrication and annealing of this stack was not part of this work, and further details can be found in [99].

Gd:HfO_2 capacitors

The top and bottom TiN electrodes were RF sputtered at room temperature starting from TiN targets in an Alliance Concept DP 650 sputter tool. In the process, a power of 200 W and a chamber pressure of $5{\cdot}10^{-3}$ mbar with a 30 sccm Ar flow were used. The 21 nm thick Gd:HfO_2 layer was deposited by PLD starting from a 3.5% Gd:HfO_2 target supplied by Kurt J. Lesker. The deposition procedure requires a heat-up stage in which the chamber temperature is raised and stabilized at 330 °C with an internal pressure of 10^{-6} mbar in N_2 environment. Then, a pressure of 0.1 mbar is reached and subsequently maintained during deposition by an O_2 flow of 20 sccm. A thickness of 21 nm of Gd:HfO_2 is deposited by 2800 pulses in about two minutes with a fluence of 1.5 J/cm^2. The heating is then turned off and the material is passively let to cool down before being extracted from the tool. The annealing of the stack was performed in the temperature range 400 - 550 °C, either in N_2 or O_2 environments, in a JetFirst 200 by Qualiflow Therm. The final stack, from bottom to top, is Si/TiN/Gd:HfO_2/TiN, see Fig. A.1c. The fabrication and annealing of this stack was part of this work and was realized in the CMi facility in EPFL.

Si:HfO_2 MFIS heterostructures

A dry oxidation process is used to grow 4 nm of SiO_2 on top of Si and then Si:HfO_2 is directly grown on that. This is accomplished by ALD on a Beneq TFS200 at 300 °C using TEMA-Hf and SAM.24 precursors for Hf and Si respectively. The cycle ratio enabled to have a 3.4% doping. A top TiN electrode is then RF sputtered at room T starting from TiN targets on a Alliance Concept DP 650 with a power of 200 W and a chamber pressure of $5{\cdot}10^{-3}$ mbar, with a 30 sccm Ar flow. Finally, the gate stack is annealed at 600 °C for 2 min in N_2 in a JetFirst 200 by Qualiflow Therm. The final stack, from bottom to top, is Si/SiO_2/Si:HfO_2/TiN, see Fig. A.1d. The fabrication and annealing of this stack took place in CMi, EPFL, but were not part of this work, and further details can be found in [89].

HZO MFIM heterostructures

The bottom and top TiN electrodes were reactively sputtered at room temperature. The HZO layer was deposited by ALD at 260 °C using TEMA-Hf and TEMA-Zr precursors with water as oxygen source. The Ta_2O_5 dielectric layer was deposited on top of HZO by reactive sputtering at room temperature. The annealing was carried out in N_2 at 500 °C for 20 s. The final stack, from bottom to top, is Si/TiN/HZO/Ta_2O_5/TiN, see Fig. A.1e. The fabrication and annealing of this stack was not part of this work, and further details can be found in [35].

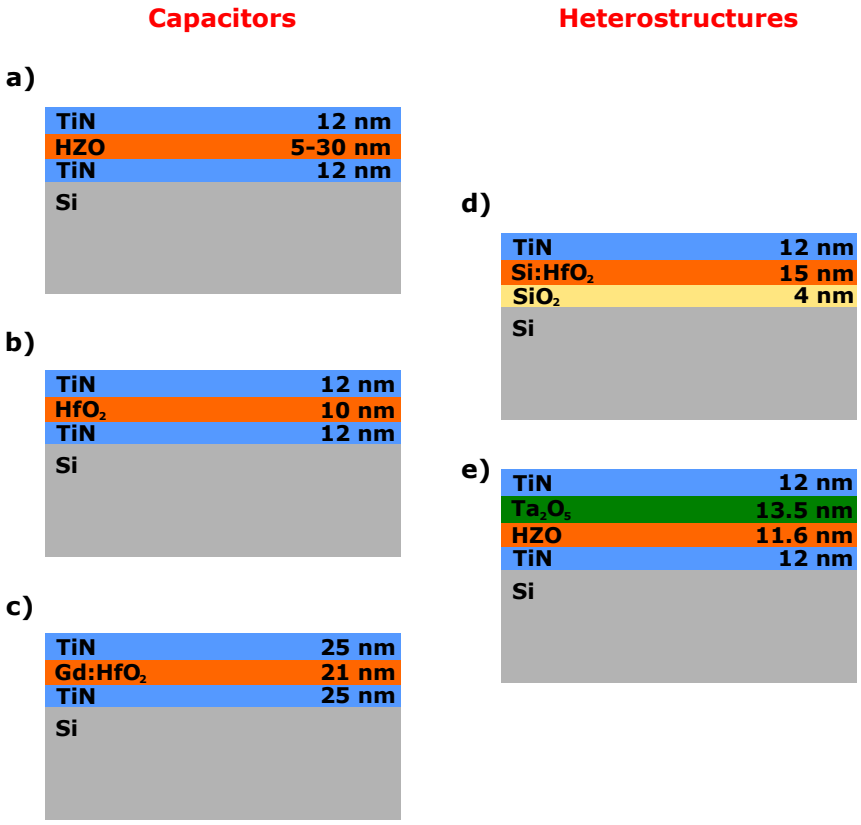

Figure A.1: Material stack until top electrode for all the samples used in this work: capacitor structures include a) HZO, b) undoped HfO_2 and c) Gd:HfO_2; heterostructures are d) Si:HfO_2 MFIS and e) HZO MIFM.

A.2 Top contact deposition and patterning of the structures

All the material stacks reported above terminate with a top TiN layer. In order to enable electrical and electromechanical characterization, a top layer of conducting material is deposited and then the substrate is patterned. This was always executed in CMi as part of this work and will be described once since it is the same for all structures. It is important to mention that, already before the annealing step, the wafers on which the thin films were deposited are diced into approximately squared chips of 1-1.5 cm side. This allows to have a greater output and try different annealing conditions on otherwise identical film. The externally fabricated samples are instead already received in form of chips.

First the top contact material is sputtered, and this is either Pt or W, the latter just used for the electrical characterization of Gd:HfO_2. For both materials the sputtering occurs in a DP 650 by Alliance Concept at room temperature with a power of 250 W and with a chamber pressure of $5{\cdot}10^{-3}$ mbar maintained by an Ar flow of 30 sccm.

The square or rectangular chips are thermally dehydrated by placing them for a few minutes on a hotplate at a temperature of 110-120 °C. This is necessary in order to ensure a better adhesion and remove water from the substrate surface. Next, they are vacuum-clamped to a chuck on a turntable and few droplets of liquid photoresist AZ 1512 are deposited on top of them with a pipette, until the surface is fully covered. The chip is then spun at 5000 rpm for 1 minute in order to obtain a uniform thickness of 1.1 µm. The amount of photoresist, the duration of the process and the rotational speed are critical in that they affect the uniformity and thickness of the polymer layer. During the spin coating procedure the liquid photoresist becomes denser by losing most of the solvent. Right after the spin coating is terminated, the chip is placed on a hotplate for 70 s, where the temperature is carefully controlled to be 100 °C. This baking process hardens the photoresist and further reduces the amount of residual solvent, stabilizing the polymer film and preparing it for the subsequent step. Once more, here the process temperature and duration are critical: a too low thermal budget leaves the film tacky and unstable, a too high thermal budget risks to excessively dry or even burn the photoresist. All the processes listed above, that is thermal dehydration, spin coating and post-deposition baking are performed on a SSE SB20 manual coater in CMi.

The following step consists in exposing selected regions of the photoresist by preparing a mask file that contains the coordinates of the regions to expose; in this way it is possible to obtain the desired pattern on the photoresist. The photolithography mask is fed to a MLA 150 laser writer by Heidelberg Instruments in CMi. A dose of 65 µC/cm^2 of near UV light (λ = 405 nm) with a defocus of -2 is used to expose the photoresist. Since AZ 1512 is a positive photoresist, the negative of the mask is exposed. The critical requirement of this part of the process is calculating the right laser exposure dose according to the thickness of the photoresist and the reflectivity of the bottom layer. This work mainly required the realization of square regions with side varying from a minimum of 5 to a maximum of 50 µm; an example of a mask used in this work is reported in Fig. A.2.

After exposure, the photoresist has to be developed. The chips are placed in a beaker and submerged by developer AZ 726 MIF for 1 minute: this is sufficient to dissolve all the exposed polymer and leave just square islands that will be used to pattern capacitors. The chips are properly rinsed and cleaned and then placed again on a hotplate at 115 °C for 105 s to perform a post-development baking, also called reflow. This process is critical in that it reduces redeposition of material during the subsequent etching step and allows to remove the photoresist more easily at the end of the process.

At this stage the photoresist is patterned but the substrate is not: the next step is then dry etching of the photoresist to transfer the pattern to the materials stack and effectively create capacitors. This is accomplished by Ion Beam Etching (IBE) in a Veeco Nexus IBE350. Since the tool can only process 100 mm wafers, the chips are glued to a wafer before being inserted in the chamber. With the purpose of achieving a good uniformity, maximum 4-5 chips at a time are glued to the wafer, in order to have them all close to the center. In addition, during the process the wafer holder rotates and is placed with a tilt of -10 ° so as to ensure a uniformly distributed etching, which is performed by a beam of Ar ions generated with a voltage of 300 V and a

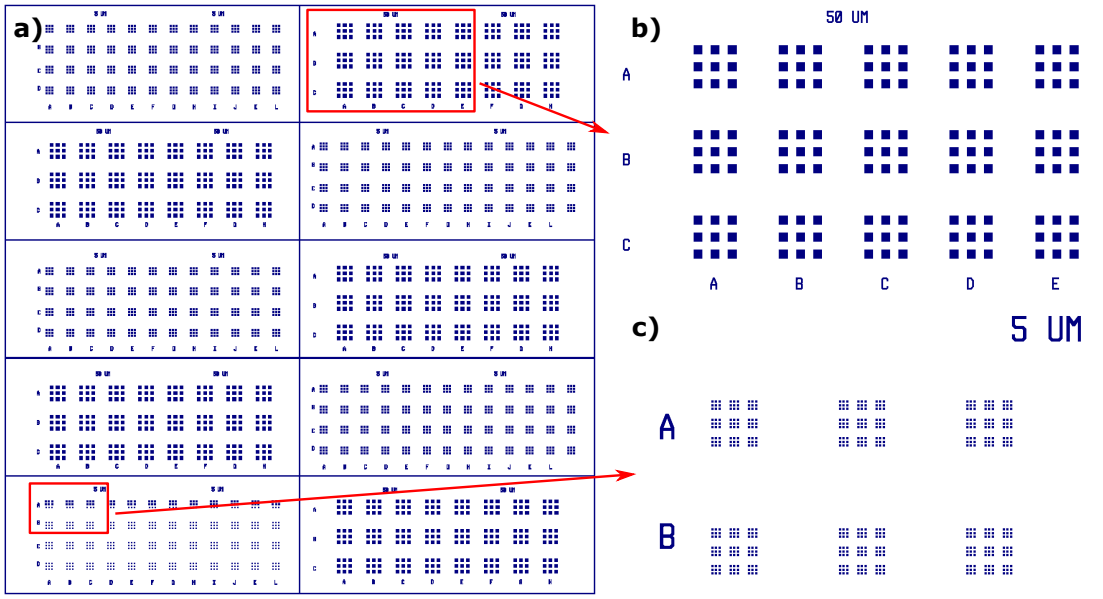

Figure A.2: a) The 1x1 cm^2 photolithography mask used in this work, with zoomed areas showing the square features of b) 50x50 and c) 5x5 μm^2.

current of 500 mA. This low power recipe is preferred because it keeps the temperature low, preventing a burning of the photoresist, and takes approximately 180-200 s. This physical etching procedure is not selective over the elements but can be controlled by a Secondary Ion Mass Spectroscopy (SIMS) tool that detects which material is currently being sputtered: when the FE layer is detected, the process is continued for just a few seconds to make sure that all top TiN is etched and then the process is stopped. A run at higher power on a dummy wafer is always performed first in order to heat up the ion beam. The materials stack after IBE consists of a uniform layer of Si/TiN/FE with isolated islands of TiN/Pt/photoresist on top of it. This structure is particularly useful in order to have a common bottom electrode which facilitates the contact for electrical and electromechanical measurements.

The final step of the process flow is the removal of the photoresist that is left on top of the capacitor structures: first the chips are exposed to a low-power O_2 plasma for 60 s and then by a 1165 UFT remover bath at 70 °C which lasts a few hours. The chips are then rinsed, dried and finally ready to be measured. Fig. A.3a shows an optical microscope picture of 50x50 μm^2 capacitors on an HZO film while Fig. A.3b offers a SEM detail of a 5x5 μm^2 capacitor on Gd:HfO_2, showing that the real size is actually slightly smaller than nominal.

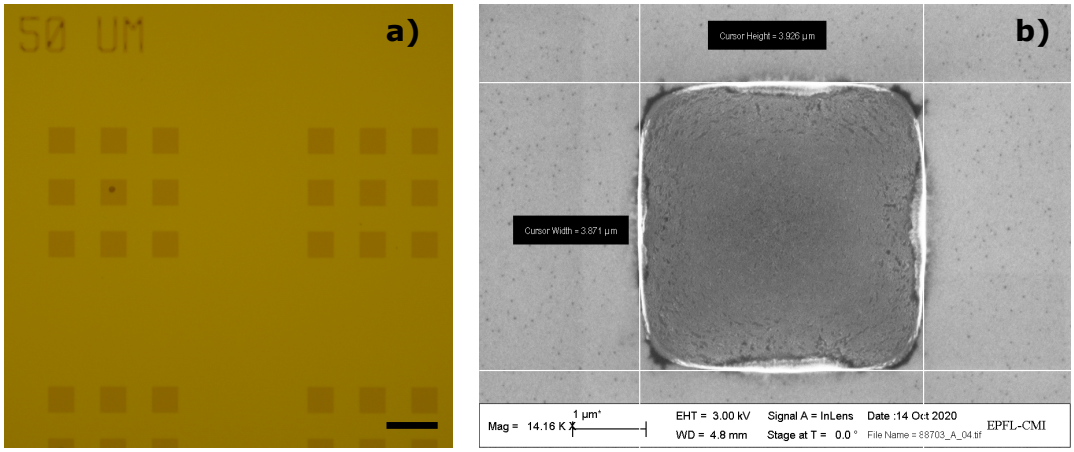

Figure A.3: a) Optical microscope picture of 50x50 µm^2 structures patterned on a HZO film (scale bar = 100 µm) and b) SEM detail of a 5x5 µm^2 capacitor on Gd:HfO_2, where it can be seen that the side length is approximately 4 µm.

Bibliography

[1] T. S. Böscke, J. Müller, D. Bräuhaus, U. Schröder, and U. Böttger, "Ferroelectricity in hafnium oxide thin films," *Applied Physics Letters*, vol. 99, no. 10, p. 102 903, Sep. 2011, ISSN: 00036951. DOI: 10.1063/1.3634052.

[2] U. Schroeder, C. S. Hwang, and H. Funakubo, *Ferroelectricity in Doped Hafnium Oxide: Materials, Properties and Devices*. Elsevier, 2019, p. 570, ISBN: 9780081024300. DOI: 10.1016/C2017-0-01145-X.

[3] A. Chen, "A review of emerging non-volatile memory (NVM) technologies and applications," *Solid-State Electronics*, vol. 125, pp. 25–38, Nov. 2016, ISSN: 00381101. DOI: 10.1016/j.sse.2016.07.006.

[4] M. H. Park, Y. H. Lee, T. Mikolajick, U. Schroeder, and C. S. Hwang, "Review and perspective on ferroelectric HfO2-based thin films for memory applications," *MRS Communications*, vol. 8, no. 03, pp. 795–808, Sep. 2018, ISSN: 2159-6859. DOI: 10.1557/mrc.2018.175.

[5] T. Mikolajick, U. Schroeder, and S. Slesazeck, "The Past, the Present, and the Future of Ferroelectric Memories," *IEEE Transactions on Electron Devices*, vol. 67, no. 4, pp. 1434–1443, Apr. 2020, ISSN: 0018-9383. DOI: 10.1109/TED.2020.2976148.

[6] M. Bohr, R. Chau, T. Ghani, and K. Mistry, "The High-k Solution," *IEEE Spectrum*, vol. 44, no. 10, pp. 29–35, Oct. 2007, ISSN: 0018-9235. DOI: 10.1109/MSPEC.2007.4337663.

[7] S. Guha and V. Narayanan, "High- κ /Metal Gate Science and Technology," *Annual Review of Materials Research*, vol. 39, no. 1, pp. 181–202, Aug. 2009, ISSN: 1531-7331. DOI: 10.1146/annurev-matsci-082908-145320.

[8] M. H. Park, D. H. Lee, K. Yang, J.-Y. Park, G. T. Yu, H. W. Park, M. Materano, T. Mittmann, P. D. Lomenzo, T. Mikolajick, U. Schroeder, and C. S. Hwang, "Review of defect chemistry in fluorite-structure ferroelectrics for future electronic devices," *Journal of Materials Chemistry C*, vol. 8, no. 31, pp. 10 526–10 550, 2020, ISSN: 2050-7526. DOI: 10.1039/D0TC01695K.

[9] J. Valasek, "Piezo-Electric and Allied Phenomena in Rochelle Salt," *Physical Review*, vol. 17, no. 4, pp. 475–481, Apr. 1921, ISSN: 0031-899X. DOI: 10.1103/PhysRev.17.475.

[10] A. von Hippel, R. G. Breckenridge, F. G. Chesley, and L. Tisza, "High dielectric constant ceramics," *Industrial & Engineering Chemistry*, vol. 38, no. 11, pp. 1097–1109, Nov. 1946, ISSN: 0019-7866. DOI: 10.1021/ie50443a009.

[11] J. G. Bergman, J. H. McFee, and G. R. Crane, "Pyroelectricity and Optical Second Harmonic Generation in Polyvinylidene Fluoride Films," *Applied Physics Letters*, vol. 18, no. 5, pp. 203–205, Mar. 1971, ISSN: 0003-6951. DOI: 10.1063/1.1653624.

[12] A. Devonshire, "XCVI. Theory of barium titanate," *The London, Edinburgh, and Dublin Philosophical Magazine and Journal of Science*, vol. 40, no. 309, pp. 1040–1063, 1949. DOI: 10.1080/14786444908561372.

[13] D. Damjanovic, "Ferroelectric, dielectric and piezoelectric properties of ferroelectric thin films and ceramics," *Reports on Progress in Physics*, vol. 61, no. 9, pp. 1267–1324, Sep. 1998, ISSN: 0034-4885. DOI: 10.1088/0034-4885/61/9/002.

[14] D. Damjanovic, "Hysteresis in Piezoelectric and Ferroelectric Materials," in *The Science of Hysteresis*, vol. 3, Elsevier, 2006, pp. 337–465, ISBN: 9780124808744. DOI: 10.1016/B978-012480874-4/50022-1.

[15] T. Schenk, "Formation of Ferroelectricity in Hafnium Oxide Based Thin Films," Final dissertation, Technische Universität Dresden, 2016.

[16] L. D. Landau, "On the theory of phase transisions," *Zh. Exsp. Teor. Fiz.*, vol. 7, pp. 19–32, 1937.

[17] V. L. Ginzburg, "On the dielectric properties of ferroelectric (Segnette-electric) crystals and barium titanate," *Zh. Exsp. Teor. Fiz.*, vol. 15, pp. 739–749, 1945.

[18] A. Devonshire, "Theory of ferroelectrics," *Advances in Physics*, vol. 3, no. 10, pp. 85–130, Apr. 1954, ISSN: 0001-8732. DOI: 10.1080/00018735400101173.

[19] M. E. Lines and A. M. Glass, *Principles and Applications of Ferroelectrics and Related Materials*. Oxford University Press, Feb. 2001, ISBN: 9780198507789. DOI: 10.1093/acprof:oso/9780198507789.001.0001.

[20] F. Preisach, " ber die magnetische Nachwirkung," *Zeitschrift f r Physik*, vol. 94, no. 5-6, pp. 277–302, May 1935, ISSN: 1434-6001. DOI: 10.1007/BF01349418.

[21] S. V. Kalinin, Y. Kim, D. D. Fong, and A. N. Morozovska, "Surface-screening mechanisms in ferroelectric thin films and their effect on polarization dynamics and domain structures," *Reports on Progress in Physics*, vol. 81, no. 3, p. 036 502, Mar. 2018, ISSN: 0034-4885. DOI: 10.1088/1361-6633/aa915a.

[22] R. Landauer, D. R. Young, and M. E. Drougard, "Polarization Reversal in the Barium Titanate Hysteresis Loop," *Journal of Applied Physics*, vol. 27, no. 7, pp. 752–758, Jul. 1956, ISSN: 0021-8979. DOI: 10.1063/1.1722477.

[23] R. Landauer, "Electrostatic Considerations in BaTiO 3 Domain Formation during Polarization Reversal," *Journal of Applied Physics*, vol. 28, no. 2, pp. 227–234, Feb. 1957, ISSN: 0021-8979. DOI: 10.1063/1.1722712.

[24] A. Kolmogoroff, "Zur Statistik der Kristallisationsvorgänge in Metallen," Russian, *Izv. Akad. Nauk SSSR, Ser. Mat.*, vol. 1937, pp. 355–359, 1937, ISSN: 0373-2436.

[25] M. Avrami, "Kinetics of Phase Change. II Transformation-Time Relations for Random Distribution of Nuclei," *The Journal of Chemical Physics*, vol. 8, no. 2, pp. 212–224, Feb. 1940, ISSN: 0021-9606. DOI: 10.1063/1.1750631.

[26] H. Orihara, S. Hashimoto, and Y. Ishibashi, "A Theory of D-E Hysteresis Loop Based on the Avrami Model," *Journal of the Physical Society of Japan*, vol. 63, no. 3, pp. 1031–1035, Mar. 1994, ISSN: 0031-9015. DOI: 10.1143/JPSJ.63.1031.

[27] A. K. Tagantsev, I. Stolichnov, N. Setter, J. S. Cross, and M. Tsukada, "Non-Kolmogorov-Avrami switching kinetics in ferroelectric thin films," *Physical Review B*, vol. 66, no. 21, p. 214 109, 2002, ISSN: 0163-1829. DOI: 10.1103/PhysRevB.66.214109.

[28] N. Setter, D. Damjanovic, L. Eng, G. Fox, S. Gevorgian, S. Hong, A. Kingon, H. Kohlstedt, N. Y. Park, G. B. Stephenson, I. Stolitchnov, A. K. Taganstev, D. V. Taylor, T. Yamada, and S. Streiffer, "Ferroelectric thin films: Review of materials, properties, and applications," *Journal of Applied Physics*, vol. 100, no. 5, p. 051 606, Sep. 2006, ISSN: 0021-8979. DOI: 10.1063/1.2336999.

[29] M. Pešić, F. P. G. Fengler, L. Larcher, A. Padovani, T. Schenk, E. D. Grimley, X. Sang, J. M. LeBeau, S. Slesazeck, U. Schroeder, and T. Mikolajick, "Physical Mechanisms behind the Field-Cycling Behavior of HfO 2 -Based Ferroelectric Capacitors," *Advanced Functional Materials*, vol. 26, no. 25, pp. 4601–4612, Jul. 2016, ISSN: 1616301X. DOI: 10.1002/adfm.201600590.

[30] M. H. Park, H. J. Kim, Y. J. Kim, T. Moon, and C. S. Hwang, "The effects of crystallographic orientation and strain of thin Hf 0.5Zr0.5O2 film on its ferroelectricity," *Applied Physics Letters*, vol. 104, no. 7, p. 072 901, Feb. 2014, ISSN: 00036951. DOI: 10.1063/1.4866008.

[31] M. Hoffmann, U. Schroeder, T. Schenk, T. Shimizu, H. Funakubo, O. Sakata, D. Pohl, M. Drescher, C. Adelmann, R. Materlik, A. Kersch, and T. Mikolajick, "Stabilizing the ferroelectric phase in doped hafnium oxide," *Journal of Applied Physics*, vol. 118, no. 7, p. 072 006, Aug. 2015, ISSN: 0021-8979. DOI: 10.1063/1.4927805.

[32] J. F. Ihlefeld, D. T. Harris, R. Keech, J. L. Jones, J. P. Maria, and S. Trolier-McKinstry, "Scaling Effects in Perovskite Ferroelectrics: Fundamental Limits and Process-Structure-Property Relations," *Journal of the American Ceramic Society*, vol. 99, no. 8, pp. 2537–2557, 2016, ISSN: 15512916. DOI: 10.1111/jace.14387.

[33] T. Shiraishi, K. Katayama, T. Yokouchi, T. Shimizu, T. Oikawa, O. Sakata, H. Uchida, Y. Imai, T. Kiguchi, T. J. Konno, and H. Funakubo, "Impact of mechanical stress on ferroelectricity in (Hf 0.5 Zr 0.5)O 2 thin films," *Applied Physics Letters*, vol. 108, no. 26, p. 262 904, Jun. 2016, ISSN: 0003-6951. DOI: 10.1063/1.4954942.

[34] T. Schenk, M. Hoffmann, J. Ocker, M. Pešić, T. Mikolajick, and U. Schroeder, "Complex internal bias fields in ferroelectric hafnium oxide," *ACS Applied Materials and Interfaces*, vol. 7, no. 36, pp. 20 224–20 233, Sep. 2015, ISSN: 19448252. DOI: 10.1021/acsami.5b05773.

[35] M. Hoffmann, F. P. G. Fengler, M. Herzig, T. Mittmann, B. Max, U. Schroeder, R. Negrea, P. Lucian, S. Slesazeck, and T. Mikolajick, "Unveiling the double-well energy landscape in a ferroelectric layer," *Nature*, vol. 565, no. 7740, pp. 464–467, Jan. 2019, ISSN: 0028-0836. DOI: 10.1038/s41586-018-0854-z.

[36] F. P. G. Fengler, M. Hoffmann, S. Slesazeck, T. Mikolajick, and U. Schroeder, "On the relationship between field cycling and imprint in ferroelectric Hf 0.5 Zr 0.5 O 2," *Journal of Applied Physics*, vol. 123, no. 20, p. 204 101, May 2018, ISSN: 0021-8979. DOI: 10.1063/1.5026424.

[37] A. K. Tagantsev, I. Stolichnov, E. L. Colla, and N. Setter, "Polarization fatigue in ferroelectric films: Basic experimental findings, phenomenological scenarios, and microscopic features," *Journal of Applied Physics*, vol. 90, no. 3, pp. 1387–1402, Aug. 2001, ISSN: 0021-8979. DOI: 10.1063/1.1381542.

[38] D. Shin, R. Arróyave, and Z.-K. Liu, "Thermodynamic modeling of the Hf–Si–O system," *Calphad*, vol. 30, no. 4, pp. 375–386, Dec. 2006, ISSN: 03645916. DOI: 10.1016/j.calphad.2006.08.006. arXiv: 0708.4239.

[39] T. S. Boscke, J. Muller, D. Brauhaus, U. Schroder, and U. Bottger, "Ferroelectricity in hafnium oxide: CMOS compatible ferroelectric field effect transistors," in *2011 International Electron Devices Meeting*, IEEE, Dec. 2011, pp. 24.5.1–24.5.4, ISBN: 978-1-4577-0505-2. DOI: 10.1109/IEDM.2011.6131606.

[40] M. D. Hanwell, D. E. Curtis, D. C. Lonie, T. Vandermeersch, E. Zurek, and G. R. Hutchison, "Avogadro: an advanced semantic chemical editor, visualization, and analysis platform," *Journal of Cheminformatics*, vol. 4, no. 1, p. 17, Dec. 2012, ISSN: 1758-2946. DOI: 10.1186/1758-2946-4-17.

[41] S. Summerfelt, T. Moise, K. Udayakumar, K. Boku, K. Remack, J. Rodriguez, J. Gertas, H. McAdams, S. Madan, J. Eliason, J. Groat, D. Kim, P. Staubs, M. Depner, and R. Bailey, "High-Density 8Mb 1T-1C Ferroelectric Random Access Memory Embedded Within a Low-Power 130nm Logic Process," in *2007 Sixteenth IEEE International Symposium on the Applications of Ferroelectrics*, IEEE, May 2007, pp. 9–10, ISBN: 978-1-4244-1333-1. DOI: 10.1109/ISAF.2007.4393151.

[42] T. Mikolajick, S. Slesazeck, M. H. Park, and U. Schroeder, "Ferroelectric hafnium oxide for ferroelectric random-access memories and ferroelectric field-effect transistors," *MRS Bulletin*, vol. 43, no. 5, pp. 340–346, May 2018, ISSN: 0883-7694. DOI: 10.1557/mrs.2018.92.

[43] S. Mueller, J. Mueller, A. Singh, S. Riedel, J. Sundqvist, U. Schroeder, and T. Mikolajick, "Incipient ferroelectricity in Al-doped HfO 2 thin films," *Advanced Functional Materials*, vol. 22, no. 11, pp. 2412–2417, 2012, ISSN: 1616301X. DOI: 10.1002/adfm.201103119.

[44] S. Mueller, C. Adelmann, A. Singh, S. Van Elshocht, U. Schroeder, and T. Mikolajick, "Ferroelectricity in Gd-Doped HfO 2 Thin Films," *ECS Journal of Solid State Science and Technology*, vol. 1, no. 6, N123–N126, Jan. 2012, ISSN: 2162-8769. DOI: 10.1149/2.002301jss.

[45] J. Muller, T. S. Boscke, S. Muller, E. Yurchuk, P. Polakowski, J. Paul, D. Martin, T. Schenk, K. Khullar, A. Kersch, W. Weinreich, S. Riedel, K. Seidel, A. Kumar, T. M. Arruda, S. V. Kalinin, T. Schlosser, R. Boschke, R. van Bentum, U. Schroder, and T. Mikolajick, "Ferroelectric hafnium oxide: A CMOS-compatible and highly scalable approach to future ferroelectric memories," in *2013 IEEE International Electron Devices Meeting*, IEEE, Dec. 2013, pp. 10.8.1–10.8.4, ISBN: 978-1-4799-2306-9. DOI: 10.1109/IEDM.2013.6724605.

[46] T. Schenk, S. Mueller, U. Schroeder, R. Materlik, A. Kersch, M. Popovici, C. Adelmann, S. Van Elshocht, and T. Mikolajick, "Strontium doped hafnium oxide thin films: Wide process window for ferroelectric memories," in *2013 Proceedings of the European Solid-State Device Research Conference (ESSDERC)*, IEEE, Sep. 2013, pp. 260–263, ISBN: 978-1-4799-0649-9. DOI: 10.1109/ESSDERC.2013.6818868.

[47] T. Olsen, U. Schröder, S. Müller, A. Krause, D. Martin, A. Singh, J. Müller, M. Geidel, and T. Mikolajick, "Co-sputtering yttrium into hafnium oxide thin films to produce ferroelectric properties," *Applied Physics Letters*, vol. 101, no. 8, p. 082 905, Aug. 2012, ISSN: 0003-6951. DOI: 10.1063/1.4747209.

[48] U. Schroeder, E. Yurchuk, J. Müller, D. Martin, T. Schenk, P. Polakowski, C. Adelmann, M. I. Popovici, S. V. Kalinin, and T. Mikolajick, "Impact of different dopants on the switching properties of ferroelectric hafniumoxide," *Japanese Journal of Applied Physics*, vol. 53, no. 8S1, 08LE02, Aug. 2014, ISSN: 0021-4922. DOI: 10.7567/JJAP.53.08LE02.

[49] M. H. Park, Y. H. Lee, H. J. Kim, Y. J. Kim, T. Moon, K. D. Kim, J. Müller, A. Kersch, U. Schroeder, T. Mikolajick, and C. S. Hwang, "Ferroelectricity and Antiferroelectricity of Doped Thin HfO 2 -Based Films," *Advanced Materials*, vol. 27, no. 11, pp. 1811–1831, Mar. 2015, ISSN: 09359648. DOI: 10.1002/adma.201404531.

[50] J. Müller, T. S. Böscke, D. Bräuhaus, U. Schröder, U. Böttger, J. Sundqvist, P. Kücher, T. Mikolajick, and L. Frey, "Ferroelectric Zr 0.5 Hf 0.5 O 2 thin films for nonvolatile memory applications," *Applied Physics Letters*, vol. 99, no. 11, p. 112 901, Sep. 2011, ISSN: 0003-6951. DOI: 10.1063/1.3636417.

[51] M. H. Park, Y. H. Lee, H. J. Kim, T. Schenk, W. Lee, K. D. Kim, F. P. G. Fengler, T. Mikolajick, U. Schroeder, and C. S. Hwang, "Surface and grain boundary energy as the key enabler of ferroelectricity in nanoscale hafnia-zirconia: a comparison of model and experiment," *Nanoscale*, vol. 9, no. 28, pp. 9973–9986, 2017, ISSN: 2040-3364. DOI: 10.1039/C7NR02121F.

[52] S. J. Kim, J. Mohan, S. R. Summerfelt, and J. Kim, "Ferroelectric Hf0.5Zr0.5O2 Thin Films: A Review of Recent Advances," *JOM*, vol. 71, no. 1, pp. 246–255, Jan. 2019, ISSN: 1047-4838. DOI: 10.1007/s11837-018-3140-5.

[53] D. Lehninger, R. Olivo, T. Ali, M. Lederer, T. Kämpfe, C. Mart, K. Biedermann, K. Kühnel, L. Roy, M. Kalkani, and K. Seidel, "Back-End-of-Line Compatible Low-Temperature Furnace Anneal for Ferroelectric Hafnium Zirconium Oxide Formation," *physica status solidi (a)*, vol. 217, no. 8, p. 1 900 840, Apr. 2020, ISSN: 1862-6300. DOI: 10.1002/pssa.201900840.

[54] E. Yurchuk, J. Müller, S. Knebel, J. Sundqvist, A. P. Graham, T. Melde, U. Schröder, and T. Mikolajick, "Impact of layer thickness on the ferroelectric behaviour of silicon doped hafnium oxide thin films," *Thin Solid Films*, vol. 533, pp. 88–92, Apr. 2013, ISSN: 00406090. DOI: 10.1016/j.tsf.2012.11.125.

[55] C. Richter, T. Schenk, M. H. Park, F. A. Tscharntke, E. D. Grimley, J. M. LeBeau, C. Zhou, C. M. Fancher, J. L. Jones, T. Mikolajick, and U. Schroeder, "Si Doped Hafnium Oxide-A "Fragile" Ferroelectric System," *Advanced Electronic Materials*, vol. 3, no. 10, p. 1 700 131, Oct. 2017, ISSN: 2199160X. DOI: 10.1002/aelm.201700131.

[56] H. J. Kim, M. H. Park, Y. J. Kim, Y. H. Lee, W. Jeon, T. Gwon, T. Moon, K. D. Kim, and C. S. Hwang, "Grain size engineering for ferroelectric Hf 0.5 Zr 0.5 O 2 films by an insertion of Al 2 O 3 interlayer," *Applied Physics Letters*, vol. 105, no. 19, p. 192 903, Nov. 2014, ISSN: 0003-6951. DOI: 10.1063/1.4902072.

[57] R. Materlik, C. Künneth, and A. Kersch, "The origin of ferroelectricity in Hf1−xZrxO2: A computational investigation and a surface energy model," *Journal of Applied Physics*, vol. 117, no. 13, p. 134 109, 2015, ISSN: 0021-8979. DOI: 10.1063/1.4916707.

[58] T. Schenk, N. Godard, A. Mahjoub, S. Girod, A. Matavz, V. Bobnar, E. Defay, and S. Glinsek, "Toward Thick Piezoelectric HfO 2 -Based Films," *physica status solidi (RRL) – Rapid Research Letters*, vol. 14, no. 3, p. 1 900 626, Mar. 2020, ISSN: 1862-6254. DOI: 10.1002/pssr.201900626.

[59] U. Schroeder, C. Richter, M. H. Park, T. Schenk, M. Pešić, M. Hoffmann, F. P. G. Fengler, D. Pohl, B. Rellinghaus, C. Zhou, C.-C. Chung, J. L. Jones, and T. Mikolajick, "Lanthanum-Doped Hafnium Oxide: A Robust Ferroelectric Material," *Inorganic Chemistry*, vol. 57, no. 5, pp. 2752–2765, Mar. 2018, ISSN: 0020-1669. DOI: 10.1021/acs.inorgchem.7b03149.

[60] X. J. Lou, "Polarization fatigue in ferroelectric thin films and related materials," *Journal of Applied Physics*, vol. 105, no. 2, p. 024 101, Jan. 2009, ISSN: 0021-8979. DOI: 10.1063/1.3056603.

[61] Y. A. Genenko, J. Glaum, M. J. Hoffmann, and K. Albe, "Mechanisms of aging and fatigue in ferroelectrics," *Materials Science and Engineering: B*, vol. 192, no. C, pp. 52–82, Feb. 2015, ISSN: 09215107. DOI: 10.1016/j.mseb.2014.10.003.

[62] F. P. G. Fengler, M. Pešić, S. Starschich, T. Schneller, C. Künneth, U. Böttger, H. Mulaosmanovic, T. Schenk, M. H. Park, R. Nigon, P. Muralt, T. Mikolajick, and U. Schroeder, "Domain Pinning: Comparison of Hafnia and PZT Based Ferroelectrics," *Advanced Electronic Materials*, vol. 3, no. 4, p. 1 600 505, Apr. 2017, ISSN: 2199160X. DOI: 10.1002/aelm.201600505.

[63] H.-Y. Chen and F.-H. Lu, "Oxidation behavior of titanium nitride films," *Journal of Vacuum Science & Technology A: Vacuum, Surfaces, and Films*, vol. 23, no. 4, pp. 1006–1009, Jul. 2005, ISSN: 0734-2101. DOI: 10.1116/1.1914815.

[64] M. H. Park, H. J. Kim, Y. J. Kim, W. Jeon, T. Moon, and C. S. Hwang, "Ferroelectric properties and switching endurance of Hf 0.5 Zr 0.5 O 2 films on TiN bottom and TiN or RuO 2 top electrodes," *physica status solidi (RRL) - Rapid Research Letters*, vol. 8, no. 6, pp. 532–535, Jun. 2014, ISSN: 18626254. DOI: 10.1002/pssr.201409017.

[65] W. Hamouda, A. Pancotti, C. Lubin, L. Tortech, C. Richter, T. Mikolajick, U. Schroeder, and N. Barrett, "Physical chemistry of the TiN/Hf 0.5 Zr 0.5 O 2 interface," *Journal of Applied Physics*, vol. 127, no. 6, p. 064 105, Feb. 2020, ISSN: 0021-8979. DOI: 10.1063/1.5128502.

[66] M. Hyuk Park, H. Joon Kim, Y. Jin Kim, W. Lee, T. Moon, and C. Seong Hwang, "Evolution of phases and ferroelectric properties of thin Hf 0.5 Zr 0.5 O 2 films according to the thickness and annealing temperature," *Applied Physics Letters*, vol. 102, no. 24, p. 242 905, Jun. 2013, ISSN: 0003-6951. DOI: 10.1063/1.4811483.

[67] P. D. Lomenzo, Q. Takmeel, S. Moghaddam, and T. Nishida, "Annealing behavior of ferroelectric Si-doped HfO2 thin films," *Thin Solid Films*, vol. 615, pp. 139–144, Sep. 2016, ISSN: 00406090. DOI: 10.1016/j.tsf.2016.07.009.

[68] A. G. Chernikova, D. S. Kuzmichev, D. V. Negrov, M. G. Kozodaev, S. N. Polyakov, and A. M. Markeev, "Ferroelectric properties of full plasma-enhanced ALD TiN/La:HfO 2 /TiN stacks," *Applied Physics Letters*, vol. 108, no. 24, p. 242 905, Jun. 2016, ISSN: 0003-6951. DOI: 10.1063/1.4953787.

[69] M. H. Park, C.-C. Chung, T. Schenk, C. Richter, K. Opsomer, C. Detavernier, C. Adelmann, J. L. Jones, T. Mikolajick, and U. Schroeder, "Effect of Annealing Ferroelectric HfO 2 Thin Films: In Situ, High Temperature X-Ray Diffraction," *Advanced Electronic Materials*, vol. 4, no. 7, p. 1 800 091, Jul. 2018, ISSN: 2199160X. DOI: 10.1002/aelm.201800091.

[70] Y. Goh, S. H. Cho, S.-H. K. Park, and S. Jeon, "Oxygen vacancy control as a strategy to achieve highly reliable hafnia ferroelectrics using oxide electrode," *Nanoscale*, vol. 12, no. 16, pp. 9024–9031, 2020, ISSN: 2040-3364. DOI: 10.1039/D0NR00933D.

[71] R. Cao, Y. Wang, S. Zhao, Y. Yang, X. Zhao, W. Wang, X. Zhang, H. Lv, Q. Liu, and M. Liu, "Effects of Capping Electrode on Ferroelectric Properties of Hf 0.5 Zr 0.5 O 2 Thin Films," *IEEE Electron Device Letters*, vol. 39, no. 8, pp. 1207–1210, Aug. 2018, ISSN: 0741-3106. DOI: 10.1109/LED.2018.2846570.

[72] S. J. Kim, D. Narayan, J.-G. Lee, J. Mohan, J. S. Lee, J. Lee, H. S. Kim, Y.-C. Byun, A. T. Lucero, C. D. Young, S. R. Summerfelt, T. San, L. Colombo, and J. Kim, "Large ferroelectric polarization of TiN/Hf 0.5 Zr 0.5 O 2 /TiN capacitors due to stress-induced crystallization at low thermal budget," *Applied Physics Letters*, vol. 111, no. 24, p. 242 901, Dec. 2017, ISSN: 0003-6951. DOI: 10.1063/1.4995619.

[73] P. Polakowski and J. Müller, "Ferroelectricity in undoped hafnium oxide," *Applied Physics Letters*, vol. 106, no. 23, p. 232 905, Jun. 2015, ISSN: 0003-6951. DOI: 10.1063/1.4922272.

[74] T. Shimizu, K. Katayama, T. Kiguchi, A. Akama, T. J. Konno, O. Sakata, and H. Funakubo, "The demonstration of significant ferroelectricity in epitaxial Y-doped HfO2 film," *Scientific Reports*, vol. 6, no. 1, p. 32 931, Dec. 2016, ISSN: 2045-2322. DOI: 10.1038/srep32931.

[75] Y. Wei, P. Nukala, M. Salverda, S. Matzen, H. J. Zhao, J. Momand, A. S. Everhardt, G. Agnus, G. R. Blake, P. Lecoeur, B. J. Kooi, J. Íñiguez, B. Dkhil, and B. Noheda, "A rhombohedral ferroelectric phase in epitaxially strained Hf0.5Zr0.5O2 thin films," *Nature Materials*, vol. 17, no. 12, pp. 1095–1100, Dec. 2018, ISSN: 1476-1122. DOI: 10.1038/s41563-018-0196-0. arXiv: 1801.09008.

[76] T. Li, N. Zhang, Z. Sun, C. Xie, M. Ye, S. Mazumdar, L. Shu, Y. Wang, D. Wang, L. Chen, S. Ke, and H. Huang, "Epitaxial ferroelectric Hf 0.5 Zr 0.5 O 2 thin film on a buffered YSZ substrate through interface reaction," *Journal of Materials Chemistry C*, vol. 6, no. 34, pp. 9224–9231, 2018, ISSN: 2050-7526. DOI: 10.1039/C8TC02941E.

[77] H. Y. Yoong, H. Wu, J. Zhao, H. Wang, R. Guo, J. Xiao, B. Zhang, P. Yang, S. J. Pennycook, N. Deng, X. Yan, and J. Chen, "Epitaxial Ferroelectric Hf 0.5 Zr 0.5 O 2 Thin Films and Their Implementations in Memristors for Brain-Inspired Computing," *Advanced Functional Materials*, vol. 28, no. 50, p. 1 806 037, Dec. 2018, ISSN: 1616-301X. DOI: 10.1002/adfm.201806037.

[78] J. Lyu, I. Fina, J. Fontcuberta, and F. Sánchez, "Epitaxial Integration on Si(001) of Ferroelectric Hf 0.5 Zr 0.5 O 2 Capacitors with High Retention and Endurance," *ACS Applied Materials & Interfaces*, vol. 11, no. 6, pp. 6224–6229, Feb. 2019, ISSN: 1944-8244. DOI: 10.1021/acsami.8b18762.

[79] D. Zhou, J. Xu, Q. Li, Y. Guan, F. Cao, X. Dong, J. Müller, T. Schenk, and U. Schröder, "Wake-up effects in Si-doped hafnium oxide ferroelectric thin films," *Applied Physics Letters*, vol. 103, no. 19, p. 192 904, Nov. 2013, ISSN: 0003-6951. DOI: 10.1063/1.4829064.

[80] M. H. Park, H. J. Kim, Y. J. Kim, Y. H. Lee, T. Moon, K. D. Kim, S. D. Hyun, and C. S. Hwang, "Study on the size effect in Hf 0.5 Zr 0.5 O 2 films thinner than 8 nm before and after wake-up field cycling," *Applied Physics Letters*, vol. 107, no. 19, p. 192 907, Nov. 2015, ISSN: 0003-6951. DOI: 10.1063/1.4935588.

[81] H. J. Kim, M. H. Park, Y. J. Kim, Y. H. Lee, T. Moon, K. D. Kim, S. D. Hyun, and C. S. Hwang, "A study on the wake-up effect of ferroelectric Hf 0.5 Zr 0.5 O 2 films by pulse-switching measurement," *Nanoscale*, vol. 8, no. 3, pp. 1383–1389, 2016, ISSN: 2040-3364. DOI: 10.1039/C5NR05339K.

[82] T. Y. Lee, K. Lee, H. H. Lim, M. S. Song, S. M. Yang, H. K. Yoo, D. I. Suh, Z. Zhu, A. Yoon, M. R. MacDonald, X. Lei, H. Y. Jeong, D. Lee, K. Park, J. Park, and S. C. Chae, "Ferroelectric Polarization-Switching Dynamics and Wake-Up Effect in Si-Doped HfO 2," *ACS Applied Materials & Interfaces*, vol. 11, no. 3, pp. 3142–3149, Jan. 2019, ISSN: 1944-8244. DOI: 10.1021/acsami.8b11681.

[83] T. Schenk, U. Schroeder, M. Pešić, M. Popovici, Y. V. Pershin, and T. Mikolajick, "Electric Field Cycling Behavior of Ferroelectric Hafnium Oxide," *ACS Applied Materials & Interfaces*, vol. 6, no. 22, pp. 19 744–19 751, Nov. 2014, ISSN: 1944-8244. DOI: 10.1021/am504837r. arXiv: arXiv:1408.1149.

[84] S. Starschich, S. Menzel, and U. Böttger, "Evidence for oxygen vacancies movement during wake-up in ferroelectric hafnium oxide," *Applied Physics Letters*, vol. 108, no. 3, p. 032 903, Jan. 2016, ISSN: 0003-6951. DOI: 10.1063/1.4940370.

[85] F. Huang, X. Chen, X. Liang, J. Qin, Y. Zhang, T. Huang, Z. Wang, B. Peng, P. Zhou, H. Lu, L. Zhang, L. Deng, M. Liu, Q. Liu, H. Tian, and L. Bi, "Fatigue mechanism of yttrium-doped hafnium oxide ferroelectric thin films fabricated by pulsed laser deposition," *Physical Chemistry Chemical Physics*, vol. 19, no. 5, pp. 3486–3497, 2017, ISSN: 1463-9076. DOI: 10.1039/C6CP07501K.

[86] P. Buragohain, C. Richter, T. Schenk, H. Lu, T. Mikolajick, U. Schroeder, and A. Gruverman, "Nanoscopic studies of domain structure dynamics in ferroelectric La:HfO 2 capacitors," *Applied Physics Letters*, vol. 112, no. 22, p. 222 901, May 2018, ISSN: 0003-6951. DOI: 10.1063/1.5030562.

[87] H. Mulaosmanovic, J. Ocker, S. Müller, U. Schroeder, J. Müller, P. Polakowski, S. Flachowsky, R. van Bentum, T. Mikolajick, and S. Slesazeck, "Switching Kinetics in Nanoscale Hafnium Oxide Based Ferroelectric Field-Effect Transistors," *ACS Applied Materials & Interfaces*, vol. 9, no. 4, pp. 3792–3798, Feb. 2017, ISSN: 1944-8244. DOI: 10.1021/acsami.6b13866.

[88] N. Gong, X. Sun, H. Jiang, K. S. Chang-Liao, Q. Xia, and T. P. Ma, "Nucleation limited switching (NLS) model for HfO 2 -based metal-ferroelectric-metal (MFM) capacitors: Switching kinetics and retention characteristics," *Applied Physics Letters*, vol. 112, no. 26, p. 262 903, Jun. 2018, ISSN: 0003-6951. DOI: 10.1063/1.5010207.

[89] C. Gastaldi, M. Cavalieri, A. Saeidi, É. O'Connor, F. Bellando, I. Stolichnov, and A. M. Ionescu, "Negative Capacitance in HfO2 gate stacks structures with and without metal interlayer," *IEEE Transactions on Electron Devices [submitted, under review]*,

[90] R. Landauer, "Can capacitance be negative?" *Collect. Phenom.*, vol. 2, no. 167, 1976.

[91] S. Salahuddin and S. Datta, "Use of Negative Capacitance to Provide Voltage Amplification for Low Power Nanoscale Devices," *Nano Letters*, vol. 8, no. 2, pp. 405–410, Feb. 2008, ISSN: 1530-6984. DOI: 10.1021/nl071804g. arXiv: 0707.2073.

[92] J. Íñiguez, P. Zubko, I. Luk'yanchuk, and A. Cano, "Ferroelectric negative capacitance," *Nature Reviews Materials*, vol. 4, no. 4, pp. 243–256, Apr. 2019, ISSN: 2058-8437. DOI: 10.1038/s41578-019-0089-0.

[93] I. Luk'yanchuk, Y. Tikhonov, A. Sené, A. Razumnaya, and V. M. Vinokur, "Harnessing ferroelectric domains for negative capacitance," *Communications Physics*, vol. 2, no. 1, p. 22, Dec. 2019, ISSN: 2399-3650. DOI: 10.1038/s42005-019-0121-0. arXiv: 1811.12103.

[94] C. S. Hwang, *Atomic Layer Deposition for Semiconductors*, C. S. Hwang, Ed. Boston, MA: Springer US, 2014, vol. 9781461480, pp. 1–263, ISBN: 978-1-4614-8053-2. DOI: 10.1007/978-1-4614-8054-9.

[95] B. C. Mallick, C.-T. Hsieh, K.-M. Yin, Y. A. Gandomi, and K.-T. Huang, "Review—On Atomic Layer Deposition: Current Progress and Future Challenges," *ECS Journal of Solid State Science and Technology*, vol. 8, no. 4, N55–N78, May 2019, ISSN: 2162-8769. DOI: 10.1149/2.0201903jss.

[96] K. D. Kim, Y. H. Lee, T. Gwon, Y. J. Kim, H. J. Kim, T. Moon, S. D. Hyun, H. W. Park, M. H. Park, and C. S. Hwang, "Scale-up and optimization of HfO2-ZrO2 solid solution thin films for the electrostatic supercapacitors," *Nano Energy*, vol. 39, no. April, pp. 390–399, Sep. 2017, ISSN: 22112855. DOI: 10.1016/j.nanoen.2017.07.017.

[97] V. Miikkulainen, M. Leskelä, M. Ritala, and R. L. Puurunen, "Crystallinity of inorganic films grown by atomic layer deposition: Overview and general trends," *Journal of Applied Physics*, vol. 113, no. 2, p. 021 301, Jan. 2013, ISSN: 0021-8979. DOI: 10.1063/1.4757907.

[98] T. Mittmann, F. P. Fengler, C. Richter, M. H. Park, T. Mikolajick, and U. Schroeder, "Optimizing process conditions for improved Hf1−xZrxO2 ferroelectric capacitor performance," *Microelectronic Engineering*, vol. 178, pp. 48–51, Jun. 2017, ISSN: 01679317. DOI: 10.1016/j.mee.2017.04.031.

[99] T. Mittmann, M. Materano, P. D. Lomenzo, M. H. Park, I. Stolichnov, M. Cavalieri, C. Zhou, C.-C. Chung, J. L. Jones, T. Szyjka, M. Müller, A. Kersch, T. Mikolajick, and U. Schroeder, "Origin of Ferroelectric Phase in Undoped HfO 2 Films Deposited by Sputtering," *Advanced Materials Interfaces*, vol. 1900042, p. 1 900 042, Apr. 2019, ISSN: 2196-7350. DOI: 10.1002/admi.201900042.

[100] M. C. Rao, "Pulsed Laser Deposition - Ablation Mechanism and Applications," *International Journal of Modern Physics: Conference Series*, vol. 22, pp. 355–360, Jan. 2013, ISSN: 2010-1945. DOI: 10.1142/S2010194513010362.

[101] F. V. E. Hensling, C. Xu, F. Gunkel, and R. Dittmann, "Unraveling the enhanced Oxygen Vacancy Formation in Complex Oxides during Annealing and Growth," *Scientific Reports*, vol. 7, no. 1, p. 39 953, Feb. 2017, ISSN: 2045-2322. DOI: 10.1038/srep39953.

[102] I. Stolichnov, M. Cavalieri, E. Colla, T. Schenk, T. Mittmann, T. Mikolajick, U. Schroeder, and A. M. Ionescu, "Genuinely Ferroelectric Sub-1-Volt-Switchable Nanodomains in Hf x Zr (1– x) O 2 Ultrathin Capacitors," *ACS Applied Materials & Interfaces*, vol. 10, no. 36, pp. 30 514–30 521, Sep. 2018, ISSN: 1944-8244. DOI: 10.1021/acsami.8b07988.

[103] G. Esteves, K. Ramos, C. M. Fancher, and J. L. Jones, "LIPRAS : Line-Profile Analysis Software Peak Fitting with LIPRAS," no. March, pp. 1–4, 2017. DOI: 10.13140/RG.2.2.29970.25282/3.

[104] S. Gates-Rector and T. Blanton, "The Powder Diffraction File: a quality materials characterization database," *Powder Diffraction*, vol. 34, no. 4, pp. 352–360, Dec. 2019, ISSN: 0885-7156. DOI: 10.1017/S0885715619000812.

[105] A. Jain, S. P. Ong, G. Hautier, W. Chen, W. D. Richards, S. Dacek, S. Cholia, D. Gunter, D. Skinner, G. Ceder, and K. A. Persson, "Commentary: The Materials Project: A materials genome approach to accelerating materials innovation," *APL Materials*, vol. 1, no. 1, p. 011 002, Jul. 2013, ISSN: 2166-532X. DOI: 10.1063/1.4812323.

[106] M. Hoffmann, T. Schenk, I. Kulemanov, C. Adelmann, M. Popovici, U. Schroeder, and T. Mikolajick, "Low Temperature Compatible Hafnium Oxide Based Ferroelectrics," *Ferroelectrics*, vol. 480, no. 1, pp. 16–23, May 2015, ISSN: 0015-0193. DOI: 10.1080/00150193.2015.1012401.

[107] X. Zhao and D. Vanderbilt, "First-principles study of structural, vibrational, and lattice dielectric properties of hafnium oxide," *Physical Review B*, vol. 65, no. 23, p. 233 106, Jun. 2002, ISSN: 0163-1829. DOI: 10.1103/PhysRevB.65.233106. arXiv: 0202454 [cond-mat].

[108] E. D. Grimley, T. Schenk, X. Sang, M. Pešić, U. Schroeder, T. Mikolajick, and J. M. LeBeau, "Structural Changes Underlying Field-Cycling Phenomena in Ferroelectric HfO 2 Thin Films," *Advanced Electronic Materials*, vol. 2, no. 9, p. 1 600 173, Sep. 2016, ISSN: 2199160X. DOI: 10.1002/aelm.201600173.

[109] D. R. Islamov, A. G. Chernikova, M. G. Kozodaev, A. M. Markeev, T. V. Perevalov, V. A. Gritsenko, and O. M. Orlov, "Leakage currents mechanism in thin films of ferroelectric Hf 0.5 Zr 0.5 O 2," *Journal of Physics: Conference Series*, vol. 864, no. 1, p. 012 002, Jun. 2017, ISSN: 1742-6588. DOI: 10.1088/1742-6596/864/1/012002.

[110] G. Haugstad, *Atomic Force Microscopy*, 1. Hoboken, NJ, USA: John Wiley & Sons, Inc., Aug. 2012, vol. 41, pp. 3–49, ISBN: 9781118360668. DOI: 10.1002/9781118360668.

[111] A. L. Kholkin, S. V. Kalinin, A. Roelofs, and A. Gruverman, "Review of Ferroelectric Domain Imaging by Piezoresponse Force Microscopy," in *Scanning Probe Microscopy*, January, New York, NY: Springer New York, 2007, pp. 173–214, ISBN: 978-0-387-28667-9. DOI: 10.1007/978-0-387-28668-6_7.

[112] D. Martin, J. Müller, T. Schenk, T. M. Arruda, A. Kumar, E. Strelcov, E. Yurchuk, S. Müller, D. Pohl, U. Schröder, S. V. Kalinin, and T. Mikolajick, "Ferroelectricity in Si-Doped HfO 2 Revealed: A Binary Lead-Free Ferroelectric," *Advanced Materials*, vol. 26, no. 48, pp. 8198–8202, Dec. 2014, ISSN: 09359648. DOI: 10.1002/adma.201403115.

[113] A. Chernikova, M. Kozodaev, A. Markeev, D. Negrov, M. Spiridonov, S. Zarubin, O. Bak, P. Buragohain, H. Lu, E. Suvorova, A. Gruverman, and A. Zenkevich, "Ultrathin Hf 0.5 Zr 0.5 O 2 Ferroelectric Films on Si," *ACS Applied Materials & Interfaces*, vol. 8, no. 11, pp. 7232–7237, Mar. 2016, ISSN: 1944-8244. DOI: 10.1021/acsami.5b11653.

[114] K. Lee, T. Y. Lee, S. M. Yang, D. H. Lee, J. Park, and S. C. Chae, "Ferroelectricity in epitaxial Y-doped HfO 2 thin film integrated on Si substrate," *Applied Physics Letters*, vol. 112, no. 20, p. 202 901, May 2018, ISSN: 0003-6951. DOI: 10.1063/1.5020688.

[115] A. Chouprik, S. Zakharchenko, M. Spiridonov, S. Zarubin, A. Chernikova, R. Kirtaev, P. Buragohain, A. Gruverman, A. Zenkevich, and D. Negrov, "Ferroelectricity in Hf 0.5 Zr 0.5 O 2 Thin Films: A Microscopic Study of the Polarization Switching Phenomenon and Field-Induced Phase Transformations," *ACS Applied Materials & Interfaces*, vol. 10, no. 10, pp. 8818–8826, Mar. 2018, ISSN: 1944-8244. DOI: 10.1021/acsami.7b17482.

[116] A. Chouprik, M. Spiridonov, S. Zarubin, R. Kirtaev, V. Mikheev, Y. Lebedinskii, S. Zakharchenko, and D. Negrov, "Wake-Up in a Hf 0.5 Zr 0.5 O 2 Film: A Cycle-by-Cycle Emergence of the Remnant Polarization via the Domain Depinning and the Vanishing of the Anomalous Polarization Switching," *ACS Applied Electronic Materials*, vol. 1, no. 3, pp. 275–287, Mar. 2019, ISSN: 2637-6113. DOI: 10.1021/acsaelm.8b00046.

[117] R. K. Vasudevan, N. Balke, P. Maksymovych, S. Jesse, and S. V. Kalinin, "Ferroelectric or non-ferroelectric: Why so many materials exhibit "ferroelectricity" on the nanoscale," *Applied Physics Reviews*, vol. 4, no. 2, p. 021 302, Jun. 2017, ISSN: 1931-9401. DOI: 10.1063/1.4979015. arXiv: 1701.01128.

[118] N. Balke, P. Maksymovych, S. Jesse, A. Herklotz, A. Tselev, C. B. Eom, I. I. Kravchenko, P. Yu, and S. V. Kalinin, "Differentiating Ferroelectric and Nonferroelectric Electromechanical Effects with Scanning Probe Microscopy," *ACS Nano*, vol. 9, no. 6, pp. 6484–6492, 2015, ISSN: 1936086X. DOI: 10.1021/acsnano.5b02227.

[119] N. Balke, S. Jesse, P. Yu, Ben Carmichael, S. V. Kalinin, and A. Tselev, "Quantification of surface displacements and electromechanical phenomena via dynamic atomic force microscopy," *Nanotechnology*, vol. 27, no. 42, p. 425 707, Oct. 2016, ISSN: 0957-4484. DOI: 10.1088/0957-4484/27/42/425707. arXiv: 1603.07203.

[120] N. Balke, S. Jesse, B. Carmichael, M. B. Okatan, I. I. Kravchenko, S. V. Kalinin, and A. Tselev, "Quantification of in-contact probe-sample electrostatic forces with dynamic atomic force microscopy," *Nanotechnology*, vol. 28, no. 6, p. 065 704, Feb. 2017, ISSN: 0957-4484. DOI: 10.1088/1361-6528/aa5370.

[121] N. Balke, S. Jesse, Q. Li, P. Maksymovych, M. Baris Okatan, E. Strelcov, A. Tselev, and S. V. Kalinin, "Current and surface charge modified hysteresis loops in ferroelectric thin films," *Journal of Applied Physics*, vol. 118, no. 7, p. 072 013, Aug. 2015, ISSN: 0021-8979. DOI: 10.1063/1.4927811.

[122] S. Jesse, A. P. Baddorf, and S. V. Kalinin, "Dynamic behaviour in piezoresponse force microscopy," *Nanotechnology*, vol. 17, no. 6, pp. 1615–1628, Mar. 2006, ISSN: 0957-4484. DOI: 10.1088/0957-4484/17/6/014. arXiv: 0509427 [cond-mat].

[123] S. V. Kalinin, B. J. Rodriguez, S.-H. Kim, S.-K. Hong, A. Gruverman, and E. A. Eliseev, "Imaging mechanism of piezoresponse force microscopy in capacitor structures," *Applied Physics Letters*, vol. 92, no. 15, p. 152 906, Apr. 2008, ISSN: 0003-6951. DOI: 10.1063/1.2905266.

[124] S. V. Kalinin, A. N. Morozovska, L. Q. Chen, and B. J. Rodriguez, "Local polarization dynamics in ferroelectric materials," *Reports on Progress in Physics*, vol. 73, no. 5, p. 056 502, May 2010, ISSN: 0034-4885. DOI: 10.1088/0034-4885/73/5/056502.

[125] S. Starschich, D. Griesche, T. Schneller, R. Waser, and U. Böttger, "Chemical solution deposition of ferroelectric yttrium-doped hafnium oxide films on platinum electrodes," *Applied Physics Letters*, vol. 104, no. 20, p. 202 903, May 2014, ISSN: 0003-6951. DOI: 10.1063/1.4879283.

[126] S. Starschich, T. Schenk, U. Schroeder, and U. Boettger, "Ferroelectric and piezoelectric properties of Hf 1-x Zr x O 2 and pure ZrO 2 films," *Applied Physics Letters*, vol. 110, no. 18, p. 182 905, May 2017, ISSN: 0003-6951. DOI: 10.1063/1.4983031.

[127] B. J. Rodriguez, C. Callahan, S. V. Kalinin, and R. Proksch, "Dual-frequency resonance-tracking atomic force microscopy," *Nanotechnology*, vol. 18, no. 47, p. 475 504, Nov. 2007, ISSN: 0957-4484. DOI: 10.1088/0957-4484/18/47/475504.

[128] S. Jesse, S. V. Kalinin, R. Proksch, A. P. Baddorf, and B. J. Rodriguez, "The band excitation method in scanning probe microscopy for rapid mapping of energy dissipation on the nanoscale," *Nanotechnology*, vol. 18, no. 43, p. 435 503, Oct. 2007, ISSN: 0957-4484. DOI: 10.1088/0957-4484/18/43/435503.

[129] S. Jesse, A. P. Baddorf, and S. V. Kalinin, "Switching spectroscopy piezoresponse force microscopy of ferroelectric materials," *Applied Physics Letters*, vol. 88, no. 6, p. 062 908, Feb. 2006, ISSN: 0003-6951. DOI: 10.1063/1.2172216.

[130] A. Labuda and R. Proksch, "Quantitative measurements of electromechanical response with a combined optical beam and interferometric atomic force microscope," *Applied Physics Letters*, vol. 106, no. 25, pp. 1–5, 2015, ISSN: 00036951. DOI: 10.1063/1.4922210.

[131] J. Müller, P. Polakowski, S. Mueller, and T. Mikolajick, "Ferroelectric Hafnium Oxide Based Materials and Devices: Assessment of Current Status and Future Prospects," *ECS Journal of Solid State Science and Technology*, vol. 4, no. 5, N30–N35, Feb. 2015, ISSN: 2162-8769. DOI: 10.1149/2.0081505jss.

[132] J. Muller, T. S. Boscke, U. Schroder, S. Mueller, D. Brauhaus, U. Bottger, L. Frey, and T. Mikolajick, "Ferroelectricity in Simple Binary ZrO2 and HfO2," *Nano Lett*, vol. 12, no. 8, pp. 4318–4323, 2012, ISSN: 1530-6992. DOI: 10.1021/nl302049k.

[133] É. O'Connor, M. Halter, F. Eltes, M. Sousa, A. Kellock, S. Abel, and J. Fompeyrine, "Stabilization of ferroelectric Hf x Zr 1−x O 2 films using a millisecond flash lamp annealing technique," *APL Materials*, vol. 6, no. 12, p. 121 103, Dec. 2018, ISSN: 2166-532X. DOI: 10.1063/1.5060676.

[134] D. Zhou, Y. Guan, M. M. Vopson, J. Xu, H. Liang, F. Cao, X. Dong, J. Mueller, T. Schenk, and U. Schroeder, "Electric field and temperature scaling of polarization reversal in silicon doped hafnium oxide ferroelectric thin films," *Acta Materialia*, vol. 99, pp. 240–246, Oct. 2015, ISSN: 13596454. DOI: 10.1016/j.actamat.2015.07.035.

[135] J. Müller, U. Schröder, T. S. Böscke, I. Müller, U. Böttger, L. Wilde, J. Sundqvist, M. Lemberger, P. Kücher, T. Mikolajick, and L. Frey, "Ferroelectricity in yttrium-doped hafnium oxide," *Journal of Applied Physics*, vol. 110, no. 11, p. 114 113, Dec. 2011, ISSN: 0021-8979. DOI: 10.1063/1.3667205.

[136] T. Shimizu, K. Katayama, T. Kiguchi, A. Akama, T. J. Konno, and H. Funakubo, "Growth of epitaxial orthorhombic YO 1.5 -substituted HfO 2 thin film," *Applied Physics Letters*, vol. 107, no. 3, p. 032 910, Jul. 2015, ISSN: 0003-6951. DOI: 10.1063/1.4927450.

[137] M. H. Park, T. Schenk, C. M. Fancher, E. D. Grimley, C. Zhou, C. Richter, J. M. LeBeau, J. L. Jones, T. Mikolajick, and U. Schroeder, "A comprehensive study on the structural evolution of HfO2 thin films doped with various dopants," *Journal of Materials Chemistry C*, vol. 5, no. 19, pp. 4677–4690, 2017, ISSN: 2050-7526. DOI: 10.1039/C7TC01200D.

[138] M. G. Kozodaev, A. G. Chernikova, E. V. Korostylev, M. H. Park, U. Schroeder, C. S. Hwang, and A. M. Markeev, "Ferroelectric properties of lightly doped La:HfO 2 thin films grown by plasma-assisted atomic layer deposition," *Applied Physics Letters*, vol. 111, no. 13, p. 132 903, Sep. 2017, ISSN: 0003-6951. DOI: 10.1063/1.4999291.

[139] Y. Sharma, D. Barrionuevo, R. Agarwal, S. P. Pavunny, and R. S. Katiyar, "Ferroelectricity in Rare-Earth Modified Hafnia Thin Films Deposited by Sequential Pulsed Laser Deposition," *ECS Solid State Letters*, vol. 4, no. 11, N13–N16, Sep. 2015, ISSN: 2162-8742. DOI: 10.1149/2.0031511ssl.

[140] J. Lyu, I. Fina, R. Solanas, J. Fontcuberta, and F. Sánchez, "Growth Window of Ferroelectric Epitaxial Hf 0.5 Zr 0.5 O 2 Thin Films," *ACS Applied Electronic Materials*, vol. 1, no. 2, pp. 220–228, Feb. 2019, ISSN: 2637-6113. DOI: 10.1021/acsaelm.8b00065.

[141] Q. Shao, X. Wang, W. Jiang, Y. Chen, X. Zhang, L. Tu, T. Lin, H. Shen, X. Meng, A. Liu, and J. Wang, "Ferroelectric properties of gradient doped Y 2 O 3 :HfO 2 thin films grown by pulsed laser deposition," *Applied Physics Letters*, vol. 115, no. 16, p. 162 902, Oct. 2019, ISSN: 0003-6951. DOI: 10.1063/1.5121858.

[142] S. Choopun, R. D. Vispute, W. Noch, A. Balsamo, R. P. Sharma, T. Venkatesan, A. Iliadis, and D. C. Look, "Oxygen pressure-tuned epitaxy and optoelectronic properties of laser-deposited ZnO films on sapphire," *Applied Physics Letters*, vol. 75, no. 25, pp. 3947–3949, Dec. 1999, ISSN: 0003-6951. DOI: 10.1063/1.125503.

[143] J. Y. Paek, I. Chang, J. H. Park, S. Ji, and S. W. Cha, "A study on properties of yttrium-stabilized zirconia thin films fabricated by different deposition techniques," *Renewable Energy*, vol. 65, pp. 202–206, May 2014, ISSN: 09601481. DOI: 10.1016/j.renene.2013.08.043.

[144] H. Ikeda, S. Goto, K. Honda, M. Sakashita, A. Sakai, S. Zaima, and Y. Yasuda, "Structural and Electrical Characteristics of HfO 2 Films Fabricated by Pulsed Laser Deposition," *Japanese Journal of Applied Physics*, vol. 41, no. Part 1, No. 4B, pp. 2476–2479, Apr. 2002, ISSN: 0021-4922. DOI: 10.1143/JJAP.41.2476.

[145] Y. X. Guo, Y. F. Liu, C. W. Zou, Z. M. Qi, Y. Y. Wang, Y. Q. Xu, X. L. Wang, F. Zhang, and R. Zhou, "Oxygen pressure induced structure, morphology and phase-transition for VO2/c-sapphire films by PLD," *Applied Physics A: Materials Science and Processing*, vol. 115, no. 4, pp. 1245–1250, 2014, ISSN: 14320630. DOI: 10.1007/s00339-013-7972-0. arXiv: 0207277 [hep-th].

[146] M. Cavalieri, É. O'Connor, C. Gastaldi, I. Stolichnov, and A. M. Ionescu, "Experimental Investigation of Pulsed Laser Deposition of Ferroelectric Gd:HfO 2 in a CMOS BEOL Compatible Process," *ACS Applied Electronic Materials*, vol. 2, no. 6, pp. 1752–1758, Jun. 2020, ISSN: 2637-6113. DOI: 10.1021/acsaelm.0c00319.

[147] M. H. Park, H. J. Kim, Y. J. Kim, T. Moon, K. D. Kim, Y. H. Lee, S. D. Hyun, and C. S. Hwang, "Study on the internal field and conduction mechanism of atomic layer deposited ferroelectric Hf 0.5 Zr 0.5 O 2 thin films," *Journal of Materials Chemistry C*, vol. 3, no. 24, pp. 6291–6300, 2015, ISSN: 2050-7526. DOI: 10.1039/C5TC01074H.

[148] T. Shimizu, T. Yokouchi, T. Oikawa, T. Shiraishi, T. Kiguchi, A. Akama, T. J. Konno, A. Gruverman, and H. Funakubo, "Contribution of oxygen vacancies to the ferroelectric behavior of Hf 0.5 Zr 0.5 O 2 thin films," *Applied Physics Letters*, vol. 106, no. 11, p. 112 904, Mar. 2015, ISSN: 0003-6951. DOI: 10.1063/1.4915336.

[149] Y. H. Lee, H. J. Kim, T. Moon, K. D. Kim, S. D. Hyun, H. W. Park, Y. B. Lee, M. H. Park, and C. S. Hwang, "Preparation and characterization of ferroelectric Hf 0.5 Zr 0.5 O 2 thin films grown by reactive sputtering," *Nanotechnology*, vol. 28, no. 30, p. 305 703, Jul. 2017, ISSN: 0957-4484. DOI: 10.1088/1361-6528/aa7624.

[150] J. Lyu, I. Fina, R. Bachelet, G. Saint-Girons, S. Estandía, J. Gázquez, J. Fontcuberta, and F. Sánchez, "Enhanced ferroelectricity in epitaxial Hf 0.5 Zr 0.5 O 2 thin films integrated with Si(001) using SrTiO 3 templates," *Applied Physics Letters*, vol. 114, no. 22, p. 222 901, Jun. 2019, ISSN: 0003-6951. DOI: 10.1063/1.5096002.

[151] A. K. Tagantsev and I. A. Stolichnov, "Injection-controlled size effect on switching of ferroelectric thin films," *Applied Physics Letters*, vol. 74, no. 9, pp. 1326–1328, Mar. 1999, ISSN: 0003-6951. DOI: 10.1063/1.123539.

[152] L. Chen, V. Nagarajan, R. Ramesh, and A. L. Roytburd, "Nonlinear electric field dependence of piezoresponse in epitaxial ferroelectric lead zirconate titanate thin films," *Journal of Applied Physics*, vol. 94, no. 8, p. 5147, 2003, ISSN: 00218979. DOI: 10.1063/1.1610242.

[153] M. Dawber, P. Chandra, P. B. Littlewood, and J. F. Scott, "Depolarization corrections to the coercive field in thin-film ferroelectrics," *Journal of Physics: Condensed Matter*, vol. 15, no. 24, pp. L393–L398, Jun. 2003, ISSN: 0953-8984. DOI: 10.1088/0953-8984/15/24/106. arXiv: 0307293 [cond-mat].

[154] A. K. Tagantsev, M. Landivar, E. Colla, and N. Setter, "Identification of passive layer in ferroelectric thin films from their switching parameters," *Journal of Applied Physics*, vol. 78, no. 4, pp. 2623–2630, 1995, ISSN: 00218979. DOI: 10.1063/1.360122.

[155] G. Gerra, A. K. Tagantsev, and N. Setter, "Surface-Stimulated Nucleation of Reverse Domains in Ferroelectrics," *Physical Review Letters*, vol. 94, no. 10, p. 107 602, Mar. 2005, ISSN: 0031-9007. DOI: 10.1103/PhysRevLett.94.107602.

[156] A. K. Tagantsev, L. E. Cross, and J. Fousek, *Domains in Ferroic Crystals and Thin Films*. New York, NY: Springer New York, 2010, ISBN: 978-1-4419-1416-3. DOI: 10.1007/978-1-4419-1417-0.

[157] A. I. Khan, M. Hoffmann, K. Chatterjee, Z. Lu, R. Xu, C. Serrao, S. Smith, L. W. Martin, C. Hu, R. Ramesh, and S. Salahuddin, "Differential voltage amplification from ferroelectric negative capacitance," *Applied Physics Letters*, vol. 111, no. 25, p. 253 501, Dec. 2017, ISSN: 0003-6951. DOI: 10.1063/1.5006958. arXiv: 1709.10451.

[158] D. J. R. Appleby, N. K. Ponon, K. S. K. Kwa, B. Zou, P. K. Petrov, T. Wang, N. M. Alford, and A. O'Neill, "Experimental Observation of Negative Capacitance in Ferroelectrics at Room Temperature," *Nano Letters*, vol. 14, no. 7, pp. 3864–3868, Jul. 2014, ISSN: 1530-6984. DOI: 10.1021/nl5017255.

[159] I. Stolichnov, M. Cavalieri, C. Gastaldi, M. Hoffmann, U. Schroeder, T. Mikolajick, and A. M. Ionescu, "Intrinsic or nucleation-driven switching: An insight from nanoscopic analysis of negative capacitance Hf 1−x Zr x O 2 -based structures," *Applied Physics Letters*, vol. 117, no. 17, p. 172 902, Oct. 2020, ISSN: 0003-6951. DOI: 10.1063/5.0021272.

[160] D. Kwon, S. Cheema, N. Shanker, K. Chatterjee, Y.-H. Liao, A. J. Tan, C. Hu, and S. Salahuddin, "Negative Capacitance FET With 1.8-nm-Thick Zr-Doped HfO 2 Oxide," *IEEE Electron Device Letters*, vol. 40, no. 6, pp. 993–996, Jun. 2019, ISSN: 0741-3106. DOI: 10.1109/LED.2019.2912413.

Relevant publications

Journal articles

[1] I. Stolichnov, M. Cavalieri, C. Gastaldi, M. Hoffmann, U. Schroeder, T. Mikolajick, and A. M. Ionescu, "Intrinsic or nucleation-driven switching: An insight from nanoscopic analysis of negative capacitance Hf 1−x Zr x O 2 -based structures," *Applied Physics Letters*, vol. 117, no. 17, p. 172 902, Oct. 2020, ISSN: 0003-6951. DOI: 10.1063/5.0021272.

[2] M. Cavalieri, É. O'Connor, C. Gastaldi, I. Stolichnov, and A. M. Ionescu, "Experimental Investigation of Pulsed Laser Deposition of Ferroelectric Gd:HfO 2 in a CMOS BEOL Compatible Process," *ACS Applied Electronic Materials*, vol. 2, no. 6, pp. 1752–1758, Jun. 2020, ISSN: 2637-6113. DOI: 10.1021/acsaelm.0c00319.

[3] T. Mittmann, M. Materano, P. D. Lomenzo, M. H. Park, I. Stolichnov, M. Cavalieri, C. Zhou, C.-C. Chung, J. L. Jones, T. Szyjka, M. Müller, A. Kersch, T. Mikolajick, and U. Schroeder, "Origin of Ferroelectric Phase in Undoped HfO 2 Films Deposited by Sputtering," *Advanced Materials Interfaces*, vol. 1900042, p. 1 900 042, Apr. 2019, ISSN: 2196-7350. DOI: 10.1002/admi.201900042.

[4] I. Stolichnov, M. Cavalieri, E. Colla, T. Schenk, T. Mittmann, T. Mikolajick, U. Schroeder, and A. M. Ionescu, "Genuinely Ferroelectric Sub-1-Volt-Switchable Nanodomains in Hf x Zr (1– x) O 2 Ultrathin Capacitors," *ACS Applied Materials & Interfaces*, vol. 10, no. 36, pp. 30 514–30 521, Sep. 2018, ISSN: 1944-8244. DOI: 10.1021/acsami.8b07988.

[5] C. Gastaldi, M. Cavalieri, A. Saeidi, É. O'Connor, F. Bellando, I. Stolichnov, and A. M. Ionescu, "Negative Capacitance in HfO2 gate stacks structures with and without metal interlayer," *IEEE Transactions on Electron Devices [submitted, under review]*,

MATTEO CAVALIERI

Based in: Lausanne, CH
Tel: +41 77 5052098
Mail: matteo.cavalieri10@gmail.com
Skype: matteo.cavalieri10
LinkedIn: linkedin.com/in/m-cavalieri
Languages: Italian, English, French, Spanish

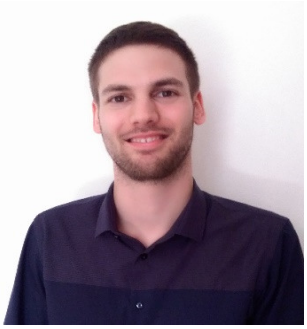

WORKING EXPERIENCE

Feb 2017-Feb 2021

PhD in Materials Science and Engineering at Nanolab, EPFL École Polytechnique Fédérale de Lausanne (Lausanne, Switzerland)
Thesis project on ferroelectricity in HfO_2 thin films. In parallel, I assisted the teaching of Dr. I. Stolichnov and Prof. A. Ionescu.

Oct 2012-Jun 2013

Internship in Team UniBo Motorsport (Bologna, Italy)
Main task was: developing a cooling system for brake discs of a racing car participating in the Formula Student (SAE) international competition, performing material selection and designing the relative manufacturing steps

2006-2014

Working to support the studies (Rimini, London)
Full-time and part-time jobs as warehouse worker and then waiter, with role of team leader acquired in time; cash responsibility and orders management among my duties

EDUCATION

Sep 2014- Jul 2016

MSc in Materials Science and Engineering (Final score: 8.5/10)
Delft University of Technology (Delft, Netherlands)
Relevant modules: structure and properties of materials, materials for measurements and control devices, relation between properties and microstructure, laboratory of materials characterization, thin film materials (project on properties and characterization of graphene);
Additional projects on: storage devices focused on Li-ion batteries, recycling of engineering materials

Nov 2015-Jul 2016	*MSc Thesis: Transfer of CVD single layer h-BN for optomechanical characterization of suspended devices.* *Delft University of Technology and Kavli Institute of Nanoscience* Main tasks are: 1) cleanroom fabrication of suitable substrates, 2) developing a transfer technique for h-BN, 3) characterization of h-BN by means of AFM, laser interferometry and Raman spectroscopy and 4) data analysis on Matlab
Sep 2010-Nov 2013	**BSc in Mechanical Engineering (Final score: 105/110)** **Universitá di Bologna (Bologna, Italy)** Final dissertation: Mechanical properties of graphene reinforced nanocomposites Relevant modules: materials science, machine design, mechanical and thermal measurements and testing Switched from Energy Engineering because it was not challenging and focused on what I liked Additional modules from Energy Engineering: metallurgy, mechanical behaviour of materials, machines and energetic systems, mechanics applied to machines

OTHER ACTIVITIES

Jan 2017-present	**Volunteering** at Action Parrainages, EVAM. Main tasks: help the integration of refugees in Lausanne by organizing and attending social events and cultural activities
Dec 2016-Jan 2017	**Volunteering** experience in northern Uganda, Africa. Main tasks: involving the community and especially the kids of Paimol (Gulu district) in activities of different nature, from simple team building games to raising awareness towards the importance of education
Sep 2010-Jul 2012	**Founder and vice-president** of Drama, a cultural association aimed to arrange social events for children and teenagers in my province Main tasks: bureaucratic and practice events organization, recruiting artists or other personalities for events, presenting and hosting events
Sep 2007-May 2010	**Volunteer** in a municipality centre helping children with their homework and organizing recreational activities for them